Design, Synthesis and Biological Evaluation of Indole Related Heterocycles as Anti-cancer Agents

THESIS

Submitted in partial fulfillment

of the requirements for the degree of

DOCTOR OF PHILOSOPHY

by

Monika Malik

Under the Supervision of

Prof. Dalip Kumar

and

Co-supervision of

Prof. Kavita Shah

BIRLA INSTITUTE OF TECHNOLOGY AND SCIENCE, PILANI

(RAJASTHAN)

September-2024

BIRLA INSTITUTE OF TECHNOLOGY AND SCIENCE, PILANI

CERTIFICATE

This is to certify that the thesis titled **"Design, Synthesis and Biological Evaluation of Indole Related Heterocycles as Anti-cancer Agents"** and submitted by Ms. **Monika Malik** ID No: **2019PHXF0015P** for award of Ph.D. of the Institute embodies original work done by her under my supervision.

Signature of the Supervisor:

Name in capital block letters: **PROF. DALIP KUMAR**

Designation: **Senior Professor**

Date:

Signature of the Co-supervisor:

Name in capital block letters: **PROF. KAVITA SHAH**

Designation: **Professor**

Date: 03/10/2024

Dedicated to

My Family, Friends and

Teachers

Acknowledgements

I would like to begin by expressing my heartfelt gratitude to "**God**" for granting me the strength, knowledge, and ability to undertake and successfully complete this research study. It is with immense pleasure that I reflect on the countless cherished moments and the individuals who have stood by my side throughout this journey. Their unwavering support, guidance, motivation, and blessings at every stage have been instrumental in helping me achieve this significant milestone in my life.

I would like to express my deepest gratitude to Prof. Dalip Kumar for his invaluable guidance and mentorship throughout my Ph.D. journey. I am sincerely thankful to him for providing me with the opportunity to work in a supportive environment, which allowed me to develop both as a researcher and as an individual. It has been a privilege to work under his supervision and to benefit from his vast expertise in the field. His dedication to research, as well as his constant encouragement, has motivated me to stay focused and optimistic during the challenges of my Ph.D. tenure. I am especially grateful for the opportunities he provided me to mentor undergraduate and new students in the laboratory, enriching my experience and shaping my leadership skills. Prof. Dalip Kumar's unwavering support, both academically and personally, has been instrumental in my growth, and I will always remain thankful for his trust and belief in my abilities.

I extend my heartfelt gratitude to my co-supervisor, Dr. Kavita Shah from Purdue University, USA, for her invaluable guidance and unwavering support throughout my research journey. Specifically, during my OVDF (Overseas Visiting Doctoral Fellowship) tenure, I had the privilege of working closely under Dr. Shah's mentorship for 1.5 years. I acquired a wealth of knowledge and expertise, particularly in the field of biology. Dr. Shah's guidance played a pivotal role in shaping my understanding and proficiency in my research domain. Her continuous encouragement and insightful feedback have not only enriched my academic endeavors but also instilled in me a deeper appreciation for scientific inquiry. Working alongside her during my OVDF experience was both enlightening and enriching, as I had the opportunity to learn from her vast experience and expertise. I am truly grateful to Dr. Kavita Shah for her mentorship, patience, and dedication, which have been instrumental in my growth and development as a researcher.

I am grateful to the past and current Vice-Chancellors, Directors, Deans, and Associate Deans of Birla Institute of Technology & Science, Pilani (BITS Pilani), for granting me the opportunity to

Monika Malik

ABSTRACT

Cancer is one of the prominent causes of death worldwide. To identify potent and selective anticancer drugs with reduced side effects is a serious concern to medicinal chemists. Medicinal chemists are actively engaged in the quest for such drugs, focusing on specific targets such as anti-mitotic agents (Tubulin inhibitors), Cyclin dependent Kinases, and FICD inhibitors. Tubulin, a pivotal protein in cellular processes like mitosis and intracellular transport, has emerged as a key target for anticancer therapy. Additionally, dysregulated kinase activity frequently correlates with cancer progression, therefore, kinase is another promising target for anticancer therapeutics. The thesis deals with the design, synthesis and anticancer activity studies of novel indolyl heterocycles. Moreover, *in silico* binding modes for synthesiszed compounds have also been investigated using molecular modeling and toxicity predication. The thesis is divided into seven chapters.

The **First Chapter** of the thesis provides brief introduction about the physical and chemical properties of indole and an overview of anticancer research and treatments of various types of cancers with special emphasizes on chemotherapy and classification of anticancer drugs present in market. Further, the chapter provides information for the rational design of novel indole containing chemical entities as potent anticancer agents. Also, it describes the current problems associated with the existing anticancer drugs and the scope for developing novel indole-based compounds by structural modifications of existing natural and synthetic bioactive indole anticancer agents with improved anticancer properties. The **Second Chapter** of the thesis is divided in two parts. **Part 2A** of this chapter reports, the copper-mediated cross-coupling reactions of *N*-Boc-3-indolylsulfoximines with aryl iodides, we produced a diverse series of *N*-arylated indolylsulfoximines in excellent yields. From the prepared series of *N*-arylated indolylsulfoximines, compound **11K** (1.28 μM) was selectively cytotoxic against MCF7 cells and **11j** (2.68 μM) was selectively cytotoxic against 22Rv1 cells. The compound **11l** bearing fluorine at the C_6-position of indole, endowed broad cytotoxicity against C4-2, PC3, 22Rv1 and MCF7 with IC_{50} values of 8.1, 3.51, 1.91, and 1.7 μM, respectively. HEK293 cells (normal kidney cells) were not affected by these compounds, suggesting their specificity for cancer cells. In **Part 2B**, colchicine sulfoximine analogues were synthesized and found to exhibit significant inhibition of tubulin polymerization.

The **third Chapter** of the thesis focuses on investigating the potential of *N*-aryl indolylsulfoximines as anticancer agents, with a specific emphasis on their activity against Cyclin-Dependent Kinases (CDKs). Particularly, compound **23g** emerged as a potent CDK5/p25 inhibitor with an IC_{50} value of 1.12 μM, showcasing selectivity over CDK2 and CDK1. *N*-aryl indolylsulfoximines exhibited promising selectivity with an IC_{50} value of 2.15 μM for CDK5/p25. Additionally, the docking results of potent compound (binding affinity= -8.5 Kcal/mol) demonstrated a strong correlation with the *in vitro* outcomes. The **Fourth Chapter** entails indolyl-1,2,4-triazoles prepared from the cyclization of acylhydrazides and thioimidate in good to excellent yields (95%). The most active compound exhibited cytotoxicity towards acute HeLa cell line (IC_{50} = 3.5 μM). Preliminary mechanism of action study of the most potent compound showed inhibition of tubulin polymerization. The **Fifth Chapter** of the thesis, divided into two parts. **Part 5A** describes environmentally friendly synthesis of α-cyano bis(indolyl)chalcones, followed by their *in vitro* evaluation against six human cancer cell lines. One of α-cyano bis(indolyl)chalcone emerged as the most potent and selective against the C4-2 prostate cancer cell line, displaying an IC_{50} value of 0.98 μM. In **Part 5B** the synthesized α-cyano bis(indolyl)chalcones were screened for FICD inhibition activity. In AMPylation assay, α-cyano bis(indolyl)chalcones demonstrated significant potency, with an IC_{50} value of 7.9 μM. Interestingly, our findings revealed certain molecules displaying notable affinity for ATP binding site. The **Chapter Six** describes two efficient synthetic methodologies for the preparation of diverse and biologically active β-oxo amides and benzo[a]carbazoles. The copper-catalyzed strategy enables the synthesis of β-oxo amides using iodonium salts under mild reaction conditions. Additionally, the developed approach offers a convenient route to diversely substituted benzo[a]carbazoles from 3-substituted acetylindoles and diaryliodonium salts under Pd-catalyzed neutral conditions. Finally, in the **Seventh chapter** of the thesis, summary of the thesis is presented along with the future scope of the research work.

TABLE OF CONTENTS

Chapter 1: Introduction

Chapter 2: Sulfoximine Functionalized Anti-cancer Agents

Part 2B: Design, Synthesis, *in-silico* Studies and Biological Evaluation of Novel Sulfoximine Modified Colchicine Derivative as Potent Tubulin-Targeting Anti-cancer Agents

Chapter 4: Design and Facile Synthesis of Indolyl-1,2,4-triazoles as Tubulin Interacting Anti-cancer Agents

Chapter 5: Design, Synthesis and Anti-cancer activity of Novel α-cyano bis(indolyl)chalcones

Part 5A: L-Proline catalysed synthesis and *in-silico* Studies of Novel α-cyano bis(indolyl)chalcones as Potential Anti-cancer Agents

Part 5B: Design and Synthesis of FICD Inhibitors

Chapter 6: Diaryliodonium Salts promoted Versatile Approach to Diverse β-Oxo Amides and Potent Benzo[*a*]carbazoles

Chapter 7: Conclusions and Future Scope

Appendices

LIST OF TABLES

LIST OF FIGURES

LIST OF ABBREVATIONS

Abbreviation	Description
AcOH	Acetic Acid
PSs	Photosensitizers
acac	Acetylacetonate
ACN	Acetonitrile
Ar	Aryl
Aq.	Aqueous
atm	Atmosphere
t-BuOK	Potassium $tert$-butoxide
HPLC	High Performance Liquid Chromatography
^{13}C	Carbon-13
^{19}F	Fluorine-19
$CDCl_3$	Deuterated Chloroform
p-Cymene	1-Methyl-4-(propan-2-yl)benzene
$Cu(OAc)_2$	Cupric Acetate
Calc.	Calculated
λabs	Absorption Wavelengths
MTT	(3-(4,5-Dimethylthiazol-2-yl)-2,5-diphenyltetrazolium
IC_{50}	Half Maximal Inhibitory Concentration
nM	Nanomolar
μM	Micromolar
nm	Nanometer
d	Doublet
dd	Doublet of Doublet

DCB	1,4-Dichlorobenzene
DCE	1,2-Dichloroethane
DCM	Dichloromethane
DMA	Dimethylacetamide
DME	Dimethoxyethane
DMF	*N,N*-Dimethylformamide
DMSO-*d₆*	Deuterated Dimethylsulfoxide
DMSO	Dimethylsulfoxide
ESI-MS	Electron Spray Ionization-Mass Spectrometry
Et$_2$O	Diethyl Ether
EtOAc	Ethyl Acetate
EtOH	Ethanol
EWG	Electron Withdrawing Group
EDG	Electron Donating Group
equiv.	Equivalent
FT-IR	Fourier Transform Infrared
g	Gram
h	Hours
HRMS	High Resolution Mass Spectrometry
Hz	Hertz
^{i}Pr	Isopropyl
IBD	Iodobenzene Diacetate
PIFA	Phenyliodine Bis(trifluoroacetate)
HTIB	[Hydroxy(tosyloxy)iodo]benzene
J	Coupling Constant

K_2CO_3	Potassium Carbonate
mp	Melting point
m	Multiplet
mL	Millilitre
mg	Milligram
MHz	Megahertz
min	Minutes
mmol	Millimole
mol %	Mole Percent
MeOH	Methanol
NaOAc	Sodium Acetate
NMR	Nuclear Magnetic Resonance
Nu	Nucleophile
o	Ortho
p	Para
m	Meta
Phen	1,10-Phenanthroline
PIDA	Phenyl Iodonium Diacetate
ppm	Parts Per Million
Q-TOF	Quadrupole Time of Flight
r.t.	Room Temperature
s	Singlet
t	Triplet
td	Triplet of Doublets
TFA	Trifluoroacetic Acid

THF	Tetrahydrofuran
TLC	Thin Layer Chromatography
p-TSA or *p*-TsOH	*p*-Toluenesulfonic Acid
UV	Ultraviolet
$Zn(OAc)_2$	Zinc Acetate
ROS	Reactive Oxygen Species
A549	Lung Cancer Cell Line
GPCR	G-protein Coupled Receptors
DABCO	1,4-Diazabicyclo[2.2.2]octane
PET	Positron Emission Tomography
ED_{50}	Effective dose 50%
SAR	Structure-Activity Relationship
TMSCl	Trimethylsilyl Chloride
ADME	Absorption, Distribution, Metabolism, Excretion
CDKs	Cyclin Dependent Kinases
AR	Androgen Receptors
ATP	Adenosine Triphosphate
PAINS	Pan Assay Interference
GI	Gastro-intestine
MTs	Microtubules
MW	Microwave
MTAs	Microtubule Targetting Agents
CBS	Colchicine Binding site
CA-4	Combretastatin A-4

α	Alpha
β	Beta
ºC	Degree Centigrade
FICD	Filamentation Induced by cAMP Domain
MW (g/mol)	Molecular Weight
Log $P_{o/w}$	Lipophilicity
Log S	Water Solubility
BBB	Blood Brain Barrier
PGP	P-glycoprotein
BOILED-Egg	Brain Or IntestinaL EstimateD permeation
yolk	Yellow Area
CP	Conventional Procedure
PDB	Protein Data Bank
PC3	Prostate Cancer Cell Line
MCF7	Breast Cancer Cell Line

Chapter 1

Introduction
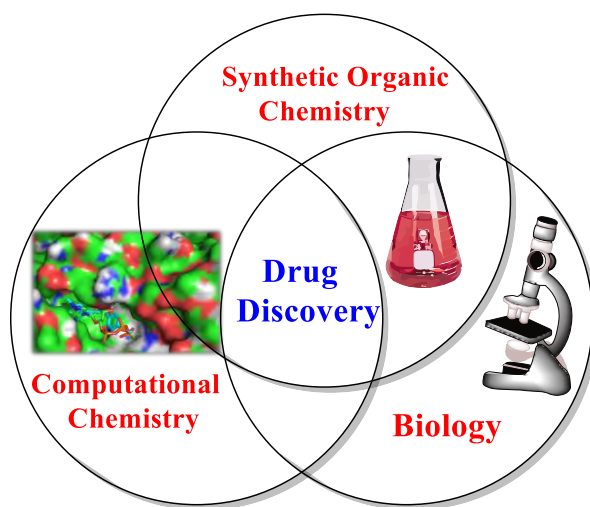
1. Introduction

1.1 Cancer Research in Drug Discovery

Drug discovery is a multifaceted process aimed at identifying potential therapeutic agents, employing a combination of computational, experimental, translational, and clinical models.[1] Despite significant advancements in biotechnology and our understanding of biological systems, drug discovery remains a challenging, time-consuming, and costly endeavor, often plagued by a high attrition rate of new therapeutic candidates. At its core, drug design involves the innovative creation of new medications based on the understanding of a biological target. Essentially, it entails designing molecules that complement the shape and charge of the molecular target they interact with and bind it at perticular target. While drug design frequently utilizes computer modeling techniques and bioinformatics approaches, it may also rely on other methods in the era of big data.[2]

Modern drug design is an integrated and long-term process that entails significant financial investment, costing tens to hundreds of millions of dollars from candidate compound trials to FDA approval.[3] Preclinical drug design trials involve a combination of *in silico*, *in vitro*, and *in vivo* experiments, with advancements in information technology and big data accelerating the pace of drug discovery by facilitating the construction of highly effective and targeted databases. There are several stages in the drug discovery process that require numerous skills and the use of various advanced technological platforms (often a combination of computational and experimental approaches) to validate targets and search for therapeutic agents.[4] When initial experimental compounds have been sufficiently optimized to be selective, potent and safe in preliminary *in vitro* experiments and animal models, they can be nominated as drug candidates.

Cancer poses a major health challenge and remains a leading cause of death worldwide. According to the World Health Organization the number of cancer cases in the world will increase to 22 million by 2030.[7] Liver, breast and prostate are among the most common types of cancer diseases. Several ways have been discovered and reported for inhibiting cancer diseases, such as surgery, chemotherapy, radiation therapy, targeted therapy, immunotherapy, hormonal therapy, bio-logical therapy, and photodynamic therapy.[5] More recently, targeted therapy has shown great potential in addressing drugs toward cancer cells of specific genes and proteins without attacking the healthy cells.
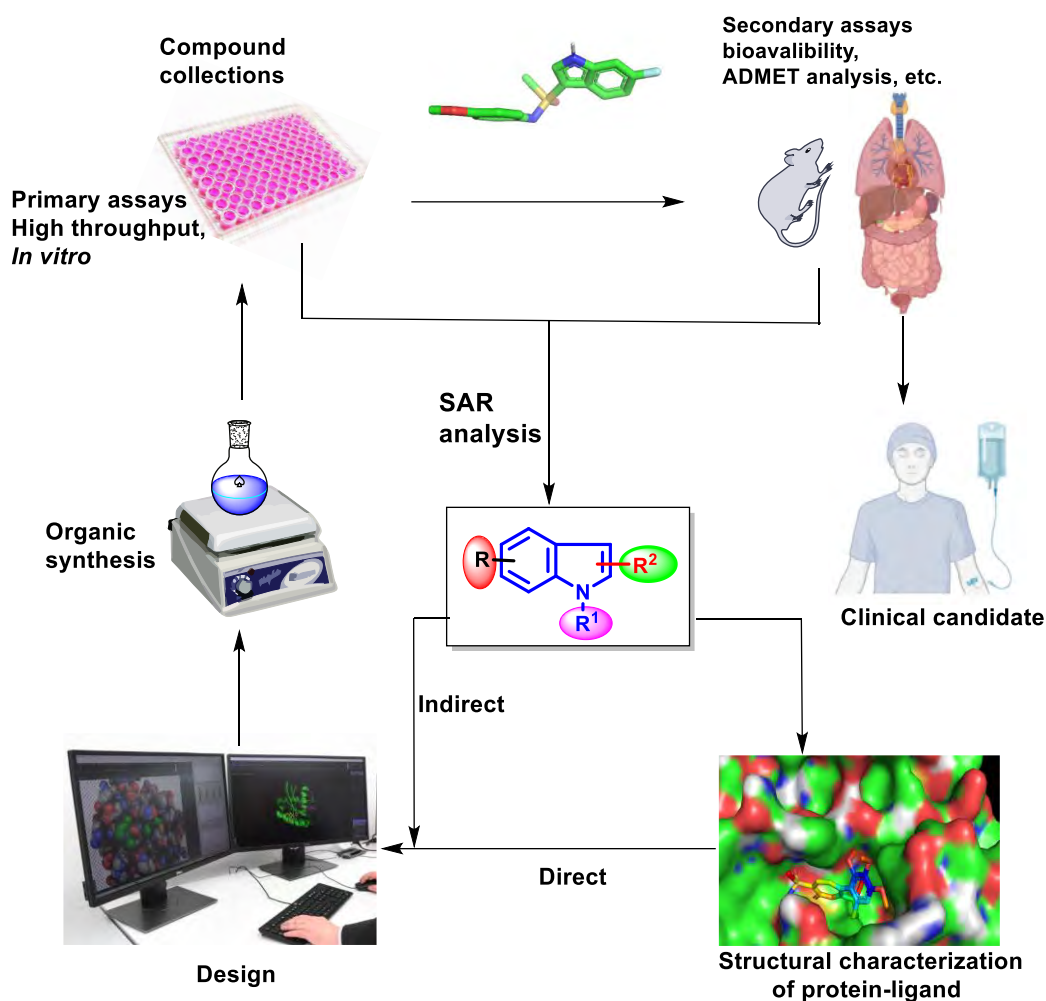
Figure 1.1 Drug Discovery Cycle

The high mortality rate associated with HCC can be largely attributed to its widespread prevalence and the inadequacy of conventional chemotherapy as an effective treatment.[8] FDA-approved drugs such as Sorafenib and Regorafenib were used as multi-kinase inhibitors for the treatment of HCC; however, this treatment can only improve patient's median survival for about 3 to 10 months.[9] Addressing these challenges necessitates the development of novel and effective chemotherapeutics in medicinal chemistry, despite the existence of several drugs for various cancers.[10]

Efforts to reduce the cancer-related death rate have garnered considerable attention from governments, societies, the pharma industry, and scientific communities, with hopes for the rapid development of effective and safe drugs for cancer treatment. Despite remarkable advancements in biological sciences and our understanding of disease biology, the creation of new, practical, and innovative small molecule drugs remains a challenging, time-consuming, and costly endeavor.[11] This undertaking necessitates collaboration across multidisciplinary fields, including medicinal chemistry, computational chemistry and biology (Figure 1.2).

Computational methods have become crucial tools in drug discovery projects and are now essential to new drug development approaches. These methods expedite and streamline the drug development process, making it more efficient and cost-effective.
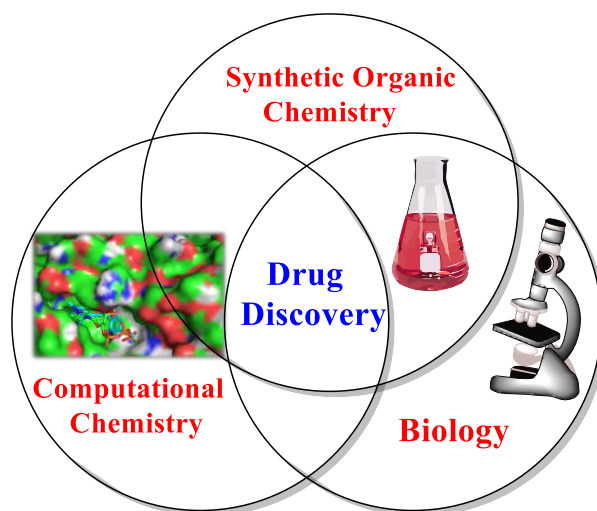
Figure 1.2 Multidisciplinary fields in drug discovery

Cancer remains one of the most challenging health issues globally, with its complex and heterogeneous nature posing significant hurdles in effective treatment strategies. Despite advancements in medical science, the quest for novel and potent anticancer agents continues. The development of such agents requires a multifaceted approach, integrating diverse disciplines including medicinal chemistry, molecular biology, computational modeling and pharmacology. Our efforts towards the design, synthesis, *in silico* analysis, and biological evaluation of indolyl heterocycles as promising anti-cancer agents targets tubulin, Cyclin Dependent Kinases and FICD.

Tubulin, a crucial protein involved in cellular processes such as mitosis and intracellular transport, has emerged as a prime target for anticancer therapy. Disruption of tubulin dynamics can lead to cell cycle arrest and apoptosis, making it an attractive target for drug development.[11, 12] Kinases, on the other hand are enzymes that regulate various signaling pathways involved in cell proliferation, differentiation, and survival.[13] Dysregulation of kinase activity is often associated with cancer progression, making them another promising target for anticancer drug development. Additionally, FICD (Filamentation induced by cAMP domain) a protein involved in cellular stress response and post-translational modification, is emerging as a promising target for cancer therapy. Its role in essential cellular processes, including adaptation to adverse conditions, makes it an attractive target for disrupting cancer cell growth and survival. By targeting FICD, it may be possible to hinder dysregulated cellular processes implicated in tumor development and progression. This highlights FICD as a potential avenue

for the development of novel cancer therapies. Heterocyclic compounds are of immense chemical and biological significance. In particular, azaheterocycles (nitrogen containing heterocycles) such as pyrrole, oxazoles, imidazoles, thiazoles, oxadiazoles, quinolines, pyrimidines and indoles are structural constituents of many natural as well as synthetic bioactive drug-like molecules.[14]

Nitrogen-containing heterocyclic compounds have gained prominence in the synthetic and pharmaceutical industries because of their diverse biological actions.[15] For example, these actions include anti-microbial,[16, 17] anticancer,[18, 19] anti-malarial,[20] anti-HIV,[21] and anti-tubercular activities.[22] Among the nitrogen-containing heterocycles, indole and derived compounds possess remarkable anti-tuberculosis,[23] anti-inflammatory,[24] and anti-cancer activities.[25] The intriguing indole moiety is well-known for its anticancer activities and occurs widely in numerous natural products such as vinblastine and vincristine, which can be used to treat breast cancer, testicular cancer, ovarian cancer, and neck and prostate cancer.[26] There is significant evidence that indole can be linked to a variety of other anticancer compounds.

Indole-based heterocycles offer a versatile scaffold for the design of anti-cancer agents due to their diverse biological activities and structural flexibility. The planar structure of indole allows for facile modifications to tailor pharmacological properties and enhance target specificity. Moreover, indole derivatives have demonstrated promising anticancer activity through various mechanisms, including inhibition of tubulin polymerization, interference with kinase signaling pathways and modulation of cellular stress response mechanisms. While working towards the identification of anti-cancer agents, the thesis research work aims to achieve the following objectives

1. Design, synthesis and characterization of novel indole derived compounds.

2. Biological evaluation of synthesized compounds using different human cancerous cell lines. And utilization of computational methods for *in silico* screening and molecular modeling to predict the binding interactions of synthesized compounds with their respective targets (Tubulin, Kinases and FICD).

Through a multidisciplinary approach encompassing organic synthesis, computational modeling and biological assays, thesis aims to contribute to the discovery of novel anticancer agents with improved efficacy and reduced off-target effects. The findings from this research hold potential for the development of innovative therapies for combating cancer and improving patient outcomes.

1.2 Indole

Indole is a pervasive and naturally occurring heterocyclic compound, featuring a six-membered benzene ring fused to a five-membered pyrrole ring (Figure 1.3)[27]. Following Huckel′s rule of aromaticity, indole, with its 10 electrons, exhibits aromatic properties. Similar to benzene, it is prone to electrophilic substitution reactions. Molecular orbital studies have revealed that the 3-position of indole is particularly reactive towards electrophilic substitution reactions. Under basic conditions, indoles can undergo N-substitution reactions due to the slightly acidic nature of the -NH bond in indole.[28] The first synthesis of indole was achieved in 1866 by Adolf von Baeyer.[29] Owing to the diverse applications of the indole scaffold in both biological and pharmacological fields, numerous synthetic schemes have been published. Among the most prominent and widely used methods are reported by Fisher,[30] Bischler,[31] Hemetsberger, Nenitzescu, Bartoli,[32] and others.[33] Owing to its bioavailability and pharmacological applications, indole is considered as the most privileged scaffold in heterocyclic chemistry.
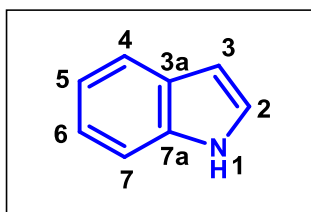
Figure 1.3 Structure of Indole

1.2.1 Chemical Reactivity

Indole and simple alkyl indoles are colorless crystalline solids found to be stable in air and soluble in most organic solvents. Indole presents a planar conjugated system with 10 π-electrons, and its IUPAC name is 1H-benzo[*b*]pyrrole. In terms of chemical behavior, indole shares similarities with pyrrole, particularly in its weak basicity. Its pKa value, a measure of acid strength, is recorded at -3.63, indicating that it is a very weak base. Despite its weak basic nature, indole and its derivatives exhibit a diverse range of physical and chemical properties, making them versatile compounds for various applications in both biological and synthetic chemistry. Although indole is a weak base, it and its derivatives display a wide array of physical and chemical properties, contributing to their versatility in various applications within biological and synthetic chemistry. The electron-rich pyrrole ring within indole renders it particularly prone to electrophilic substitution reactions, distinguishing it from its benzene counterpart.[34] This unique combination of aromaticity and reactivity makes indole a highly valued heterocyclic nucleus in medicinal chemistry.

1.3 Cancer and its Treatment

1.3.1 FDA-Approved Anti-cancer Drugs

Indole is considered as one of the most important nitrogen heterocycles that have gained considerable interest in last decade due to its multiple bioactivities (Figure 1.4). It is evidenced by the fact that recently, U.S. Food and Drug Administration (FDA) databases have disclosed the importance of nitrogen-containing heterocycles in drug discovery.[10, 35, 36]

1. Vincritine (R=CHO) (Tubulin inhibitor)
2. Vinorelbine (R=CH$_3$) (Tubulin inhibitor)
FDA Approved in 1963 (**1**) and 1994 (**2**)

3
Colchicine

4
Frovatriptan
FDA Approved in 2001

5
Sunitinib (Kinase inhibitor)
FDA Approved in 2006

6
Carvedilol phosphate
FDA Approved in 2006

7
Panobinostat lactate
FDA Approved in 2015

8
Osimertinib mesylate (Kinase inhibitor)
FDA Approved in 2015

9
Midostaurin (Kinase inhibitor)
FDA Approved in 2017

10
Entrectinib
FDA Approved in 2019

11
Pemigatinib (Kinase inhibitor)
FDA Approved in 2020

12
Abemaciclib (Breast cancer)
FDA Approved in 2023

13
Talazoparib (Prostate cancer)
FDA Approved in 2023

Figure 1.4 FDA-approved anti-cancer drugs

1.3.2 Chemotherapeutic Approaches

Chemotherapy is the use of drugs or chemical entities to kill cancer cells. These drugs specifically target fast-dividing cancer cells, which are more susceptible to their effects compared to normal, healthy cells. However, chemotherapy is not always able to distinguish between cancerous and healthy cells, it can also affect normal cells that undergo rapid division, leading to the side effects commonly associated with this treatment.[37]

1.3.3 Types of Chemotherapy Drugs Targets

Chemotherapy drugs can be divided into several groups based on various factors such as how they affect chemical substances within the cancer cell, what part of the cell cycle the drug affects, chemical structure and their relationship to another drug. Depending on the mechanism of action, chemotherapy can be divided into alkylating agents, antimetabolites, topoisomerase inhibitors, mitotic spindle inhibitors, and others.[38, 39]

Each new year, FDA approves the use of new drugs for cancer treatments, but due to multiple drug resistance and serious side effects, current treatments become non-ideal therapy; because of that, great efforts to discover a new agent with fewer toxic effects are necessary.[40, 41] Many new chemical structures were designed and synthesized regarding cancer's biological targets, such as cyclin-dependent kinase (CDK), epidermal growth factor (EGF), DNA topoisomerase and tubulin proteins.[42] These targets were classified as the main targets of new anticancer candidates and with regards to this, tubulin and CDKs are considered as the most useful and strategic molecular targets for antitumor drugs (Figure 1.5).
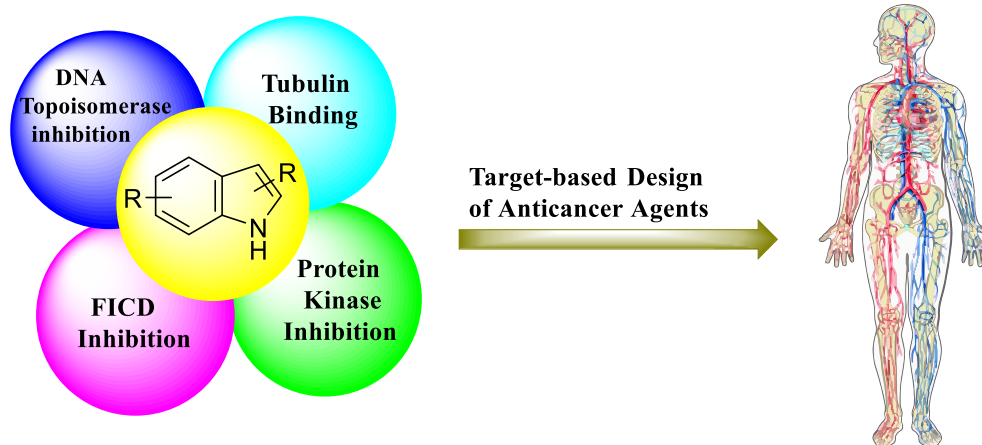
Figure 1.5 Target based design of indole-derived anti-cancer agents

1.3.3.1 Anti-mitotic Agents: Tubulin Inhibition

Antimitotic agents have been the most successful pharmacological agents for the treatment of cancer. The term "antimitotic agent" has traditionally been synonymous with tubulin targeting compounds. The vast majority of these molecules act by binding to the protein tubulin, an α, β-heterodimer that forms the core of the microtubule. Microtubules (MTs) are tubular polymers and are major cytoskeletal components in eukaryotic cells.

Tubulin is a globular protein comprising α,β-heterodimers, which polymerize to form the biopolymers of microtubules. Being the third major component of the cytoskeleton, microtubules play a critical role in cell division, in addition to aiding in both inter and intra-cellular movement and maintaining cell shape.[43] Microtubules are vital components of cell division and have become attractive targets for anti-cancer agents. In cancer treatment, both polymerizing and depolymerizing agents are utilized to disrupt the dynamic assembly and disassembly of microtubules, critical processes for cell division. Polymerizing agents like taxanes and epothilones stabilize microtubules by promoting their assembly, leading to the formation of stable structures that disrupt mitosis and induce apoptosis in rapidly dividing cancer cells. Conversely, depolymerizing agents such as vinca alkaloids, colchicine, and nocodazole inhibit microtubule polymerization, causing disassembly and cell cycle arrest. These agents effectively disrupt cancer cell proliferation and survival by altering the delicate balance of microtubule dynamics. (Figure 1.6)
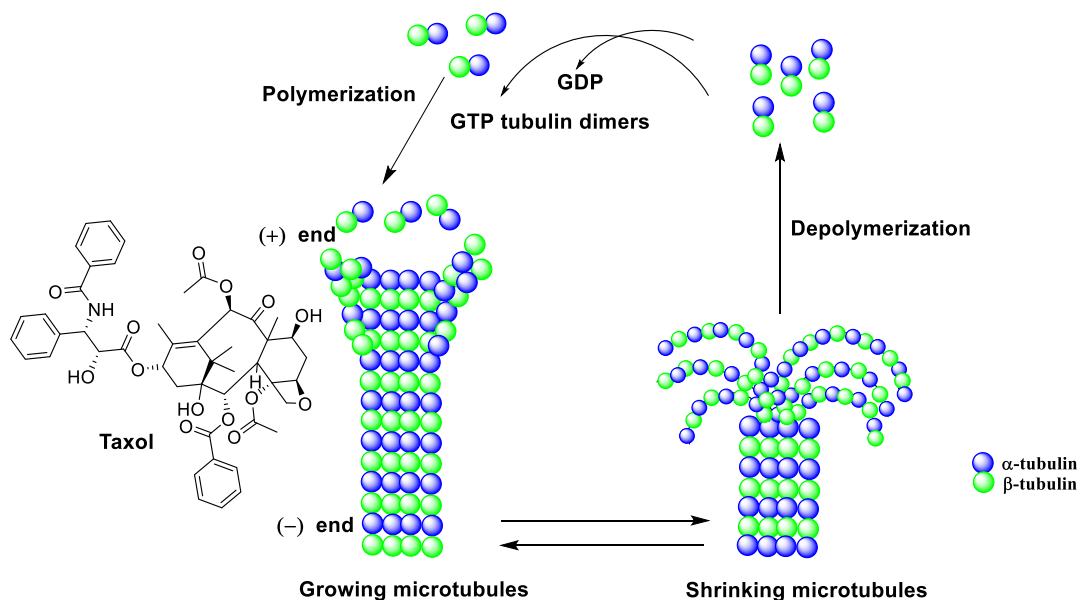
Figure 1.6 Structure and dynamic instability of microtubules

By specifically targeting microtubule depolymerization, these agents effectively hinder cancer cell proliferation and survival, offering promising avenues for cancer therapy. The vinca alkaloids (vincristine, vinblastine, and vinorelbine)[44] and colchicine destabilize tubulin by inhibiting the polymerization of tubulin (Figure 1.7). Molecular docking explorations have revealed specific interactions of these inhibitors in the active sites of tubulin protein.[45] Colchicine binding is considered to be a universal property of higher eukaryotic tubulin. Therefore, many researchers are focusing their efforts on developing compounds that bind to the colchicine site to find new drugs that can address the limitations of existing tubulin targeting drugs.[46, 47] The colchicine binding site contains three hydrophobic pockets that serve as the main locations for ligand interactions, as well as two hydrophilic sites that are prone to forming additional hydrogen bonds with ligands that add stability to the interactions. Hydrophobic pocket I is the main target for compounds in the 'deep binding mode' category, whereas hydrophobic pocket II is the major CBSI binding pocket. Hydrophobic pocket II is occupied by the TMP moiety of numerous CBSIs (such as combretastatin A analogues and ABI analogues). Hydrophobic pocket III is located at the interface of the α, β-subunit.[48] Due to the small volume of the colchicine site cavity and the relatively simple structure of the corresponding inhibitors, the research on colchicine inhibitors has attracted much attention in recent years.
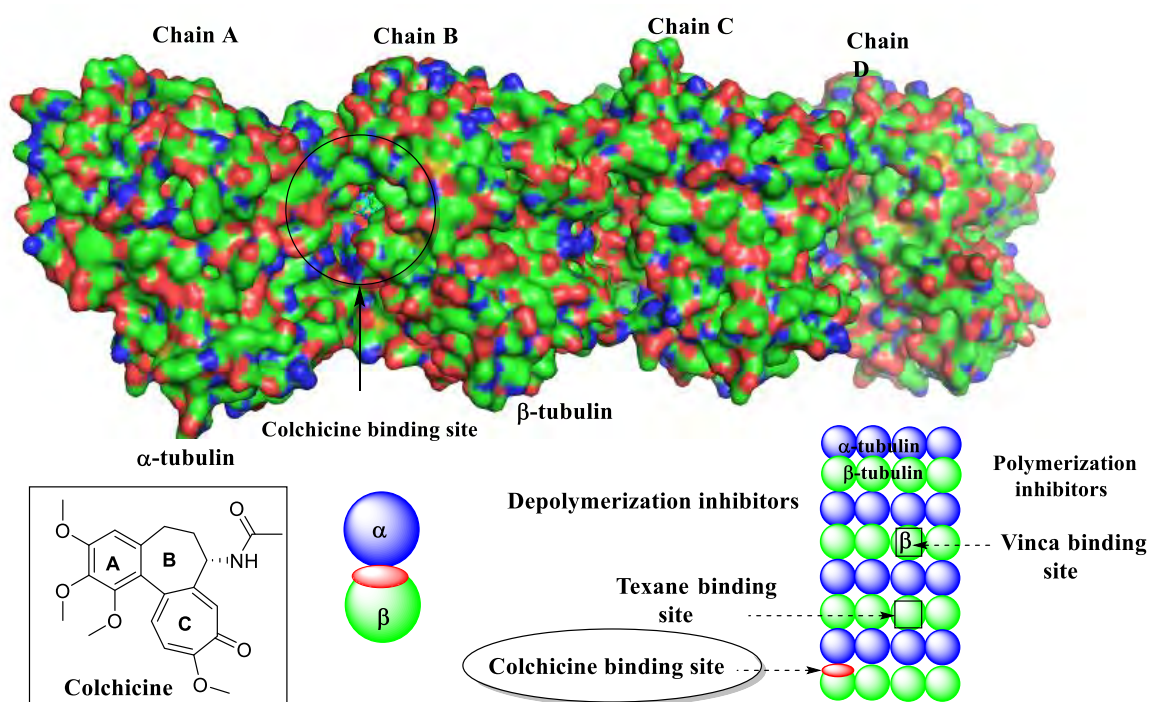
Figure 1.7 Binding sites of tubulin protein

1.3.3.1.1 Colchicine Binding Site Inhibitors

Colchicine binding site inhibitors are a class of compounds that target the colchicine-binding site on tubulin, a key protein involved in the formation of microtubules. By binding to this site, these inhibitors disrupt the polymerization of tubulin into microtubules, thereby interfering with crucial cellular processes such as cell division and intracellular transport.

In 2024, Zhu *et al.* demonstrated the potent inhibitory activity of compound **14** against tubulin assembly, with an IC_{50} value of 1.68 μM. Furthermore, **14** exhibited significant growth inhibitory effects on three human cancer cell lines, including MCF-7, A549, and Hela, with IC_{50} values ranging from 0.21 to 0.46 μM. Additionally, **14** induced apoptosis, arrested the cell cycle in the G2/M phase, and disrupted the cellular microtubule network, highlighting its promising anti-cancer properties.[45] Similarly, in 2024, Wang *et al.* reported the remarkable inhibitory activities of compound **15** against MCF-7, A549, and HepG2 cancer cells, with IC_{50} values ranging from 1.79-40.55 nM in Figure 1.8. These inhibitory effects were superior to those of the standard drugs cisplatin and colchicine. Additionally, compound **15** was found to inhibit tubulin polymerization, further demonstrating its potential as a tubulin inhibitor.[12]
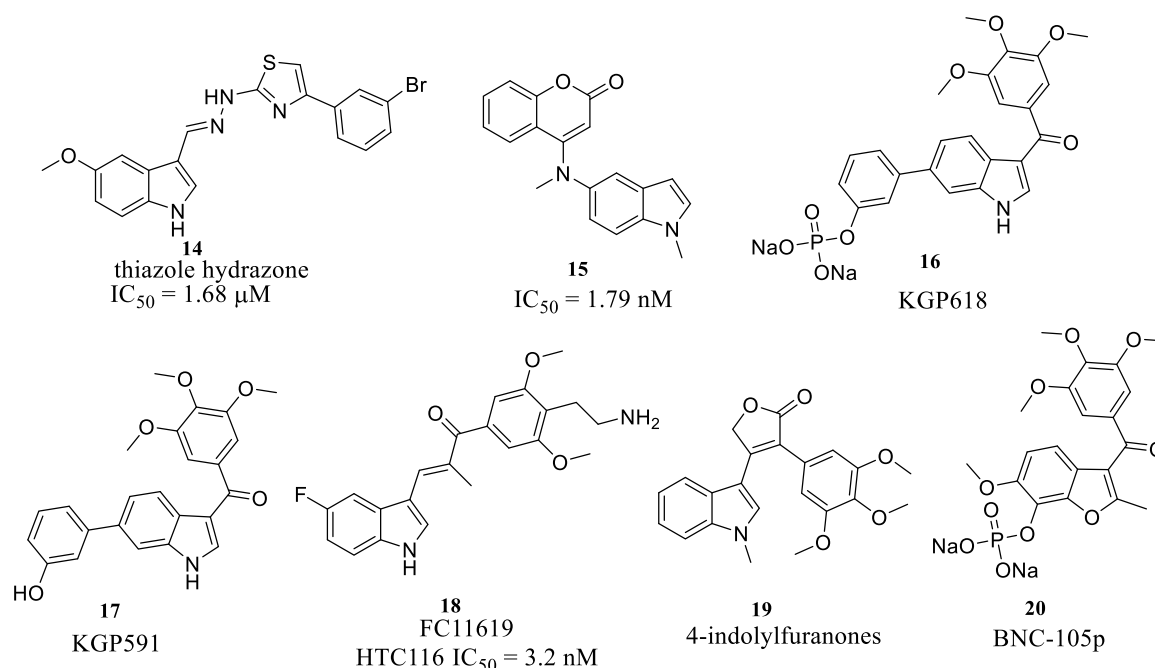
Figure 1.8 Representative anti-tubulin CBS inhibitors

Furthermore, Kevin *et al.* in 2024 reported promising analogues, including KGP591 (**17**), which induced significant G2/M arrest, disrupted microtubule structure and cell morphology, and inhibited cell migration in MDAMB-231 breast cancer cells. Molecular docking studies provided insights into the key interactions of KGP591 (**17**) at the colchicine site. Additionally, the phosphate prodrug salt KGP618 (**16**), derived from KGP591 (**17**), demonstrated significant

efficacy in reducing bioluminescence signal in an orthotopic model of kidney cancer (RENCA-luc) in BALB/c mice, indicating its potential as a vascular disrupting agent (VDA).[49] Moreover, in 2023, Zhuang *et al.* developed Fluoro-substituted indole-chalcone FC116 derivatives, among which FC11619 (**18**) exhibited potent cytotoxicity against HCT-116 CRC cells in low nanomolar range. **18** induced G2/M phase arrest, increased reactive oxygen species (ROS) production, and targeted tubulin in CRC cells. *In vivo* studies demonstrated that **18** significantly suppressed tumor growth, outperforming Taxol in terms of efficacy (Figure 1.8).[50] Several other potent tubulin inhibitors have been identified, such as BPROL075, 4-indolylfuranones (**19**), and BNC-105p (**20**) which exert their activity through colchicine binding site. Notably, indole structures have been identified as key components in these inhibitors, suggesting the significance of the indole nucleus in tubulin inhibition.[50]

1.3.3.1.2 Tubulin Role in the Cell Cycle: Mechanism of Action

Tubulin plays a critical role in multiple phases of the cell cycle, particularly in the processes of cell division and chromosome segregation. An overview about the involvement of tubulin in the cell cycle is provided below.

During interphase, the non-dividing phase of the cell cycle, tubulin is essential for maintaining the cytoskeleton and providing structural support to the cell. It forms microtubule networks that help in intracellular transport, cell shape maintenance, and organelle positioning. In prophase, tubulin plays a key role in the assembly of the mitotic spindle, a microtubule-based structure responsible for the proper segregation of chromosomes during cell division. Tubulin molecules polymerize to form spindle microtubules, which capture and organize the chromosomes. During metaphase, the chromosomes align at the center of the cell, forming the metaphase plate. The mitotic spindle, composed of microtubules, helps to position and align the chromosomes accurately. Tubulin provides the structural framework for spindle formation and ensures proper chromosome attachment. In anaphase, tubulin enables the separation of sister chromatids by mediating the poleward movement of chromosomes. Tubulin subunits depolymerize from the kinetochore microtubules attached to the centromeres, resulting in chromosome segregation towards opposite poles of the cell. Tubulin also plays a role in the final stages of cell division. During telophase, tubulin helps in the reformation of the nuclear envelope around the segregated chromosomes. In cytokinesis, tubulin is involved in the formation of the contractile ring, which constricts the cell at the equator and leads to the physical separation of the two daughter cells. (Figure 1.9)

11
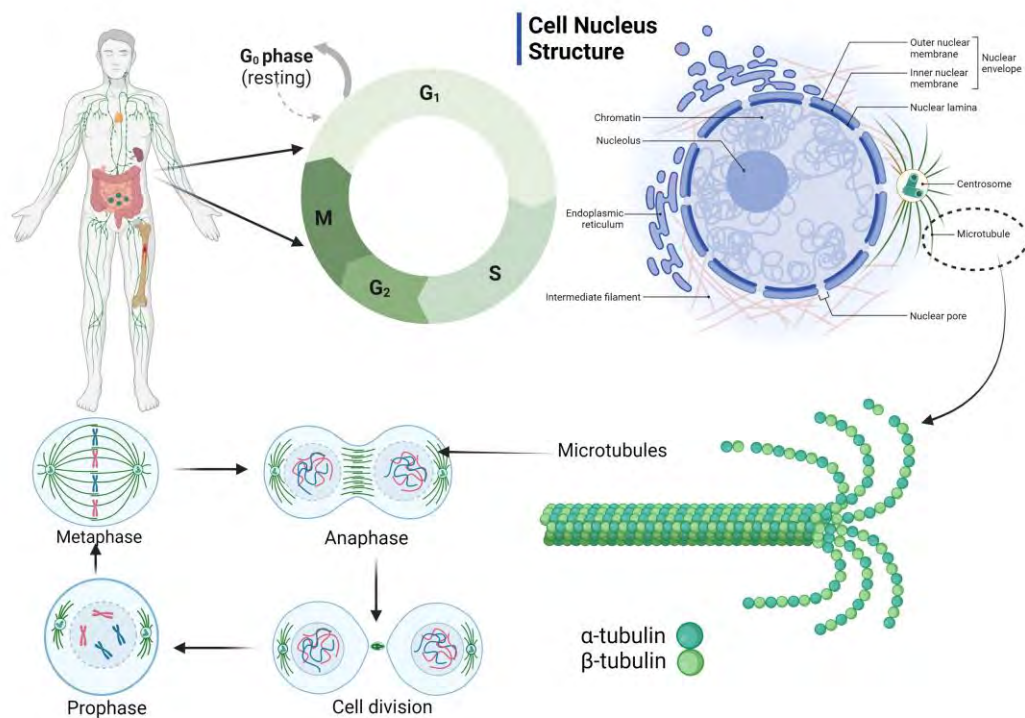
Figure 1.9 Role of microtubules in cell cycle

Disruption of tubulin dynamics leads to cell cycle arrest in the G2/M phase and induction of apoptosis.[51] The crystal structure of β-tubulin reveals important structural information about the C-terminal and N-terminal regions of this protein. These regions play essential roles in tubulin assembly, interactions with other proteins, and binding of small molecule ligands or drugs.

C-terminal of β-Tubulin

The C-terminal region of beta tubulin is located at the end of the protein chain. It contains a conserved sequence that is crucial for tubulin polymerization and microtubule formation. The C-terminal residues of β-tubulin interact with the N-terminal region of another β-tubulin subunit, promoting the head-to-tail assembly of tubulin dimers into protofilaments, which subsequently form the microtubule structure. These interactions involve both hydrophobic and electrostatic interactions, contributing to the stability and integrity of the microtubule lattice. Furthermore, the C-terminal tail of β-tubulin extends outward from the microtubule surface and serves as a binding site for microtubule-associated proteins (MAPs) and motor proteins. MAPs play a role in regulating microtubule dynamics, cross-linking microtubules, and determining their spatial organization within the cell. Motor proteins, such as kinesins and dyneins, bind to the C-terminal tails of β-tubulin and utilize the microtubule tracks for intracellular transport and cell motility. (Figure 1.10)

N-terminal of β-Tubulin

The N-terminal region of beta tubulin is located at the opposite end of the protein chain. It participates in the assembly of tubulin subunits into protofilaments and also plays a role in protein-protein interactions. The N-terminal segment of β-tubulin interacts with the C-terminal region of alpha tubulin within the tubulin dimer, stabilizing the overall structure.
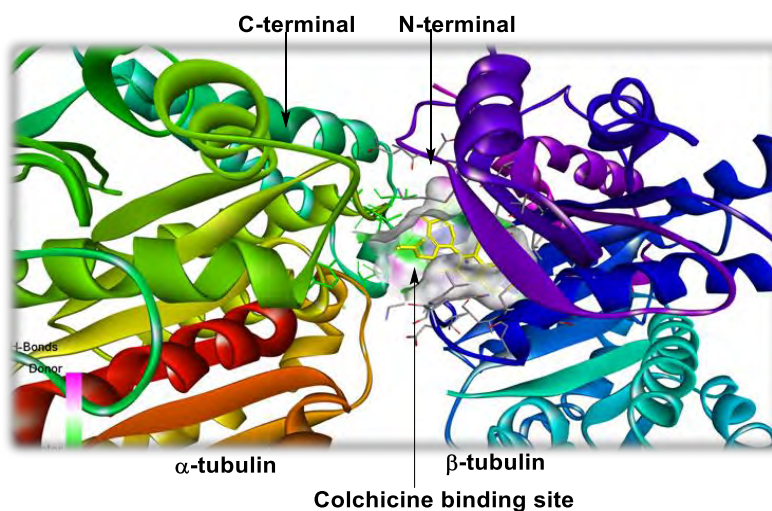
Figure 1.10 C-terminal and N-terminal regions of β-tubulin

The N-terminal domain of β-tubulin also contains the colchicine binding site, which is a pharmacologically important region targeted by tubulin inhibitors such as colchicine itself and its derivatives. (Figure 1.10) The binding of colchicine disrupts microtubule assembly by preventing tubulin polymerization and interfering with the normal functioning of microtubules. Understanding the interactions between colchicine or other tubulin inhibitors and the N-terminal region of beta tubulin is crucial for the development of new therapeutic agents targeting microtubules in cancer treatment.

1.3.3.1.3 Tubulin Inhibitors: Dual Role as Vascular Disrupting Agents (VDAs)

Several tubulin inhibitors have demonstrated VDA activity through their ability to disrupt microtubule dynamics not only in cancer cells but also in endothelial cells lining tumor blood vessels. By binding to tubulin and interfering with microtubule assembly, these agents destabilize the cytoskeleton of endothelial cells, leading to vascular collapse and cessation of blood flow within the tumor. Additionally, tubulin inhibitors can induce endothelial cell apoptosis, further contributing to vascular disruption. (Figure 1.11)

One of the well-known tubulin inhibitors with VDA activity is combretastatin A-4 phosphate (CA4P), a derivative of combretastatin A-4.[52] CA4P has been shown to selectively target tumor vasculature and induce extensive vascular shutdown in preclinical models of cancer.
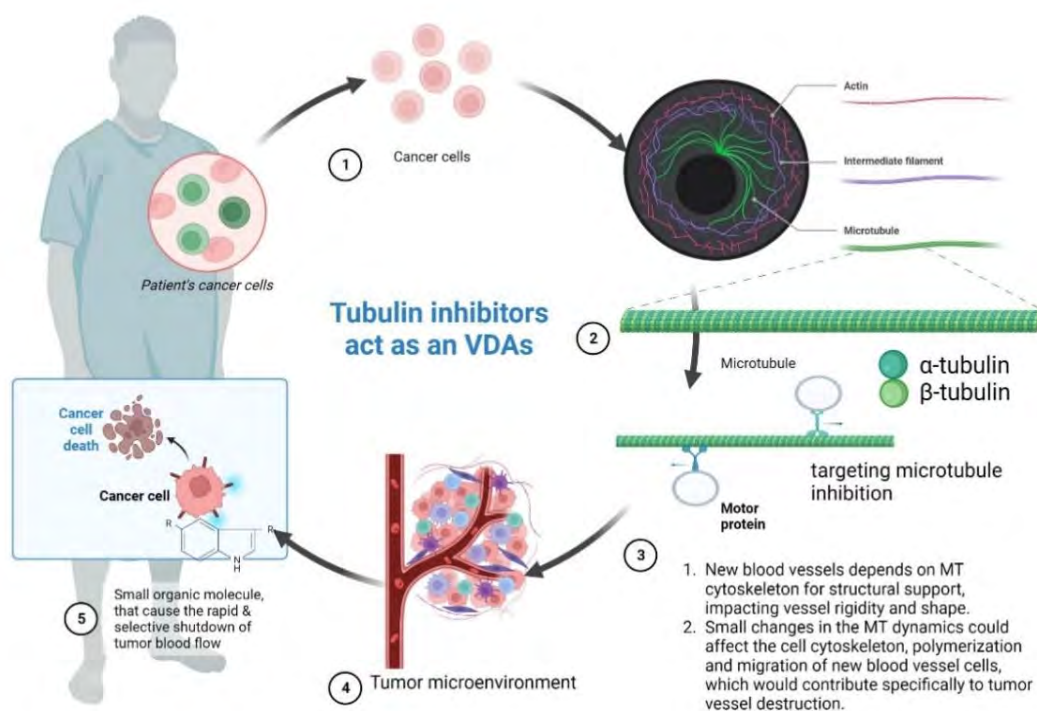
Figure 1.11 Tubulin inhibitors as Vascular Disrupting Agents (VDAs)

Clinical studies have demonstrated its efficacy as a VDA in combination with chemotherapy or radiation therapy for the treatment of various solid tumors, including non-small cell lung cancer and colorectal cancer. Other tubulin inhibitors, such as vinblastein and colchicine have also exhibited VDA activity in preclinical studies. These agents disrupt microtubule dynamics in both cancer cells and endothelial cells, leading to vascular collapse and tumor necrosis. While their clinical utility as VDAs may be limited due to systemic toxicity, efforts are underway to develop novel tubulin inhibitors with improved tumor-selective VDA activity and reduced off-target effects.[53]

Colchicine presents significant challenges in cancer therapy due to its non-selectivity, poor water solubility, narrow therapeutic window and potential for inducing drug resistance. Firstly, its indiscriminate binding to tubulin affects both cancerous and normal cells, leading to adverse effects and limiting its therapeutic potential. Additionally, its low water solubility impedes optimal drug delivery and may require special formulations for effective administration. Several colchicine-site agents have been investigated as vascular disrupting agents (VDAs) in clinical trials for cancer therapy. Unlike other inhibitors, colchicine-site inhibitors are not substrates of P-glycoprotein (P-gp) or affected by the overexpression of βIII-tubulin. Moreover, they have the ability to target tumor vasculatures and disrupt existing blood vessels.

Despite their promising clinical successes, the efficacy of microtubule-targeting agents (MTAs) is hindered by the development of drug resistance, dose-limiting toxicity, and poor water solubility.[54] Hence, there is a critical need to develop novel therapeutic strategies capable of overcoming these limitations.

1.3.3.2 Inhibition of DNA-Topoisomerases in Anti-cancer Drug

Topoisomerases represent crucial targets in the realm of anticancer drug development, as they play pivotal roles in regulating changes in DNA structure during the cell cycle. Topoisomerase inhibitors are designed to impede the action of these enzymes, thereby disrupting DNA replication and leading to cell death. The typical way that both topoisomerase I and II inhibitors work is that the inhibitor binds to the topoisomerase molecule and it makes the enzyme nonfunctional by blocking the ability of the topoisomerase to bind the DNA back together after it has been cut. Therefore, cuts are made to either one or both strands of the DNA molecule which are never repaired, ultimately leading to death of the cell.[55]

Chen *et al.* devised a strategy to enhance drug efficacy by developing hybrid molecules. They synthesized a series of indolizino[6,7-b]indoles, incorporating two pharmacophores: a, β-carboline group and a bis(hydroxymethyl)pyrrole group. These hybrids exhibited inhibitory effects on both topoisomerase I/II and DNA cross-linking abilities.[56] Notably, the hybrid derivative BO-1978 (**21**) demonstrated effectiveness in suppressing lung adenocarcinoma A549 cells by inhibiting Topo I/II and inducing DNA cross-links, resulting in DNA damage and subsequent cell cycle arrest. Topoisomerase II inhibitors encompass well-known drugs such as doxorubicin, etoposides, and mitoxantrone. Camptothecin (CPT) (**22**) was originally discovered in 1966 by M. E. Wall and M. C. Wani during systematic screenings of natural products for anticancer properties from the bark and stem of Camptotheca acuminata. Demonstrated to be effective against a wide range of tumors, its molecular target has been firmly established as human DNA topoisomerase I.[57] Cryptolepine hydrochloride (**23**), an indoloquinoline alkaloid isolated from the roots of Cryptolepis sanguinolenta, operates by intercalating into DNA and inhibiting topoisomerase II, as well as DNA synthesis. Synthetic analogues of Cryptolepine, such as IQDMA (**24**) and compound (**25**), (Figure 1.12) have shown significant anticancer activity through their interaction with DNA.[58]

Podophyllotoxin (PPT) (**26**), also known as podofilox, is a non-alkaloid toxin lignan extracted from the roots and rhizomes of Podophyllum species, possessing potent anticancer activity. Modified analogues of Podophyllotoxin, such as Etoposide have demonstrated improved

efficacy against various cancers including lung, testicular, lymphoma non-lymphocytic leukemia, and glioblastoma.[58]

BO-1978 (**21**)

Camptothecin (**22**)
Topoisomerase II inhibitors

Cryptolepine (**23**)
Topoisomerase II inhibitors

IQDMA (**24**)

Benzo-pyrido-indole (**25**)

Podophyllotoxin (**26**)
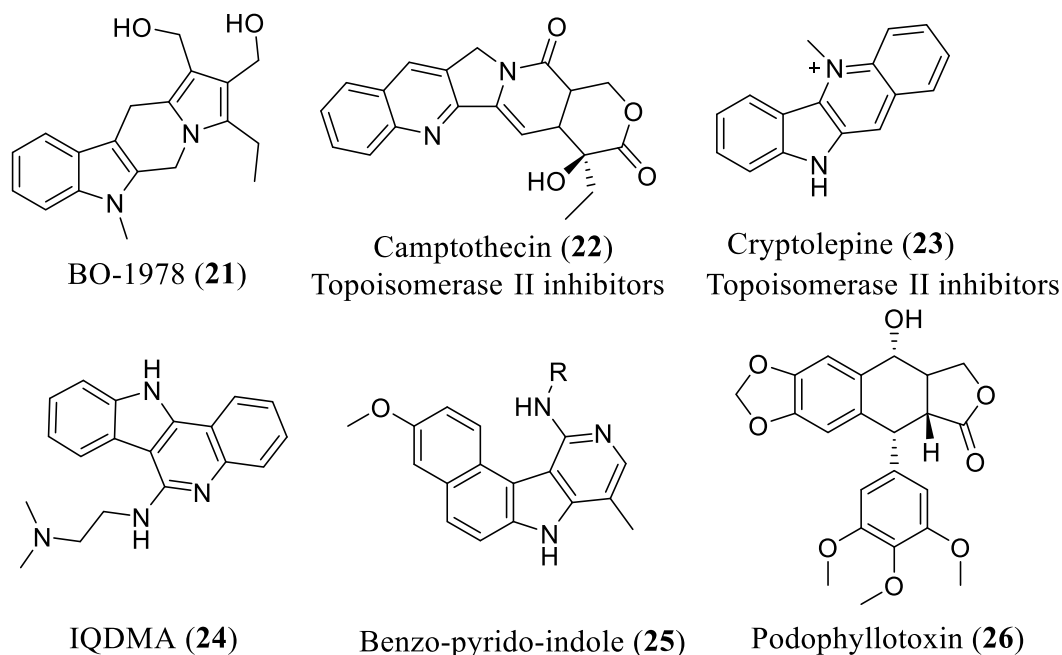
Figure 1.12 Structures of topoisomerase inhibitors **21-26**

1.3.3.3 Targeting Protein Kinases in Cancer Therapy: A Crucial Approach

Protein kinases play a pivotal role in cell signaling pathways, making them a prime focus in contemporary cancer treatment strategies. This enzyme family, comprising over 500 members encoded by approximately 2% of eukaryotic genes, regulates fundamental cellular processes through phosphorylation of proteins. Dysregulated kinase activity is a hallmark of cancer, driving tumorigenesis by promoting aberrant cell signaling.[59] As a result, protein kinases have emerged as prominent targets for anti-cancer drug development in the last two decades. In particular, cyclin-dependent kinases (CDKs) have garnered significant attention in the quest for effective anticancer agents.

1.3.3.3.1 Exploring Cyclin-Dependent Kinase Targets

To date, twenty different CDKs have been reported in mammalian cells and about the same number of cyclins.[60] However, not all of them are regulators of cell cycle progression, and several of these kinases are involved in multiple functions (Figure 1.13).[61] Indeed, more recent research has revealed the existence of specific CDK/Cyclin heterodimers whose functional implications are being uncovered in transcriptional processes and other non-cell cycle functions, as well as in pathological settings.[62] Hence, the functional diversity of this small group of protein kinases is important, and it is now fully recognized that CDK/Cyclins are

involved in a wide variety of biological processes, for example, transcriptional regulation, metabolism, neuronal differentiation and development.
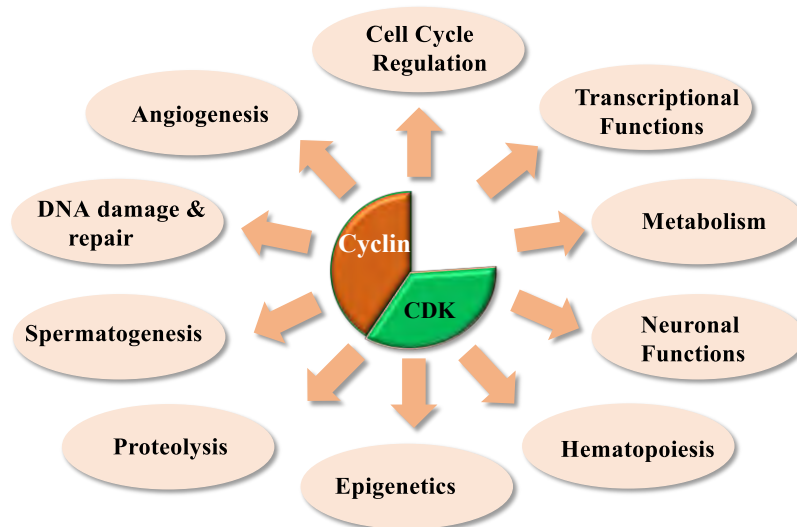
Figure 1.13 Functional Diversity of Cyclin-dependent Kinases

1.3.3.3.1.1 Cyclin-Dependent Kinases: Key Players in Cancer Progression

In physiological conditions, activation of CDK/Cyclin kinases is tightly controlled both spatially and temporally. However, the dysregulation of CDK/Cyclins in numerous human cancers disrupts the coordinated cycle of cell growth and proliferation, leading to uncontrolled cell proliferation, a hallmark feature of cancer cells.[63, 64] In fact, together with mutations in proto-oncogenes, mutations leading to hyperactivation of CDK activity (Figure 1.14A) have been found in human cancer genomes, and confer selective growth advantage to cells, whilst mutations that inactivate checkpoint regulators, tumour suppressor genes or CKIs result in loss of cell cycle inhibition.[65]
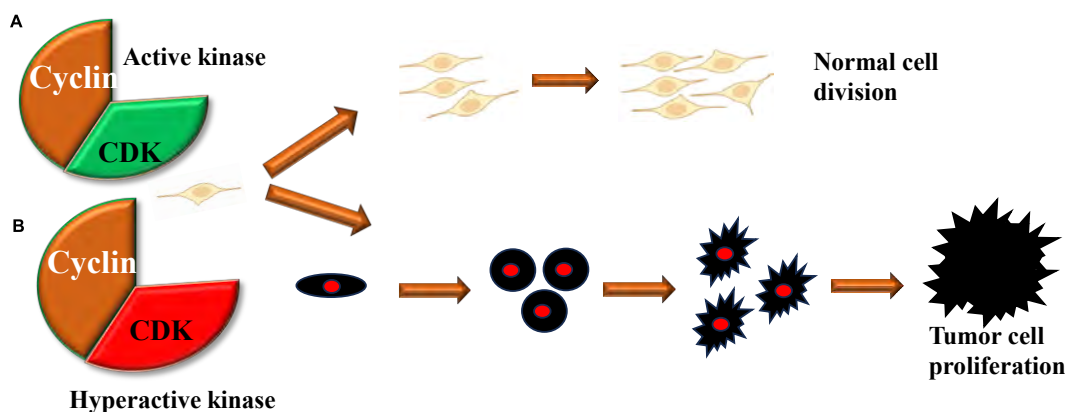
Figure 1.14 Cyclin-dependent kinases under normal and hyperactive conditions

More recently, targeted therapy has shown great potential in addressing drugs toward cancer cells of specific genes and proteins without attacking the healthy cells. It is well known that protein kinases play a vital role in regulating cell function. Therefore, these proteins can be used as a molecular target for designing new cancer inhibitors. For example, it was found that most human cancers are associated with the deregulation of cyclin-dependent kinases (CDKs). CDKs are a family of serine-threonine kinases that regulate cell cycle progression *via* the phosphorylation process.[59] Among the various protein kinases, cyclin-dependent kinases (CDKs) have emerged as promising targets in cancer therapy. CDK1 is known to have a diagnostic value in oesophageal and breast cancers, while the expression of CDK2 or its activity seems to have been utilized towards the prognosis of breast, ovarian and oral cancers.[66]
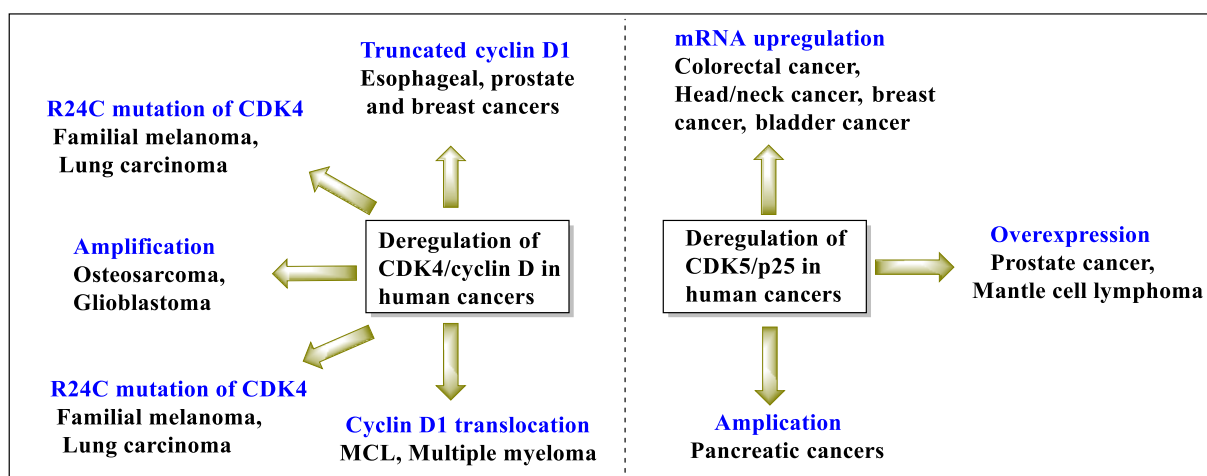
Figure 1.15 Roles of CDK4/cyclin D/CDK5/p25 in different types of cancers

In other types of cancer such as the ovarian, urinary bladder, endometrial or oral, CDK4 expression is impaired. CDK5 is known to play a role in the prostate cancer, lung cancer and breast cancer (Figure 1.15), while CDK6 is mis expressed in oral cancer. These findings underscore the multifaceted roles of CDKs in different cancer types, highlighting their potential as targets for therapeutic intervention and prognostic assessment. In particular, Cyclin-dependent kinase 5 (CDK5), a distinctive member of the CDK family, is activated upon binding with regulatory proteins, primarily p35.[59]

Cyclin-dependent kinase 5 (CDK5), a unique member of the CDK family, is activated by binding with regulatory proteins, mainly p35.[67] Its activation is crucial in central nervous system (CNS) development and neurodegeneration. Recent findings suggest that CDK5 also plays important roles in regulating various biological and pathological processes, including cancer progression. In the context of prostate cancer, CDK5 phosphorylates the androgen receptor (AR), promoting cancer cell proliferation. Clinical evidence indicates that CDK5

levels correlate with prostate cancer progression. Inhibition of CDK5 inhibits prostate cancer cell growth, while drug-induced CDK5 hyperactivation leads to apoptosis. Blocking CDK5 activity using small interfering RNAs or roscovitine, a pan-CDK inhibitor, reduces cellular AR protein levels and induces prostate cancer cell death.[68] Thus, CDK5 plays a crucial role in prostate cancer cell growth, with AR regulation being a significant pathway. (Figure 1.16)
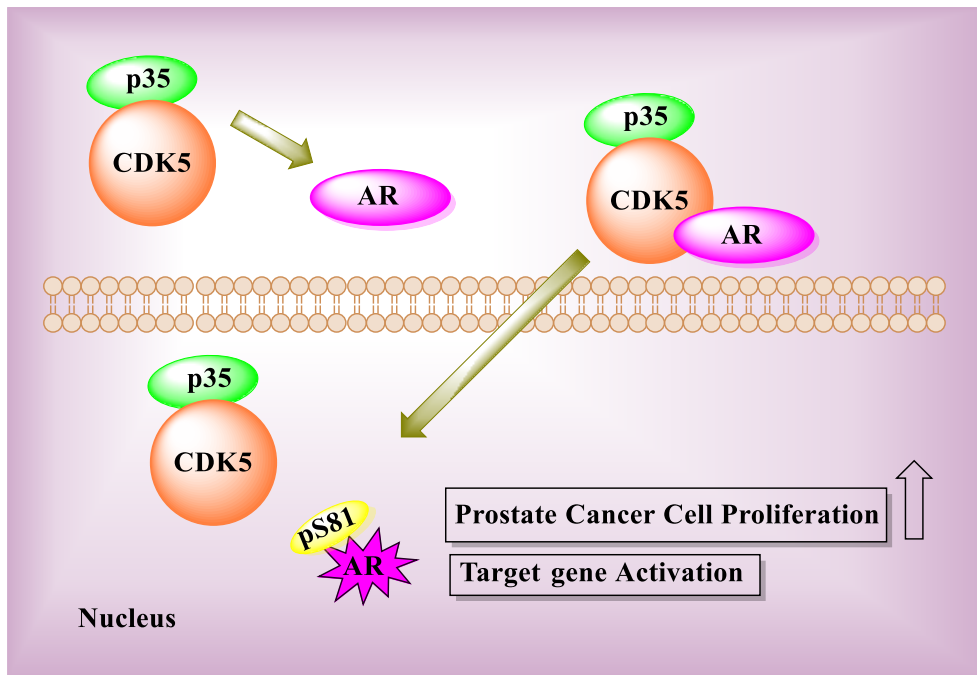
Figure 1.16 CDK5 and p35 regulation of androgen receptor (AR) protein

2019, Lin *et al.* clinical finding suggests that CDK5 and p35 certainly play crucial roles in the development of prostate cancer. These data provide the first confirmation of the connection between CDK5 and AR in prostate cancer cells and prostate carcinoma specimens, suggesting that phosphorylation of AR by direct interaction with CDK5 protects AR protein against degradation by the ubiquitin–proteasome mechanism. Altogether, it suggests that p35 is also critical to CDK5 and AR regulation and their functions. An illustration of CDK5 and AR regulation in prostate cancer cells is shown in figure 1.16.[69]

1.3.3.3.2 Small-molecules Kinase Inhibitors

Targeting the ATP-binding pocket of kinases, a highly conserved area in the kinase domain, is how small-molecule kinase inhibitors work. These inhibitors can impede the transfer of phosphate groups from ATP to their substrate proteins by binding to this pocket, which inhibits the activity of kinases and subsequent signalling pathways. Competitive inhibition, non-competitive inhibition, and allosteric inhibition are the three major categories into which small-

molecule kinase inhibitors methods of action can be divided. For binding to the ATP-binding pocket of the kinase, competitive inhibitors engage in competition with ATP. This kind of inhibition can be reversed, and it is often removed by raising the level of ATP. Due to the structural similarities among kinases, maintaining selectivity is essential. The structures of molecules are quite diverse and they are generally constituted or derived from various heterocyclic families such as purines, pyrimidines, indoles, pyrazoles, thiazoles, or derived from natural products such as staurosporine or flavones.[70]

Although a wide variety of ATP-competitive compounds have been proposed to inhibit these kinases, and there are several successful examples in clinical trials, including Tucatibib (**27**), Ribociclib (**28**), Palbociclib (**30**) and Roscovitine (**31**) this class of compounds still faces issues with respect to selectivity there are still many issues in the development of anticancer inhibitors that target the ATP pocket. Indeed, one of the major issues associated with ATP-competitive inhibitors is their limited specificity which leads to important cytotoxic side effects and poor tolerability, since the dose administered necessary to inhibit the kinase target often induces off-target effects that limit efficacy.[71] No specific-CDK5 inhibitors have entered clinical trials, and inhibition of CDK5 activity using pan-CDK inhibitors such as dinaciclib and roscovitine (**31**) is the most common strategy in clinical trials (Figure 1.17).

The challenge consists in developing drugs which inhibit CDK/Cyclin hyperactivity with high efficiency, specificity and selectivity, whilst eliciting minimal toxic side-effects and emergence of resistance over time. To address this challenge, it is essential to understand the nature of the pathology, of the dysregulation, dysfunction, and to define the molecular features of the target. The first step therefore consists in characterizing the biological relevance and targetability, as well as the mechanistic and structural features of the target as thoroughly as possible, so as to identify a specific pocket or interface within the target of interest.[72]

Lapatinib (**34**) is a HER2- targeted therapies that have completely changed how HER2- positive breast cancer is treated. Serine/threonine kinases known as CDK4/6 are essential for controlling the cell cycle (Finn *et al.,* 2016). For breast cancer, CDK4/6 inhibitors such as ribociclib (**28**) and palbociclib (**30**) have been developed as targeted treatments. These inhibitors are currently authorized for the treatment of hormone receptor-positive, and HER2-negative metastatic breast cancer since they exhibited effectiveness in clinical trials (Braal *et al.,* 2021). Palbociclib (**30**) is an orally bioavailable drug that showed good pharmacokinetic properties in rats. With a desirable selectivity profile and pharmacokinetic behavior, it was identified as a drug candidate in 2004 for the treatment of cancer and is under evaluation in different tumor types, including mantle cell lymphoma (MCL), melanoma and sarcoma. February 2015 and on basis

of positive phase II data, the FDA granted an accelerated approval in the USA for palbociclib in combination with letrozole, an aromatase inhibitor, as a frontline treatment for postmenopausal women with ER-positive/HER2-negative metastatic breast cancer (mBC).

Figure 1.17 Potent CDK inhibitors

Palbociclib (Ibrance Pfizer), is the first molecule in CDK4 and CDK6 inhibitor class to achieve regulatory approval and it has paved the way for the exploration of the biology of these G1 targets which are emerging as the most promising ones in the cell cycle arena.[73]

Potent and orally bioavailable CDK4 inhibitors, Daiichi Sankyo (**32**) has designed and evaluated novel thieno[2,3-d]pyrimidine hydrazone analogs (Figure 1.19). The introduction of a thiazole group at the hydrazone part led to marked enhancement of chemical stability under acidic conditions relative to the initial hit. Preclinical CDK4 and CDK6 inhibitors: Novartis and Astex (**33**) reported the identification and structure guided optimization of a series of 4-(pyrazolyl)pyrimidines affording compound 3 as a highly selective and orally active CDK4 and CDK6 inhibitor (Figure 1.17).[74]

1.3.3.4 Alkylating Agents

Alkylating agents were one of the earliest classes of drugs used in the treatment of cancer. The biggest weakness of most cancer cells is that they are very sensitive to DNA damage. Alkylating agents work by reacting with the proteins that bound together to form the very delicate double helix structure of a DNA molecule, adding an alkyl group to some or all of them. This structure of DNA prevents the proteins from linking up as they should and causing breakage of the DNA strands and ultimately the death of the cancer cells. These drugs will kill cells in all phases of the cell cycle. Chlormethine (**35**), also known as nitrogen mustard, is sold under the brand name Mustargen.(Figure 1.18) This alkylating agent works by binding to DNA, crosslinking two strands and preventing cell multiplication. Chlormethine (**35**) binds to the *N*-7 nitrogen on the DNA base guanine. Cyclophosphamide (**37**) is nitrogen mustard from oxazaphosphorine group works like Chlormethine.
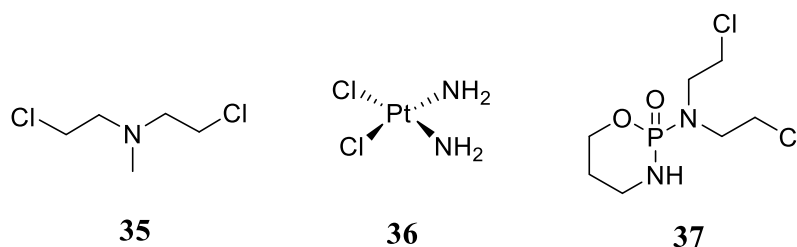
Figure 1.18 Representative alkylating agents as anticancer drugs

Generally, Cyclophosphamide (**37**) is used to treat cancers including lymphomas, some forms of brain cancer, leukemia and some solid tumors. It is a chemotherapy drug that works by inducing the death of certain T cells. Cisplatin (**36**) is the member of a class of platinum-containing anticancer drugs (Figure 1.18). These platinum complexes react *in vivo*, binding to and causing crosslinking of DNA, which ultimately triggers apoptosis. It is used to treat various types of cancers, including small cell lung cancer, ovarian cancer, lymphomas, bladder cancer, cervical cancer and germ cell tumors. Cisplatin is particularly effective against testicular cancer; the cure rate was improved from 10% to 85%.[75]

1.3.3.5 Antimetabolites

Antimetabolites comprise various groups of drugs used in cancer treatment, each targeting specific pathways to disrupt DNA/RNA synthesis or interfere with essential biosynthetic processes. Among these drugs, pyrimidine antagonists such as cytarabine, 5-fluorouracil (5-FU(**37**)), gemcitabine, and capecitabine play vital roles by impeding pyrimidine metabolism. They find application in treating a spectrum of cancers including colon, rectal, anal, breast, cervical, and bladder cancer. Additionally, purine antagonists like fludarabine (**40**) act by

inhibiting DNA synthesis through interference with ribonucleotide reductase and DNA polymerase activities. This class of drugs is particularly effective against both dividing and resting cells, making them valuable in the treatment of hematological malignancies like leukemias and lymphomas. (Figure 1.19) Purine analogues, such as 6-mercaptopurine (**38**), azathioprine (**39**) and cladribine, mimic purine bases and disrupt DNA and RNA synthesis, with 6-mercaptopurine finding use in treating acute lymphoblastic leukemia. Antifolates like methotrexate, pemetrexed, and pralatrexate interfere with folate metabolism, essential for DNA synthesis, while ribonucleotide reductase inhibitors like hydroxyurea disrupt DNA synthesis by inhibiting ribonucleotide reductase. These drugs exert their anticancer effects by interfering with crucial cellular processes, ultimately leading to the disruption of DNA synthesis or the induction of DNA damage, thereby inhibiting cancer cell growth and proliferation.[76]

| 5-Fluorouracil (**37**) | 6-Mercaptopurine (**38**) | Azathioprine (**39**) | Fludarabine (**40**) |
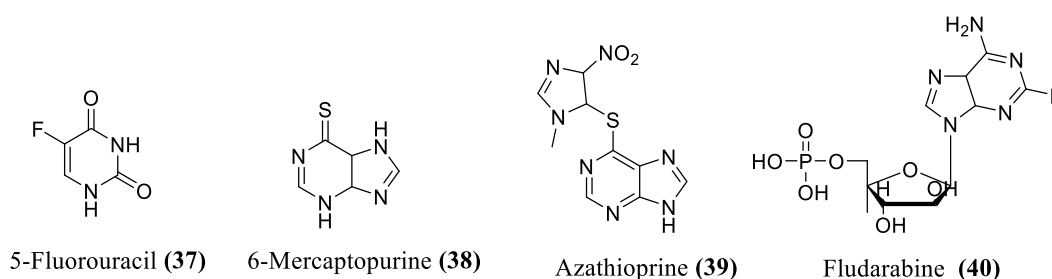
Figure 1.19 Examples of antimetabolites as anticancer agents

1.3.3.6 Other Chemotherapeutic Agents

Including some enzymes (l-asparaginase), proteasome inhibitors (bortezomib) and antibiotics (bleomycin, actinomycin D, and anthracyclines), are characterized by non-homogenous mechanisms of action. While L-asparaginase cleaves the amino acid L-asparagine essential for normal cell metabolism, bortezomib drives the cell to apoptotic death by inhibition of apoptotic protein degradation. Imatinib and erlotinib inhibit tyrosine kinases activities involved in multiple intracellular pathways associated with receptor-mediated growth signaling, leading to cellular dysfunction and subsequent cell death. Bleomycin, an antibiotic, induces formation of free radicals that cause DNA damage and the cell cycle arrest in G2 phase. Another anticancer agent, actinomycin D, intercalates into DNA and interferes in DNA transcription. Anthracyclines exhibit anti-proliferatory effects in the abovementioned processes and inhibit topoisomerase II activity.[39]

1.3.4 Drug Resistance in Cancer Chemotherapy

Drug resistance poses a significant challenge in cancer chemotherapy, with statistics indicating that over 90% of cancer-related mortalities are attributed to this phenomenon. Multidrug

resistance (MDR) in cancer cells during chemotherapy can arise from various mechanisms, including enhanced drug efflux, genetic alterations (mutations, amplifications, and epigenetic changes), (Figure 1.20) activation of growth factors, augmented DNA repair mechanisms, and increased metabolism of foreign substances.[39, 77]

These mechanisms collectively diminish the therapeutic efficacy of administered drugs, complicating tumor treatment significantly. Resistance mechanisms in cancer cells encompass diverse processes such as drug inactivation, suppression of apoptosis, alterations in drug metabolism, epigenetic modifications, changes in drug targets, enhanced DNA repair, and amplification of target genes. Integral components of cell membranes like P-glycoprotein (P-gp) and Breast Cancer Resistance Protein (BCRP) play pivotal roles in drug resistance by regulating the distribution, absorption, and excretion of various chemical compounds, including chemotherapeutic agents, thereby serving as protective mechanisms against cytotoxic substances.[39]
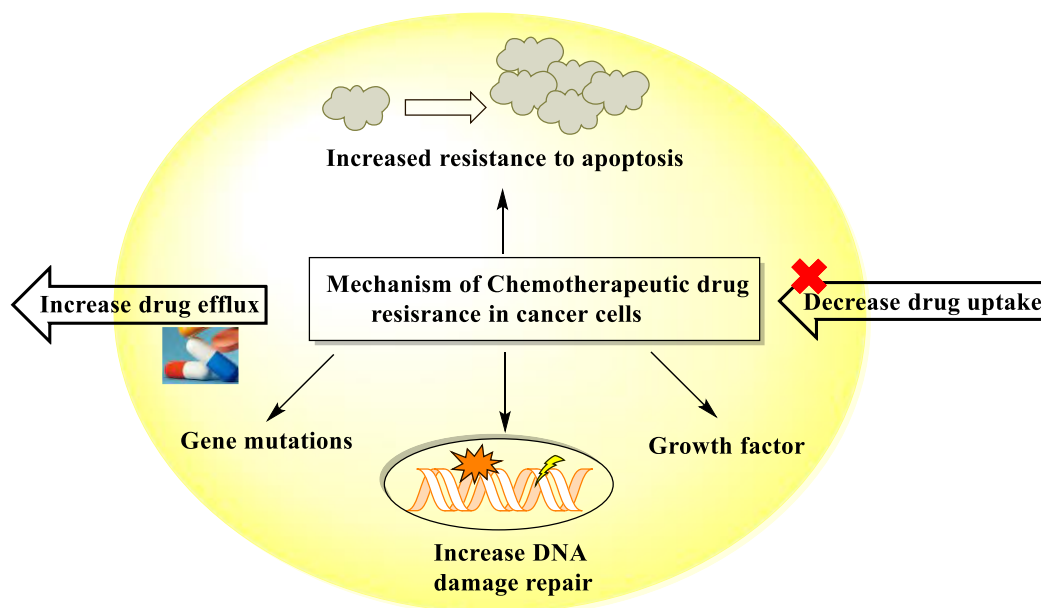
Figure 1.20 Mechanisms of chemotherapeutic drug resistance in cancer cells

In cancer therapy, the presence of P-glycoprotein (P-gp), particularly on endothelial cell surfaces, poses a significant obstacle. P-gp impedes the penetration of chemotherapeutic drugs into specific sites, notably hindering the treatment of brain tumors due to the challenges in crossing the blood-brain barrier (BBB). Additionally, the inadequate blood supply in large tumors diminishes the effectiveness of chemotherapy by restricting drug delivery. While P-gp shields the brain from harmful compounds, it simultaneously hampers the access of therapeutic agents, complicating cancer treatment. Overcoming this barrier often requires higher concentrations of drugs, which can lead to systemic toxicity. The heightened efflux of drugs

mediated by P-gp serves as a crucial mechanism contributing to cancer cell resistance against chemotherapy.[78]

Gene mutations commonly observed in tumor cells are considered a primary contributor to the failure of chemotherapy treatment. According to Duesberg *et al.,* the development of multidrug resistance (MDR) in cancer cells can be best explained by their aneuploid nature. Aneuploidy, characterized by an abnormal number of chromosomes, is suggested to lead to the loss of drug-sensitive genes or alterations in biochemical pathways during mitosis, thereby contributing to chemotherapeutic drug resistance. Conversely, normal cells, which typically maintain a stable chromosome number, are more likely to retain sensitivity to drugs, adding complexity to treatment strategies.[79] Hence, the development of new anticancer drugs is imperative to address these challenges.

1.4 Indole Nucleus in Anti-cancer Research

The indole nucleus holds significant importance in the realm of anticancer drug discovery research, serving as a cornerstone for the development of potent anticancer agents. Notably, both natural and synthetic analogues containing the indole structure have demonstrated promising anticancer properties, contributing to advancements in cancer chemotherapy.[80]

Indole-based anticancer agents, whether derived from natural sources or synthesized in the laboratory, can be broadly categorized into three main groups based on their structural features:
(a) Functionalized indoles
(b) Indolylazoles as anti-cancer agents
(c) Bisindoles as anti-cancer agents

1.4.1 Functionalized Indoles

These compounds feature additional functional groups attached to the indole nucleus, imparting unique pharmacological properties and enhancing anticancer activity.

Recently, in 2023, Chen *et al.* designed and synthesized derivatives of 3(arylmethylene)indole **(41)**, evaluating their antiproliferative activities against glioma cell lines. Compound **41** exhibited remarkable antiglioma activity, along with favourable pharmacokinetic characteristics and the ability to penetrate the blood-brain barrier (BBB). Notably, compound **41** significantly improved the survival rate and inhibited the growth of orthotopic glioblastoma. Utilizing the Phospho-Totum system, Chen *et al.* identified ALK as a potential target of compound **41** for its anticancer activity (Figure 1.21). Unlike reported ALK inhibitors, may act as a novel ALK modulator, potentially interacting with the extracellular ligand-binding domain of ALK. This interaction selectively induces ERK-mediated autophagy and apoptosis under

both in vitro and in vivo conditions, highlighting its promising therapeutic potential.[81] Notably, one crucial indole derivative is 5-hydroxyindoleacetic acid (**42**), a metabolite of serotonin in the human body. Jeong *et al.* demonstrated that UVB-activated 5-hydroxyindoleacetic acid (5-HIAAUVB) induces apoptosis in prostate and bladder cancer cells through stress signaling and the apoptotic pathway. This discovery highlights its potential as a candidate for a novel photosensitizer in photodynamic therapy (PDT).[82]

Angerer and colleagues reported that methoxy-substituted 3-formyl-2-phenylindoles (**43**) exhibit activity against breast cancer cell lines (IC_{50} = 35 nM; MDA-MB-231). Additionally, compound **43** disrupts microtubule assembly with an IC_{50} of 1.5 μM. Fluorescence microscopy studies confirmed that compound **43** degrades the cytoskeleton similar to colchicine. However, the *in vivo* activity of these compounds was not satisfactory, likely due to the metabolically unstable nature of the aldehyde functional group.[83]

5-Hydroxyindole-3-acetic acid (**42**)

Indole-2-phenyl-3-carboxaldehyde (**43**)

41

44

Indibulin (**45**)

2-Aryl-3-aroylindole (**46**)

BPR0L081 (**47**)

Arylthioindole (**48**)
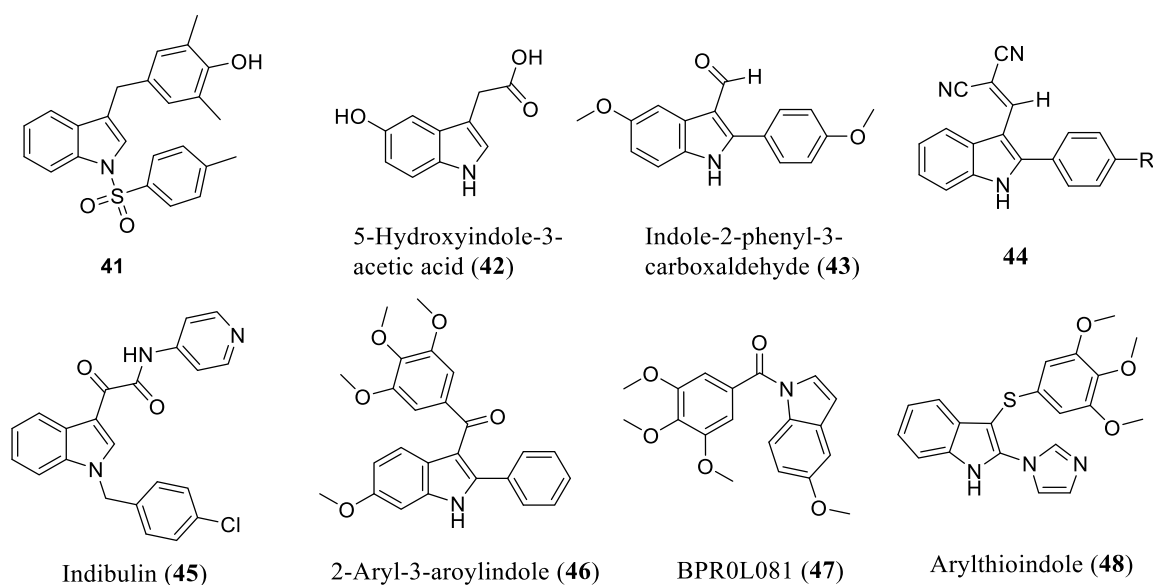
Figure 1.21 Functionalized indoles as anti-cancer agents

Indibulin (D-24851) (**45**), featuring a glyoxylamide moiety, demonstrates good *in vitro* cytotoxicity towards various human cancer cell lines, including ovarian, glioblastoma, breast, and pancreatic (IC_{50} = 0.036-0.285 μM). Its anticancer activity is attributed to the blocking of tubulin polymerization (IC_{50} = 0.3 μM) without inducing neurotoxicity in preclinical animal studies. Indibulin exhibits potent cytotoxic activity against a panel of human cancer cell lines, such as SKOV3 ovarian cancer, U87 glioblastoma and ASPC-1 pancreatic cancer cells. The promising potential of indibulin in cancer treatment stems from its simple synthetic nature, good oral bioavailability, potent *in vitro* and *in vivo* anticancer activities, efficacy against multidrug-resistant tumors and the absence of neurotoxicity.[42] Indole containing small

molecules have been identified as potent tubulin inhibitors, for example, **46**, *N*-aroylindoles (**47**), 2-heteroarylthioindoles and (**48**) (Figure 1.21).[84, 85]

1.4.2 Functionalized Indoles as Combretastatin-4 (CA-4) Analogues

Several studies have reported that the most effective antimitotic agent of this class against a variety of tumor cells is combretastatin A-4 (CA-4). CA-4 (**49**) was isolated from the South African willow species Combretum caffrum's bark in 1989.[86] CA-4 binds to colchicine-binding site on β-tubulin and inhibits microtubule polymerization, additionally, it obstructs blood flow to solid tumors and disrupts the vasculature of tumor cells causing cell death (apoptosis). Due to its structural simplicity, CA-4 (**49**) has been investigated as a leading pharmacophore to understand tubulin activities and characteristics.[87] Combretastatins have matching molecular structures with colchicine, as both contain a trimethoxyphenyl ring and the aromatic tropone ring of colchicine is related to the isovanillinyl group of combretastatin. The most promising antimitotic combretastatin is the A-4 type. It readily binds to the tubulin at the colchicine site.[88] Studies using CA-4 Structure-Activity Relationship (SAR) have identified three crucial structural elements essential for its anti-tubulin activity. These include (i) the 3,4,5-trimethoxy moiety on ring A; (ii) the cis configuration bridge (B) of both aromatic rings (the trans-orientation is inactive); and (iii) the presence of a small substituent on ring C, such as a methoxy group (Figure 1.22). The aromatic rings in CA-4 can adopt the best binding orientation for interactions with colchicine-binding site on β-tubulin thanks to the cis-alkene structure. Unfortunately, CA-4 tends to isomerize from its active cis-configuration to its inactive trans-configuration during storage and during *in vivo* metabolism. Meanwhile, extensive structure-activity relationship (SAR) studies were performed on **49**, which demonstrated the 3,4,5-trimethoxy substitution pattern on the A-ring, 4-methoxysubstituted B-ring and cis-configuration double bond as the basis for the polymerization-inhibiting activity of microtubulin.[89]

In 2023, a new series of 4-(4-methoxyphenyl)-5-(3,4,5-trimethoxyphenyl)-4H-1,2,4-triazole-3-thiol derivatives were synthesized as analogues for the anticancer drug combretastatin A-4 (CA-4). The new CA-4 analogues were designed to meet the structural requirements of the highest expected anticancer activity of CA-4 analogues by maintaining ring A 3,4,5-trimethoxyphenyl moiety, and at the same time varying the substituents effect of the triazole moiety (ring B).
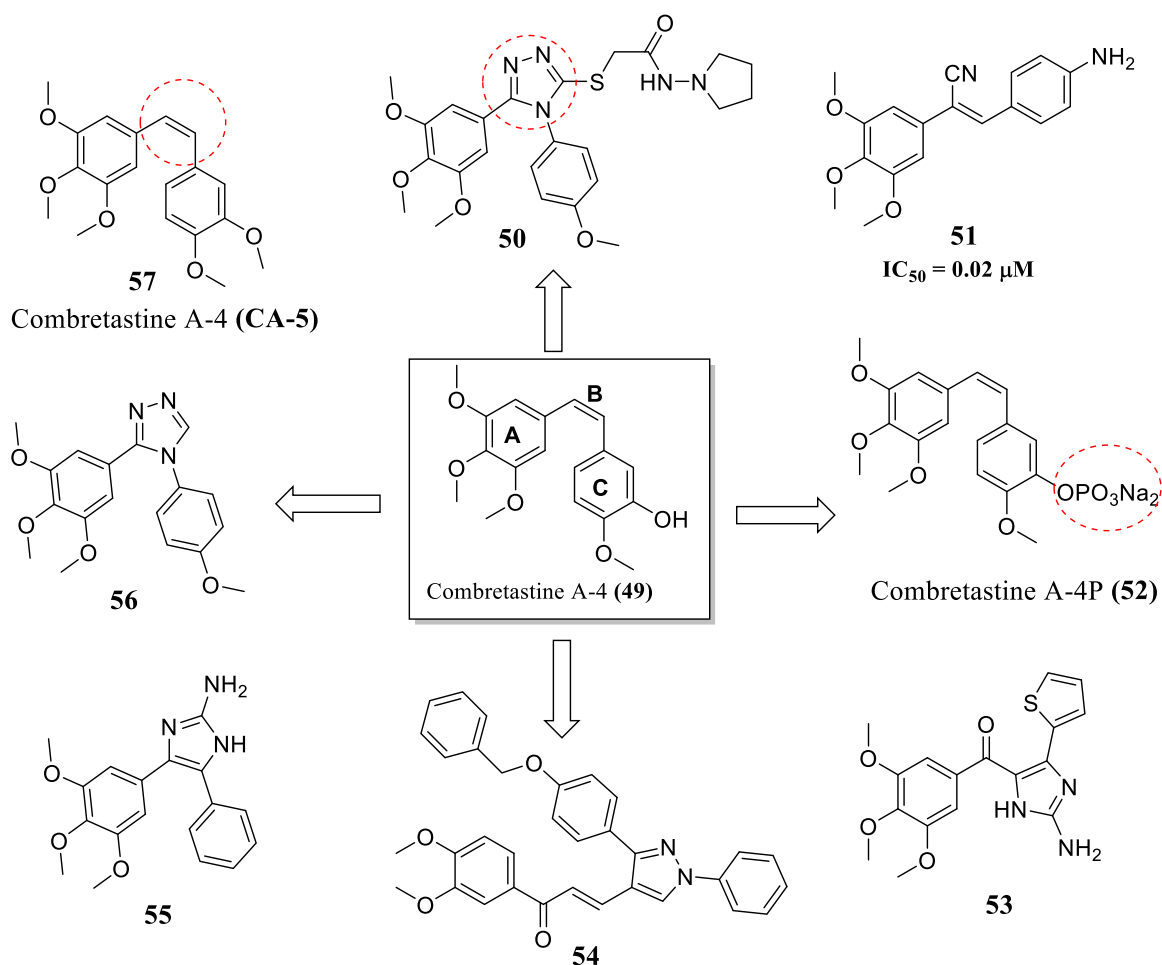
Figure 1.22 Structures of CA-4 and its analogues

Compound **50** showed strong similarity to colchicine, and it has excellent pharmacokinetics properties and a good dynamic profile. The *in vitro* anti-proliferation studies showed that compound **50** is the most cytotoxic CA-4 analog against cancer cells (IC$_{50}$ of 6.35 μM against Hep G2 hepatocarcinoma cells), and based on its selectivity index (4.7), compound **50** is a cancer cytotoxic-selective agent. As expected and similar to colchicine, compound 3-treated Hep G2 hepatocarcinoma cells were arrested at the G2/M phase resulting in induction of apoptosis. Compound **50** tubulin polymerization IC$_{50}$ (9.50 μM) and effect on Vmax of tubulin polymerization was comparable to that of colchicine (5.49 μM).[90]

Interestingly, biological evaluation of the compounds revealed that intermediate **51** had the highest anticancer activity. However, the aqueous solubility was five times lower than that of CA-4, and the activity against HCT-116 was eight times higher than that of CA-4, reaching sub-micromolar levels (IC$_{50}$ = 0.02 μM).[91] Study investigating the competency of combretastatin A-4 disodium phosphate (CA-4-DP) (**52**) to stimulate vascular effects in mouse breast carcinoma, the anti-tumor response was investigated by combining **52** with the

anticancer drug cisplatin. CA-4-DP (250 mg/kg) was found to markedly reduce tumor perfusion 30 min after injection and this effect lasted for a few hours, and after 24 h a return to normal was observed.

In 2018, a study evaluated the antiproliferative activity of several 2-aminoimidazole-carbonyl analogues of clinically relevant combretastatins A-4 (CA-4) and A-1 using a cell-based assay. Among the compounds tested, C-13 and C-21 exhibited significant antiproliferative activities against HeLa cells. Additionally, compound **53** showed more potent inhibition of proliferation in lung carcinoma (A549) cells compared to combretastatin A-4. Compound **53** also retarded the migration of A549 cells. Interestingly, **53** displayed much stronger antiproliferative effects against breast carcinoma and skin melanoma cells compared to noncancerous breast epithelial and skin fibroblast cells.[92] Some (E)-3-(3-(4-(benzyloxy)phenyl)-1-phenyl-1H-pyrazol-4-yl)-1-phenylprop-2-en-1-one conjugates were designed, synthesized and evaluated for tubulin polymerization inhibitory activity and *in vitro* cytotoxicity against breast (MCF-7), cervical (SiHa), and prostate (PC-3) cancer cell lines, as well as a normal cell line (HEK-293T). Among all the synthesized conjugates, compound **54** exhibited excellent cytotoxicity with an IC$_{50}$ value of 2.13 ± 0.80 μM (MCF-7), 4.34 ± 0.98 μM (SiHa), and 4.46 ± 0.53 μM (PC-3) against cancer cell lines. The compound did not exhibit significant toxicity to the HEK cells.[47, 93]

Medarde and coworkers synthesized some 2,3-diarylindole derivatives by mimicking the *cis* orientation of the aryls of combretastatin A-4. After screening the synthesized compounds against a panel of 60 tumoral cell lines at NCI, compound **58** displayed a remarkable cytostatic activity. The most potent activity was exerted against leukemia, non-small cell lung cancer and CNS cancer. The compound **58** exhibited significant activities for two CNS and two colon cancer cell lines.[72] Furthermore, modification of **58** led to **59**, exhibited tubulin inhibition activity with IC$_{50}$ = 4.1 μM. (Figure 1.23)
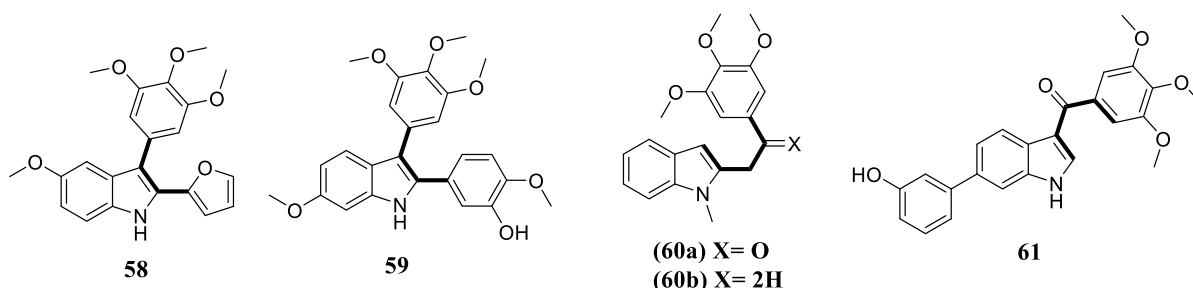
Figure 1.23 Functionalized indoles as combretastatin-4 (CA-4) analogue

In indole bearing hetero combretastatin analogues series, compound **60** showed significant anticancer activity against a panel of cancer cell lines (IC$_{50}$ = 0.3-0.6 μM).[74] Insertion of keto

functionality in **59** resulted with 1.3 times (IC$_{50}$ = 1.6 μM) more active than CA-4 (IC$_{50}$ = 2.1 μM) as a tubulin polymerization inhibitor. In 2007, Chang *et al.* prepared various aroylindoles including 2-, 3-, 4-, 5- and 6-aroylindoles and studied there antiproliferative and tubulin polymerizing inhibition activities. Interestingly, among these series of compounds, some of the analogues exhibited more potent inhibition of tubulin polymerization than the colchicine.

1.4.3 Indolylazoles as Anticancer Agents

Indole molecules connected to five or six-membered azaheterocycles fall under this category, representing a diverse class of compounds with intriguing anticancer properties. Among them, numerous indolylazoles of both natural and synthetic origin have demonstrated promising antitumor activity in Figure 1.24. Meridianins A-E (**62**) are pyrimidine class of marine alkaloids that were isolated from the tunicate *Aplidium meridianum* and found to possess potent cytotoxic and kinase inhibition activities.[94] Reyes and co-workers isolated a family of indole alkaloids, Aplicyanins (**63**) from Antarctic tunicate *Aplidium cyaneum*. The Aplicyanins (**63**) with a bromoindole nucleus and 6-tetrahydropyrimidine at C-3 position were found to be cytotoxic against human tumor cell lines including MDA-MB-231 (breast adenocarcinoma), A549 (lung carcinoma) and HT-29 (colorectal carcinoma) with inhibition of tubulin polymerization.[95] With (aminoimidazolinyl)bromoindole moiety, Discodermindole (**64**) was isolated from the marine sponge *Dirpcodermia polydiscus* and its *in vitro* anticancer activity study exhibited IC$_{50}$ values ranges 1.8-12 μg/mL against P388 (murine leukemia), A-549 (human lung) and HT-29 (human against colon) cell lines.[96]

Meridianin A-E (**62**) Discodermindole (**63**) Discodermindole (**64**)
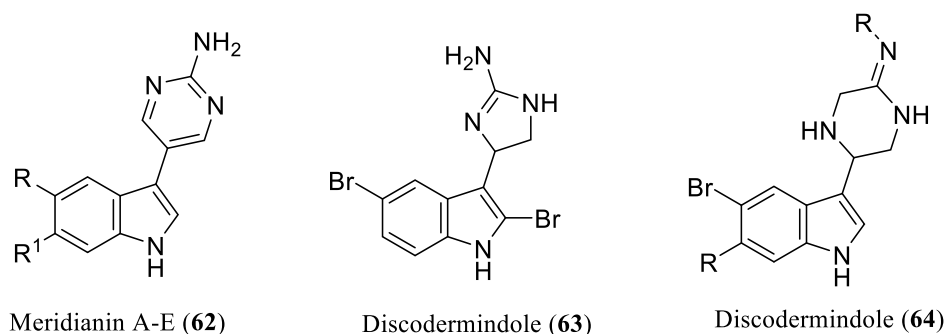
Figure 1.24 Naturally occurring cytotoxic indolylazoles

Inspired from above mentioned naturally occurring indolylazoles, various research groups prepared diverse indolylazoles by connecting azole ring through pyrrolic ring or benzene ring and evaluated their anticancer activity (as depicted in Figure 1.24).

In a recent study from 2023, Chan *et al.* introduced compound **65**, which exhibited remarkable antiproliferative activity with an average IC$_{50}$ of 4.5 nM, surpassing that of colchicine (IC$_{50}$ =

65.3 nM). Further elucidating its mechanism, the crystal structure of compound **65** in complex with tubulin was resolved using X-ray crystallography. This structural insight highlighted the enhanced binding affinity of **65** to tubulin, consequently contributing to its superior anticancer activity compared to the lead compound **66** (IC$_{50}$ = 32.5 nM). *In vivo* experiments demonstrated that **65**, administered at 5 mg/kg, exhibited significant antitumor efficacy against B16-F10 melanoma, achieving a Tumor Growth Inhibition (TGI) of 62.96%. Notably, **65** also potentiated the antitumor immunity of NP19 by activating the tumor immune microenvironment, as evidenced by the increased infiltration of tumor-infiltrating lymphocytes (TIL).[97] In 2021, Kumar *et al.* synthesized Indolyl-α-keto-1,3,4-oxadiazoles (**67**) with 3,4,5-trimethoxyphenyl motif, endowed strong cytotoxicity against U937, Jurkat, BT474 and SB cancer cells with IC$_{50}$ values of 7.1, 3.1, 4.1, and 0.8 μM, respectively. Molecular docking studies suggested a potential binding mode for **67** in the colchicine binding site of tubulin. When tested for *in vitro* tubulin polymerization, **67** inhibited tubulin polymerizations (IC$_{50}$ = 10.66 μM)[98] and induced apoptosis through caspase 3/7 activation (Figure 1.25).

65
IC$_{50}$ = 4.5 nM

66
IC$_{50}$ = 32.5 nM

Indolyl 1,3,4-oxadiazoles (**67**)

Indolyloxadiazoles (**68**)

Verubulin analogue (**69**)

70: R=H
71: R=CN

Indolyl-benzimidazole (**72**)

2-Indolyl-4-benzoyl-imidazole (**73**)
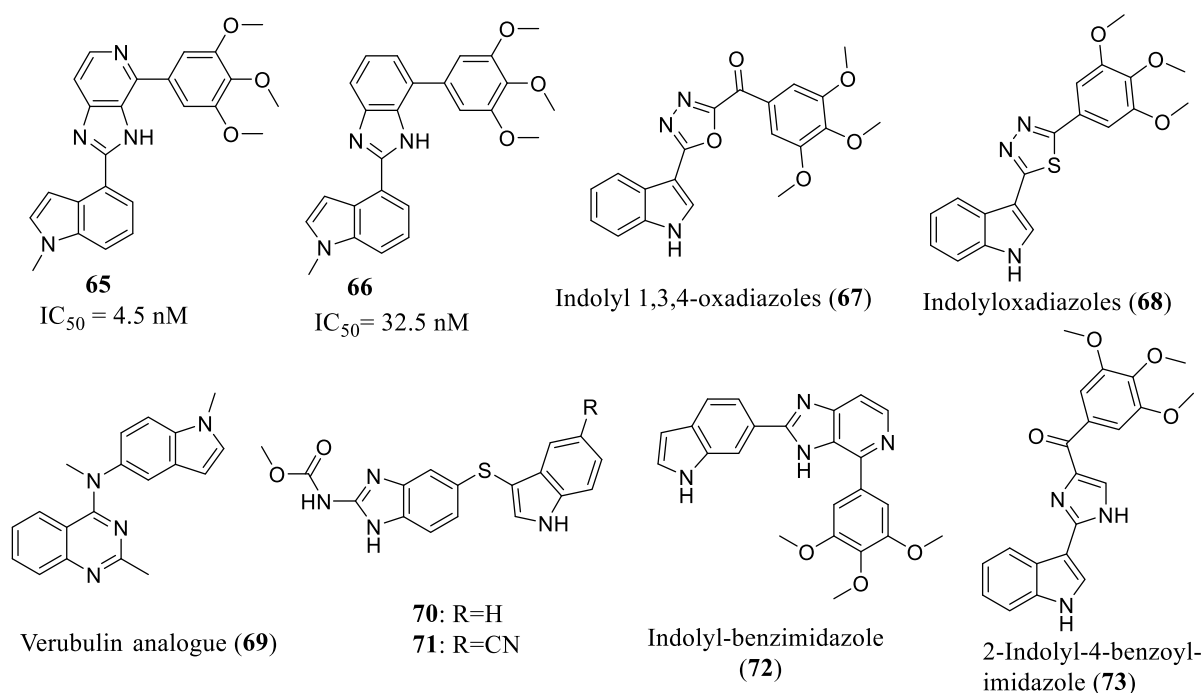
Figure 1.25 Representative synthetic indolylazoles as anticancer agents

In another study, Kumar *et al.* identified indolyloxadiazoles and indolylthiadiazoles (**68**) as analogues of Labradorins, demonstrating potent cytotoxicity and selectivity against human cancer cell lines.[99] Among these analogues, thiadiazoles analogue **68** exhibited potent anticancer activity, with the best compound showing an IC$_{50}$ of 1.42 μM against HeLa cell

lines. Additionally, analogue **68** exerted its anticancer activity by inhibiting tubulin polymerization, with an IC_{50} value of 17.5 μM.[100]

Verubulin analogue (**69**) is a previously reported CBSI that showed good vascular disrupting effects and induced apoptosis in both sensitive and multi-drug resistant phenotypes. Although it passed a Phase IIb clinical trial, further development was suspended due to the economic reasons. Compound **69**, an analogue of verubulin designed and synthesized by Katharina's group, showed comparable antiproliferative activity with verubulin against nine tumor cell lines with low nanomolar IC_{50} values (0.4-5.8 nM).[101] **70** and **71** were reported as benzimidazole carbamate analogues and **71** showed moderate antiproliferative activity against A549 and HT1080 with IC_{50} values of 5.07 μM and 0.95 μM, respectively. (Figure 1.24) They significantly suppressed microtubule polymerization and caused inhibition of tubulin assembly. Miller and co-workers synthesized a series of indolyl-imidazoles (**72**) as promising cytotoxic agents towards the melanoma and prostate cancer cell lines which exhibited their activity through modulation of tubulin polymerizations (IC_{50}= 5-57 nM), also were found to be effective against P-glycoprotein (P-gp) mediated multiple drug resistance (MDR) and taxol resistance cells.[102, 103]

These findings underscore the promising potential of indolylazoles as anticancer agents, offering insights into novel therapeutic strategies for combating cancer. In 2012, Li *et al.* identified the indolyl-benzoylimidazole (**73**) as antiproliferative agents (IC_{50} = 3.8 nM; melanoma and prostate cancers). (Figure 1.25) Compound **73** can effectively overcome Pgp mediated multidrug resistance and paclitaxel resistance cancer cell lines. Mechanism of action showed that the compound **73** exert their anticancer activity through inhibition of tubulin polymerizations.[104]

1.4.4 Bisindoles as Anti-cancer Agents

Bisindoles are an important class of alkaloids, in which two indole nuclei are separated by a heterocyclic ring or linear spacer or any functional group as depicted in Figure 1.28. Bisindole alkaloids have drawn significant attention due to their diverse biological properties including antiviral, antimicrobial and anticancer.[105] Bisindole alkaloids generally isolated from marine source including sponges, coelenterates, tunicates, and bryozoans and exhibited anticancer activity (Figure 1.26). For instance, Topsentins A-C (**74**), which feature a ketoimidazole moiety as a linker between two indole rings and are isolated from the marine sponge Topsentia genitrix, have been found to inhibit tumor cell proliferation (IC_{50}= 4–40 μM).[106] Similarly, the

imidazole-bearing bisindole alkaloids Nortopsentins A–C (**75**), isolated from Spongosorites ruetzleri, exhibited in vitro cytotoxicity against P388 cells (IC$_{50}$= 4.5–20.7 μM).[107]

In 2023, Jan *et al.* conducted a study focused on synthesizing novel bis-indole analogues containing a phenyl linker derived from indole phytoalexins. The synthesis involved the reaction of [1-(tert-butoxycarbonyl)indol-3-yl]methyl isothiocyanate with p-phenylenediamine to obtain the target bis-indole thiourea linked by a phenyl linker. Compound **77**, resulting from this synthesis, exhibited significant inhibition of proliferation in the lung cancer cell line A549, while showing minimal effects on non-cancerous cells. Moreover, it was demonstrated that compound **77** induced autophagy by upregulating Beclin-1, LC3A/B, Atg7, AMPK, and ULK1.
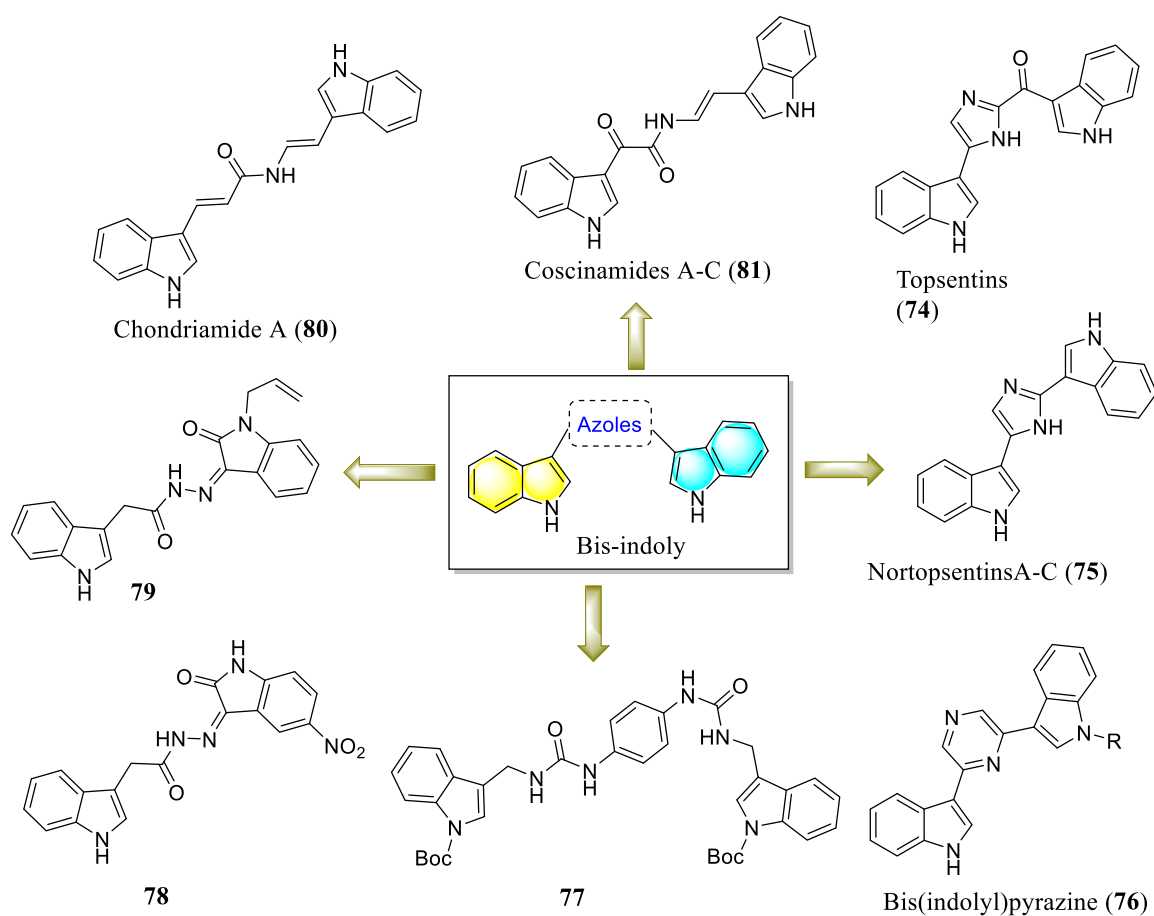
Figure 1.26 Bisindoles as anti-cancer agents

Additionally, when combined with chloroquine (CQ), an autophagy inhibitor, compound **77** led to decreased cell proliferation, G1 cell cycle arrest, and apoptosis. Furthermore, compound **77** caused depletion of glutathione (GSH) and notably enhanced the antiproliferative effect of cis-platin.[3] Wagdy and colleagues designed and synthesized a novel series of bis-indoles, analogues of Topsentin and Nortopsentin. The design strategy involved replacing the

heterocyclic spacer in the natural leads with a more flexible hydrazide linker while retaining the two peripheral indole rings.

All synthesized bis-indoles were evaluated for their antiproliferative activity against human breast cancer cell lines (MCF-7 and MDA-MB-231). Among them, compounds **78** and **79** exhibited the most potent activity against MCF-7 cells (IC$_{50}$= 0.44 ± 0.01 and 1.28 ± 0.04 μM, respectively) and induced apoptosis in MCF-7 cells. This induction of apoptosis was evidenced by the externalization of plasma membrane phosphatidylserine detected by Annexin V-FITC/PI assay. Additionally, both compounds increased the Bax/Bcl-2 ratio, caspase-3 level, and p53 level, and arrested the cell cycle primarily in the G2/M phase. Furthermore, compounds **78** and **79** displayed good selectivity toward tumor cells, as indicated by their cytotoxicity toward non-tumorigenic breast MCF-10A.[108] Bisindoles, received much attention of medicinal chemist due to their structural simplicity and broad anticancer activities. In recent years, diverse synthetic analogues of Nortopsentins **75**, have been reported by replacing imidazole ring with variety of cyclic (five-or six-membered heterocyclic rings) as well as linear chain linkers (**74-81**) as shown in figure 1.26.

1.5 Role of Computational Chemistry in Drug Discovery
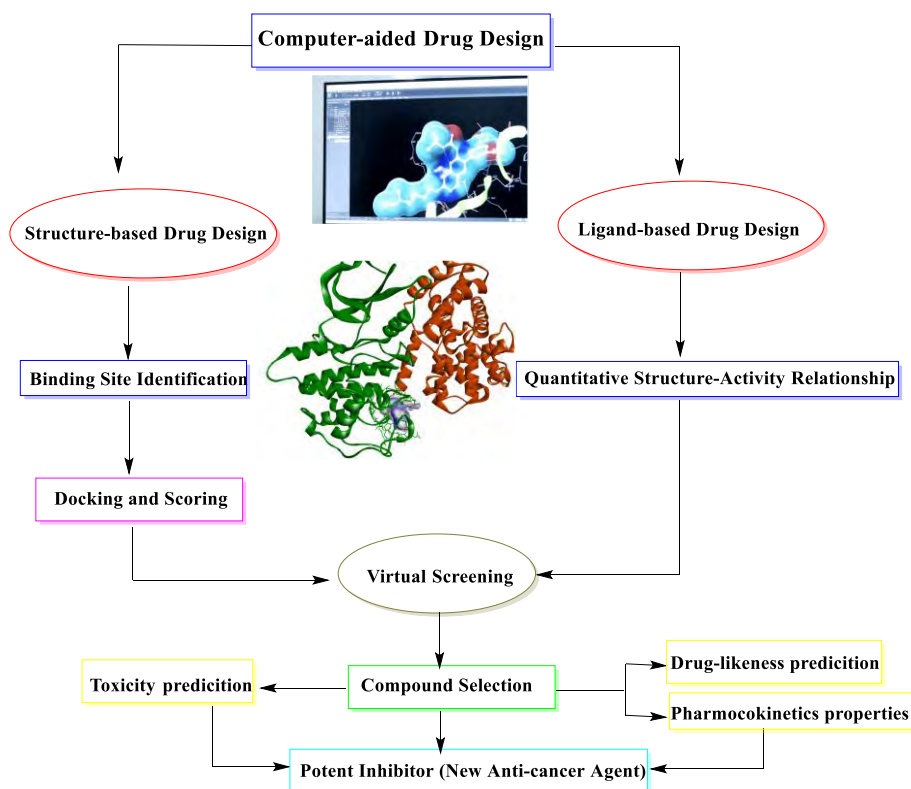
Figure 1.27 Role of computational chemistry

Computational methods have proved to play an essential role in modern drug discovery. Since computational methods could cover almost all stages of the drug discovery pipeline, the applications of computational methods in anticancer drug discoveries have shown great advantages in terms of the required investment, resources, and time. More recently, computational methods have become a potent and powerful tool in several successful cases of anticancer drug development.[109]

Computer aided drug design providing valuable insights into molecular interactions, structure-activity relationships, and pharmacokinetic properties of potential drug candidates. (Figure 1.27) *In silico* studies, including molecular modeling, virtual screening, and ADMET (absorption, distribution, metabolism, excretion, and toxicity) predictions, facilitate the identification and optimization of lead compounds with desired pharmacological properties.[110] In this context, this study aims to explore the role of indole-based compounds as anticancer agents, focusing on their molecular targets, structural diversity, and potential therapeutic applications.

1.5.1 Molecular Docking

Molecular docking is a typical structure-based protocol in rational drug design by studying and predicting the binding patterns and interaction affinities among the ligand and receptor biomolecules.[110] It could be categorized as rigid docking and flexible docking according to the flexibility of the ligands involved in the computational process. Molecular docking is a powerful computational technique used in computational chemistry for studying the interactions between small molecules (such as potential ligand) and their target biomolecules (such as proteins) at the atomic level. In the context of anti-cancer drug discovery, molecular docking plays several crucial roles.
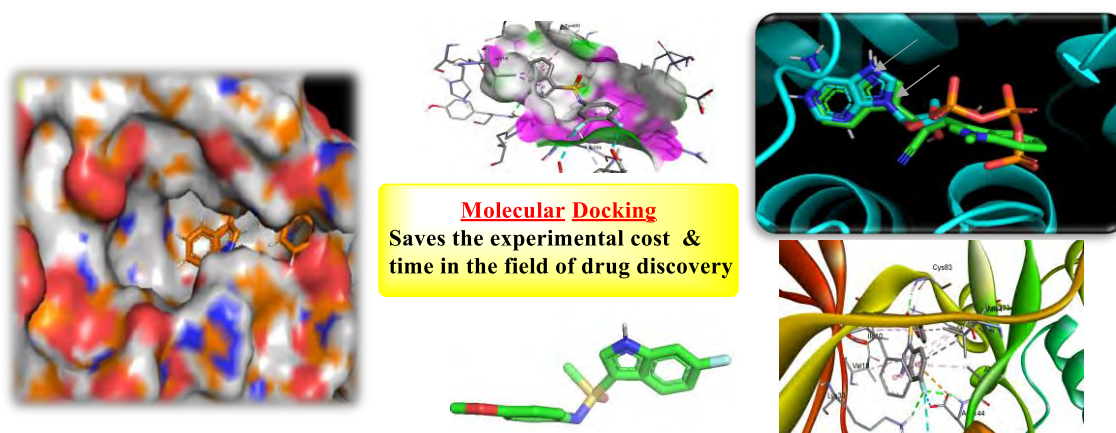
Figure 1.28 Molecular docking studies

Target Identification and Validation: Molecular docking helps in identifying potential protein targets that are involved in cancer progression or are specific to cancer cells. By docking small molecules against a library of protein structures, researchers can prioritize targets based on the strength and specificity of binding interactions.

It also provides insights into the molecular mechanisms underlying the anti-cancer activity of lead compounds. By analyzing the binding poses and interactions (Figure 1.28) between the compound and its target protein, researchers can elucidate the specific biochemical pathways or signaling cascades affected by the compound, aiding in the understanding of its mode of action.[111] Molecular docking studies conducted to explore the interactions between indolylheterocycles and key cancer-related biomolecules. For instance, in Figure 1.29, colchicine and combretastatin are depicted as standard anticancer agents, demonstrating potent interactions with tubulin protein. In 2018, Kamal *et al.* conducted preliminary activity screening, revealing significant inhibitory activity among most derivatives, with compounds **83** standing out. Compound **83** exhibited potent inhibitory activity against human prostate cancer cells DU-145, with IC_{50} values of 0.68 and 0.54 μM, respectively (Figure 1.29).
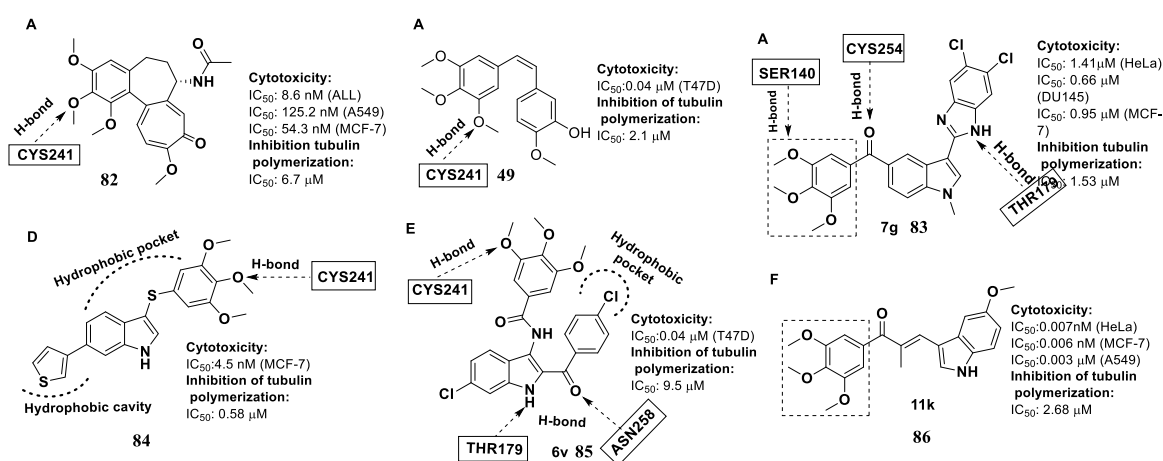
Figure 1.29 Anti-cancer agents: Docked structure of potent compounds

Subsequent studies unveiled that these compounds arrested the cell cycle at the G2/M phase and induced apoptosis in DU-145 cells. Molecular modeling studies elucidated that the TMP group of **83** accepted two hydrogen bonds from SER140 and GLN11. Additionally, the -NH group of the benzimidazole ring donated a hydrogen bond to THR179. Notably, the carbonyl group at the bridge chain exhibited a hydrogen bond interaction with CYS254, a rare occurrence in this class of tubulin inhibitors. Interactions with other active site residues, including GLN247, LEU248, LEU255, ASN258, MET259, and LYS352, were also observed. Similarly, other molecules demonstrated potent interactions as depicted in figure 1.28.

1.5.2 Toxicity Prediction

Computational methods can predict the potential toxicity of chemical compounds by assessing their interaction with biological targets or through structure-activity relationships (SAR). These predictions help identify potentially toxic compounds early in the drug discovery process, allowing researchers to prioritize safer candidates for further experimental testing. By evaluating toxicity computationally, researchers can reduce the time and resources required for experimental toxicity testing. By understanding the potential toxic effects of a compound, researchers can make informed decisions regarding its development and use, minimizing the risk of adverse reactions in patients. Absorption, Distribution, Metabolism, Excretion, and Toxicity (ADMET) properties are crucial factors that influence the pharmacokinetics and safety of drugs. Computational methods allow for the prediction of ADMET properties based on molecular structure, aiding in the optimization of drug candidates with favorable pharmacokinetic profiles and reduced toxicity. By evaluating ADMET properties computationally, researchers can identify compounds with improved bioavailability, reduced metabolism, and minimal toxicity.[112]

Drug-likeness refers to the resemblance of a compounds physicochemical properties to those of known drugs. Computational methods, such as quantitative structure-activity relationship (QSAR) modeling and molecular docking, can assess a compound's drug-likeness based on factors such as molecular weight, lipophilicity, hydrogen bonding capacity, and structural similarity to approved drugs. Evaluating drug-likeness computationally helps prioritize compounds with a higher likelihood of success in drug development, as they are more likely to possess desirable pharmacological properties and lower toxicity.[113]

By leveraging computational methods, researchers can accelerate the drug discovery process, reduce experimental costs, and improve the overall success rate of drug development programs.

1.6 Conclusions

Indole-based compounds have emerged as potent tools in the ongoing fight against life-threatening diseases, notably cancer. The field has witnessed significant progress, with a growing number of indole-based compounds advancing to pre-clinical and clinical stages. These advancements are poised to address challenges associated with chemotherapy, including drug resistance, bioavailability issues, and drug toxicity. Notably, existing cancer drugs often lead to adverse effects such as bone marrow suppression, gastrointestinal disturbances, and hair loss due to their cytotoxic effects. Additionally, many antineoplastic drugs trigger nausea and vomiting by stimulating the chemoreceptor trigger zone in the medulla. To overcome these

aforementioned problems and scientific understanding of the mechanisms of drug resistance may emerge new treatments which may develop to counteract resistance and decrease the toxicity. The present study mainly focuses on the design and synthesis of novel indole-based chemical entities for the improved anticancer activity. Design of diverse series of indole-based compounds is based on natural as well as synthetic bioactive lead molecules. By synthesizing diverse heterocycles and functionalizing positions such as C-3, C-2, and N-H on the indole ring, we conducted screening against a broad spectrum of cancer cell lines, providing insights into their mechanisms and necessary structural modifications. The initial studies on the mechanism of action of these synthesized indole-based compounds motivated us to further explore the structure-activity relationship and delve into the detailed mechanisms of action of the most promising compounds. Additionally, employing *in silico* studies aided in the identification of potential anticancer agents, complementing our experimental findings.

1.7 References

1. Zhong, W.-Z.; Zhou, S.-F., Molecular science for drug development and biomedicine. MDPI: **2014**; *15*, 20072-20078.

2. Xiao, X.; Min, J.-L.; Lin, W.-Z.; Liu, Z.; Cheng, X.; Chou, K.-C., iDrug-Target: predicting the interactions between drug compounds and target proteins in cellular networking via benchmark dataset optimization approach. *Journal of Biomolecular Structure and Dynamics* **2015,** *33* (10), 2221-2233.

3. Budovska, M.; Michalkova, R.; Kello, M.; Vaskova, J.; Mojzis, J., Design, Synthesis and Antiproliferative Evaluation of Bis-Indole Derivatives with a Phenyl Linker: Focus on Autophagy. *Molecules* **2022,** *28* (1), 251.

4. Hassan, A. S.; Moustafa, G. O.; Awad, H. M.; Nossier, E. S.; Mady, M. F., Design, synthesis, anticancer evaluation, enzymatic assays, and a molecular modeling study of novel pyrazole–indole hybrids. *ACS Omega* **2021,** *6* (18), 12361-12374.

5. Sherif, S. H.; Murthy, Y., Design and synthesis of indole-benzimidazole hybrid molecules and evaluation of their in-vitro cytotoxic activities. *Bulletin of the Chemical Society of Ethiopia* **2023,** *37* (5), 1209-1220.

6. El-Shershaby, M. H.; Ghiaty, A.; Bayoumi, A. H.; Ahmed, H. E.; El-Zoghbi, M. S.; El-Adl, K.; Abulkhair, H. S., 1, 2, 4-Triazolo [4, 3-c] quinazolines: a bioisosterism-guided approach towards the development of novel PCAF inhibitors with potential anticancer activity. *New Journal of Chemistry* **2021,** *45* (25), 11136-11152.

7.   Abbas, S. Y.; Al-Harbi, R. A.; El-Sharief, M. A. S., Synthesis and anticancer activity of thiourea derivatives bearing a benzodioxole moiety with EGFR inhibitory activity, apoptosis assay and molecular docking study. *European Journal of Medicinal Chemistry* **2020,** *198*, 112363.

8.   Man, S.; Luo, C.; Yan, M.; Zhao, G.; Ma, L.; Gao, W., Treatment for liver cancer: From sorafenib to natural products. *European Journal of Medicinal Chemistry* **2021,** *224*, 113690.

9.   Khedr, F.; Ibrahim, M. K.; Eissa, I. H.; Abulkhair, H. S.; El‑Adl, K., Phthalazine‑based VEGFR‑2 inhibitors: Rationale, design, synthesis, in silico, ADMET profile, docking, and anticancer evaluations. *Archiv Der Pharmazie* **2021,** *354* (11), 2100201.

10.   Dhuguru, J.; Skouta, R., Role of indole scaffolds as pharmacophores in the development of anti-lung cancer agents. *Molecules* **2020,** *25* (7), 1615.

11.   Cui, W.; Aouidate, A.; Wang, S.; Yu, Q.; Li, Y.; Yuan, S., Discovering anti-cancer drugs via computational methods. *Frontiers in Pharmacology* **2020,** *11*, 733.

12.   Yang, W.; Peng, H.; He, M.; Peng, Z.; Wang, G., Novel tubulin polymerization inhibitors based on the hybridization of coumarin and indole ring: Design, synthesis and bioactivities evaluation. *Journal of Molecular Structure* **2024**, 137761.

13.   Kargbo, R. B., Selective cyclin-dependent kinase inhibitors and their application in cancer therapy. ACS Publications: 2022, 13, 1561-1563.

14.   Zahoor, A. F.; Saeed, S.; Rasul, A.; Noreen, R.; Irfan, A.; Ahmad, S.; Faisal, S.; Al-Hussain, S. A.; Saeed, M. A.; Muhammed, M. T., Synthesis, Cytotoxic, and Computational Screening of Some Novel Indole–1, 2, 4-Triazole-Based S-Alkylated N-Aryl Acetamides. *Biomedicines* **2023,** *11* (11), 3078.

15.   Kerru, N.; Gummidi, L.; Maddila, S.; Gangu, K. K.; Jonnalagadda, S. B., A review on recent advances in nitrogen-containing molecules and their biological applications. *Molecules* **2020,** *25* (8), 1909.

16.   El‑Shershaby, M. H.; El‑Gamal, K. M.; Bayoumi, A. H.; El‑Adl, K.; Ahmed, H. E.; Abulkhair, H. S., Synthesis, antimicrobial evaluation, DNA gyrase inhibition, and in silico pharmacokinetic studies of novel quinoline derivatives. *Archiv Der Pharmazie* **2021,** *354* (2), 2000277.

17.   Omar, A. M.; Ihmaid, S.; Habib, E.-S. E.; Althagfan, S. S.; Ahmed, S.; Abulkhair, H. S.; Ahmed, H. E., The rational design, synthesis, and antimicrobial investigation of 2-

Amino-4-Methylthiazole analogues inhibitors of GlcN-6-P synthase. *Bioorganic Chemistry* **2020,** *99*, 103781.

18. Othman, E. M.; Fayed, E. A.; Husseiny, E. M.; Abulkhair, H. S., The effect of novel synthetic semicarbazone-and thiosemicarbazone-linked 1, 2, 3-triazoles on the apoptotic markers, VEGFR-2, and cell cycle of myeloid leukemia. *Bioorganic Chemistry* **2022,** *127*, 105968.

19. Al-Karmalawy, A. A.; Rashed, M.; Sharaky, M.; Abulkhair, H. S.; Hammouda, M. M.; Tawfik, H. O.; Shaldam, M. A., Novel fused imidazotriazines acting as promising top. II inhibitors and apoptotic inducers with greater selectivity against head and neck tumors: Design, synthesis, and biological assessments. *European Journal of Medicinal Chemistry* **2023,** *259*, 115661.

20. Baragaña, B.; Norcross, N. R.; Wilson, C.; Porzelle, A.; Hallyburton, I.; Grimaldi, R.; Osuna-Cabello, M.; Norval, S.; Riley, J.; Stojanovski, L., Discovery of a quinoline-4-carboxamide derivative with a novel mechanism of action, multistage antimalarial activity, and potent in vivo efficacy. *Journal of Medicinal Chemistry* **2016,** *59* (21), 9672-9685.

21. Mohammad, B. D.; Baig, M. S.; Bhandari, N.; Siddiqui, F. A.; Khan, S. L.; Ahmad, Z.; Khan, F. S.; Tagde, P.; Jeandet, P., Heterocyclic compounds as dipeptidyl peptidase-IV inhibitors with special emphasis on oxadiazoles as potent anti-diabetic agents. *Molecules* **2022,** *27* (18), 6001.

22. Atukuri, D.; Gunjal, R.; Holagundi, N.; Korlahalli, B.; Gangannavar, S.; Akkasali, K., Contribution of N‐heterocycles towards anti‐tubercular drug discovery (2014‐2019); predicted and reengineered molecular frameworks. *Drug Development Research* **2021,** *82* (6), 767-783.

23. Nakhi, A.; Prasad, B.; Reddy, U.; Rao, R. M.; Sandra, S.; Kapavarapu, R.; Rambabu, D.; Krishna, G. R.; Reddy, C. M.; Ravada, K., A new route to indoles via in situ desilylation–Sonogashira strategy: identification of novel small molecules as potential anti-tuberculosis agents. *Medchemcomm* **2011,** *2* (10), 1006-1010.

24. Singh, S.; Sharma, N.; Chandra, R., The indole nucleus as a selective COX-2 inhibitor and anti-inflammatory agent (2011–2022). *Organic Chemistry Frontiers* **2022,** *9* (13), 3624-3639.

25. Wan, Y.; Li, Y.; Yan, C.; Yan, M.; Tang, Z., Indole: A privileged scaffold for the design of anti-cancer agents. *European Journal of Medicinal Chemistry* **2019,** *183*, 111691.

26. Jagadeesan, S.; Karpagam, S., Novel series of N-acyl substituted indole based piperazine, thiazole and tetrazoles as potential antibacterial, antifungal, antioxidant and cytotoxic agents, and their docking investigation as potential Mcl-1 inhibitors. *Journal of Molecular Structure* **2023,** *1271*, 134013.

27. Tjitra, E.; Baker, J.; Suprianto, S.; Cheng, Q.; Anstey, N. M., Therapeutic efficacies of artesunate-sulfadoxine-pyrimethamine and chloroquine-sulfadoxine-pyrimethamine in vivax malaria pilot studies: relationship to Plasmodium vivax dhfr mutations. *Antimicrobial Agents and Chemotherapy* **2002,** *46* (12), 3947-3953.

28. Kaushik, N. K.; Kaushik, N.; Attri, P.; Kumar, N.; Kim, C. H.; Verma, A. K.; Choi, E. H., Biomedical importance of indoles. *Molecules* **2013,** *18* (6), 6620-6662.

29. Baeyer, A., Ueber die reduction aromatischer verbindungen mittelst zinkstaub. *Justus Liebigs Annalen Der Chemie* **1866,** *140* (3), 295-296.

30. Baeyer, A.; Emmerling, A., Synthese des indols. *Berichte Der Deutschen Chemischen Gesellschaft* **1869,** *2* (1), 679-682.

31. Petrova, G.; Shner, V.; Alekseeva, L.; Suvorov, N., Indole derivatives: XC. Preparation of indoles with a substituent in the benzene ring from the corresponding 2-naphthols. *Chemistry of Heterocyclic Compounds* **1974,** *10* (2), 182-185.

32. Jones, A. W.; Purwono, B.; Bowyer, P. K.; Mitchell, P. S.; Kumar, N.; Nugent, S. J.; Jolliffe, K. A.; Black, D. S., The nitration of some 4, 6-dimethoxyindoles. *Tetrahedron* **2004,** *60* (47), 10779-10786.

33. Huang, R. Y.; Franke, P. T.; Nicolaus, N.; Lautens, M., Domino C–H functionalization reactions of gem-dibromoolefins: synthesis of N-fused benzo [c] carbazoles. *Tetrahedron* **2013,** *69* (22), 4395-4402.

34. Tobisu, M.; Yamaguchi, S.; Chatani, N., Lewis Acid-Promoted Imine Synthesis by the Insertion of Isocyanides into C− H Bonds of Electron-Rich Aromatic Compounds. *Organic Letters* **2007,** *9* (17), 3351-3353.

35. Pennington, L. D.; Collier, P. N.; Comer, E., Harnessing the necessary nitrogen atom in chemical biology and drug discovery. *Medicinal Chemistry Research* **2023,** *32* (7), 1278-1293.

36. Patil, S. A.; Patil, S. A.; Patil, R., Medicinal applications of (benz) imidazole‐ and indole‐based macrocycles. *Chemical Biology & Drug Design* **2017,** *89* (4), 639-649.

37. Corrie, P. G., Cytotoxic chemotherapy: clinical aspects. *Medicine* **2008,** *36* (1), 24-28.

38. Xiao, B.; Ma, L.; Merlin, D., Nanoparticle-mediated co-delivery of chemotherapeutic agent and siRNA for combination cancer therapy. *Expert Opinion on Drug Delivery* **2017,** *14* (1), 65-73.

39. Bukowski, K.; Kciuk, M.; Kontek, R., Mechanisms of multidrug resistance in cancer chemotherapy. *International Journal of Molecular Sciences* **2020,** *21* (9), 3233.

40. Yu, B.; Du, Z.; Zhang, Y.; Li, Z.; Bian, J., Small-molecule degraders of cyclin-dependent kinase protein: A review. *Future Medicinal Chemistry* **2022,** *14* (3), 167-185.

41. Hawash, M.; Jaradat, N.; Eid, A. M.; Abubaker, A.; Mufleh, O.; Al-Hroub, Q.; Sobuh, S., Synthesis of novel isoxazole–carboxamide derivatives as promising agents for melanoma and targeted nano-emulgel conjugate for improved cellular permeability. *BMC Chemistry* **2022,** *16* (1), 47.

42. Hawash, M., Recent advances of tubulin inhibitors targeting the colchicine binding site for cancer therapy. *Biomolecules* **2022,** *12* (12), 1843.

43. Fletcher, D. A.; Mullins, R. D., Cell mechanics and the cytoskeleton. *Nature* **2010,** *463* (7280), 485-492.

44. Liu, Y.-M.; Chen, H.-L.; Lee, H.-Y.; Liou, J.-P., Tubulin inhibitors: a patent review. *Expert Opinion on Therapeutic Patents* **2014,** *24* (1), 69-88.

45. Wang, Y.-T.; Huang, X.; Cai, X.-C.; Kang, X.-X.; Zhu, H.-L., Synthesis, biological evaluation and molecular docking of thiazole hydrazone derivatives grafted with indole as novel tubulin polymerization inhibitors. *Journal of Molecular Structure* **2024,** *1301*, 137343.

46. Gargantilla, M.; Persoons, L.; Kauerová, T.; Del Río, N.; Daelemans, D.; Priego, E.-M.; Kollar, P.; Pérez-Pérez, M.-J., Hybridization approach to identify salicylanilides as inhibitors of tubulin polymerization and signal transducers and activators of transcription 3 (STAT3). *Pharmaceuticals* **2022,** *15* (7), 835.

47. Alam, M. J.; Alam, O.; Perwez, A.; Rizvi, M. A.; Naim, M. J.; Naidu, V. G.; Imran, M.; Ghoneim, M. M.; Alshehri, S.; Shakeel, F., Design, synthesis, molecular docking, and biological evaluation of pyrazole hybrid chalcone conjugates as potential anticancer agents and tubulin polymerization inhibitors. *Pharmaceuticals* **2022,** *15* (3), 280.

48. Wang, J.; Miller, D. D.; Li, W., Molecular interactions at the colchicine binding site in tubulin: An X-ray crystallography perspective. *Drug Discovery Today* **2022,** *27* (3), 759-776.

49. Ren, W.; Deng, Y.; Ward, J. D.; Vairin, R.; Bai, R.; Wanniarachchi, H. I.; Hamal, K. B.; Tankoano, P. E.; Tamminga, C. S.; Bueno, L. M., Synthesis and biological

evaluation of structurally diverse 6-aryl-3-aroyl-indole analogues as inhibitors of tubulin polymerization. *European Journal of Medicinal Chemistry* **2024,** *263*, 115794.

50. Hurysz, B.; Evans, B. A.; Laryea, R. N.; Boyer, B. E.; Coburn, T. E.; Dexter, M. S.; Edwards, M. A.; Faulkner, G. V.; Huss, R. L.; Lafferty, M. M., Synthesis, modeling, and biological evaluation of anti-tubulin indole-substituted furanones. *Bioorganic & Medicinal Chemistry Letters* **2023,** *90*, 129347.

51. Shuai, W.; Wang, G.; Zhang, Y.; Bu, F.; Zhang, S.; Miller, D. D.; Li, W.; Ouyang, L.; Wang, Y., Recent progress on tubulin inhibitors with dual targeting capabilities for cancer therapy. *Journal of Medicinal Chemistry* **2021,** *64* (12), 7963-7990.

52. Banerjee, S.; Hwang, D.-J.; Li, W.; Miller, D. D., Current advances of tubulin inhibitors in nanoparticle drug delivery and vascular disruption/angiogenesis. *Molecules* **2016,** *21* (11), 1468.

53. Hinnen, P.; Eskens, F., Vascular disrupting agents in clinical development. *British Journal of Cancer* **2007,** *96* (8), 1159-1165.

54. Al Sheikh Ali, A.; Khan, D.; Naqvi, A.; Al-Blewi, F. F.; Rezki, N.; Aouad, M. R.; Hagar, M., Design, synthesis, molecular modeling, anticancer studies, and density functional theory calculations of 4-(1, 2, 4-triazol-3-ylsulfanylmethyl)-1, 2, 3-triazole derivatives. *ACS Omega* **2020,** *6* (1), 301-316.

55. Pommier, Y., Topoisomerase I inhibitors: camptothecins and beyond. *Nature Reviews Cancer* **2006,** *6* (10), 789-802.

56. Chien, C.-M.; Yang, S.-H.; Lin, K.-L.; Chen, Y.-L.; Chang, L.-S.; Lin, S.-R., Novel indoloquinoline derivative, IQDMA, suppresses STAT5 phosphorylation and induces apoptosis in HL-60 cells. *Chemico-biological Interactions* **2008,** *176* (1), 40-47.

57. Chen, C.-W.; Wu, M.-H.; Chen, Y.-F.; Yen, T.-Y.; Lin, Y.-W.; Chao, S.-H.; Tala, S.; Tsai, T.-H.; Su, T.-L.; Lee, T.-C., A potent derivative of indolizino [6, 7-b] indole for treatment of human non–small cell lung cancer cells. *Neoplasia* **2016,** *18* (4), 199-212.

58. Liu, Y. Q.; Tian, J.; Qian, K.; Zhao, X. B.; Morris‐Natschke, S. L.; Yang, L.; Nan, X.; Tian, X.; Lee, K. H., Recent progress on C‐4‐modified podophyllotoxin analogs as potent antitumor agents. *Medicinal Research Reviews* **2015,** *35* (1), 1-62.

59. Peyressatre, M.; Prével, C.; Pellerano, M.; Morris, M. C., Targeting cyclin-dependent kinases in human cancers: from small molecules to peptide inhibitors. *Cancers* **2015,** *7* (1), 179-237.

60. Malumbres, M.; Barbacid, M., Mammalian cyclin-dependent kinases. *Trends in Biochemical Sciences* **2005,** *30* (11), 630-641.

61. Lim, S.; Kaldis, P., Cdks, cyclins and CKIs: roles beyond cell cycle regulation. *Development* **2013,** *140* (15), 3079-3093.

62. Malumbres, M., Physiological relevance of cell cycle kinases. *Physiological Reviews* **2011**.

63. Hanahan, D.; Weinberg, R. A., The hallmarks of cancer. *cell* **2000,** *100* (1), 57-70.

64. Malumbres, M.; Barbacid, M., To cycle or not to cycle: a critical decision in cancer. *Nature Reviews Cancer* **2001,** *1* (3), 222-231.

65. Greenman, C.; Stephens, P.; Smith, R.; Dalgliesh, G. L.; Hunter, C.; Bignell, G.; Davies, H.; Teague, J.; Butler, A.; Stevens, C., Patterns of somatic mutation in human cancer genomes. *Nature* **2007,** *446* (7132), 153-158.

66. Liu, J.-L.; Ma, H.-P.; Lu, X.-L.; Sun, S.-H.; Guo, X.; Li, F.-C., NF-κB induces abnormal centrosome amplification by upregulation of CDK2 in laryngeal squamous cell cancer. *International Journal of Oncology* **2011,** *39* (4), 915-924.

67. Lenjisa, J. L.; Tadesse, S.; Khair, N. Z.; Kumarasiri, M.; Yu, M.; Albrecht, H.; Milne, R.; Wang, S., CDK5 in oncology: recent advances and future prospects. *Future Medicinal Chemistry* **2017,** *9* (16), 1939-1962.

68. Oner, M.; Lin, E.; Chen, M.-C.; Hsu, F.-N.; Shazzad Hossain Prince, G.; Chiu, K.-Y.; Teng, C.-L. J.; Yang, T.-Y.; Wang, H.-Y.; Yue, C.-H., Future aspects of CDK5 in prostate cancer: from pathogenesis to therapeutic implications. *International Journal of Molecular Sciences* **2019,** *20* (16), 3881.

69. Tripathi, B. K.; Qian, X.; Mertins, P.; Wang, D.; Papageorge, A. G.; Carr, S. A.; Lowy, D. R., CDK5 is a major regulator of the tumor suppressor DLC1. *Journal of Cell Biology* **2014,** *207* (5), 627-642.

70. Sharma, P. S.; Sharma, R.; Tyagi, R., Inhibitors of cyclin dependent kinases: useful targets for cancer treatment. *Current Cancer Drug Targets* **2008,** *8* (1), 53-75.

71. Guha, M., Blockbuster dreams for Pfizer's CDK inhibitor. *Nature Biotechnology* **2013,** *31* (3), 187-188.

72. Dickson, M. A., Molecular pathways: CDK4 inhibitors for cancer therapy. *Clinical Cancer Research* **2014,** *20* (13), 3379-3383.

73. Mariaule, G.; Belmont, P., Cyclin-dependent kinase inhibitors as marketed anticancer drugs: where are we now? A short survey. *Molecules* **2014,** *19* (9), 14366-14382.

74. Sánchez-Martínez, C.; Gelbert, L. M.; Lallena, M. J.; de Dios, A., Cyclin dependent kinase (CDK) inhibitors as anticancer drugs. *Bioorganic & Medicinal Chemistry Letters* **2015,** *25* (17), 3420-3435.

75. Hadfield, J. A.; Ducki, S.; Hirst, N.; McGown, A. T., Tubulin and microtubules as targets for anticancer drugs. *Progress in Cell Cycle Research.* **2003,** *5*, 309-326.

76. Marchi, E.; O'Connor, O. A., Safety and efficacy of pralatrexate in the treatment of patients with relapsed or refractory peripheral T-cell lymphoma. *Therapeutic Advances in Hematology* **2012,** *3* (4), 227-235.

77. Luqmani, Y., Mechanisms of drug resistance in cancer chemotherapy. *Medical Principles and Practice* **2005,** *14* (Suppl. 1), 35-48.

78. Sagadevan, S.; Vennila, S.; Marlinda, A. R.; Al-Douri, Y.; Rafie Johan, M.; Anita Lett, J., Synthesis and evaluation of the structural, optical, and antibacterial properties of copper oxide nanoparticles. *Applied Physics A* **2019,** *125*, 1-9.

79. Duesberg, P.; Stindl, R.; Hehlmann, R., Explaining the high mutation rates of cancer cells to drug and multidrug resistance by chromosome reassortments that are catalyzed by aneuploidy. *Proceedings of the National Academy of Sciences* **2000,** *97* (26), 14295-14300.

80. Zhou, B.; Liu, Z.-F.; Deng, G.-G.; Chen, W.; Li, M.-Y.; Yang, L.-J.; Li, Y.; Yang, X.-D.; Zhang, H.-B., Synthesis and antitumor activity of novel N-substituted tetrahydro-β-carboline–imidazolium salt derivatives. *Organic & Biomolecular Chemistry* **2016,** *14* (39), 9423-9430.

81. Feng, L.; Chen, X.; Sheng, G.; Li, Y.; Li, Y.; Zhang, Y.; Yao, K.; Wu, Z.; Zhang, R.; Kiboku, T., Synthesis and Bioevaluation of 3-(Arylmethylene) indole Derivatives: Discovery of a Novel ALK Modulator with Antiglioblastoma Activities. *Journal of Medicinal Chemistry* **2023,** *66* (21), 14609-14622.

82. Jeong, Y.-M.; Li, H.; Kim, S. Y.; Park, W.-J.; Yun, H.-Y.; Baek, K. J.; Kwon, N. S.; Jeong, J. H.; Myung, S. C.; Kim, D.-S., Photo-activated 5-hydroxyindole-3-acetic acid induces apoptosis of prostate and bladder cancer cells. *Journal of Photochemistry and Photobiology b: Biology* **2011,** *103* (1), 50-56.

83. De Martino, G.; Edler, M. C.; La Regina, G.; Coluccia, A.; Barbera, M. C.; Barrow, D.; Nicholson, R. I.; Chiosis, G.; Brancale, A.; Hamel, E., New arylthioindoles: Potent Inhibitors of tubulin polymerization. 2. Structure− activity relationships and molecular modeling studies. *Journal of Medicinal Chemistry* **2006,** *49* (3), 947-954.

84. Brancale, A.; Silvestri, R., Indole, a core nucleus for potent inhibitors of tubulin polymerization. *Medicinal Research Reviews* **2007,** *27* (2), 209-238.

85. Gastpar, R.; Goldbrunner, M.; Marko, D.; Von Angerer, E., Methoxy-substituted 3-formyl-2-phenylindoles inhibit tubulin polymerization. *Journal of Medicinal Chemistry* **1998,** *41* (25), 4965-4972.

86. Ducki, S.; Rennison, D.; Woo, M.; Kendall, A.; Chabert, J. F. D.; McGown, A. T.; Lawrence, N. J., Combretastatin-like chalcones as inhibitors of microtubule polymerization. Part 1: Synthesis and biological evaluation of antivascular activity. *Bioorganic & Medicinal Chemistry* **2009,** *17* (22), 7698-7710.

87. Baytas, S. N., Recent advances in combretastatin A-4 inspired inhibitors of tubulin polymerization: an update. *Current Medicinal Chemistry* **2022,** *29* (20), 3557-3585.

88. Chauhan, S. S.; Singh, A. K.; Meena, S.; Lohani, M.; Singh, A.; Arya, R. K.; Cheruvu, S. H.; Sarkar, J.; Gayen, J. R.; Datta, D., Synthesis of novel β-carboline based chalcones with high cytotoxic activity against breast cancer cells. *Bioorganic & Medicinal Chemistry Letters* **2014,** *24* (13), 2820-2824.

89. Stefański, T.; Mikstacka, R.; Kurczab, R.; Dutkiewicz, Z.; Kucińska, M.; Murias, M.; Zielińska-Przyjemska, M.; Cichocki, M.; Teubert, A.; Kaczmarek, M., Design, synthesis, and biological evaluation of novel combretastatin A-4 thio derivatives as microtubule targeting agents. *European Journal of Medicinal Chemistry* **2018,** *144*, 797-816.

90. Abdul Hussein, S. A.; Razzak Mahmood, A. A.; Tahtamouni, L. H.; Balakit, A. A.; Yaseen, Y. S.; Al‑Hasani, R. A., New Combretastatin Analogs as Anticancer Agents: Design, Synthesis, Microtubules Polymerization Inhibition, and Molecular Docking Studies. *Chemistry & Biodiversity* **2023,** *20* (4), 202201206.

91. Chen, Z.-H.; Xu, R.-M.; Zheng, G.-H.; Jin, Y.-Z.; Li, Y.; Chen, X.-Y.; Tian, Y.-S., Development of Combretastatin A-4 Analogues as Potential Anticancer Agents with Improved Aqueous Solubility. *Molecules* **2023,** *28* (4), 1717.

92. Hura, N.; Sawant, A. V.; Kumari, A.; Guchhait, S. K.; Panda, D., Combretastatin-inspired heterocycles as antitubulin anticancer agents. *ACS Omega* **2018,** *3* (8), 9754-9769.

93. Karatoprak, G. Ş.; Küpeli Akkol, E.; Genç, Y.; Bardakcı, H.; Yücel, Ç.; Sobarzo-Sánchez, E., Combretastatins: an overview of structure, probable mechanisms of action and potential applications. *Molecules* **2020,** *25* (11), 2560.

94. Pauletti, P. M.; Cintra, L. S.; Braguine, C. G.; Filho, A. A. d. S.; Silva, M. L. A. e.; Cunha, W. R.; Januario, A. H., Halogenated indole alkaloids from marine invertebrates. *Marine Drugs* **2010,** *8* (5), 1526-1549.

95. Reyes, F.; Fernandez, R.; Rodríguez, A.; Francesch, A.; Taboada, S.; Avila, C.; Cuevas, C., Aplicyanins A–F, new cytotoxic bromoindole derivatives from the marine tunicate Aplidium cyaneum. *Tetrahedron* **2008,** *64* (22), 5119-5123.

96. Sun, H. H.; Sakemi, S., A brominated (aminoimidazolinyl) indole from the sponge Discodermia polydiscus. *The Journal of Organic Chemistry* **1991,** *56* (13), 4307-4308.

97. Ren, Y.; Wang, Y.; Liu, J.; Liu, T.; Yuan, L.; Wu, C.; Yang, Z.; Chen, J., X-ray crystal structure-guided discovery of novel indole analogues as colchicine-binding site tubulin inhibitors with immune-potentiating and antitumor effects against melanoma. *Journal of Medicinal Chemistry* **2023,** *66* (10), 6697-6714.

98. Tantak, M. P.; Malik, M.; Klingler, L.; Olson, Z.; Kumar, A.; Sadana, R.; Kumar, D., Indolyl-α-keto-1, 3, 4-oxadiazoles: Synthesis, anti-cell proliferation activity, and inhibition of tubulin polymerization. *Bioorganic & Medicinal Chemistry Letters* **2021,** *37*, 127842.

99. Kumar, D.; Sundaree, S.; Johnson, E. O.; Shah, K., An efficient synthesis and biological study of novel indolyl-1, 3, 4-oxadiazoles as potent anticancer agents. *Bioorganic & Medicinal Chemistry Letters* **2009,** *19* (15), 4492-4494.

100. Bhattacharya, S.; Kumar, N. M.; Ganguli, A.; Tantak, M. P.; Kumar, D.; Chakrabarti, G., NMK-TD-100, a novel microtubule modulating agent, blocks mitosis and induces apoptosis in HeLa cells by binding to tubulin. *PloS One* **2013,** *8* (10), e76286.

101. Li, W.; Yin, Y.; Shuai, W.; Xu, F.; Yao, H.; Liu, J.; Cheng, K.; Xu, J.; Zhu, Z.; Xu, S., Discovery of novel quinazolines as potential anti-tubulin agents occupying three zones of colchicine domain. *Bioorganic Chemistry* **2019,** *83*, 380-390.

102. Lu, Y.; Chen, J.; Wang, J.; Li, C.-M.; Ahn, S.; Barrett, C. M.; Dalton, J. T.; Li, W.; Miller, D. D., Design, synthesis, and biological evaluation of stable colchicine binding site tubulin inhibitors as potential anticancer agents. *Journal of Medicinal Chemistry* **2014,** *57* (17), 7355-7366.

103. Hwang, D.-J.; Wang, J.; Li, W.; Miller, D. D., Structural optimization of indole derivatives acting at colchicine binding site as potential anticancer agents. *ACS Medicinal Chemistry Letters* **2015,** *6* (9), 993-997.

104. Chen, J.; Ahn, S.; Wang, J.; Lu, Y.; Dalton, J. T.; Miller, D. D.; Li, W., Discovery of novel 2-aryl-4-benzoyl-imidazole (ABI-III) analogues targeting tubulin polymerization as antiproliferative agents. *Journal of Medicinal Chemistry* **2012,** *55* (16), 7285-7289.

105. Carbone, A.; Parrino, B.; Barraja, P.; Spanò, V.; Cirrincione, G.; Diana, P.; Maier, A.; Kelter, G.; Fiebig, H.-H., Synthesis and antiproliferative activity of 2, 5-bis (3′ - indolyl) pyrroles, analogues of the marine alkaloid nortopsentin. *Marine Drugs* **2013,** *11* (3), 643-654.

106. Bartik, K.; Braekman, J.-C.; Daloze, D.; Stoller, C.; Huysecom, J.; Vandevyver, G.; Ottinger, R., Topsentins, new toxic bis-indole alkaloids from the marine sponge Topsentia genitrix. *Canadian Journal of Chemistry* **1987,** *65* (9), 2118-2121.

107. Sakemi, S.; Sun, H. H., Nortopsentins A, B, and C. Cytotoxic and antifungal imidazolediylbis [indoles] from the sponge Spongosorites ruetzleri. *The Journal of Organic Chemistry* **1991,** *56* (13), 4304-4307.

108. Barreca, M.; Spanò, V.; Montalbano, A.; Cueto, M.; Díaz Marrero, A. R.; Deniz, I.; Erdoğan, A.; Lukić Bilela, L.; Moulin, C.; Taffin-de-Givenchy, E., Marine anticancer agents: An overview with a particular focus on their chemical classes. *Marine Drugs* **2020,** *18* (12), 619.

109. Cai, C.; Lin, H.; Wang, H.; Xu, Y.; Ouyang, Q.; Lai, L.; Pei, J., miDruglikeness: subdivisional drug-likeness prediction models using active ensemble learning strategies. *Biomolecules* **2022,** *13* (1), 29.

110. Aziz, M.; Ejaz, S. A.; Zargar, S.; Akhtar, N.; Aborode, A. T.; A. Wani, T.; Batiha, G. E.-S.; Siddique, F.; Alqarni, M.; Akintola, A. A., Deep learning and structure-based virtual screening for drug discovery against NEK7: a novel target for the treatment of cancer. *Molecules* **2022,** *27* (13), 4098.

111. Pinzi, L.; Rastelli, G., Molecular docking: shifting paradigms in drug discovery. *International Journal of Molecular Sciences* **2019,** *20* (18), 4331.

112. Sliwoski, G.; Kothiwale, S.; Meiler, J.; Lowe, E. W., Computational methods in drug discovery. *Pharmacological Reviews* **2014,** *66* (1), 334-395.

113. Roman, D. L.; Roman, M.; Som, C.; Schmutz, M.; Hernandez, E.; Wick, P.; Casalini, T.; Perale, G.; Ostafe, V.; Isvoran, A., Computational assessment of the pharmacological profiles of degradation products of chitosan. *Frontiers in Bioengineering and Biotechnology* **2019,** *7*, 214.

Chapter 2

Sulfoximine Functionalized Anti-cancer Agents

Part 2A: Design and Synthesis of

N-aryl Indolylsulfoximines: Identification

of Potent and Selective Anti-cancer Agents
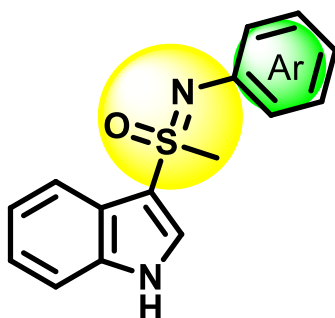
2.1 Sulfoximines

The sulfoximine moiety presents a distinctive array of intriguing characteristics, including structural diversity, advanced chemical and metabolic stability, and favourable physicochemical and *in vitro* attributes. Despite its potential, the available literature data on sulfoximine compounds have historically been limited. To address this gap, numerous studies have emerged in recent years, exploring sulfoximine-containing small molecules or their fragments, as well as other sulfur-containing functional groups through matched molecular pair analysis or investigations into related analogues. These efforts aim to comprehensively assess the physicochemical and *in vitro* properties of sulfoximine-based compounds, shedding light on their potential applications and utility.
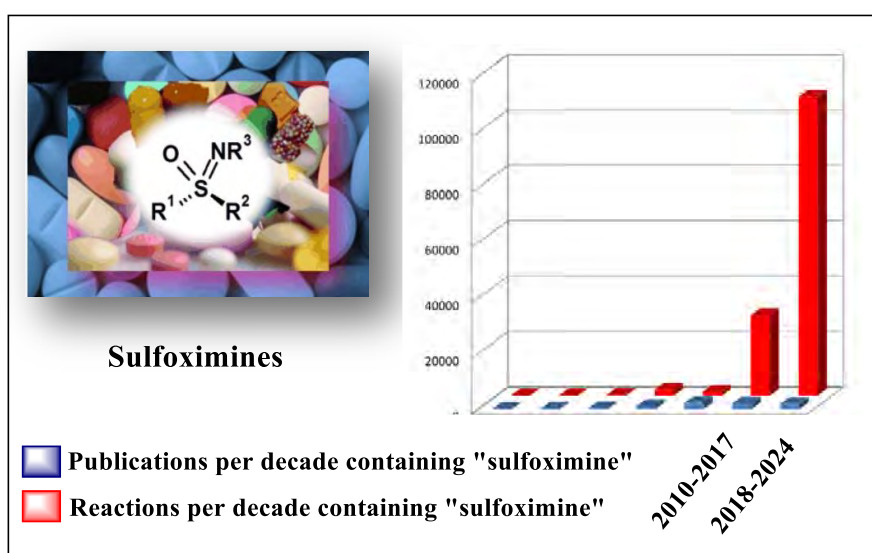
Figure 2.1 An examination of the number of publications per decade containing the keyword "sulfoximine" (represented by blue bars) and of reactions per decade featuring a sulfoximine substructure (depicted by red bars).

In this chapter, synthesis and anticancer activity studies of two series of sulfoximines have been discussed. **Part 2A** includes the design, synthesis and biological evaluation of *N*-aryl indolylsulfoximines as novel apoptosis inducing cytotoxic agents. **Part 2B** deals with the synthesis and biological evaluation of colchicine sulfoximine as anticancer agents (tubulin inhibitor).

Part 2A: Design and Synthesis of *N*-aryl Indolylsulfoximines: Identification of Potent and Selective Anti-cancer Agents

2.1.1 Introduction

In drug discovery, medicinal chemists face numerous challenges during the course of hit selection and lead generation, such as affinity and selectivity issues, toxicity concerns, the necessity to improve or tune physicochemical and ADME (absorption, distribution, metabolism and excretion) properties, or the need for novelty with regard to intellectual property (IP) generation.[1] The most prevalent techniques in lead optimization involve the systematic use of common bioisosteres.[2] In the latter approach, the aim is to discover structurally novel compounds by modifying the central core structure of known active compounds. Heterocyclic compounds are a significant source of pharmacologically active compounds, which could be obtained from organic synthesis or isolated from natural products.[3-5] Since heterocyclic compounds contain one or more heteroatoms, such as nitrogen, oxygen and sulphur, besides at least one carbon in the ring, they could be used as potential hydrogen bond donors and acceptors. Accordingly, they could bind to biological targets through intermolecular hydrogen bonds effectively. Moreover, they can regulate the lipid or aqueous solubility to yield drug molecules with improved pharmacotherapeutic properties.[6]

Microtubules (MT) are made of 10-15 protofilaments of α,β-tubulin heterodimers that associate sideways to form a polarized hollow tube. The plus end of MT is involved in polymerization and the minus end favors disassembly. They are also highly regulated by post-translational modifications including phosphorylation, acetylation, and GTP binding. Signalling cause MTs to rapidly assemble and disassemble, which enables them to participate in mitosis, organelle distribution, intracellular transport, and dendrite and axon growth.[7] The inhibition of tubulin polymerization is a well-established strategy for anticancer drug development, as MTs play an essential role in cellular processes such as mitosis, intracellular transport, and cell motility. Tubulin targeting substances are broadly categorized into microtubule stabilizing (taxanes, epothilones and discodermolide) and destabilizing (colchicine, vinca alkaloids, cryptophycins and CA-4P) agents. MT-targeting agents (MTAs) that bind to the colchicine binding site (also called CBSI) have the potential to overcome the drawbacks associated with taxanes and vinca alkaloids, owing to their structural simplicity, non-substrate nature for the multidrug resistance protein 1 (P-glycoprotein) and reasonable physicochemical properties.[8-10] Generally, anticancer agents that inhibit microtubule assembly are known as antimitotic agents. Compared to normal cells, cancer cells have the characteristics of uncontrolled proliferation, migration,

and metastasis, indicating exceptionally active microtubule dynamics.[3] Therefore, microtubules are investigated as the ideal target for anticancer therapy.[4, 5, 11] Most approved and investigated microtubule-targeting agents (MTAs) are natural or semi-synthetic compounds that interfere with microtubule dynamics, tamper with the cell division process, induce cell cycle arrest, and eventually lead to cell apoptosis.[6, 12] Some recent reports have also shown tubulin polymerization inhibitor induced ROS via mitochondrial pathways.[13]

Indole core has been continuously attracting the attention of researchers and has become a dynamic area of research due to its outstanding pharmacological properties. Indole skeleton is frequently found in many natural and synthetic chemical entities of immense biological significance. In addition, indole derivatives also display a variety of other biological activities such as anti-fungal,[13] anti-inflammatory,[14] anti-bacterial,[15] anti-viral[16] and anti-cancer [17, 18]. In the recent past, several indole containing small molecules have been identified as potent tubulin inhibitors, for example, 3-aroylindoles,[19] IMB105 [20], 2-heteroarylthioindoles, VERU-111,[21] 3-amidoindole,[22] and indolylsulfonamides.[23]
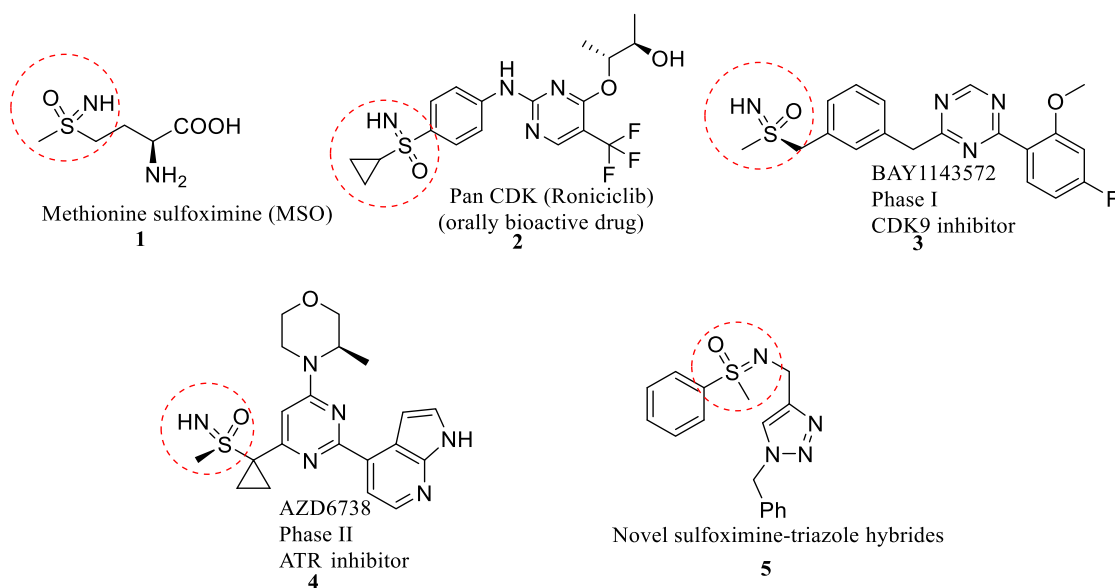
Figure 2.1.1 Biological active sulfoximines analogues

Similar to indole-derived compounds, sulfoximine derivatives have recently been emerged as interesting compounds for medicinal and synthetic chemists. Outstanding work of Bolm,[24] Bull,[25] and Lücking,[26] and Arvidsson's,[27] provided easy access to sulfoximine containing bioactive compounds. With the discovery of methionine sulfoximine **1** and its post structural modifications to glutamylcysteine synthetase inhibitor, use of chiral sulfur scaffolds in bioactive compounds has pursued with increasing interest.[27] With unique properties and potential applications, many sulfoximines containing compounds are in clinical trials such as

Roniciclib (pan-CDK inhibitor, **2**), BAY 1143572 (ATR inhibitor, **3**)[28] and AZD6738 (**4**)[29] (Figure 2.1.1).[30] In the recent past, sulfoximines have emerged as a promising class of compounds for cancer therapy due to their unique structural features and favorable pharmacokinetic properties such as better solubility in protic solvents, high stability, good physical and chemical properties, multiple hydrogen bond acceptor/donor functional groups and structural diversity.[26, 31] Sulfoximines have a chiral sulfur atom that confers stereochemical diversity and enhances their binding affinity and selectivity for target proteins. These properties suggest that the sulfoximine group has significant potential to serve as a small, hydrophilic, and stable functional group in drug discovery.

The combination of these two important chemical moieties, indoles and sulfoximines, offers a unique opportunity to develop novel compounds with potentially enhanced biological activities and therapeutic applications. As part of our efforts to develop novel anticancer agents, in the present work we have successfully synthesized and conducted cytotoxicity studies on indolylsulfoximines **9** (Figure 2.1.2).
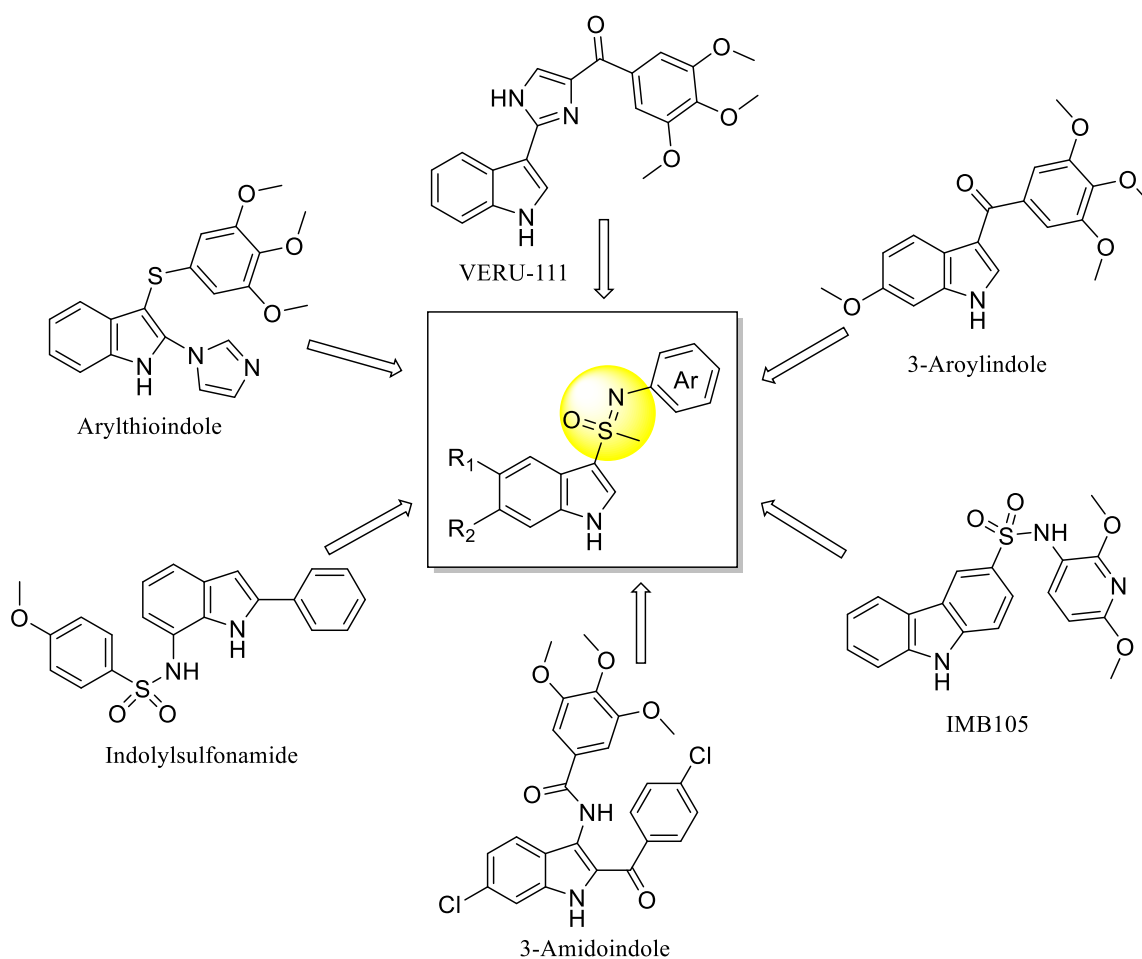
Figure 2.1.2 Rational design: Indole-based anti-cancer agents

2.1.2 Results and Discussion

2.1.2.1 Synthesis and Characterization

In the present work, indolylsulfoximines **9a-m** were prepared using the synthetic route as delineated in Scheme 3.1.1. The one-pot NH-transfer to sulfides is one of the convenient protocols to prepare NH-sulfoximines. Very recently, Bull and Luisi prepared NH-sulfoximines from sulfoxide by employing a combination of (diacetoxyiodo)benzene (IBD) and ammonium carbamate as ammonia source under metal-free conditions.[32] Subsequently, the same group described the direct conversion of sulfides into NH-sulfoximines *via* a chemoselective one-pot nitrogen and oxygen-transfer using a combination of ammonia source (ammonia in methanol, ammonium carbonate and ammonium acetate) and IBD.[33] By employing IBD and ammonium carbamate as the ammonia source, Reboul and co-workers also reported a one-pot reaction to access NH-sulfoximines from sulfides.[34] In a late-stage sulfoximation of a sulfide, Reboul et al. prepared PTEF/CDK9 inhibitor, Atuveciclib by using IBD (2.1 equiv), ammonium carbamate (1.5 equiv) in methanol.[35] However, according to the literature report more electron-rich heteroarenes such as indole were not well-tolerated.[36] Herein, we report the synthesis of indolylsulfoximines from electron-rich indolylsulfides (Scheme 2.1.1). Our modified protocol involves the preparation of key intermediate methylthioindole **8** to access indolylsulfoximines **9**. The *N*-boc-3-methylthioindoles **8a** was prepared by initial reaction of indole **6** with DMSO and trimethylsilyl chloride (TMSCl) in the presence of diisopropylamine to produce (3-methylthio)-1*H*-indole **7**.[37, 38] Next, reaction of **7** with IBD failed to generate the NH-indolylsulfoximine **9**. Therefore, NH-free indole of **7** was protected using di-*tert*-butyl dicarbonate [(Boc)₂O] to furnish *N*-boc-3-methylthioindole **8a** in good yield 92%.
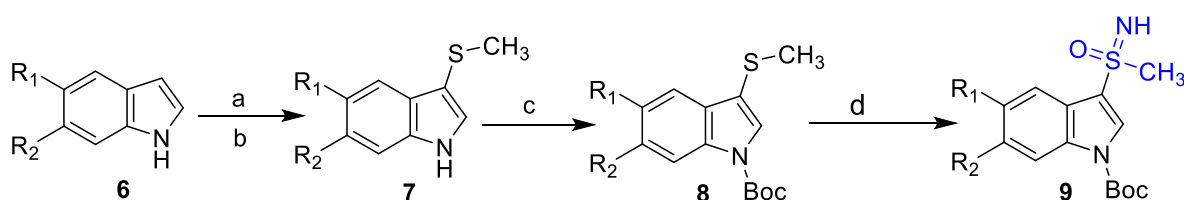
Scheme 2.1.1 Reagents and conditions: (a) DMSO (1.1 equiv), TMSCl (1.1 equiv), acetonitrile N₂-atm, 0 °C, 5 h; (b) Diisopropylamine 80 °C, 2 h; (c) [(Boc)₂O] (2.0 equiv), DMAP (1.5 equiv), THF, rt; (d) IBD (3.0 equiv), NH₂COONH₄ (2.0 equiv), methanol, 25 °C, 5 h.

Initially we treated **8a** with NH₂COONH₄ (1.5 equiv) and IBD (2.5 equiv) in methanol at room temperature for 2 h to afford **9a** in 42% yield (Table 2.1.1, entry 1). Next, experiments were carried out to minimize the excess use of IBD and ammonium carbamate. Reaction of **8a** with

1.5 equivalents of IBD and NH$_2$COONH$_4$, afforded **9a** in 37% yield (Table 2.1.1, entry 2). Further increase in equivalence (from 2.5 to 3.0) of IBD and reaction time, afforded **9a** in excellent yield (Table 2.1.1, entries 3-5). With the use of tetrahydrofuran or toluene as a reaction solvent failed to produce **9a** (Table 2.1.1, entries 6-7). Finally, we found that the use of IBD (3.0 equiv) and NH$_2$COONH$_4$ (2.0 equiv) in methanol at room temperature is the optimum reaction conditions (Table 2.1.1, entry 5) for the preparation of sulfoximine **9a**.

Table 2.1.1 Optimization for the preparation of NH sulfoximine **9a**
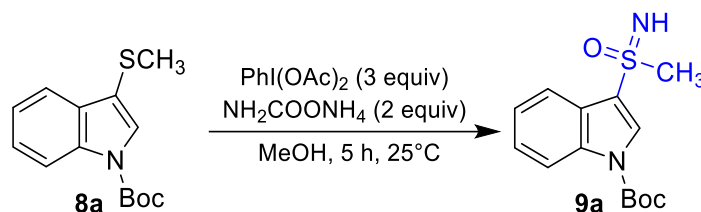
Entry	NH$_2$COONH$_4$	IBD	Solvent	Time (h)	Yield[b] (%)
1.	1.5	2.5	MeOH	2.0	42
2.	1.5	1.5	MeOH	2.0	37
3.	2.0	2.5	MeOH	4.0	72
4.	2.0	2.5	MeOH	5.0	81
5.	**2.0**	**3.0**	**MeOH**	**5.0**	**90**
6.	2.0	3.0	THF	2.0	no reaction
7.	2.0	3.0	Toluene	2.0	trace
8.	2.0	2.5	MeOH	3.5	67

With the optimized conditions in hand, the generality of the protocol was then examined with various indolylsulfides (**8b-e**). Under the identified conditions, reaction of **8b** bearing electron-donating methoxy group proceeded smoothly to afford **9b** in 85% yield (Table 2.1.2).

9a, 90%

R = OMe (**9b**, 85%)
R = Br (**9c**, 88%)

9d
89%

9e
81%
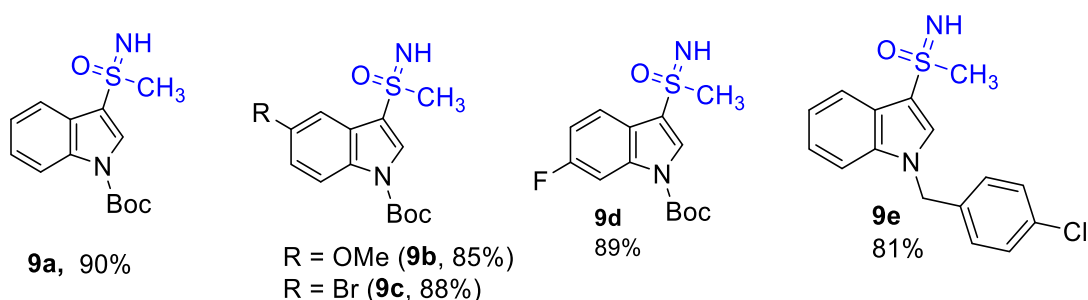
Figure 2.1.3 Structures of the prepared NH sulfoximines **9a-e**

Indole derivatives **8c** and **8d** with bromine/fluorine substituent also successfully afforded **9c** (88%) and **9d** (89%) in good yields. The tolerance of halogen group can offer tremendous potential to prepare more complex structures through various cross coupling reactions. The *N*-(4-chlorobenzylchloride) protected indole **8e** reacted smoothly under the optimized conditions

to provide **9e** in 81% yield (Figure 2.1.3). The structure of **9a** was confirmed by NMR ([1]H & [13]C) and mass spectral analysis.
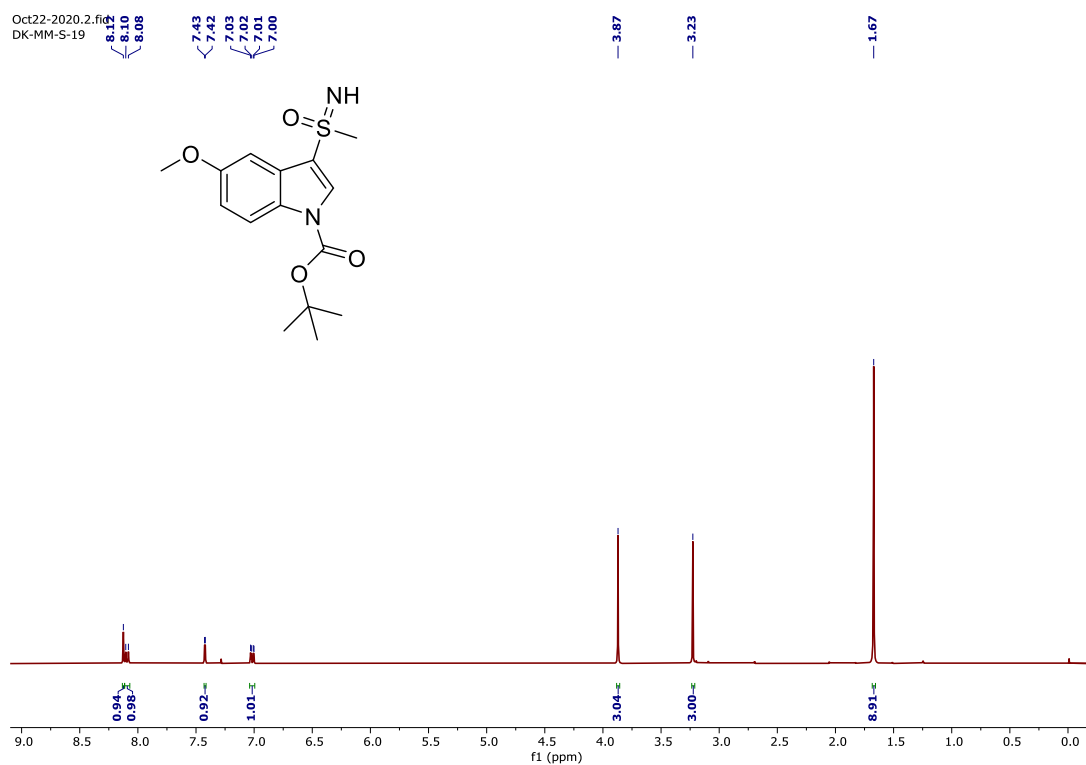
Figure 2.1.4 ^{1}H NMR spectrum of **9a**
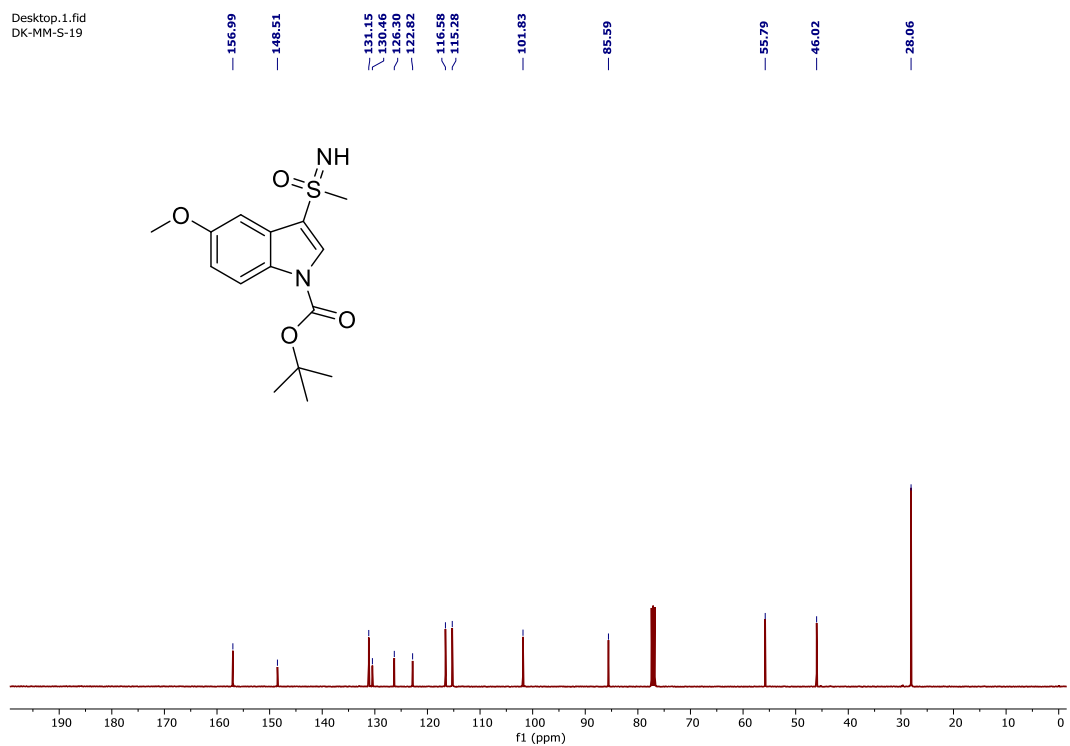
Figure 2.1.5 ^{13}C NMR spectrum of **9a**
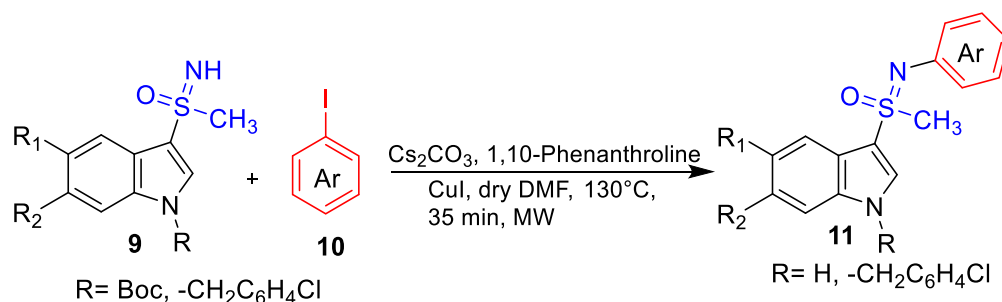
Scheme 2.1.2 Reagents and conditions: **9** (0.33 mmol, 1.0 equiv), **10** (0.39 mmol, 1.2 equiv), CuI catalyst (0.03 mmol, 0.1 equiv), 1,10-phenanthroline (0.06 mmol, 0.2 equiv), dry DMF (2.5 mL) under a N$_2$ atmosphere at 130 °C for 35 min.

Formation of **9a** was indicative by the appearance of singlets at 3.28 ppm and 8.20 ppm for methyl protons and indole C$_2$-proton, respectively in ^{1}H NMR spectrum.(Figure 2.1.4) The ^{13}C NMR spectrum of **9a** displayed a characteristic signal at 46.03 ppm due to methyl carbon of the sulfoximine moiety. (Figure 2.1.5) Similarly, other NH sulfoximines **9b-e** were characterized by their NMR spectral data.

Next, we explored the coupling reaction of NH sulfoximines **9** with aryl halides to prepare *N*-arylated indolylsulfoximines **11** as illustrated in Scheme 2.1.2 The coupling of **9a** with aryl bromide or aryl chloride failed to produce the desired product. Next, the reaction of **9a** with **10** using CuI (10 mol%) as the catalyst, 1,10-phenanthroline (20 mol%), Cs$_2$CO$_3$ (1.5 equiv) and dimethyl formamide (DMF) as solvent at 100 °C under N$_2$ atmosphere in microwave (MW) resulted in the expected *N*-phenylindole-3-carboxamide **11a** in 25% yield (Table 2.1.2, entry 1). The same coupling reaction under conventional heating took longer time (24 h) to furnish **11a** in lower yield. The use of triethylamine instead of Cs$_2$CO$_3$ as the base failed to deliver **11a** (Table 2.1.2, entry 2). When the reaction of **9a** with **10a** was performed in dry DMF, the product yield increased to 30% (Table 2.1.2, entry 3). Under similar conditions, replacement 2f ligand 1,10-phenanthroline with BINAP was unsuccessful (Table 2.1.2, entry 4). Noticeably, an increase in the temperature from 100 to 110 °C provided **11a** in 45% (Table 2.1.2, entry 5). With the increase of Cs$_2$CO$_3$ equivalents from 1.5 to 2.5 resulted in **11a** with 57 % yield (Table 2.1.2, entry 6). Conducting the reaction with dry DMF under strictly anhydrous conditions further increased the yield of **11a** to 65% (Table 2.1.2, entry 7). Furthermore, by increasing the temperature from 110 to 130°C, yield (82%) of the reaction was significantly improved to produce **11a** (Table 2.1.2, entry 8). Gratifyingly, increasing the reaction time from 30 to 35 min. produced **11a** in 91% yield (Table 2.1.2, entry 9). The reaction yields also decreased in the absence of a N$_2$ atmosphere (Table 2.1.2, entry 10). The use of DCE or THF as reaction

solvents resulted in poor yields of **11a** (Table 2.1.2, entries 11–12). Thus, based on the detailed investigations mentioned above, the optimized conditions for the coupling of **9a** with **10a** involve the use of CuI (10 mol%), 1,10-phenanthroline (20 mol%), Cs_2CO_3 (2.5 equiv) and dry DMF as a solvent at 130 °C for 35 min. under N_2 atmosphere in MW (Table 2.1.2, entry 9).

Table 2.1.2 Optimization of the coupling reaction of **9a** and **10a** [a, b]
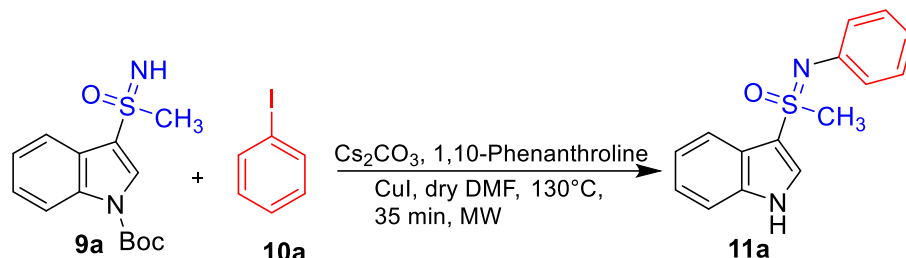
Entry	Ligand	Base (equiv)	Solvent	Temp. (℃)	Time (min.)	Yield[b] (%)
1.	1,10-phenanthroline	Cs_2CO_3 (1.5)	DMF	100	25	25
2.	1,10-phenanthroline	Et_3N	DMF	110	25	trace
3.	1,10-phenanthroline	Cs_2CO_3 (1.5)	dry DMF	100	25	30
4.	BINAP	Cs_2CO_3 (1.5)	DMF	100	25	NR[c]
5.	1,10-phenanthroline	Cs_2CO_3 (1.5)	DMF	110	25	45
6.	1,10-phenanthroline	Cs_2CO_3 (2.5)	DMF	110	25	57
7.	1,10-phenanthroline	Cs_2CO_3 (2.5)	dry DMF	110	25	65
8.	1,10-phenanthroline	Cs_2CO_3 (2.5)	dry DMF	130	30	82
9.	**1,10-phenanthroline**	**Cs_2CO_3 (2.5)**	**dry DMF**	**130**	**35**	**91**
10.	1,10-phenanthroline	Cs_2CO_3 (2.5)	DMF	130	35	71[d]
11.	1,10-phenanthroline	Cs_2CO_3 (2.5)	DCE	130	35	10
12.	1,10-phenanthroline	Cs_2CO_3 (2.5)	THF	130	35	trace

[a] Reagents and conditions: **9a** (0.33 mmol, 1.0 equiv), **10a** (0.39 mmol, 1.2 equiv), CuI catalyst (0.03 mmol, 0.1 equiv), 1,10-phenanthroline (0.06 mmol, 0.2 equiv) dry DMF (2.5 mL) under N_2 atmosphere at 130 °C for 35 min. [b] Isolated yield. [c] NR = no reaction. [d] Reaction was performed in absence of N_2 atmosphere.

After establishing the optimal reaction conditions, the protocol generality was tested using indolylsulfoximine **9a** and various aryl iodides (**10a–h**) (Table 2.1.3). The reaction of **9a** with other aryl iodides bearing electron-donating substituents such as *p*-methyl (**10b**), *p*-methoxy (**10c**) and tri-methoxy (**10d**) proceeded smoothly to afford the corresponding products **11b** (86%), **11c** (84%) and **11d** (87%) (Table 2.1.3). And the halogen substituted aryl iodides such as *p*-Br (**10e**), *p*-F (**10f**) and 3,4-difluoro (**10g**) also furnished the desired products **11e** (81%), **11f** (83%) and **11g** (85%) in high yields. Interestingly, *m*-trifluoromethyl iodobenzene **10h** afforded sulfoximine **11h** in high yield (83%).

Furthermore, we explored the viable substrate scope by employing diversely substituted indolylsulfoximines **9b-e** as given in Table 2.1.3b. The coupling reaction of 5-methoxyindolyl-sulfoximine (**9b**) with aryl iodides **10c** and **10d** proceeded smoothly to afford the corresponding products **11i** (88%) and **11j** (91%) (Table 2.1.3b).

Table 2.1.3 Synthesis of *N*-arylindolylsulfoximines[a]

a) Substrate scope of aryl iodides

11a 91%   **11b** 86%   **11c** 85%   **11d** 89%

11e 81%   **11f** 83%   **11g** 85%   **11h** 83%

b) Substrate scope of indolysulfoximines

11i 88%   **11j** 91%   **11k** 84%

11l 82%   **11m** 81%
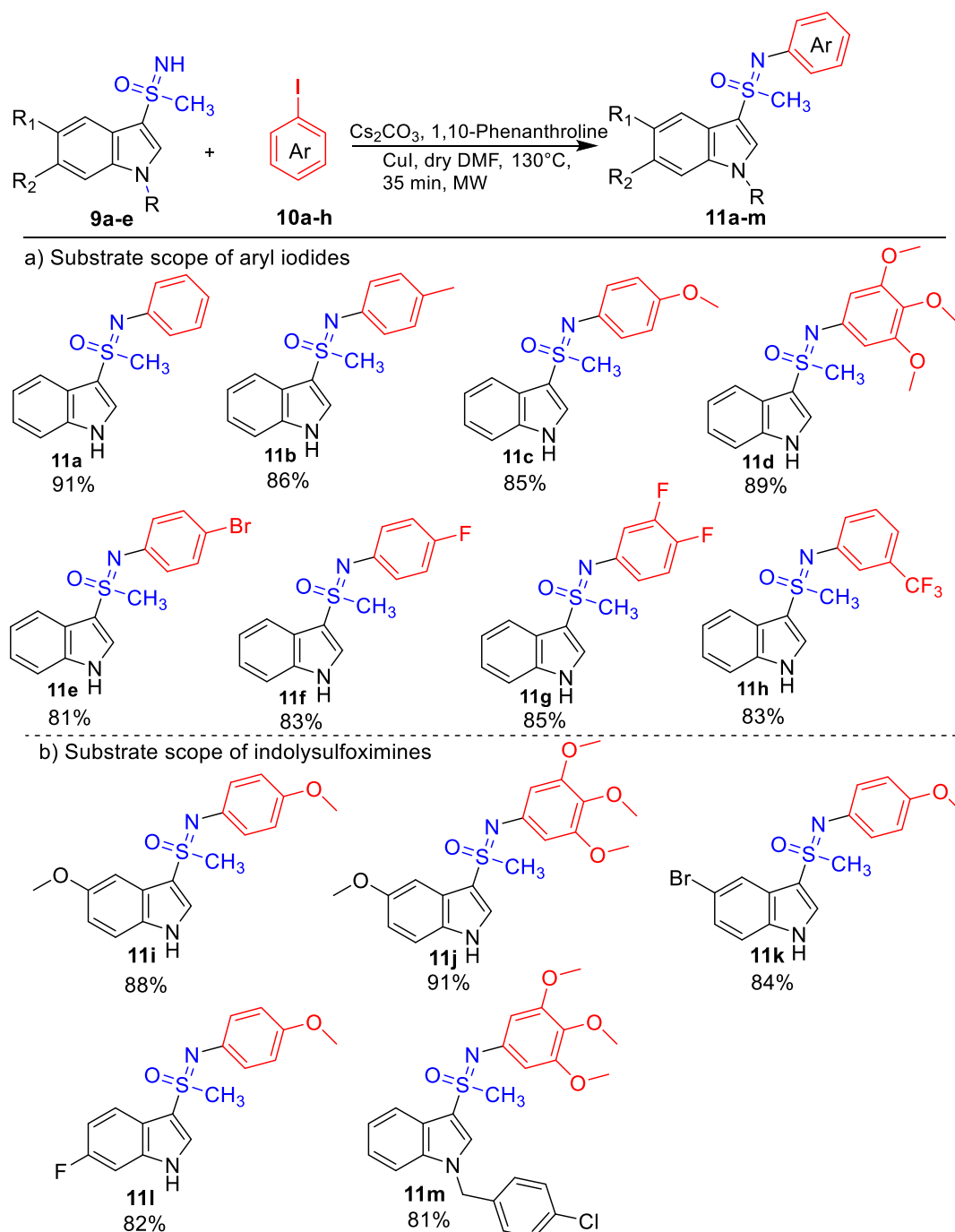
[a] Reagents and conditions: **9a-e** (0.33 mmol, 1.0 equiv), **10a-h** (0.39 mmol, 1.2 equiv), CuI catalyst (0.03 mmol, 0.1 equiv), 1,10-phenanthroline (0.06 mmol, 0.2 equiv), Cs_2CO_3 (0.82 mmol, 2.5 equiv) dry DMF (1.5 mL), under N_2 atmosphere at 130 °C, MW for 35 min.

With the use of halogen substituted NH indolylsulfoximines **9c** (C$_5$-bromine) or **9d** (C$_5$-fluorine) and *p*-methoxyiodobenzene, prepared the corresponding products **11k** and **11l** in high yields (82-85%). The coupling *N*-(4-chlorobenzylchloride) protected NH-sulfoximine **9e** and **10d** enabled to access **11m** in 81% yield (Table 2.1.3b).

The structure of **11a** was confirmed by detailed NMR (^{1}H & ^{13}C) and HRMS spectral analysis. Formation of analogues **11a** was indicative by appearance of singlets at 3.32 ppm and 7.93 ppm for methyl protons and indole C$_2$-proton in ^{1}H NMR spectrum. The ^{13}C NMR spectrum displayed a distinct peak at 46.66 ppm corresponding to the methyl carbon. The HRMS spectrum of **11a** displayed a molecular ion at 271.0860 in agreement with the expected mass for C$_{15}$H$_{14}$N$_2$OS at 271.0898. (Figure 2.1.8) Similarly, using spectroscopic data, structural elucidation of other *N*-aryl sulfoximines **11b-m** was carried out.
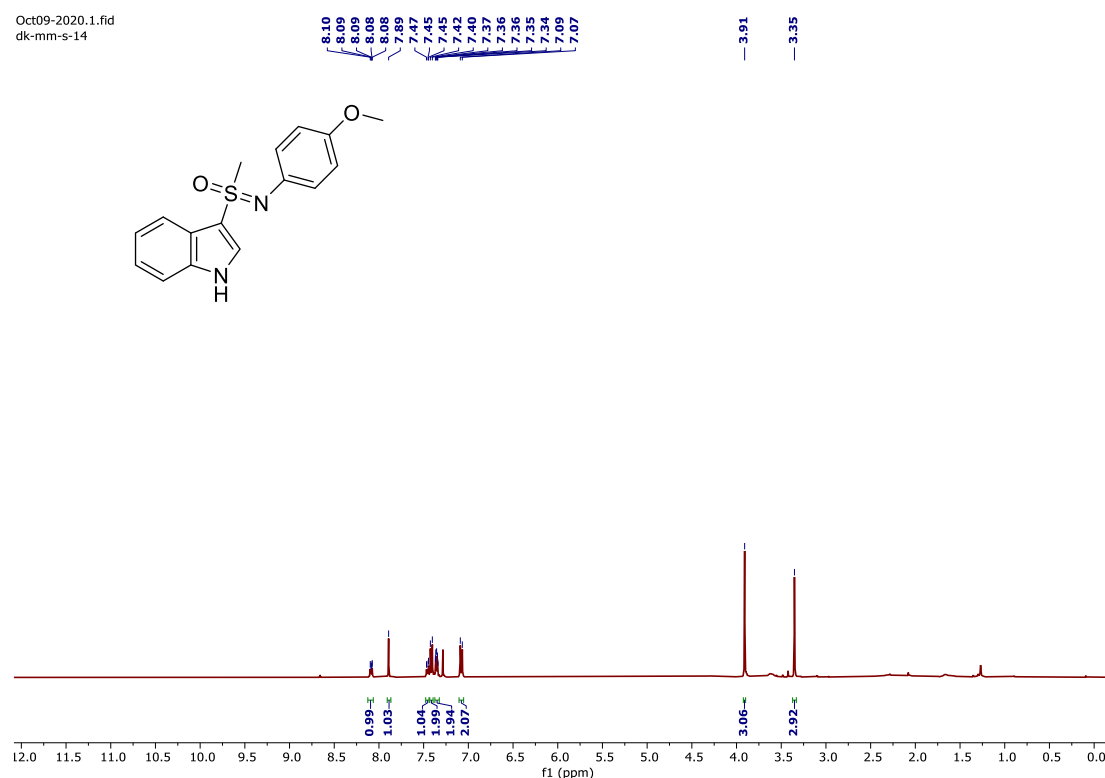
Figure 2.1.6 ^{1}H NMR spectrum of **11c**

Oct09-2020.2.fid
dk-mm-s-14
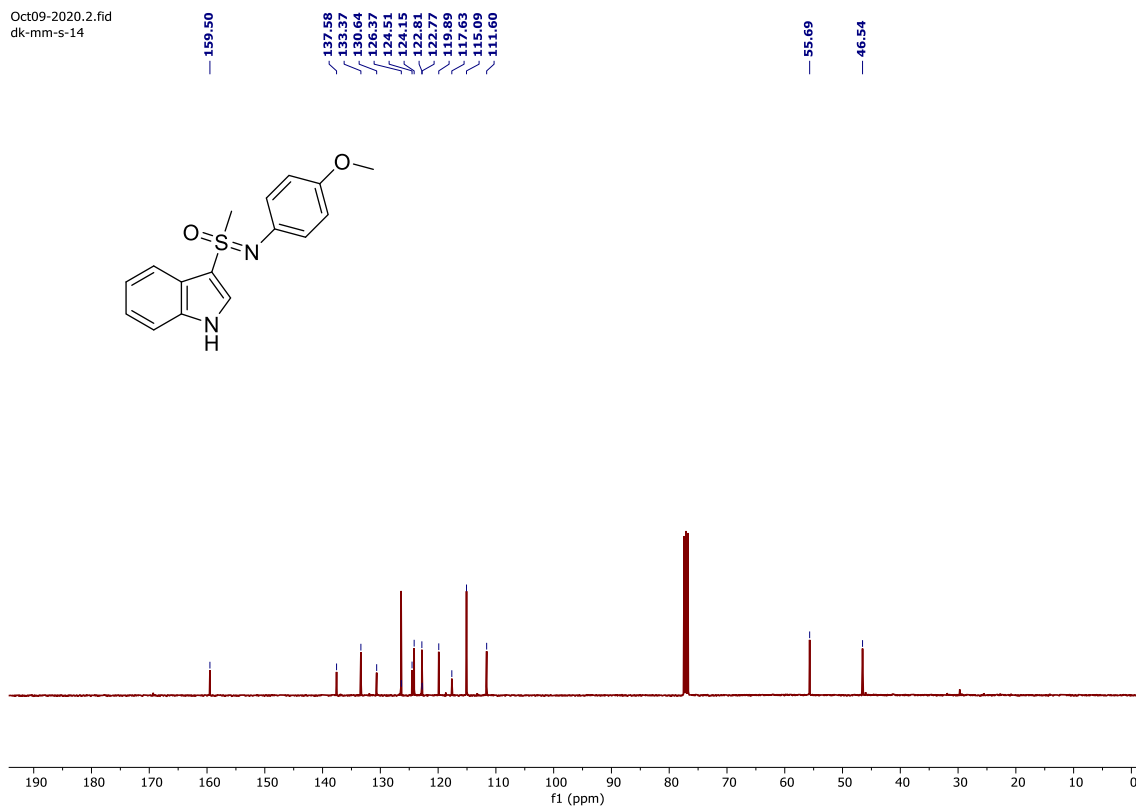
Figure 2.1.7 ^{13}C NMR spectrum of **11c**
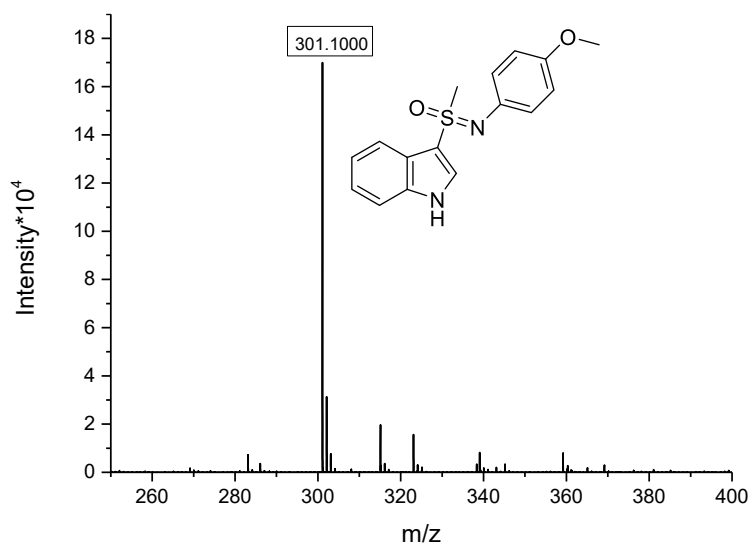
Figure 2.1.8 HRMS Spectrum of **11c**

2.1.2.2 Biological Evaluation

2.1.2.2.1 Anti-cancer Activity

Synthesized *N*-arylated indolylsulfoximine analogues **11a-m** were assessed *in vitro* for their cytotoxicity against a panel of cancer cell lines including 22Rv1, PC3 and C4-2 (human prostate cancer cells), MCF7 (human breast cancer cells) and HEK293 (normal human kidney cells) and the results are given in Table 2.1.4. The indolylsulfoximines **11c** (3.31 μM), **11i** (2.76 μM) and **11j** (2.68 μM) showed selective cytotoxicity against 22Rv1 cells. The indolylsulfoximine derivatives **11b** (2.3 μM), **11c** (1.95 μM), **11f** (3.7 μM), **11g** (1.9 μM), and **11h** (2.18 μM) displayed good cytotoxicity against C4-2 cells. The introduction of electron-donating group, for example, sulfoximine derivatives **11b** (1.6 μM), **11h** (2.0 μM), **11k** (1.28 μM) led to selective cytotoxic against MCF7 cells. Having 6-fluorine and methoxy group, compound **11l** showed high cytotoxic activity IC_{50} values ranging from 1.7 μM to 8.2 μM against the tested human cancer cell lines. The indolylsulfoximines **11a-m** were found to be non-cytotoxic to normal HEK293 cells (>40 μM), indicating their potential selectivity towards cancer cells.

Table 2.1.4 Cytotoxicity for indolylsulfoximines **11a-m** (IC_{50}, μM)

Compd	22Rv1	C4-2	PC3	MCF7	HEK293
11a	>40	**8.9±0.04**	>40	**10.0±0.04**	>40
11b	>40	**2.3±0.04**	>40	**1.6±0.06**	40
11c	**3.31±0.02**	**1.95±0.01**	**17.11±0.07**	>40	>40
11d	>40	**10.0±0.03**	**21.65±0.06**	40	>40
11e	>40	>40	**11.13±0.06**	>40	>40
11f	40	**3.7±0.1**	>40	40	>40
11g	40	**1.9±0.01**	**14.36±0.03**	>40	>40
11h	>40	**2.18±0.03**	40	**2.0±0.1**	40
11i	**2.76±0.05**	40	**12.22±0.07**	>40	>40
11j	**2.68±0.03**	>40	>40	**38.83±0.06**	>40
11k	ND	ND	ND	**1.28±0.02**	>40
11l	**1.91±0.01**	**8.2±0.02**	**3.51±0.04**	**1.7±0.02**	>40
11m	>40	40	>40	40	>40

ND* not determined

The *N*-aryl moiety with fluoro substituent (compounds **11f**, **11g**, and **11h**) is beneficial for the activity and selectivity towards C4-2 cancer cell line. Introduction of an electron-donating group in indole as well as *N*-aryl units of the sufoximines (compounds **11c**, **11i**, and **11j**) is

good for the activity (2.68-3.3 μM) and selectivity against 22Rv1 cancer cell line. The bromo and moderately electron donating groups (**11b**, **11h** and **11k**) are favourable for the activity and selectivity against MCF-7 cells (Figure 2.1.9).

R$_3$= OMe **(11l)**, CH$_3$ **(11b)**, di-F **(11g)**, CF$_3$ **(11h)** good for cytotoxicity

H, Br, OCH$_3$ favourable for the activity

fluorine group increases cytotoxicity

Free NH optimal for activity
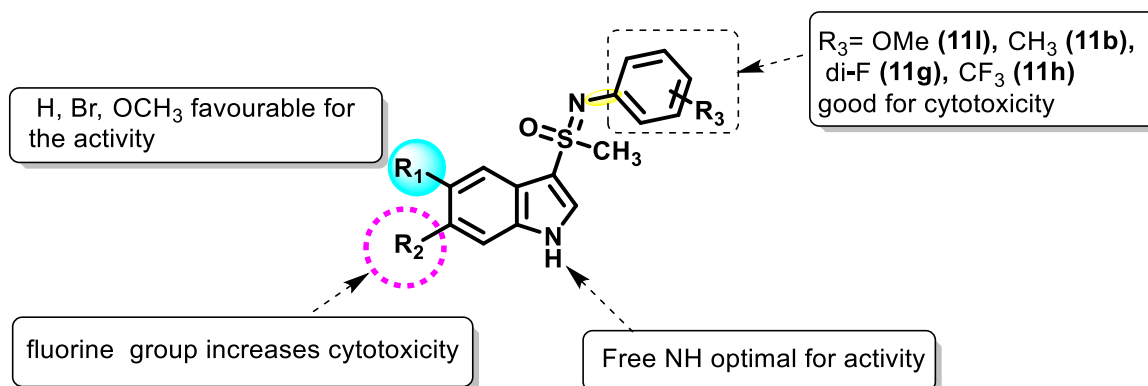
Figure 2.1.9 Structure-activity relationship analysis of compounds **11a-m**

2.1.2.2.2 Acridine Orange (AO)/Ethidium Bromide (EB) staining

Our data revealed **11l** as the most effective compound, as it showed broad selectivity. Thus, to explore the mechanism of cell death, we initially used acridine orange (AO)/ethidium bromide (EB) staining to differentiate the percentage of live and dead cells. While AO stain both live and dead cells, ethidium bromide (EB) stain only dead cells. Incubation of compound **11l** in C4-2 cells for 48 h resulted in red fluorescence, indicating that **11l** causes cell death in C4-2 cells (Figure 2.1.10).
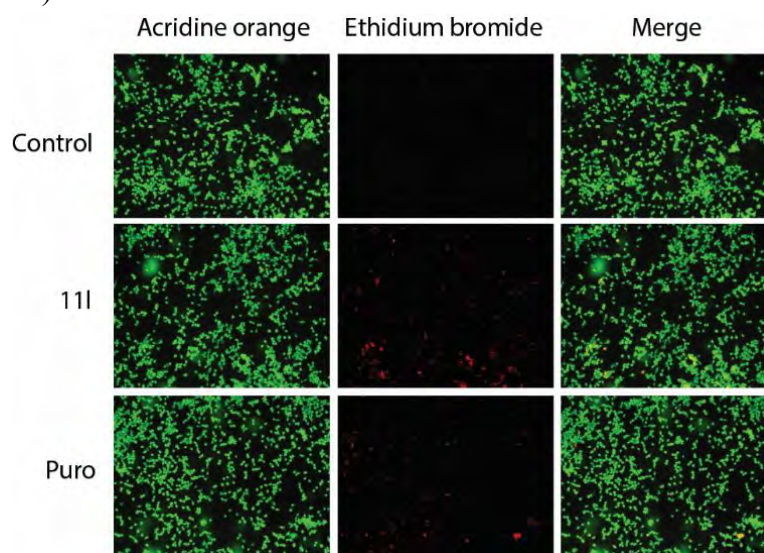
Figure 2.1.10 Fluorescent microscopic images of C4-2 prostate cancer lines treated with DMSO, **11l** and puromycin at 48 h by AO-EB staining. Control cells show green fluorescence confirming their viability. Puromycin showed considerable red fluorescence representing significant apoptosis. **11l** showed substantial apoptosis as majority of cells displayed red fluorescence.

2.1.2.2.3 Measurement of intracellular reactive oxygen species (ROS) levels

Increased ROS levels promote cell death. Thus, we evaluated whether compound **11l** induces ROS accumulation using DCFDA staining in C4-2 cells. H_2O_2-exposed C4-2 cells were used as positive controls. ROS levels were quantified in untreated and C4-2 cells treated with H_2O_2 (10 µM), and **11l** (10 µM) for 48 h. As expected, H_2O_2-treated cells displayed high DCFDA staining. **11l**-treated cells also showed increased ROS levels, indicating that **11l** may cause apoptosis *via* ROS upregulation (Figure. 2.1.11A, B). To further confirm this hypothesis, we examined p53 and c-Jun levels in C4-2 cells treated with either H_2O_2 or compound **11l**. Both p53 and c-Jun levels increased upon **11l** treatment indicating that these compounds induce cytotoxicity by upregulating apoptosis (Figure 2.1.11).
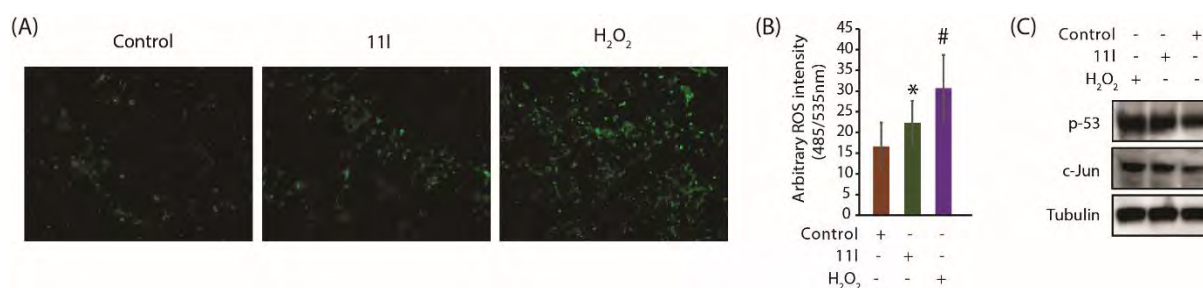
Figure 2.1.11 11l increases ROS levels in C4-2 cells. (A) C4-2 cells were treated with DMSO (vehicle control), compounds **11l** (10 µM) and H_2O_2 (positive control) for 48 h and stained with H2-DCFDA. Photographs were taken with the fluorescence microscope (Nikon) at 10X objective. (B) The bar graph shows arbitrary intensity of ROS level (green signal) among control, **11l** and H_2O_2 treated C4-2 cells. The intensity of green fluorescence was quantified using ImageJ software. Data were mean ± SE of three independent experiments. (C) Western blots show protein level of apoptotic markers p-53 and c-Jun in control, **11l** and H_2O_2 C4-2 cells. Tubulin used as the loading control.

2.1.2.2.4 11l induces mitochondrial dysfunction in C4-2 cells

Increased oxidative stress is often linked to mitochondrial dysfunction, which prompted us to investigate whether **11l** treatment could cause mitochondrial depolarization. C4-2 cells were treated with either **11l** (10 µM) or positive control puromycin for 48 h, both of which induced significant mitochondrial depolarization, thereby revealing that **11l** toxicity at least partly arises due to mitochondrial damage (Figure 2.1.12).
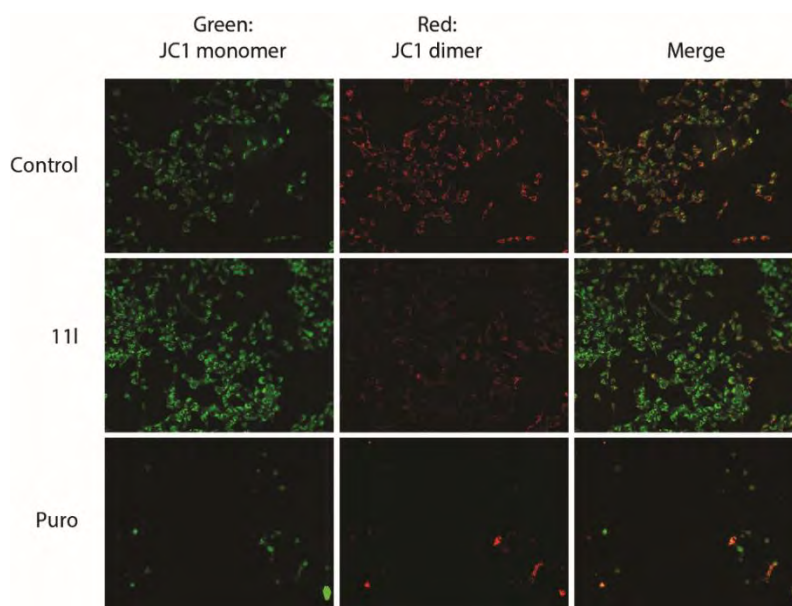
Figure 2.1.12 11l increases mitochondrial depolarization in C4-2 cells. Cells were treated with DMSO, **11l** (10 μM) and Puromycin for 48 h and stained with JC-1. Photographs were taken in FITC (green) and TRITC (red) channel at 20X objective with the fluorescence microscope (Nikon).

2.1.2.2.5 Wound healing assay

Cell migration is involved in numerous pathological processes including metastasis, tumor invasion and neoangiogenesis. As MTs are essential for cell migration, we measured the impact of **11l** on cellular motility using a wound healing assay.
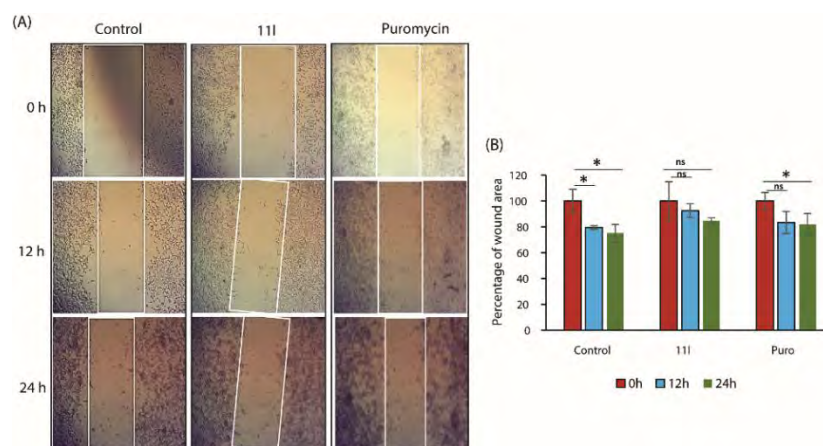
Figure 2.1.13 11l inhibits cell motility in C4-2 cells. (A) C4-2 cells were exposed to DMSO (vehicle control), compound **11l** (10 μM) and Puromycin (positive control). Scratches (wound) were made with sterile 200 μL pipette tip. Images of wounds were captured at 0, 12 and 24 h respectively. (B) The bar graph showing the relative percentage of wound healing area in **11l** and puromycin treated cells with respect to DMSO control cells. The area of wound was calculated using ImageJ software and then percentage of wound healing area was calculated using the following formula, (%) = $(A_{0h} - A_{24h})/A_{0h} \times 100$, where A_{0h} represents the area of initial wound, A_{24h} represents the area of wound at 24 h. Data are mean ± SE of three similar independent experiments.

In the wound healing assay, a mechanical scratch (wound) was created in the absence or presence of **11l** (or puromycin), and the scratches were visualized at 12 h and 24 h (Figure 2.1.13a). Treatment of **11l** indeed reduced cell motility as compared to control both after 12 h and 24 h of treatments, indicating that **11l** should exhibit anti-metastatic potential *in vivo* (Figure 2.1.13).

2.1.2.2.6 Rrestricts colony formation

Colonigenic assay was conducted to examine the effect of **11l** on colony forming ability of C4-2 cells. Compared to the DMSO treated group, **11l** treatment had a significant visible decrease in the number of colonies (Figure 2.1.14A, B). This indicates inhibitory effect of **11l** on cell proliferation.
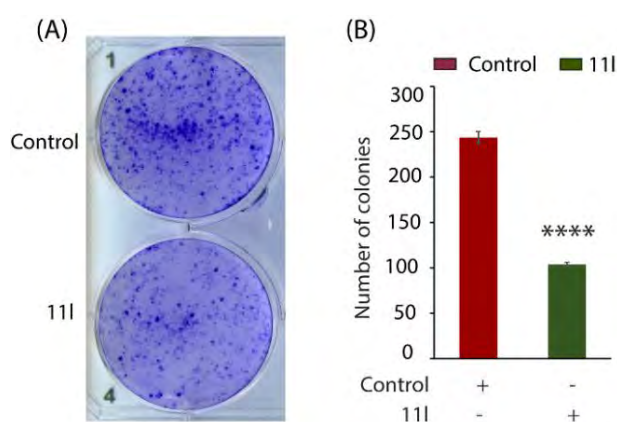
Figure 2.1.14 11l restricts colony formation in C4-2 cells. (A) Equal number of cells (1000/well) were plated in 6 well and treated with DMSO or compound **11l** (10µM). After 10 days cells were fixed, stained with crystal violet and photographed on drying. (B) Bar graph representing the number of colonies in DMSO and **11l** treated groups. The result is representative of 3 biological replicates. Student-t-test was applied for statistical significance. ****$P < 0.0001$ compared to the respective controls.

2.1.2.2.7 Induce tubulin depolymerization and cytokinesis defects

While physiological ROS levels promote cytoskeleton polymerization, oxidation stress induces the F-actin severing and impedes microtubule polymerization. As **11l** promotes oxidative stress, we next analysed whether **11l** has an impact on tubulin polymerization in C4-2 cells. Briefly, C4-2 cells were treated with **11l** for 48 h and then stained for β–tubulin antibody. The images were captured and processed in fluorescent microscope at low and high magnifications. The low magnification images show more cells displaying cytokinesis defects (Figure 2.1.15A) in **11l** treated group. In parallel, high magnification images revealed clear loss of tubulin assembly in **11l** treated group. The tubulin shrunk and condensed towards nucleus

(Figure 2.1.15B). This phenomenon suggests that **11l** promotes tubulin disassembly and cytokinesis defects.
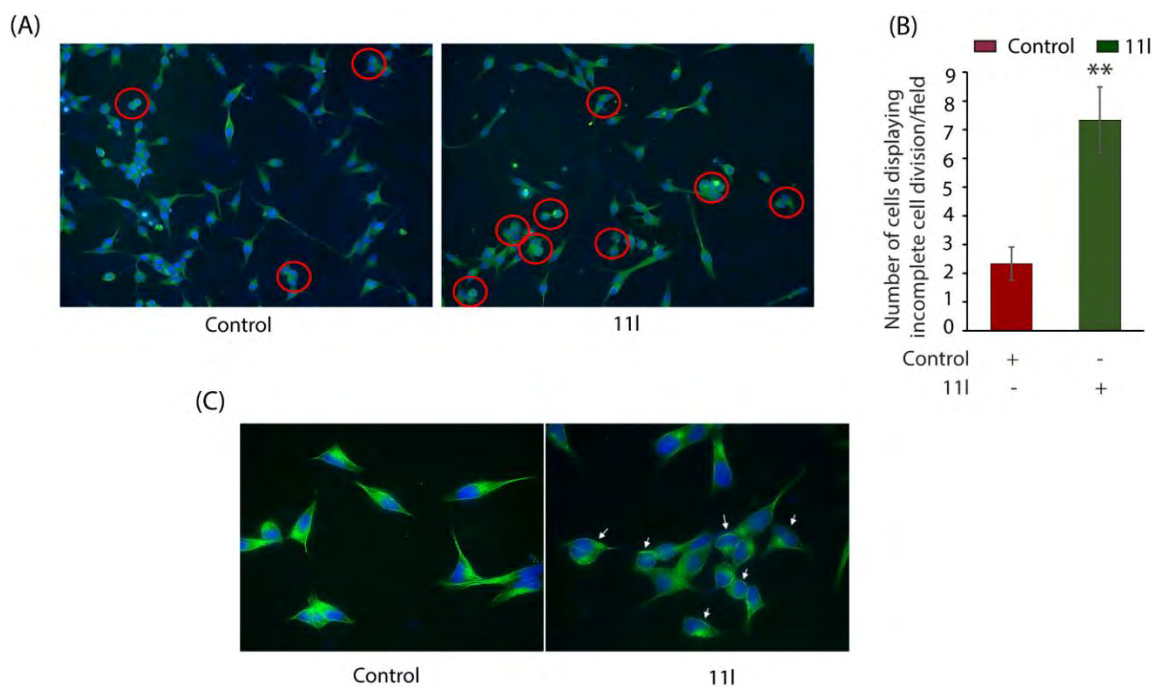
Figure 2.1.15 11l increases depolymerization of tubulin in C4-2 cells. C4-2 cells were treated with DMSO or compound 11l (10 µM) for 48 h. The fluorescence images were captured in FITC secondary antibody (green) to visualise tubulin. Nucleus were visualised by DAPI (blue). (A) Fluorescence images captured at 20X showing a greater number of cells with incomplete cytokinesis in **11l** group. (B) Bar graph showing statistical differences in incomplete cell division between control and **11l** group. Data was analysed using 3 independent replicates. For statistical significance between control and **11l** group, student t-test was applied. **$P < 0.01$. (C) Fluorescence images at 60X showing disruption and depolymerization of tubulin structures in **11l** treated group.

To further confirm whether **11l** has an impact on tubulin dynamics, we measured the relative concentrations of polymerized versus depolymerized tubulin in control and **11l**-treated 22Rv1 cells. As a positive control, colchicine was employed. Colchicine is a highly potent tubulin polymerization inhibitor. As expected, colchicine treatment significantly decreased the levels of polymerized tubulin (~30% to ~10%) as compared to control. **11l** treatment also showed considerably less polymerized tubulin (~30% to ~13%). These findings indicate that at least part of its anti-cancer effect stems from its tubulin-depolymerizing activity which could be ROS-mediated (Figure 2.1.16).
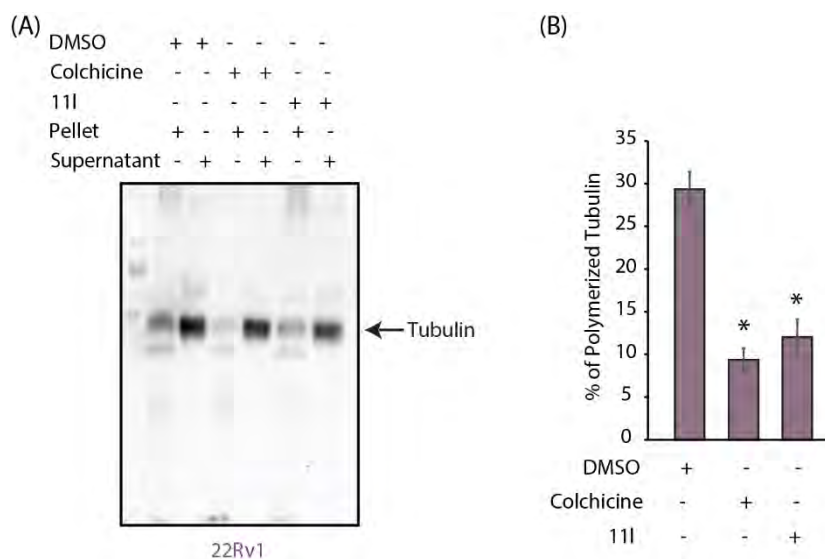
Figure 2.1.16 11l increases depolymerization of tubulin in 22Rv1 cells. (A) 22Rv1 cells were treated with DMSO, colchicine (100 nM) or compound 11l (20 μM) for 24 h. The cells were lysed in hypotonic buffer, and pellet and supernatant were separated using ultracentrifugation. Equal amounts of proteins were loaded in each lane. (B) Data analysis was performed using 3 independent replicates, and statistical significance between DMSO (control), Colchicine, and 11l-treated cells was determined using Student T-test. *P < 0.05.

2.1.2.3 ADME properties of indolylsulfoximine analogues

After the biological studies of **11a-m**, ADME (absorption, distribution, metabolism and excretion) profiling comprising size, solubility, lipophilicity and other drug-likeness properties of indolylsulfoximine derivatives were calculated using online tool Swiss ADME web tool [39] and are presented in Table 2.1.5. For a compound to be a potential lead in drug discovery, the Lipinski′s rule of five in terms of number of hydrogen bond donors less than five, number of hydrogen bond acceptors less than ten, molecular weight of compound less than 500 Dalton and octanol-water partition coefficient less than five, is expected to be followed.[39] As indicated in Table 2.1.5, compounds **11a-m** showed favourable computationally predicted ADME profiles. For all compounds, topological surface area (TPSA), the indicator of membrane penetration, was predicted between 20 and 130 Å2, was found to be within an acceptable range. According to the literature report colchicine is a poorly soluble, highly lipophilic compound that is subject to efflux transporters and extensive first-pass metabolism in the liver. These factors limit its absorption and bioavailability.

The water-octanol partition coefficient values of **11a-m** were found between 2.83 and 4.38 in compliance with several common drugs. The high values of gastrointestinal absorption (GI) for all compounds points out their potential for abnormally active drug. Similarly, the water solubility of a molecule greatly facilitates the ease of handling and synthesis. The absorption property of a drug plays a crucial role in delivering an adequate amount of the active ingredient in a small volume of pharmaceutical dosage for oral administration. In this context, the moderate water solubility (logS -4 to -5) of compounds **11a**, **11b**, **11h**, **11k**, and **11l** is noteworthy, as it suggests their potential to achieve sufficient bioavailability. By comparison, colchicine, a well-known drug with poor water solubility, has a logS of -8.01. Additionally, it is essential to consider the presence of PAINS (Pan Assay Interference) fragments in drug compounds, as they can potentially yield false-positive biological outputs and have reactive, unstable, and toxic characteristics.

The prepared set of *N*-arylated indolylsulfoximines exhibit acceptable physicochemical properties such as solubility, lipophilicity, and compliance with the Lipinski rule of five, as well as pharmacokinetic properties. These factors, taken together, suggest that this set of compounds holds promise for the development of effective therapeutic agents.

Table 2.1.5 ADME properties of *N*-arylated indolylsulfoximine analogues **11a-m**

Compds.	Molecular weight	TPSA (20 to 130 Å2)	Water Solubility	Lipophilicity (-0.7to+5.5)	GI Absorption	Lipinski Rule of five (Druglikeness property)	PAINS #alerts	HBD	HBA	Bioavalibility Score (0 to1)
11a	270.35	53.60	-4.29	3.01	High	Yes	0	1	2	0.55
11b	284.37	53.60	-4.58	3.29	High	Yes	0	1	2	0.55
11c	300.37	62.83	-4.34	2.94	High	Yes	0	1	3	0.55
11d	360.42	81.29	-4.46	2.83	High	Yes	0	1	5	0.55
11e	349.24	53.60	-5.19	3.56	High	Yes	0	1	2	0.55
11f	288.34	53.60	-4.44	3.30	High	Yes	0	1	3	0.55
11g	306.33	53.60	-4.59	3.59	High	Yes	0	1	4	0.55
11h	338.34	53.60	-5.10	4.00	Low	Yes	0	1	5	0.55
11i	330.40	54.99	-5.21	3.28	High	Yes	0	1	3	0.55
11j	390.45	73.45	-5.35	3.17	High	Yes	0	1	5	0.55
11k	379.27	62.83	-5.24	3.49	High	Yes	0	1	4	0.55
11l	**318.36**	**62.83**	**-4.49**	**3.24**	**High**	**Yes**	**0**	**1**	**4**	**0.55**
11m	484.99	70.43	-6.50	4.38	High	Yes	0	1	5	0.55
Colchicine	399.44	83.9	-8.01	3.28	Low	Yes	0	1	6	Low

2.1.3 Conclusions

By employing copper-mediated cross-coupling reactions of *N*-Boc-3-indolylsulfoximines with aryl iodides, we produced a diverse series of *N*-arylated indolylsulfoximines in excellent yields. The precursor indolylsulfoximines were easily accessed from 3-(methylthio)indole by using (diacetoxyiodo)benzene and ammonium carbamate in excellent yields. From the prepared series of *N*-arylated indolylsulfoximines with 5-bromoindole (1.28 µM) and 5-methoxyindole (2.68 µM) moieties were found to be selectively cytotoxic against MCF7 and 22Rv1 cells. **11c** was highly toxic to C4-2 cells (1.95 µM). The compound **11l** bearing fluorine at the C_6-position of indole, endowed broad cytotoxicity against C4-2, PC3, 22Rv1 and MCF7 with IC_{50} values of 8.1, 3.51, 1.91, and 1.7 µM, respectively. HEK293 cells (normal kidney cells) were not affected by these compounds, suggesting their specificity for cancer cells.

Mechanism of action studies suggested that potent compound displayed increased endogenous level of ROS, leading to the increased level of p-53 and c-jun, which ultimately induces apoptosis. Compound **11l** also inhibits tubulin assembly, which could be due to increased oxidative stress. The developed reaction conditions for the synthesis of indolylsulfoximines analogues will be useful for further structural modifications to identify interesting class of anti-cancer agents.

2.1.4 Biology Protocols

2.1.4.1 MTT assay

C4-2, PC-3 and 22Rv1 prostate cancer cells were grown in RPMI 1640 media. HEK293 (human kidney cells) and MCF7 (human breast cancer cells) were maintained in Dulbecco's modified Eagle's media (DMEM). All media were supplemented with 10% FBS, streptomycin (100 µg/mL) and penicillin (100 I.U./mL). For MTT assay, 5 x 10^3 cells/well were seeded in 96-well plates. After 12 h, cells were treated with different concentrations of **11a-m** in a range from 0.1 µM - 40 µM. 0.1% DMSO (vehicle control) was used as control. After 48 h, old media was removed, cells were washed with PBS followed by addition of 100 µL of serum free media and MTT (5mg/ml) cocktail (4:1 ratio) in each well. Cells were incubated for 4 h at 37 °C. MTT was then aspirated, cells were washed with PBS, and then 100 µL DMSO was added to dissolve the formazan crystals. The absorbance was measured at 570 nm using Tecan Spectrafluor Plus. Relative inhibition was calculated as mean absorbance of treated cells/mean absorbance of DMSO treated cells (negative control). The IC_{50} values and dose response curve were obtained by nonlinear regression analysis [non-linear regression (sigmoidal dose response

with variable slope)] using Graph Pad Prism, version 6.0 software (Graph Pad Software Inc., CA, USA).

2.1.4.2 JC-1 staining

To examine the effect of compound **11l** on mitochondrial health and apoptosis, JC-1 staining was performed. Briefly, 0.25×10^5 C4-2 cells were seeded on 12 mm coverslip. After 12 h, the cells were treated with DMSO, **11l** (10 µM) or Puromycin (1µg/ml) for 48 h. The cells were washed with PBS and incubated with JC-1 dye in PBS (2 µM) for 20 min. Cells were washed and images were captured in a fluorescent microscope (Nikon) using FITC (green) and TRITC (red) channels. The healthy mitochondria show more J-aggregates results in emission of orange fluorescence in the TRITC channel whereas the unhealthy or mitochondrial depolarization (marker of cellular apoptosis) results in a loss of JC-1 accumulation and shifting of fluorescence more towards green.

2.1.4.3 Acridine orange-Ethidium Bromide staining

To examine the effect of **11l** compound on the permeability of plasma membrane, chromatin condensation and nuclear morphology, Acridine orange (AO) /Ethidium bromide (EB) staining was performed. Briefly, 0.25×10^5 C4-2 cells were seeded on 12 mm coverslip in 24-well plates. 12 h later, the cells were treated with DMSO, **11l** (10 µM) or Puromycin (1µg/ml) for 48 h. The old media was removed, cells were washed with PBS followed by incubation with the AO/EB (100 µg/mL AO and 100 µg/mL EB) dye mixture in PBS for 20 min. Cells were washed with PBS and imaged in a fluorescent microscope (Nikon) using FITC (green) and TRITC (red) channels. AO permeates through all cells, hence the nucleus appears green, whereas EB appears red only when the cytoplasmic membrane integrity is lost (as in late apoptosis or in necrosis).

2.1.4.4 Measurement of intracellular reactive oxygen species (ROS) levels

To examine the intracellular ROS levels, the 2′,7′-dichlorofluorescein diacetate (H$_2$DCFDA) fluorogenic dye was used. Briefly, 0.25×10^5 C4-2 cells were seeded on 12 mm coverslip, treated with DMSO, **11l** (10 µM) or H$_2$O$_2$ (10 µM) and incubated for 48 h. Cells were washed with PBS and incubated with 100 µl of H$_2$DCFDA in PBS (final concentration 2 µM) for 40 min at 37°C. Thereafter the cells were washed with PBS and intracellular ROS level was observed and imaged using FITC channel in a Nikon inverted fluorescent microscope.

2.1.4.5 Wound healing assay

To investigate the effect of **11l** on migrations of cells, a wound-healing/scratch assay was performed. Briefly, 0.6×10^6 C4-2 cells/well were plated into a 6-well plate and incubated to reach 90% confluence. An equal size wound/scratch was made using a 200 µL tip. Extra detached cells were removed by washing cells with serum-free media. The medium with DMSO, **11l** (10 µM) or Puromycin (1µg/ml) were then added for 48 h. The images of wounds were captured at 0, 12, 24 and 48 h after treatment using inverted microscope (AmScope) under 4X magnification. The percentage wound closure was calculated using the following formula: Wound closure (%) = $(A_{0h} - A_{48h})/A_{0h} \times 100$, where A_{0h} represents the area of initial wound, A_{48h} represents the area of wound at 48 h.

2.1.4.6 Western blot analysis

C4-2 cells were treated with DMSO, **11l** (10 µM) or puromycin (1µg/ml) for 48 h. Cells were washed with PBS and lysed in modified RIPA lysis buffer. The proteins were resolved by 12% SDS-PAGE gel electrophoresis, and transferred at polyvinylidene difluoride (PVDF) membrane, followed by blocking in 5% skim milk (0.1% TBST). The membrane was incubated overnight at 4 ºC with p53 (1:1000), c-Jun (1:1000) or tubulin (1:5000) primary antibodies. p53 and c-Jun antibodies were purchased from Santa Cruz Biotech (USA). Tubulin hybridoma was purchased from Developmental Studies Hybridoma Bank (DHSB). PVDF membrane was washed with 0.1% TBST and incubated with secondary antibody (HRP-conjugated) for 1 h at room temperature. The proteins were visualized using chemiluminescence detection reagent (Pierce Biotechnology) in GeneGnomeXRQ chemiluminescence imager.

2.1.4.7 Tubulin polymerization assay

22Rv1 cells were plated 16 h prior to the treatment with the corresponding drugs. The cells were treated with either 20 µM of 11l or 100 nM of colchicine for 24 h at 37 ºC. Colchicine was used as a positive control. The cells were lysed using hypotonic buffer (1 mM $MgCl_2$, 2 mM EGTA, 0.5% NP40, 2 mM phenylmethylsulfonyl fluoride, 20 mM Tris HCl pH 6.8). Ultracentrifugation was used to separate the pellet and supernatant containing the polymerized and depolymerized tubulin respectively. The lysis buffer was used to resuspend the pellet followed by a Bradford assay for protein quantification. Equal amounts of the pellet and supernatant fractions were loaded onto a 12% SDS-PAGE gel, and immunoblotting was used for tubulin detection. The percentage of polymerized tubulin was calculated by using the formula% P=P/(P+S) $\times 100$.[40]

2.1.4.8 Immunofluorescence

22Rv1 cells were plated in on poly-lysine -coated cover slips. After 16 h, the cells were treated with DMSO (control), Colchicine and **11l**, respectively. After 24 h, the cells were fixed and permeabilized with iced cold methanol. A blocking solution (2% BSA and 1% Triton X-100 in 1X PBS) was used for non-specific blocking for 1 h. The poly-lysine-coated cover slips containing cells were subsequently incubated with tubulin primary antibody overnight at 4 °C. The conjugated secondary antibody goat anti-mouse-FITCwas used for 3 h in the dark, and images were captured using a BZ-X810 Keyence fluorescence microscope.

2.1.5 Experimental Section

2.1.5.1 General Methods

All the laboratory reagents were purchased from Sigma-Aldich, Alfa Aesar and Spectrochem India Pvt. Ltd and used without further purification. The reactions were monitored by thin layer chromatography and performed on Merck pre-coated plates (silica gel 60 F_{254}, 0.2mm). Column chromatographic purification of products was carried out using silica gel (100-200 mesh) and ethyl acetate/hexane mixture was used for elution. ^{1}H NMR spectra and ^{13}C NMR spectra were recorded at 400 MHz and 100 MHz using $CDCl_3$ and DMSO-d_6 solutions. Chemical shifts are given in ppm relative to the residual solvent peak (^{1}H NMR: $CDCl_3$ δ 7.26; DMSO-d_6 δ 2.50; ^{13}C NMR: $CDCl_3$ δ 77.0; DMSO-d_6 δ 39.52) with multiplicity (s = singlet, d = doublet, t = triplet, q = quartet, m = multiplet), coupling constants (*J*, in Hz) and integration. Melting points were determined by using E-Z melting point apparatus and are uncorrected. High-resolution mass data (HRMS) were obtained on IMQ-TOF 6560 Agilent, Purdue University, USA.

2.1.5.2 General procedure for the synthesis of compounds 6 and 8: To a solution of indole **6** (1.5 g, 0.21 mmol) in acetonitrile (5 mL), DMSO (1.1 equiv) and TMSCl (1.1 equiv) were added in one portion at 0 °C. The reaction mixture was allowed to reflux for 3 h (the reaction was closely monitored by TLC). Upon completion of the reaction, solid sulfonium salt (93% yield) was filtered washed with ethyl acetate and directly used for next step. Next, sulfonium salt and diisopropylamine were refluxed for 2 h at 80 °C under nitrogen atmosphere. Cooled the reaction mixture at room temperature, diisopropylamine was evaporated to dryness in vacuo. The residue thus obtained was purified by column chromatography (Hexane/EtOAc) to furnish 3-methylthioindole **7a** in 90% yield.

Further reaction of 3-methylthioindole **7a** (1 g, 5 mmol) with Boc$_2$O (2.18 g, 10 mmol) in the presence of *N,N*-dimethylpyridin-4-amine (0.915 g, 7.5 mmol) the reaction mixture was stirred magnetically at 0-25 °C temperature until TLC revealed the complete consumption of the starting material. Solvent was evaporated on the rota-vapor and the reaction mixture poured into water (150 mL) and organic layer was extracted in ethylacetate (2 × 40 mL). The extracted organic layer was washed with saturated sodium bicarbonate (50 mL) and brine (50 mL) solution. Evaporated the organic phase under reduced pressure and the residue obtained was purified by silica gel column chromatography (ethyl acetate: hexane as eluent) to obtain pure *N*-boc-3-methylthioindole (off white solid at 4 °C) **8a** in 92% yield. Similarly, compounds **8b-e** were prepared in 92-95% yields.

2.1.5.3 General experimental procedure for the synthesis of indolylsulfoximine (9a-e)

To a methanolic solution of *N*-boc-3-methylthioindole **8** (1 mmol) was added, IBD (3 mmol), and ammonium carbamate (2 mmol) at 25 °C temperature. The contents were stirred until completion of the reaction as monitored by the TLC. The solvent was evaporated under reduced pressure by using a rota evaporator. The residue thus obtained was purified by silica gel column chromatography (ethyl acetate: hexane as eluent) to get the sulfoximine **9a** in 90% yield. Similarly, sulfoximines **9b** and **-9e** were prepared in 81% and 89% yields, respectively.

N-boc-3-indolylsulfoximine (9a):
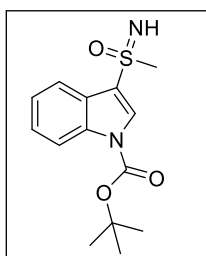
Off-white solid, 90% yield, mp 120-126°C; ^{1}H NMR (400 MHz, CDCl$_3$) δ 8.27 (d, *J* = 8.2 Hz, 1H), 8.20 (s, 1H), 8.02 (d, *J* = 7.8 Hz, 1H), 7.50 – 7.38 (m, 2H), 3.28 (s, 3H), 1.71 (s, 9H). ^{13}C NMR (100 MHz, CDCl$_3$) δ 148.57, 135.99, 130.98, 125.94, 125.39, 124.36, 123.30, 119.98, 115.76, 85.80, 46.03, 28.09.

5-methoxy-N-Boc-3-indolylsulfoximine (9b):
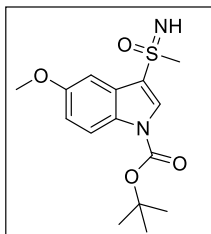
White solid, 85% yield, mp 122-126 °C; ^{1}H NMR (400 MHz, CDCl$_3$) δ 8.12 (s, 1H), 8.09 (d, *J* = 9.2 Hz, 1H), 7.42 (d, *J* = 2.5 Hz, 1H), 7.02 (dd, *J* = 9.2, 2.5 Hz, 1H), 3.87 (s, 3H), 3.23 (s, 3H), 1.67 (s, 9H); ^{13}C NMR (100 MHz, CDCl$_3$) δ 156.99, 148.51, 131.15, 130.46, 126.30, 116.58, 115.28, 101.83, 85.59, 55.79, 46.02, 28.06.

5-bromo-*N*-Boc-3-indolylsulfoximine (9c):
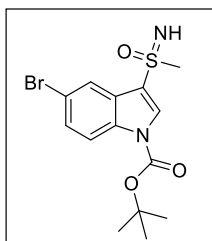
Off-white solid, 88% yield, mp 125-129 °C; ^{1}H NMR (400 MHz, CDCl$_3$) δ 8.20 – 8.17 (m, 2H), 8.14 (d, *J* = 8.9 Hz, 1H), 7.55 (dd, *J* = 8.9, 2.1 Hz, 1H), 3.26 (s, 3H), 1.70 (s, 9H); ^{13}C NMR (100 MHz, CDCl$_3$) δ 148.21, 134.68, 131.74, 129.01, 127.01, 122.82, 122.75, 118.02, 117.20, 86.31, 46.29, 29.70, 28.06.

6-fluoro-*N*-Boc-3-indolylsulfoximine (9d):
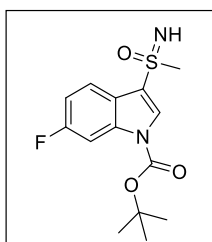
Off-white solid, 89% yield, mp 128-133 °C ^{1}H NMR (400 MHz, CDCl$_3$) δ 8.16 (s, 1H), 8.03 – 7.87 (m, 2H), 7.15 (t, *J* = 9.0 Hz, 1H), 3.25 (s, 3H), 1.70 (s, 9H); ^{13}C NMR (100 MHz, CDCl$_3$) δ 162.75, 160.33, 148.30, 136.31, 131.11, 123.46, 121.73, 120.99, 112.99, 112.75, 103.29, 103.01, 86.24, 46.25, 28.04.

4-chloro-benzylchloride-3-indolylsulfoximine (9e):
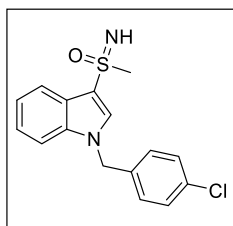
White solid, 81% yield, mp 140-144 °C. ^{1}H NMR (400 MHz, CDCl$_3$) δ 8.09-8.05 (m, 1H), 7.73 (s, 1H), 7.35-7.33 (m, 4H), 7.32 (s, 1H), 7.13 (d, *J* = 8.5 Hz, 2H), 5.33 (s, 2H), 3.26 (s, 3H); ^{13}C NMR (100 MHz, CDCl$_3$) δ 136.98, 134.41, 133.85, 132.87, 129.33, 128.56, 124.82, 123.84, 122.49, 120.13, 117.91, 50.29, 46.82.

2.1.5.4 General experimental procedure for *N*-arylindol yl sulfoximines (11a-m):

A mixture of indolylsulfoximine **9** (0.33 mmol), aryl iodide (0.39 mmol), 1,10-phenanthroline (0.062 mmol), CuI (0.03 mmol), Cs$_2$CO$_3$ (0.82 mmol) in dry DMF (3mL) was taken into 10 mL microwave vial. The vial was evacuated and filled with nitrogen. Reaction continued until consumption of starting materials as shown by thin layer chromatography. After completion of the reaction, the contents were allowed to reach room temperature. Poured the contents into crushed ice and extracted with chloroform (3×100 mL), washed with saturated brine (3×50 mL), dried over anhydrous sodium sulfate, removed excess of solvent and purified by column chromatography (ethyl acetate: hexane as eluent) to obtain products **11a-m** in high yields.

N-phenyl-1*H*-indole-3-sulfoximine (11a):
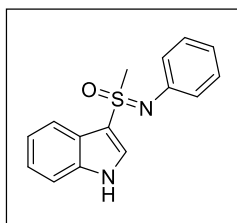
Colorless oil at 25°C, 91% yield. ^{1}H NMR (400 MHz, CDCl$_3$) δ 8.12 (dd, J = 7.2, 2.1 Hz, 1H), 7.93 (s, 1H), 7.62 – 7.55 (m, 3H), 7.55 – 7.48 (m, 4H), 7.39 – 7.35 (m, 2H), 3.32 (s, 3H); ^{13}C NMR (100 MHz, CDCl$_3$) δ 137.95, 137.09, 132.83, 130.02, 128.30, 124.88, 124.81, 124.23, 122.88, 120.08, 111.58, 46.66. HRMS (ESI) *m/z* calcd for C$_{15}$H$_{14}$N$_2$OS: 271.0860 (M + H)$^+$, found: 271.0898.

4-tolyl-*N*-phenyl-1*H*-indole-3-sulfoximine (11b):
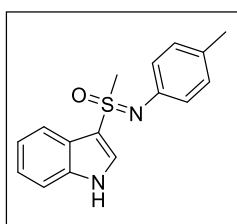
Colorless oil at 25°C, 86% yield. ^{1}H NMR (400 MHz, CDCl$_3$) δ 8.12 – 8.07 (m, 1H), 7.92 (s, 1H), 7.53 – 7.49 (m, 1H), 7.38 (s, 3H), 7.37 – 7.34 (m, 2H), 3.34 (s, 3H), 2.48 (s, 3H); ^{13}C NMR (100 MHz, CDCl$_3$) δ 138.44, 137.24, 135.34, 133.11, 130.54, 124.76, 124.68, 124.15, 122.83, 119.96, 118.29, 111.65, 111.61, 46.46, 21.17. HRMS (ESI) *m/z* calcd for C$_{16}$H$_{16}$N$_2$OS: 285.1017 (M + H)$^+$, found: 285.1050.

4-methoxy-*N*-phenyl-1*H*-indole-3-sulfoximine (11c):
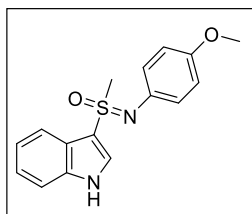
Colorless oil at 25°C, 85% yield. ^{1}H NMR (400 MHz, CDCl$_3$) δ 8.12 – 8.06 (m, 1H), 7.89 (s, 1H), 7.48 – 7.44 (m, 1H), 7.41 (d, J = 8.9 Hz, 2H), 7.37 – 7.33 (m, 2H), 7.08 (d, J = 8.9 Hz, 2H), 3.91 (s, 3H), 3.35 (s, 3H). ^{13}C NMR (100 MHz, CDCl$_3$) δ 159.50, 137.58, 133.37, 130.64, 126.37, 124.51, 124.15, 122.81, 122.77, 119.89, 117.63, 115.09, 111.60, 55.69, 46.54. HRMS (ESI) *m/z* calcd for C$_{16}$H$_{16}$N$_2$O$_2$S: 301.0966 (M + H)$^+$, found: 301.1000.

3,4,5-trimethoxy-*N*-phenyl-1*H*-indole-3-sulfoximine (11d):
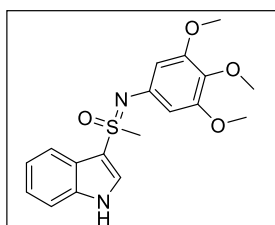
White solid, 87% yield; ^{1}H NMR (400 MHz, CDCl$_3$) δ 8.10 (dd, J = 6.1, 2.7 Hz, 1H), 7.96 (s, 1H), 7.57 (dd, J = 6.0, 3.1 Hz, 1H), 7.38 (dd, J = 6.2, 3.2 Hz, 2H), 6.72 (s, 2H), 3.94 (s, 3H), 3.92 (s, 6H), 3.37 (s, 3H); ^{13}C NMR (100 MHz, CDCl$_3$) δ 154.08, 137.96, 137.27, 133.50, 133.21, 124.62, 124.35, 123.01, 120.03, 111.68, 102.59, 61.08, 56.45, 46.46. HRMS (ESI) *m/z* calcd for C$_{18}$H$_{20}$N$_2$O$_4$S: 361.1177 (M + H)$^+$, found: 361.1209.

4-bromo-*N*-phenyl-1*H*-indole-3-sulfoximine(11e):
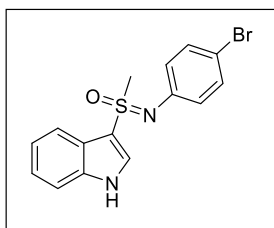
Colorless oil at 25°C, 81% yield; ^{1}H NMR (400 MHz, CDCl$_3$) δ 9.13 (s, 1H), 7.95 (d, *J* = 8.2 Hz, 1H), 7.80 (s, 1H), 7.45 (d, *J* = 7.5 Hz, 1H), 7.31 (s, 2H), 7.18 (d, *J* = 8.1 Hz, 2H), 6.99 (d, *J* = 8.1 Hz, 2H), 3.37 (s, 3H); ^{13}C NMR (100 MHz, CDCl$_3$) δ 144.94, 136.44, 131.71, 131.60, 124.77, 124.05, 123.61, 122.61, 119.57, 114.17, 112.30, 46.63. HRMS (ESI) *m/z* calcd for C$_{15}$H$_{13}$BrN$_2$OS: 347.9932 and 349.9911 (M + H)$^+$, found: 348.9991 and 350.9973.

4-fluoro-*N*-phenyl-1*H*-indole-3-sulfoximine (11f):
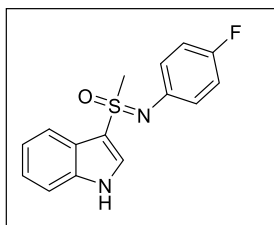
Colorless oily at 25°C, 83% yield; ^{1}H NMR (400 MHz, CDCl$_3$) δ 8.14 – 8.10 (m, 1H), 7.89 (s, 1H), 7.52 – 7.46 (m, 3H), 7.41 – 7.37 (m, 2H), 7.31 (d, *J* = 8.1 Hz, 2H), 3.33 (s, 3H); ^{13}C NMR (101 MHz, CDCl$_3$) δ 163.34, 160.86, 137.30, 133.98, 132.81, 126.90, 126.82, 124.67, 124.37, 122.97, 120.14, 117.14, 116.91, 111.30, 46.66. HRMS (ESI) *m/z* calcd for C$_{15}$H$_{13}$FN$_2$OS: 289.0766 (M + H)$^+$, found: 289.0801.

3,4-difluoro-*N*-phenyl-1*H*-indole-3-sulfoximine (11g):
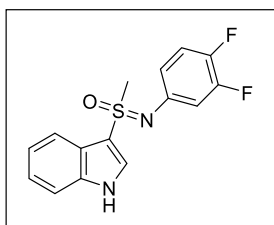
Colorless oil at 25°C, 85% yield; ^{1}H NMR (400 MHz, DMSO-*d*$_6$) δ 8.15 (s, 1H), 8.02 – 7.98 (m, 1H), 7.92 (ddd, *J* = 11.3, 7.1, 2.6 Hz, 1H), 7.71 (dt, *J* = 10.4, 8.9 Hz, 1H), 7.61 – 7.54 (m, 2H), 7.40 – 7.33 (m, 2H), 3.19 (s, 3H) ; ^{13}C NMR (100 MHz, DMSO-*d*$_6$) δ 136.59, 133.40, 125.04, 124.53, 122.91, 122.41, 120.87, 120.50, 119.16, 118.97, 115.48, 115.29, 111.82, 47.17. ^{19}F NMR (376 MHz, DMSO) δ -135.34, -135.40, -139.01, -139.07. HRMS (ESI) *m/z* calcd for C$_{15}$H$_{12}$F$_2$N$_2$OS: 307.0672 (M + H)$^+$, found: 307.0707.

3-trifluoromethyl-*N*-phenyl-1*H*-indole-3-sulfoximine (11h):
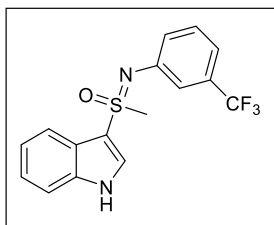
Light orange oil at 25°C, 83% yield. ^{1}H NMR (400 MHz, CDCl$_3$) δ 8.08 (dd, *J* = 8.7, 5.2 Hz, 1H), 7.93 (s, 1H), 7.80 – 7.76 (m, 2H), 7.76 – 7.71 (m, 1H), 7.22 – 7.13 (m, 2H), 3.32 (s, 3H); ^{13}C NMR (100 MHz, CDCl$_3$) δ 138.47, 136.76, 132.24, 130.71, 127.92, 124.81, 124.62, 123.18, 121.71, 120.26, 111.02, 46.53. HRMS (ESI) *m/z* calcd for C$_{16}$H$_{13}$F$_3$N$_2$OS: 339.0734 (M + H)$^+$, found: 339.0769.

5-methoxy-1*H*-indol-3yl(4-methoxy-*N*-phenyl)-1*H*-indole-3-sulfoximine(11i):
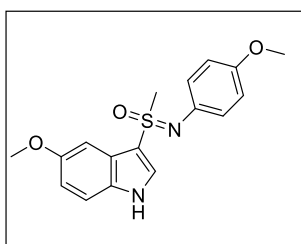
Yellow oil, at 25°C 88% yield; ^{1}H NMR (400 MHz, CDCl$_3$) δ 7.86 (s, 1H), 7.51 (d, *J* = 2.4 Hz, 1H), 7.43 – 7.38 (m, 2H), 7.34 (d, *J* = 9.1 Hz, 1H), 7.09 – 7.05 (m, 2H), 6.98 (dd, *J* = 9.1, 2.4 Hz, 1H), 3.92 (s, 3H), 3.91 (s, 3H), 3.38 (s, 3H); ^{13}C NMR (100 MHz, CDCl$_3$) δ 159.48, 156.40, 133.45, 132.48, 130.74, 126.20, 125.30, 115.07, 114.83, 112.62, 100.85, 55.98, 55.67, 46.27; HRMS (ESI) *m/z* calcd for C$_{17}$H$_{18}$N$_2$O$_3$S: 331.1072 (M + H)$^+$, found: 331.1102.

5-methoxy-1*H*-indol-3-yl)(3,4,5-tri-methoxyphenyl)sulfoximine (11j):
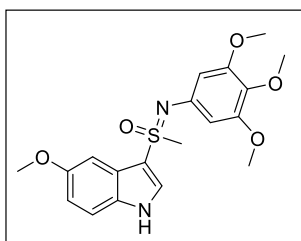
White solid, 91% yield. ^{1}H NMR (400 MHz, CDCl$_3$) δ 7.87 (s, 1H), 7.52 (d, *J* = 2.4 Hz, 1H), 7.45 (d, *J* = 9.1 Hz, 1H), 7.00 (dd, *J* = 9.0, 2.5 Hz, 1H), 6.70 (s, 2H), 3.93 (s, 3H), 3.92 (d, *J* = 2.3 Hz, 9H), 3.32 (s, 3H).; ^{13}C NMR (100 MHz, CDCl$_3$) δ 155.79, 154.02, 137.18, 133.98, 133.48, 131.58, 125.91, 119.44, 114.05, 113.23, 102.65, 60.62, 56.68, 55.99, 47.11. HRMS (ESI) *m/z* calcd for C$_{19}$H$_{22}$N$_2$O$_5$S: 391.1283 (M+H)$^+$, found: 391.1326.

(5-bromo-1*H*-indol-3-yl)(4-methoxyphenyl)sulfoximine (11k):
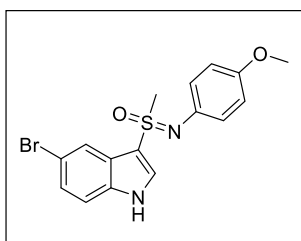
Light yellow oil, at 25°C 84% yield; ^{1}H NMR (400 MHz, CDCl$_3$) δ 8.26 (d, *J* = 1.9 Hz, 1H), 7.93 (s, 1H), 7.46 – 7.37 (m, 3H), 7.31 (d, *J* = 8.8 Hz, 1H), 7.10 – 7.05 (m, 2H), 3.91 (s, 3H), 3.39 (s, 3H).); ^{13}C NMR (100 MHz, CDCl$_3$) δ 159.74, 136.27, 134.33, 130.18, 127.29, 126.37, 126.06, 122.54, 116.45, 115.19, 113.10, 55.70, 46.68. HRMS (ESI) *m/z* calcd for C$_{16}$H$_{15}$BrN$_2$O$_2$S: 379.0038 (M+H)$^+$, found: 379.0905.

(6-fluoro-*1H*-indol-3yl)(4-methoxyphenyl)sulfoximine (11l):

Colorless oil, 82% yield; ^{1}H NMR (400 MHz, CDCl$_3$) δ 9.24 (s, 1H), 8.31 (d, *J* = 9.0 Hz, 1H), 7.87 (s, 1H), 7.85 (s, 1H), 7.70 (d, *J* = 8.1 Hz, 1H), 7.39 (d, *J* = 9.0 Hz, 2H), 7.09 (dd, *J* = 8.7, 2.0 Hz, 2H), 3.91 (s, 3H), 3.34 (s, 3H).); ^{13}C NMR (100 MHz, CDCl$_3$) δ 159.67, 159.60, 137.84, 137.72, 136.33, 133.72, 130.31, 126.26, 123.29, 120.96, 118.38, 115.20, 111.81, 111.56, 98.29, 98.02, 55.69, 46.71; HRMS (ESI) *m/z* calcd for C$_{16}$H$_{15}$FN$_2$O$_2$S: 319.0872 (M+H)$^+$, found: 319.0905.
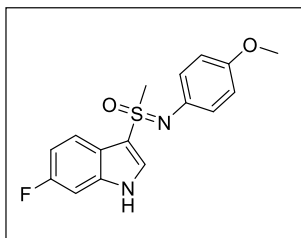
(1-(4-chlorobenzyl)-1*H*-indol-3yl)(methyl)3,4,5-trimethoxyphenyl)sulfoximine (11m):
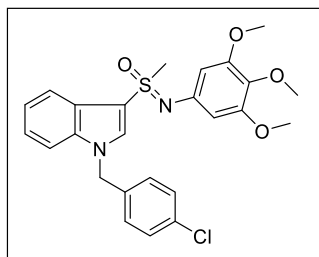
Off-white solid, 81% yield. ^{1}H NMR (400 MHz, CDCl$_3$) δ 8.05 (s, 1H), 7.78 (s, 1H), 7.33 (s, 2H), 7.31 (s, 1H), 7.03 (d, *J* = 8.3 Hz, 2H), 6.37 (s, 2H), 5.32 (s, 2H), 3.75 (s, 3H), 3.67 (s, 6H), 3.50 (s, 3H).^{13}C NMR (100 MHz, CDCl$_3$) δ 153.09, 136.93, 134.71, 134.51, 133.57, 129.38, 128.41, 124.79, 124.09, 122.84, 120.10, 110.92, 101.04, 60.89, 55.88, 50.39, 46.14. HRMS (ESI) *m/z* calcd for C$_{25}$H$_{25}$ClN$_2$O$_4$S: 486.1194 (M+H)$^+$, found: 485.1280.

2.1.6 References

1. Mäder, P.; Kattner, L., Sulfoximines as rising stars in modern drug discovery? Current status and perspective on an emerging functional group in medicinal chemistry. *Journal of Medicinal Chemistry* **2020,** *63* (23), 14243-14275.

2. Sun, H.; Tawa, G.; Wallqvist, A., Classification of scaffold-hopping approaches. *Drug Discovery Today* **2012,** *17* (7-8), 310-324.

3. Harris, C. C.; Hollstein, M., Clinical implications of the p53 tumor-suppressor gene. *New England Journal of Medicine* **1993,** *329* (18), 1318-1327.

4. Honore, S.; Pasquier, E.; Braguer, D., Understanding microtubule dynamics for improved cancer therapy. *Cellular and Molecular Life Sciences CMLS* **2005,** *62* (24), 3039-3056.

5. Pellegrini, F.; Budman, D. R., Tubulin function, action of antitubulin drugs, and new drug development. *Cancer Investigation* **2005,** *23* (3), 264-273.

6. Jordan, M. A.; Wilson, L., Microtubules as a target for anticancer drugs. *Nature Reviews Cancer* **2004,** *4* (4), 253-265.

7. Khachatryan, H.; Olszowy, B.; Barrero, C. A.; Gordon, J.; Perez-Leal, O., Identification of Inhibitors of Tubulin Polymerization Using a CRISPR-Edited Cell Line with Endogenous Fluorescent Tagging of β-Tubulin and Histone H1. *Biomolecules* **2023,** *13* (2), 249.

8. Chen, J.; Wang, Z.; Li, C.-M.; Lu, Y.; Vaddady, P. K.; Meibohm, B.; Dalton, J. T.; Miller, D. D.; Li, W., Discovery of novel 2-aryl-4-benzoyl-imidazoles targeting the colchicines binding site in tubulin as potential anticancer agents. *Journal of Medicinal Chemistry* **2010,** *53* (20), 7414-7427.

9. Chen, J.; Li, C.-M.; Wang, J.; Ahn, S.; Wang, Z.; Lu, Y.; Dalton, J. T.; Miller, D. D.; Li, W., Synthesis and antiproliferative activity of novel 2-aryl-4-benzoyl-imidazole

derivatives targeting tubulin polymerization. *Bioorganic & Medicinal Chemistry* **2011,** *19* (16), 4782-4795.

10. Chen, J.; Ahn, S.; Wang, J.; Lu, Y.; Dalton, J. T.; Miller, D. D.; Li, W., Discovery of novel 2-aryl-4-benzoyl-imidazole (ABI-III) analogues targeting tubulin polymerization as antiproliferative agents. *Journal of Medicinal Chemistry* **2012,** *55* (16), 7285-7289.

11. Tantak, M. P.; Klingler, L.; Arun, V.; Kumar, A.; Sadana, R.; Kumar, D., Design and synthesis of bis (indolyl) ketohydrazide-hydrazones: Identification of potent and selective novel tubulin inhibitors. *European Journal of Medicinal Chemistry* **2017,** *136*, 184-194.

12. Etienne-Manneville, S., From signaling pathways to microtubule dynamics: the key players. *Current Opinion in Cell Biology* **2010,** *22* (1), 104-111.

13. Cao, X.; Sun, Z.; Cao, Y.; Wang, R.; Cai, T.; Chu, W.; Hu, W.; Yang, Y., Design, synthesis, and structure–activity relationship studies of novel fused heterocycles-linked triazoles with good activity and water solubility. *Journal of Medicinal Chemistry* **2014,** *57* (9), 3687-3706.

14. Feng, Z.; Lu, X.; Gan, L.; Zhang, Q.; Lin, L., Xanthones, a promising anti-inflammatory scaffold: structure, activity, and drug likeness analysis. *Molecules* **2020,** *25* (3), 598.

15. Gao, F.; Wang, T.; Xiao, J.; Huang, G., Antibacterial activity study of 1, 2, 4-triazole derivatives. *European Journal of Medicinal Chemistry* **2019,** *173*, 274-281.

16. Ren, Y.; Ma, Y.; Cherukupalli, S.; Tavis, J. E.; Menéndez-Arias, L.; Liu, X.; Zhan, P., Discovery and optimization of benzenesulfonamides-based hepatitis B virus capsid modulators via contemporary medicinal chemistry strategies. *European Journal of Medicinal Chemistry* **2020,** *206*, 112714.

17. Sravanthi, T.; Manju, S., Indoles—A promising scaffold for drug development. *European Journal of Pharmaceutical Sciences* **2016,** *91*, 1-10.

18. Gao, F.; Zhang, X.; Wang, T.; Xiao, J., Quinolone hybrids and their anti-cancer activities: An overview. *European Journal of Medicinal Chemistry* **2019,** *165*, 59-79.

19. La Regina, G.; Sarkar, T.; Bai, R.; Edler, M. C.; Saletti, R.; Coluccia, A.; Piscitelli, F.; Minelli, L.; Gatti, V.; Mazzoccoli, C., New arylthioindoles and related bioisosteres at the sulfur bridging group. 4. Synthesis, tubulin polymerization, cell growth inhibition, and molecular modeling studies. *Journal of Medicinal Chemistry* **2009,** *52* (23), 7512-7527.

20. Wang, Y.-M.; Hu, L.-X.; Liu, Z.-M.; You, X.-F.; Zhang, S.-H.; Qu, J.-R.; Li, Z.-R.; Li, Y.; Kong, W.-J.; He, H.-W., N-(2, 6-dimethoxypyridine-3-yl)-9-methylcarbazole-3-sulfonamide as a novel tubulin ligand against human cancer. *Clinical Cancer Research* **2008,** *14* (19), 6218-6227.

21. De Martino, G.; La Regina, G.; Coluccia, A.; Edler, M. C.; Barbera, M. C.; Brancale, A.; Wilcox, E.; Hamel, E.; Artico, M.; Silvestri, R., Arylthioindoles, potent inhibitors of tubulin polymerization. *Journal of Medicinal Chemistry* **2004,** *47* (25), 6120-6123.

22. Chen, P.; Zhuang, Y.-X.; Diao, P.-C.; Yang, F.; Wu, S.-Y.; Lv, L.; You, W.-W.; Zhao, P.-L., Synthesis, biological evaluation, and molecular docking investigation of 3-amidoindoles as potent tubulin polymerization inhibitors. *European Journal of Medicinal Chemistry* **2019,** *162*, 525-533.

23. Chiou, C. T.; Chen, G. S.; Chen, M. L.; Li, H.; Shi, L.; Huang, X. H.; Dai, W. M.; Chern, J. W., Synthesis of anti‐microtubule N‐(2‐Arylindol‐7‐yl) benzenesulfonamide derivatives and their antitumor mechanisms. *ChemMedChem* **2010,** *5* (9), 1489-1497.

24. Frings, M.; Bolm, C.; Blum, A.; Gnamm, C., Sulfoximines from a medicinal chemist's perspective: physicochemical and in vitro parameters relevant for drug discovery. *European Journal of Medicinal Chemistry* **2017,** *126*, 225-245.

25. Bull, J. A.; Degennaro, L.; Luisi, R., Straightforward strategies for the preparation of NH-sulfoximines: a serendipitous story. *Synlett* **2017,** *28* (19), 2525-2538.

26. Lücking, U., Sulfoximines: a neglected opportunity in medicinal chemistry. *Angewandte Chemie International Edition* **2013,** *52* (36), 9399-9408.

27. Chinthakindi, P. K.; Naicker, T.; Thota, N.; Govender, T.; Kruger, H. G.; Arvidsson, P. I., Sulfonimidamides in medicinal and agricultural chemistry. *Angewandte Chemie International Edition* **2017,** *56* (15), 4100-4109.

28. Lücking, U.; Scholz, A.; Lienau, P.; Siemeister, G.; Kosemund, D.; Bohlmann, R.; Briem, H.; Terebesi, I.; Meyer, K.; Prelle, K., Identification of atuveciclib (BAY 1143572), the first highly selective, clinical PTEFb/CDK9 inhibitor for the treatment of cancer. *ChemMedChem* **2017,** *12* (21), 1776-1793.

29. Foote, K. M.; Nissink, J. W. M.; McGuire, T.; Turner, P.; Guichard, S.; Yates, J. W.; Lau, A.; Blades, K.; Heathcote, D.; Odedra, R., Discovery and characterization of AZD6738, a potent inhibitor of ataxia telangiectasia mutated and Rad3 related (ATR) kinase with application as an anticancer agent. ACS Publications: 2018.

30. Sirvent, J. A.; Lücking, U., Novel pieces for the emerging picture of sulfoximines in drug discovery: synthesis and evaluation of sulfoximine analogues of marketed drugs and advanced clinical candidates. *ChemMedChem* **2017,** *12* (7), 487-501.

31. Lücking, U., Neglected sulfur (VI) pharmacophores in drug discovery: exploration of novel chemical space by the interplay of drug design and method development. *Organic Chemistry Frontiers* **2019,** *6* (8), 1319-1324.

32. Zenzola, M.; Doran, R.; Degennaro, L.; Luisi, R.; Bull, J. A., Transfer of electrophilic NH using convenient sources of ammonia: direct synthesis of NH sulfoximines from sulfoxides. *Angewandte Chemie* **2016,** *128* (25), 7319-7323.

33. Tota, A.; Zenzola, M.; Chawner, S. J.; St John-Campbell, S.; Carlucci, C.; Romanazzi, G.; Degennaro, L.; Bull, J. A.; Luisi, R., Synthesis of NH-sulfoximines from sulfides by chemoselective one-pot N-and O-transfers. *Chemical Communications* **2017,** *53* (2), 348-351.

34. Lohier, J.-F.; Glachet, T.; Marzag, H.; Gaumont, A.-C.; Reboul, V., Mechanistic investigation of the NH-sulfoximination of sulfide. Evidence for λ 6-sulfanenitrile intermediates. *Chemical Communications* **2017,** *53* (12), 2064-2067.

35. Glachet, T.; Franck, X.; Reboul, V., Late-Stage Sulfoximination: Improved Synthesis of the Anticancer Drug Candidate Atuveciclib. *Synthesis* **2019,** *51* (04), 971-975.

36. Reisenbauer, J. C.; Green, O.; Franchino, A.; Finkelstein, P.; Morandi, B., Late-stage diversification of indole skeletons through nitrogen atom insertion. *Science* **2022,** *377* (6610), 1104-1109.

37. Xie, Y.; Zhou, B.; Zhou, S.; Zhou, S.; Wei, W.; Liu, J.; Zhan, Y.; Cheng, D.; Chen, M.; Li, Y., Sulfimine‐Promoted Fast O Transfer: One‐step Synthesis of Sulfoximine from Sulfide. *ChemistrySelect* **2017,** *2* (4), 1620-1624.

38. Bellesia, F.; Ghelfi, F.; Grandi, R.; Pagnoni, U. M.; Pinetti, A., The reaction of pyrroles with trimethylhalosilanes‐dialkyl sulfoxides. *Journal of Heterocyclic Chemistry* **1993,** *30* (3), 617-621.

39. Daina, A.; Michielin, O.; Zoete, V., SwissADME: a free web tool to evaluate pharmacokinetics, drug-likeness and medicinal chemistry friendliness of small molecules. *Scientific Reports* **2017,** *7* (1), 1-13.

40. S.W.L. Chu, S. Badar, D.L. Morris, M.H. Pourgholami, potent inhibition of tubulin polymerisation and proliferation of paclitaxel-resistant 1A9PTX22 human ovarian cancer cells by albendazole. *Anticancer Research* **2009**, *29*, 3791-3796.

Chapter 2

Sulfoximine Functionalized Anti-cancer Agents

Part 2B: Design, Synthesis, *in-silico* Studies and Biological Evaluation of Novel Sulfoximine Modified Colchicine Derivatives as Potent Anti-cancer Agents
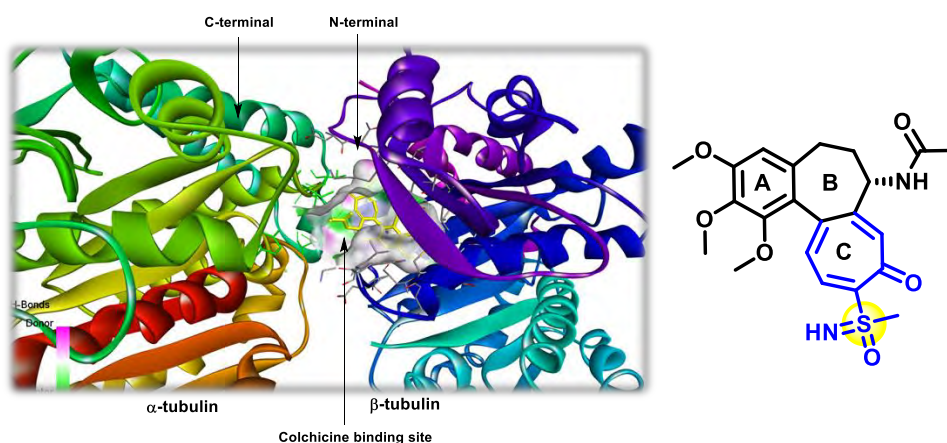
2.2.1 Introduction

In 2009, the U.S. Food and Drug Administration (FDA) approved colchicine (**1**) as a monotherapy drug for treating acute gout flares and familial Mediterranean fever.[3] This natural alkaloid, derived from plants like Colchicum, Merendera, and Gloriosa, boasts a rich history in medicine, dating back to ancient times.[4] Tubulin is considered as one of the most useful and strategic molecular targets for antitumor drugs.[5] Microtubules play a critical role in mitosis and cell division and are regarded as an excellent target for anticancer therapy.[2] Microtubules made of α-and β-tubulin heterodimers in eukaryotic cells and are vital components of the cytoskeleton which are involved in numerous cellular processes such as cell signaling, cell motility and intracellular vesicle transport.[6-8] Microtubules form highly dynamics mitotic spindles, which are vital for the suitable orientation and segregation of chromosomes; disruption of this equilibrium will lead to cell cycle arrest or cell apoptosis.[9,10] Although microtubule-targeting agents have been widely used in the clinical treatment of different human cancers, their clinical application in cancer therapy is limited by both intrinsic and acquired drug resistance and adverse toxicities. Despite the progress in the administration of microtubule targeting agents for the treatment of patients with cancer, currently, there are few FDA-approved tubulin inhibitors targeting the colchicine binding site.[11] This has encouraged medicinal chemists to design and discover the novel antimitotic agents that bind to the colchicine binding site for cancer therapy.[12-14]

Colchicine´s potent antimitotic properties have positioned it as a promising candidate for cancer treatment. However, its clinical utility in cancer therapy has been restrained by inherent toxicity and the emergence of multidrug resistance (MDR).[15] To address these challenges, extensive efforts have been dedicated to chemically modifed colchicine to mitigate its adverse effects while preserving its therapeutic benefits. The ability of colchicine-binding site ligands to also exert an antiangiogenic effect. In recent years, a variety of colchicine-binding site compounds such as combretastatin **4** has been identified as small-molecule vascular disrupting agents (VDAs) as shown in figure 2.2.1.[16] And other tubulin inhibitors, such as vinblastine and colchicine have also exhibited VDA activity in preclinical studies. By threatening the blood supply of tumors such compounds suppress the formation of new vessels and destroy already formed capillaries.[16] The design and discovery of new tubulin inhibitors (TIs) targeting the colchicine binding site appears an attractive path for improving and advancing tubulin inhibitors.
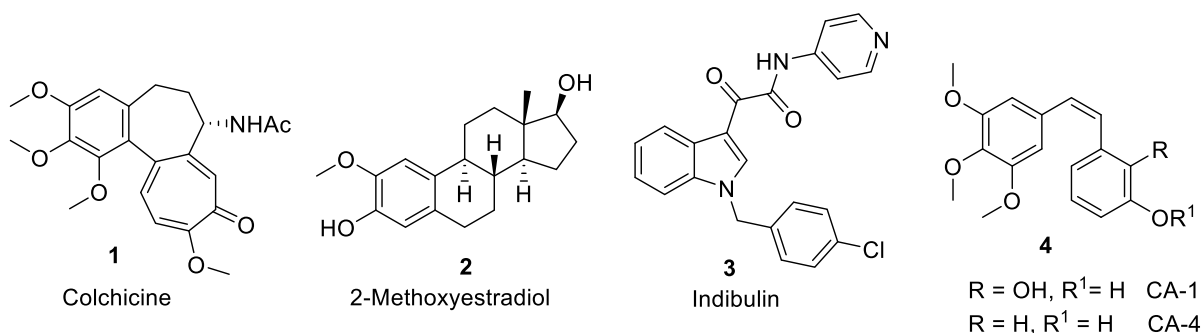
Figure 2.2.1 Colchicine and its binding site′s inhibitors

2.2.1.1 Rational Design of Colchicine Derivatives

Colchicine, a naturally occurring alkaloid, consists of three rings: a trimethoxy benzene ring (ring A), a seven-membered ring carrying an acetamido group at its C7 position (ring B), and a methoxy tropone ring (ring C). Studies have demonstrated that the A and C rings of colchicine play crucial roles in its high binding affinity to tubulin; any structural modification to these rings affects its antimitotic activity.

Role of the A-ring: The A-ring of colchicine is essential for tubulin binding, and substitution of methoxy substituents with methyl group significantly reduces its potency for tubulin. Notably, the size of methyl group in A-ring also influences tubulin binding. Insertion of bulky groups into A-ring, as seen in colchicine, leads to loss of activity.[17]
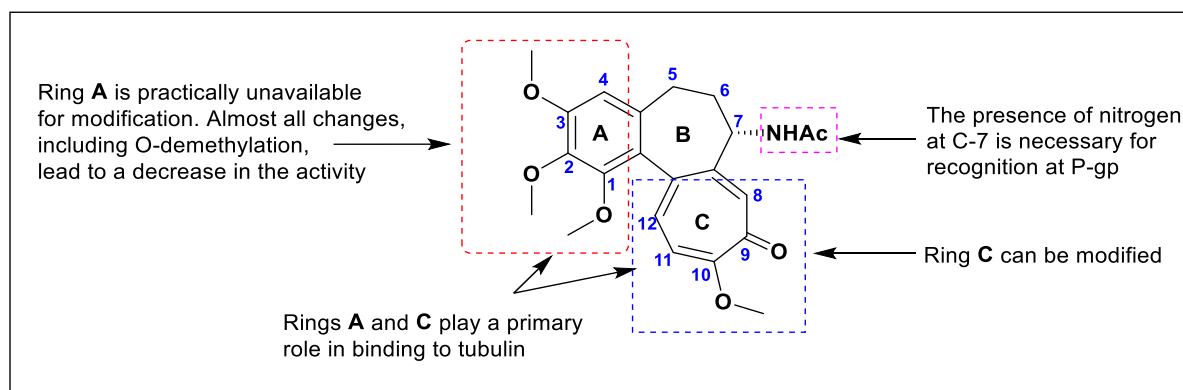
Figure 2.2.2 Possible sites for structural modification of colchicine

Role of the B-ring: While A and C rings are crucial for tubulin binding, the B-ring, though not essential, also plays a significant role towards the cytotoxicity of colchicine derivatives. Substitutions at C-7 position of the B-ring have resulted in active compounds (Figure 2.2.2). Modification of the B-ring terminal acetamide (**5**) has shown promise in overcoming multidrug resistance in cancer (Figure 2.2.3).

Role of the C-ring: The C-ring of colchicine plays a crucial role in its interaction with tubulin. Substituting the 10-OCH_3 group on the C-ring of colchicine with NH_2 group has shown a more pronounced antitumor effect and less toxicity compared to colchicine at optimal doses. The ease of synthetic manipulation at C-ring, coupled with the associated decrease in biological activity, is advantageous for prodrug design. Various colchicine C-ring modified compounds have been synthesized and evaluated. These findings suggested that the compounds with smaller linkers exhibit the highest potency against colorectal cancer cells. Additionally, a series of 10 amine derivatives of colchicine (**6**),[18] synthesized by modification at the C(10)-OCH_3 position of C-ring, have been evaluated for their *in-vitro* cytotoxicity against four human tumor cell lines (Figure 2.2.3). Among these compounds, the most active derivative with bis(2-methoxyethyl)amine substituent (**8**) was found show activity ranging from nanomolar to submicromolar concentrations and improved selectivity index.[19]

Moreover, ZD6126 (**7**) is a novel vascular-targeting prodrug developed by AstraZeneca (Macclesfield, UK).[20] Compound **7** was developed for its tubulin-binding properties and its ability to induce vascular damage in tumours. ZD6126 is a water-soluble prodrug of the tubulin-binding agent NAC. *In vivo*, ZD6126 rapidly induces a large reduction in vascular volume and extensive necrosis in a murine tumour model, consistent with vascular rather than cytotoxic effects.[21] Compound **7** is structurally similar to colchicine, with potential antiangiogenesis and antineoplastic activities, and used in the treatment of metastatic colorectal cancer. However, the study was terminated at phase II because of apparent cardiotoxicity at pharmacological doses.[22] Structure-activity relationship studies have been instrumental in deciphering the structural elements necessary for tubulin binding. Modifications, such as substitution of a methoxyl group at C-10 position with a thiomethyl group (compounds **9** and **10**; figure 2.2.3)[23] have been explored to improve molecular stability and binding affinity to tubulin. *In vitro* and *in vivo* studies, for the treatment of mice infected with L1210 and P388 leukaemia using colchicine and its analogues showed that thiocolchicine **9**, are able to bind strongly to tubulin owing to the -SCH_3 group and not the -OCH_3 group on the C (10) of its tropolonic ring (Figure 2.2.3). On the contrary, pesudothiocolchicine, which holds an -SCH_3 group at C-9), and isothiocolchicine (**11**), which possesses a -SCH_3 group at C (11), showed no binding affinity to tubulin.[24] Thus, many studies focused on the modification of the substituent at C-10 in the search for colchicine analogues with improved activity, lower toxicity or a reduced tendency toward drug resistance.
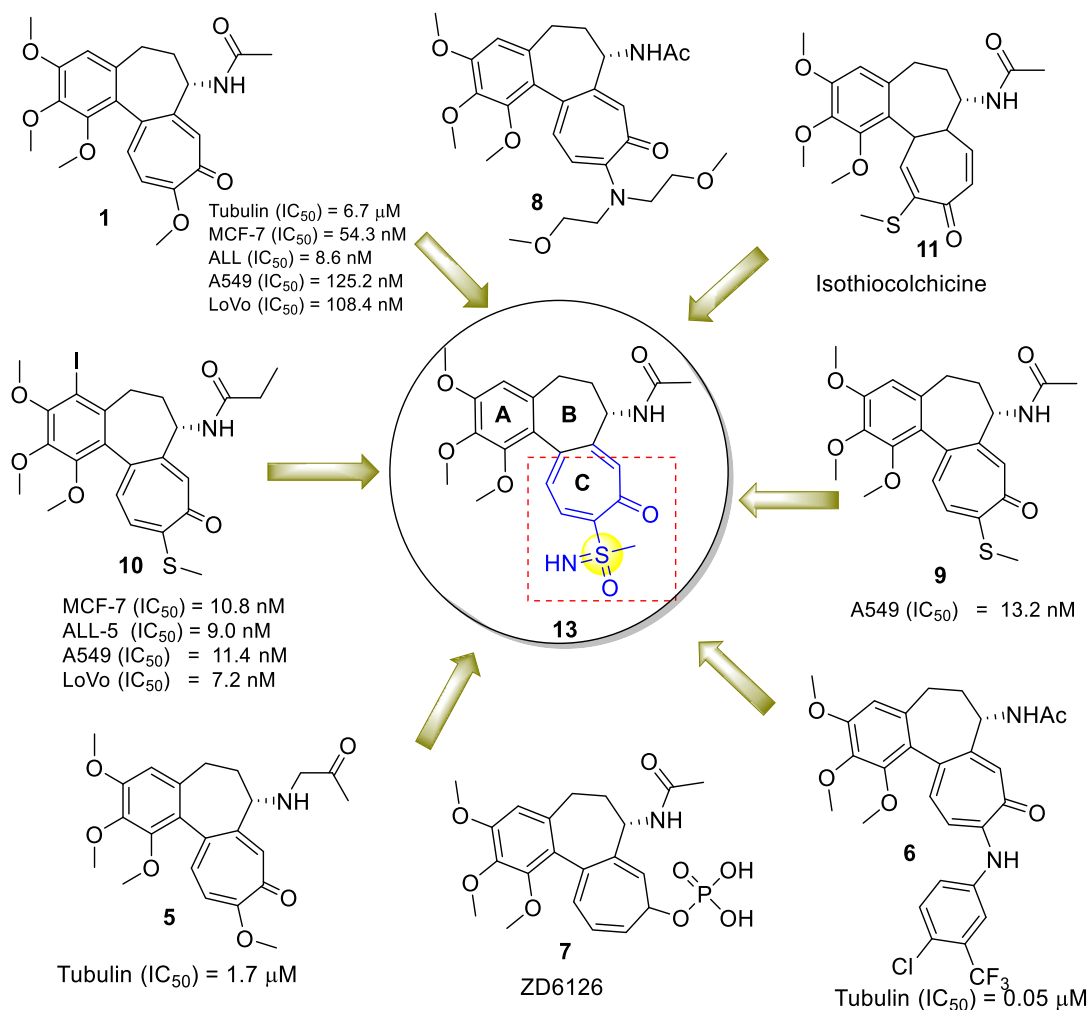
Figure 2.2.3 Rational design of the current work

In the recent past, sulfoximines have emerged as a promising class of compounds for cancer therapy due to their unique structural features and favorable pharmacokinetic properties such as better solubility in protic solvents, high stability, good physical and chemical properties, multiple hydrogen bond acceptor/donor functional groups and structural diversity.[25, 26] Sulfoximines also have a chiral sulfur atom, giving them different shapes that can enhance their ability to bind to specific proteins. These properties suggest that the sulfoximine group has significant potential to serve as a small, hydrophilic and stable functional group in drug discovery.

The combination of colchicine and sulfoximine moiety offers an unique opportunity to develop novel drug with potentially enhanced biological activities and therapeutic applications. In our previous work we reported indolylsulfoximine derivaties which showed selective cytotoxicity against various cancerous cells.[27] As part of our efforts to develop novel anticancer agents, in

the present work we have successfully synthesized colchicine analogues (**12** and **13**) and evaluated their tubulin activity.

2.2.2 Results and Discussion

2.2.2.1 Synthesis and Characterization

The design of the novel colchicine derivatives was based on the bioisosteric modifications of C-ring of colchicine and structural optimization of the lead compound **13** according to the structure-activity relationship (SAR) and molecular modeling studies results. The colchicine-based target compound was synthesized by utilizing reaction conditions, recently reported by in our previous work.[27] Formation of key precursor thiocolchicine **12** (96% yield) to access colchicine sulfoximine **13**, involves the reaction of colchicine with sodium methanethiolate in water (Scheme 2.2.1).
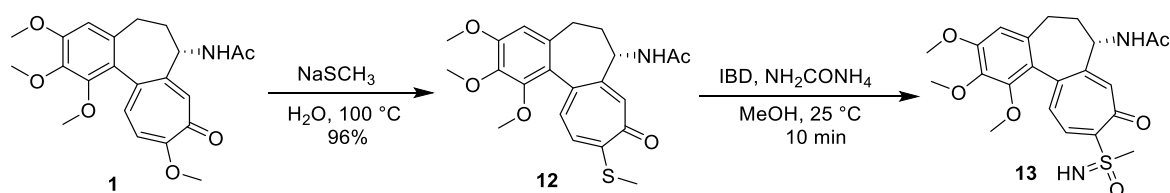
Scheme 2.2.1. Reagents and conditions: (a) NaSCH₃ (2.5 equiv), H₂O, 100 °C, 1h; (b) IBD (2.5 equiv), NH₂COONH₄ (2.0 equiv), methanol, 25 °C, 10 min.

Initially we treated **12** with NH₂COONH₄ (2.0 equiv) and IBD (3.0 equiv) in methanol at room temperature for 30 min to afford **13** in 48% yield (Table 2.2.1, entry 1). Next, experiments were carried out to minimize the excess use of IBD. Reaction of **12** with 1.5 equivalents of IBD afforded **13** in 37% yield (Table 2.2.1, entry 2). Decrease in reaction temperature to 10 °C and with the use of 1.5 equivalents of IBD afforded **13** in 25% yield (Table 2.2.1, entry 3). Increase in equivalence of IBD (from 1.5 to 2.5) afforded **13** in 63% yield (Table 2.2.1, entry 4). Further reduction in reaction time up to 15 min, afforded **13** in 26% (Table 2.2.1, entry 5). When the reaction temperature increased to 25 °C and reduced the reaction time up to 10 min, **13** was formed in 87% yield (Table 2.2.1, entry 6). Peforming the reaction in acetonitrile or toluene led to **13** only in trace amount (Table 2.2.1, entries 7-8).

Finally, we found that the use of IBD (2.5 equiv) and NH_2COONH_4 (2.0 equiv) in methanol at room temperature is the optimum reaction conditions (Table 2.2.1, entry 6) for the preparation of colchicine sulfoximine **13**.

Table 2.2.1 Optimization of conditions to prepare colchicine sulfoximine **13**[a]
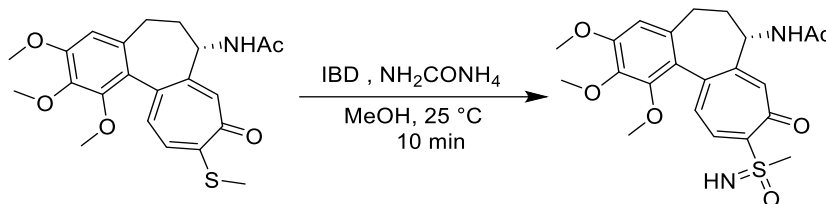
Entry	Solvent	Temp.	IBD (equiv.)	Time (min.)	Yield[b]
1.	MeOH	25	3.0	30	48
2.	MeOH	25	1.5	30	37
3.	MeOH	10	1.5	30	25
4.	MeOH	10	2.5	30	63
5.	MeOH	10	2.5	15	26
6.	**MeOH**	**25**	**2.5**	**10**	**87**
7.	ACN	25	2.5	10	trace
8.	Toluene	25	2.5	10	29

[a]Reagents and conditions: IBD (2.5 equiv), NH_2COONH_4 (2.0 equiv), methanol, 25 °C, 10 min.
[b]Isolated yield.

The chemical structure of **13** was confirmed by its spectral data. Formation of **13** was indicative by the appearance of characteristic signals in proton NMR spectrum at 2.4 ppm for methyl protons of sulfoximine moiety (Figure 2.2.4). The ^{13}C NMR spectrum of **13** exhibited a characteristic signal at 51.03 ppm (Figure 2.2.5) due to methyl carbon of the Sulfoximine group. The HRMS spectrum of **13** displayed a molecular ion at 447.1615 in agreement with the expected mass at 447.1545 for $C_{22}H_{26}N_2O_6S$ (Figure 2.2.6).
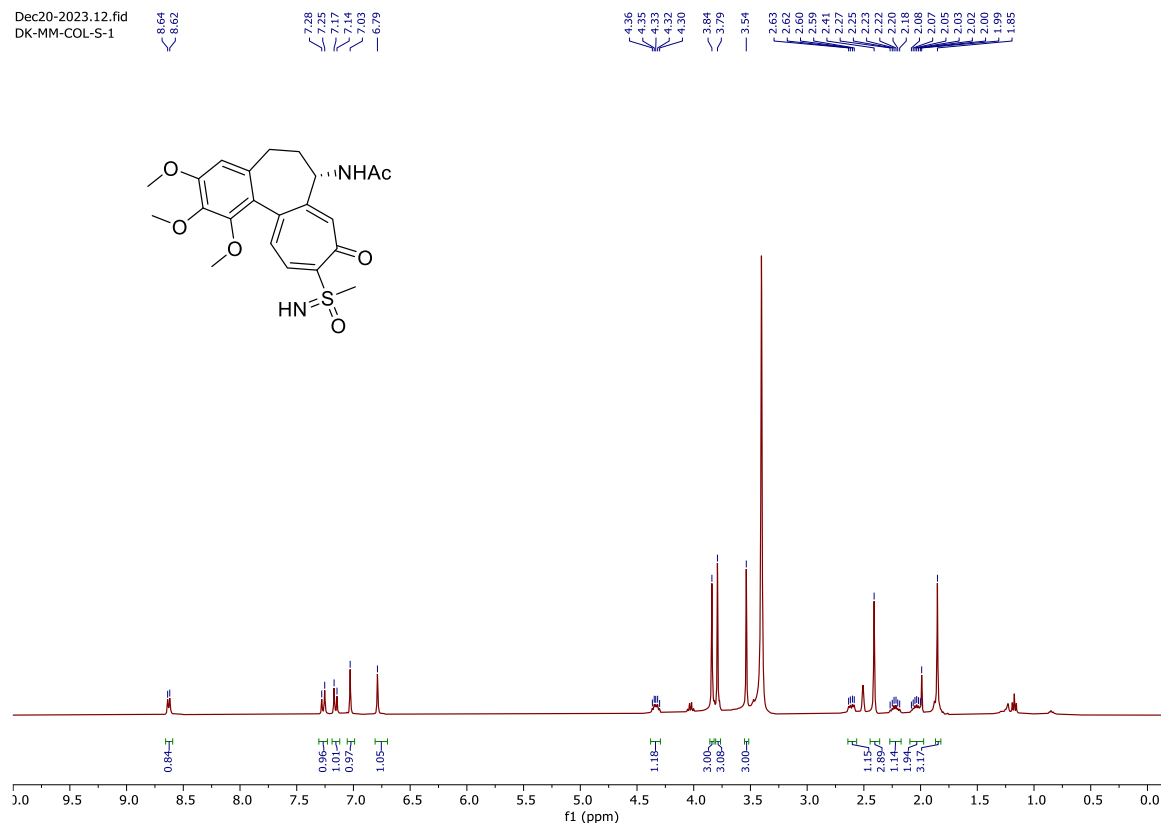
Figure 2.2.4 ^{1}H NMR spectrum of **13**
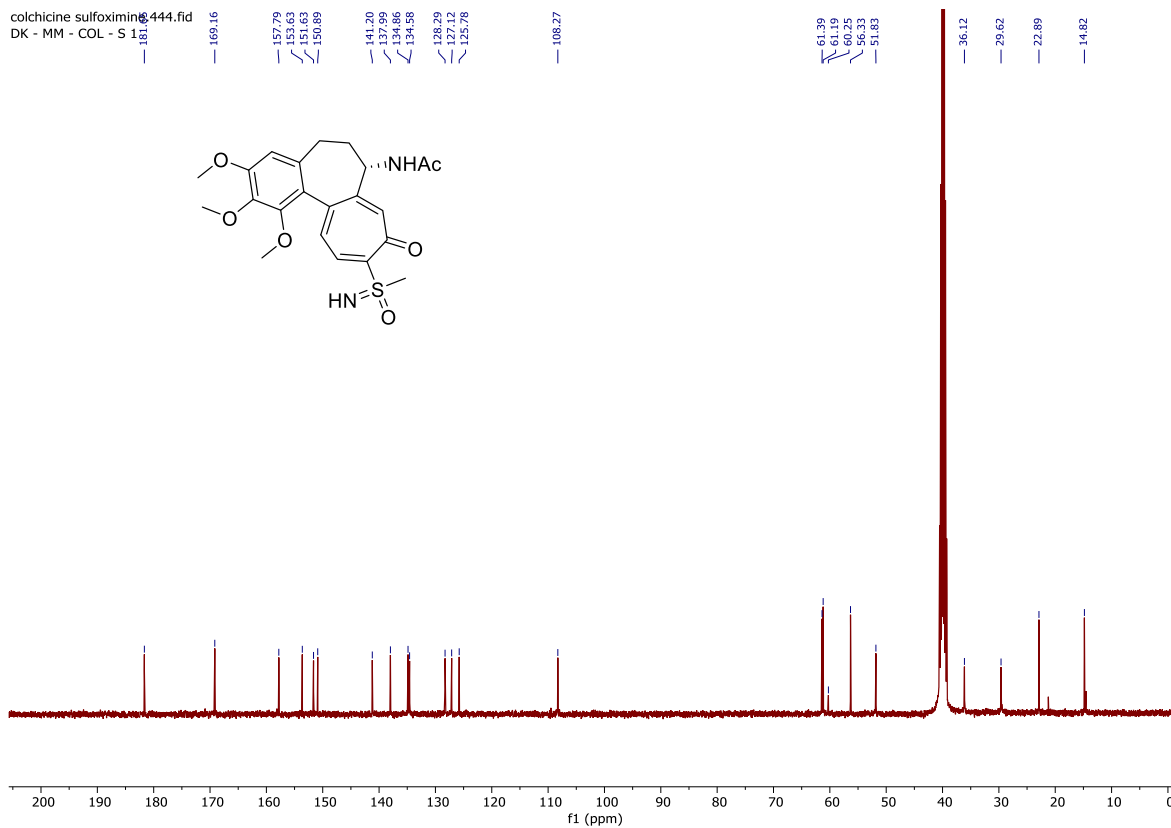
Figure 2.2.5 ^{13}C NMR spectrum of **13**
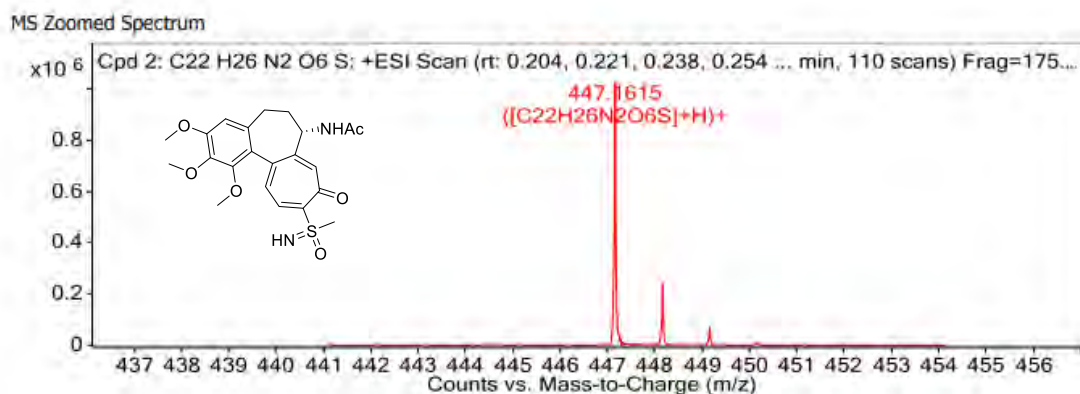
Figure 2.2.6 HRMS spectrum of compound **13**

Purity of the synthesized compounds was found to be more than 98% as determined by WATERS 515 HPLC reverse phase system with a C-18 column (5μm, 4.6 × 250 mm) and PDA detector using a flow rate of 1 mL/min. and a gradient of acetonitrile (Figure 2.2.7).
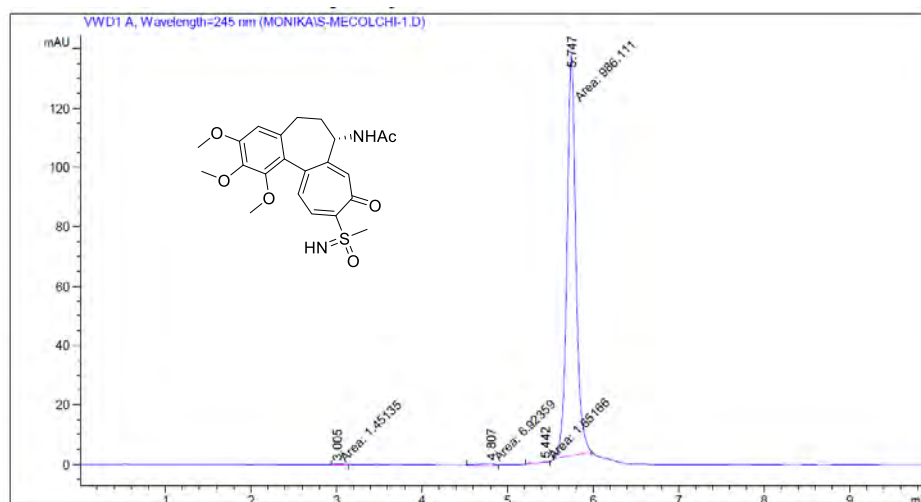
Figure 2.2.7 HPLC traces of compound **13**

2.2.2.2 Biological Evaluation

2.2.2.2.1 Anti-cancer Activity

The synthesized colchicine analogues **12-13** were evaluated for their cytotoxicity against PC3 cancer cell line, representing human prostate cancer cells, *in vitro*. Compound **12** displayed notable inhibitory activity, achieving over 77% suppression of prostate cancer cells *in vitro*. Moreover, compound **13**, which incorporates a sulfoximine functional group, exhibited even higher levels of inhibition, with over 80% suppression of cancer cells. The enhanced cytotoxicity observed with compound **13** suggests that the incorporation of the sulfoximine moiety is beneficial for its activity.

2.2.2.2.2 Tubulin Polymerization Assay

In vitro Tubulin Polymerization Assay: Tubulin (10 μM) was mixed with different concentration of compounds and polymerization reaction was initiated by incubating the tubulin-compound mixture in polymerization buffer (1 mM $MgSO_4$, 1 mM EGTA, 1.0 M monosodium glutamate, pH 6.8) at 37 °C by adding 1 mM GTP in the assembly. Tubulin polymerization reaction was monitor by light scattering at 350 nm using V-630 Jasco Spectrophotometer. Colchicine used as a positive control inhibitor of tubulin polymerization. (Figure 2.2.8). To investigate whether the antiproliferative activity of colchicine analogues **12** and **13** are due to interactions with tubulin, the most cytotoxic analogue, **13**, was evaluated for its tubulin activity. Compound **13** caused a decrease in tubulin polymerization in a dose dependent manner as shown in figure 2.2.8. Compound **13** inhibited microtubule formation, a critical part of cell division, very close to colchicine inhibition. Tubulin polymerization assay suggests that the colchicine sulfoximine **13** exhibited anticancer activity effect through the inhibition of tubulin polymerization as shown in figure 2.2.8. To gain better understanding on the potency of **13** and guide further SAR studies, we proceeded to examine the interactions of **12** and**13** with tubulin crystal structure (PDB code: 1SA0).
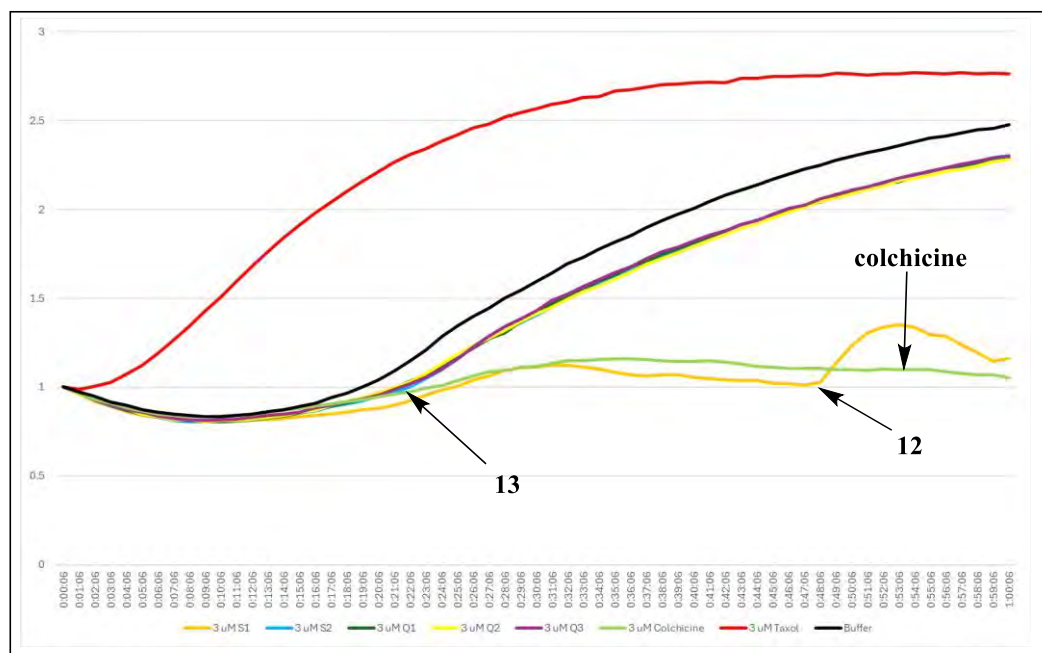
Figure 2.2.8 Tubulin polymerization inhibition (**12** and**13**)

2.2.2.2.3 Solubility Assay

The solubility analysis of compound **13** was performed using UV-visible spectroscopy to quantify its solubility in water. Initially, a series of known concentrations of compound **13** (ranging from 10 µg/mL to 100 µg/mL) was prepared, and their absorbance values were measured using a UV spectrophotometer. A total of ten concentrations (10, 20, 30, 40, 50, 60, 70, 80, 90, and 100 µg/mL) were analyzed to establish a calibration curve. The resulting data was subjected to linear regression analysis, producing the equation Y = 0.0028x + 0.0016, where Y represents the absorbance and x represents the concentration of compound **13** in µg/mL. The linear regression was fitted to ensure the line passed through the origin (0, 0), meaning that no absorbance was recorded when no compound was present. For the solubility determination in pure water, a stock solution of compound **13** was prepared at a concentration of 1 mg/mL (2.2 mM). The stock solution was prepared by dissolving 1 mg of compound **13** in 1 mL of water. To evaluate the solubility of compound **13**, a sample from this stock solution was added to a 5 mL volumetric flask already containing 5 mL of distilled water.

Using the established calibration curve and linear equation (Y = 0.0029x + 0.0032), the absorbance of the unknown concentration of compound **13** was used to calculate its concentration in water. By substituting the measured absorbance value into the equation, the solubility of compound **13** in pure water was determined.
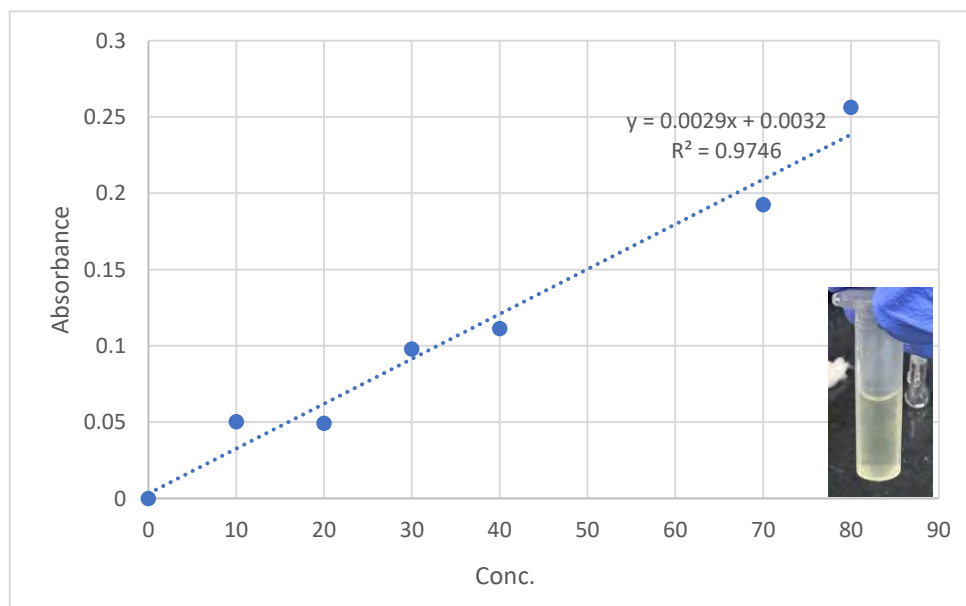
Figure 2.2.8a Linear regression analysis of compound **13**

2.2.3 Computational Studies

2.2.3.1 Molecular Docking

Colchicine disrupts tubulin polymerization throughout the cell cycle by binding to β-tubulin at its interface with α-tubulin. This binding induces a distortion in the conformation of the αβ-hetero-dimer of tubulin, which in turn disrupts the lateral contacts necessary for polymerization.[28] Consequently, tubulin becomes destabilized, impeding its ability to form polymerized structures. Tubulin-Colchicine binding has been extensively studied and the Colchicine Binding Site (CBS) is well explained in figure 2.2.9. The C-terminal and N-terminal regions of beta tubulin play significant roles in tubulin assembly, microtubule structure and interactions with other proteins. The C-terminal tail is involved in protein-protein interactions and serves as a binding site for MAPs and motor proteins. The N-terminal region participates in tubulin assembly and contains the colchicine binding site, which is targeted by tubulin inhibitors.

Molecular docking study was carried out using AutoDock vina Software, where the prepared compounds were docked into the colchicine binding site of tubulin. The binding mode of the designed compounds was studied to determine the essential pharmacophoric features of the new compounds. The X-ray crystallographic enzyme tubulin complex with colchicine (PDB ID: 1SA0) (Figure 2.2.10), showed the presence of an essential hydrogen bond with CYS241, in addition to hydrophobic interaction. The selected pose of the new compounds out of eight poses that showed similarity to the binding mode compared to the reference ligand (colchicine) is considered the best pose (Figure 2.2.10). The presented docking study showed similar binding mode between the lead compounds and the docked molecules. **13** exhibited H-bonding interaction with CYS241; Pi-sigma: LEU248; Hydrophobic interactions: LEU255, ALA250, LEU242, ALA354 and LYS352 (Figure 2.2.11). Binding was validated by the overlapping of the docked ligand binding position with co-crystallized colchicine (Figure 2.2.12).

The binding mode and the binding free energy of the biologically active synthesized compounds are summarized in Table 2.2.2. Where the molecular docking of the new compounds revealed that compounds **12** showing MET259 and **13** retained the essential H-bond with CYS241 . Compound **13** showed the highest binding affinity (-7.5 Kcal/mol) compared to colchicine (-6.8 Kcal/mol) as given in Table 2.2.2.
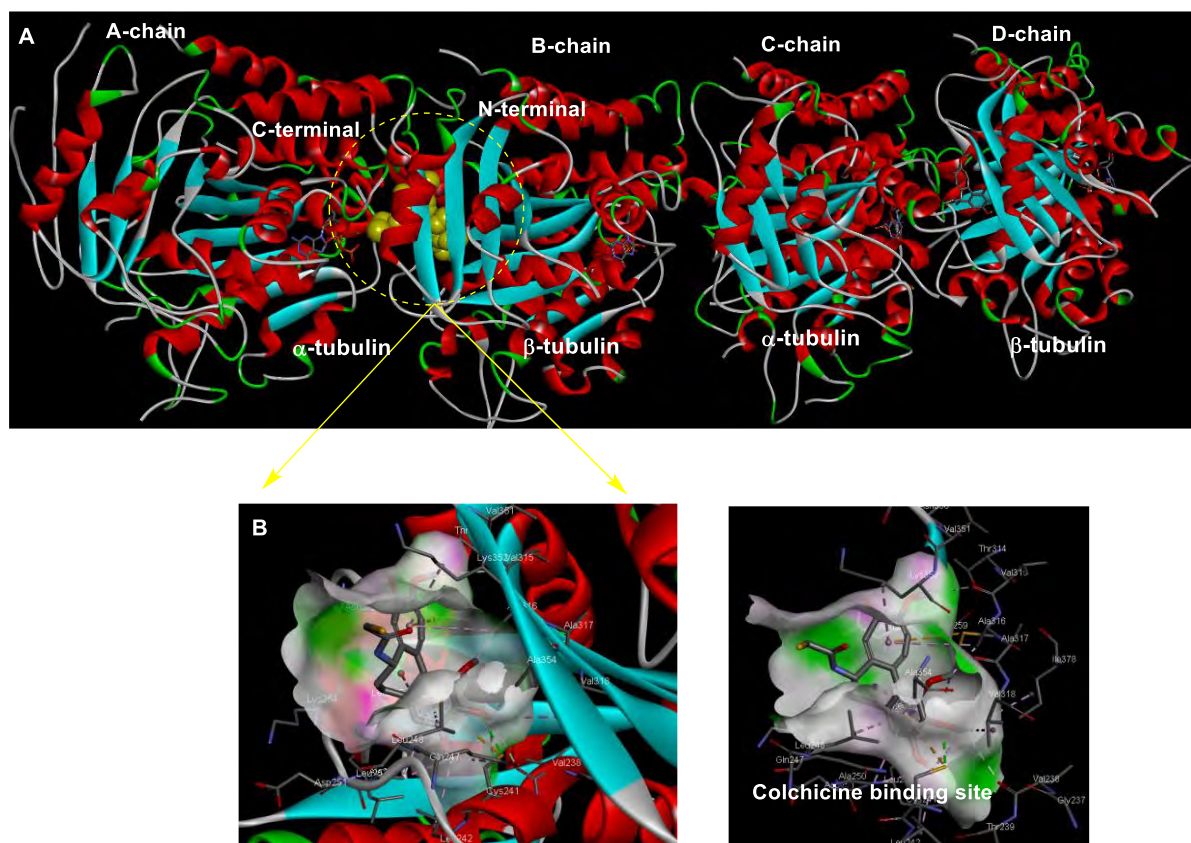
Figure 2.2.9 (A) Crystal structure of αβ-tubulin heterodimers showing the binding sites of colchicine. (B) Interactions of colchicine with the colchicine-binding site of tubulin.
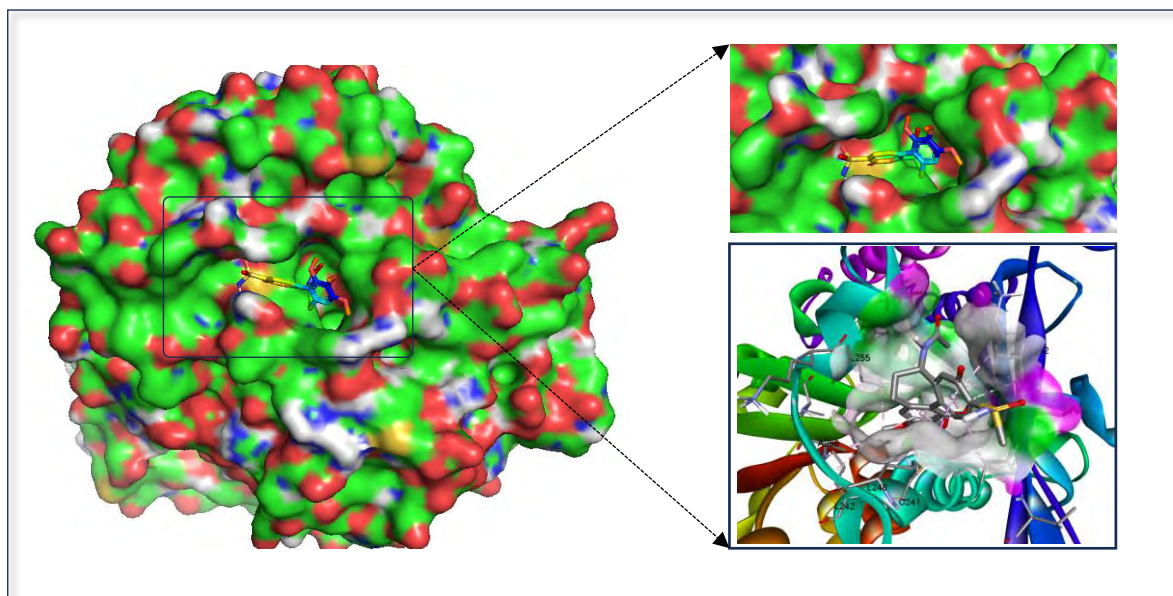
Figure 2.2.10 Surface representation of sulfoximine colchicine, binding at colchicine binding site.
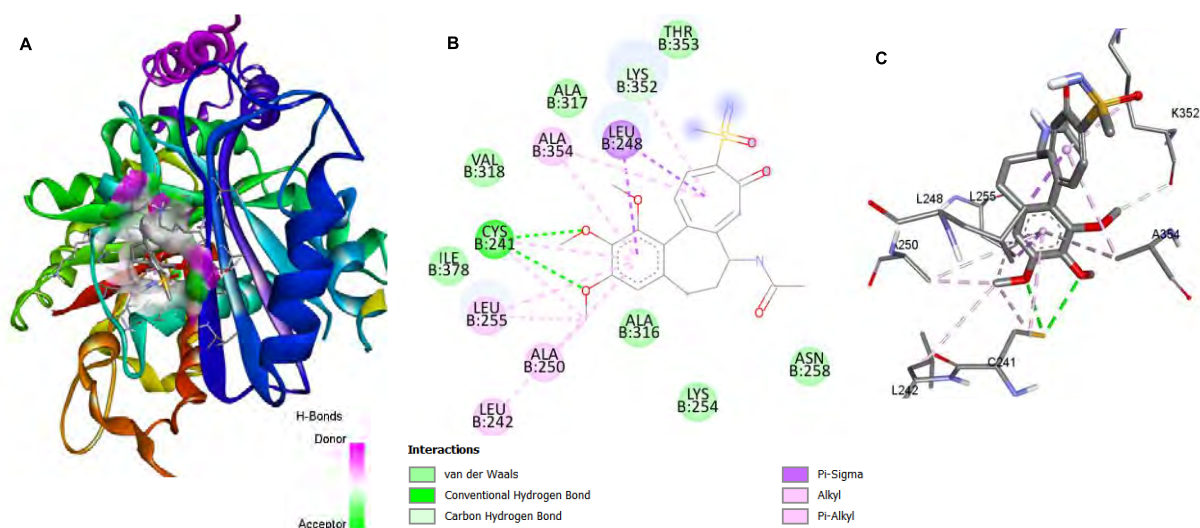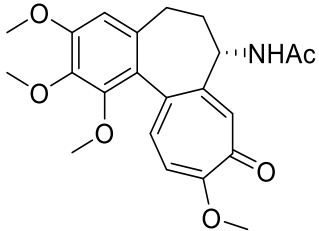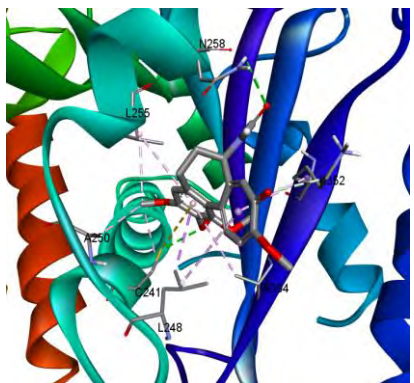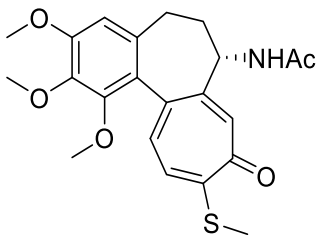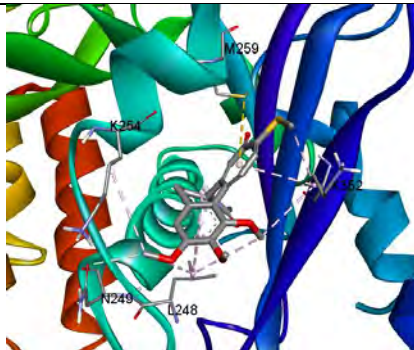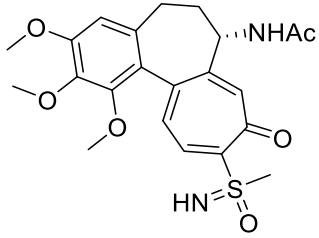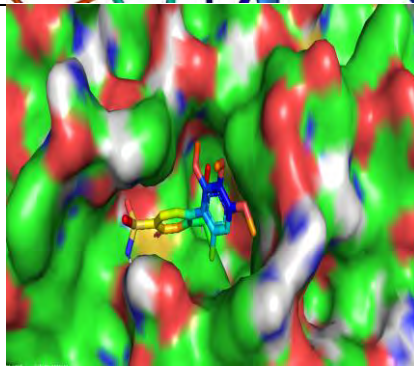
Figure 2.2.11 Molecular modeling study of colchicine sulfoximine (**13**) with tubulin (PDB code: 1SA0). (B) **13** binds to β-tubulin (surface). (B) 2D Ligand-protein interactions between **13** and β-tubulin. (C) 3D protein-ligand interactions. The green dotted lines represent hydrogen bond interaction, and the other lines represent the amino acids showing hydrophobic interaction with protein.
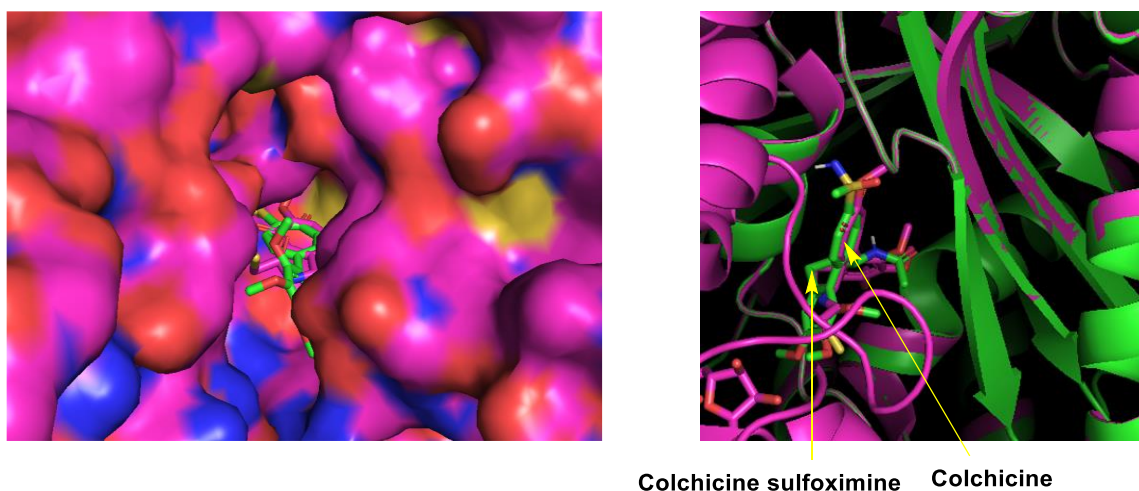
Figure 2.2.12 Overlapping shows the binding mode of compound **13** with colchicine, at the active site of colchicine in tubulin. The binding mode observed for **13** was very similar to that for colchicine and perfectly overlapped in the co-crystallized tubulin structure.

Table 2.2.2 Binding location and orientation of colchicine and its derivatives on α-β tubulin as predicted by Autodock Vina scoring function and compounds with specified residues interacting with each ligand via (hydrogen bonding or hydrophobic interactions) in the binding pocket of β tubulin are listed in the last column.

Compounds	Binding pose	Binding Affinity (Kcal/mol)	Protein-ligand interactions
1.		-6.8	H-bonding: CYS241, ASN258; Hydrophobic interactions: LEU255, ALA250, LEU242, ALA354, LYS352
12.		-7.0	Pi-sulfur: MET 259; Hydrophobic interactions: ASN255, LEU248, LYS352
13.		**-7.5**	Potent H-bonding: CYS241, Pi-sigma: LEU248; Hydrophobic interactions: LEU255, ALA250, LEU242, ALA354, LYS352

2.2.3.2 Pharmacokinetic Prediction

After the molecular docking studies of synthesized compounds, ADME (absorption, distribution, metabolism and excretion) profiling comprising size, solubility, lipophilicity and other drug-likeness properties of colchicine derivatives were calculated using software [29] and are presented in Table 2.2.3.

For a compound to be a potential lead in drug discovery, the Lipinski′s rule of five in terms of number of hydrogen bond donors less than five, number of hydrogen bond acceptors less than ten, molecular weight of compound less than 500 Dalton and octanol-water partition coefficient less than five, is expected to be followed.[29] As indicated in Table 2.2.3, compound **13** showed favourable computationally predicted ADME profiles. For all compounds, topological surface area (TPSA), the indicator of membrane penetration, was predicted between 20 and 130 Å2, was found to be within the range. The test results can be seen in Table 2.2.3. The results of the tests in the gastrointestinal absorption parameter showed that ligand **13** (with the high result) are suitable for oral use. P-glycoprotein (P-gp) is an ATP-dependent phosphorglycoprotein found in the cell membrane, playing a crucial role in drug transport across cell membranes. It is a highly dynamic and efficient efflux transporter that interacts with a wide range of drugs, affecting their absorption, distribution, and elimination in the body. P-gp acts as a protective barrier by pumping out drugs and toxins from cells, thereby reducing their intracellular concentrations. This mechanism is particularly important in tissues with high exposure to xenobiotics, such as the intestine, liver, kidney, and blood-brain barrier. By actively transporting drugs out of cells, P-gp can decrease drug efficacy and contribute to multidrug resistance in cancer cells. In clinical settings, P-gp activity is particularly relevant in the context of multidrug resistance in cancer chemotherapy. In the occurrence of several drug–drug interactions, drug metabolism through the cytochrome P450 (CYP) system has emerged as a significant determinant. CYP belongs to the hemethiolate class of enzymes that catalyse the oxidation of a wide variety of xenobiotics and pharmaceutical agents. Six different P450 isozymes that play important roles in drug metabolism have been identified, such as CYP1A2, CYP2C19, CYP2C9, CYP2D6, CYP2E1 and CYP3A4.[30] The most important human hepatic CYP isoform found mainly in the liver and the intestine is CYP3A4, which quantitatively constitutes up to 50% of the total hepatic P450 content. It promisingly contributes towards the metabolism of major marketed therapies including antibiotics, anaesthetics, steroids and cancer chemotherapeutics.[31, 32]

Table 2.2.3 ADME properties of colchicine analogues **12-13**

S.No.	ADME parameters		Colchicine (1)	Thiocolchicine (12)	Col. Sulfoximine (13)
1.	**Physicochemical parameters**	Mol. Wt (g/mol)	399.44	415.50	460.54
		H-bond donors	1	1	2
		H-bond acceptors	6	5	7
		No. of rotatable bonds	6	6	6
		TPSA	83.09 Å	99.16 Å	123.16 Å
		No. heavy atom	29	29	32
2.	**Water solubility**	Log S (SILICOC-IT)	-6.66 Poorly soluble	-7.01 Poorly soluble	-5.01 Soluble
3.	**Lipophilicity**	CLog P	2.36	2.89	1.87
4.	**Pharmacokinetics**	GI absorption	High	High	High
		BBB	No	No	No
		Bioavailability	low	0.55	0.55
		Skin permeation (log Kp)	-8.01 cm/s	-7.58 cm/s	-7.43 cm/s
		P-gp substrate	Yes	Yes	Yes
		CYP enzyme inhibitors: CYP1A2	No	No	No
		CYP2C19	No	Yes	No
		CYP2C9	No	Yes	No
		CYP2D6	Yes	Yes	No
		CYP3A4	Yes	Yes	Yes
5.	**Druglikeness**	Lipinski rule	Yes	Yes	Yes
		Ghose rule	Yes	Yes	Yes
		Veber rule	Yes	Yes	Yes
		Egan rule	Yes	Yes	Yes
6.	**Medicinal Chemistry**	Synthetic accessibility	3.87	3.88	5.27

Furthermore, CYP enzymes metabolize the majority of marketed drugs; thus, it is important to characterize the interactions of potential new therapies with members of this enzyme. The results of yes, in the cytochrome inhibitor parameter, will indicate that ligand can act as an inhibitor in the process of cytochrome metabolism, while no results will show that the ligand

cannot act as an inhibitor in the process of cytochrome metabolism. The test results show that ligands **12** and **13** were cytochrome inhibitors (CYP2D6 and CYP3A4). The higher bioavailability of the compound indicates that it can be better used orally. Based on the results obtained from the parameter (Figure 2.2.13), compound **13** have good bioavailability score. In figure 2.2.13, the pink area represents the optimal range for each physicochemical property of oral bioavailability (LIPO-lipophilicity, SIZE-size, POLAR-polarity, INSOLU-solubility, INSATU-saturation and FLEX-flexibility), while the red lines represent compounds.
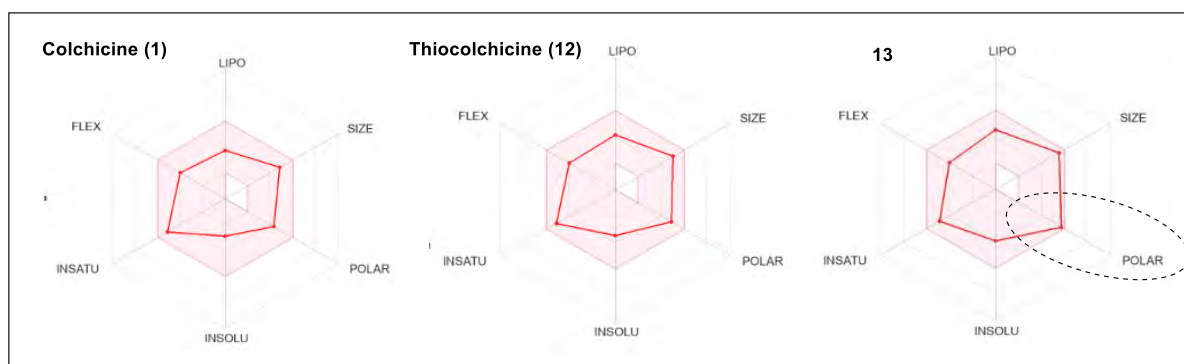
Figure 2.2.13 Oral bioavailability radar charts for the studied compounds. **13** have good bioavailability score and more hydrophilic in nature.

2.2.4 Conclusions

In this chapter, synthesis and anticancer activity of the colchicine sulfoximine analogue derived from the colchicine has been described. High yielding synthesis of compound **13** involves the reaction of thiocolchicine with IBD and ammonium carbamate. Cytotoxicity study shows that compound **13** was showing more than 80% inhibition of prostate cancerous cells. Tubulin polymerization assay showed that the thiocolchicine **12** and sulfoximine **13** are potent inhibitors of tubulin polymerization. Incorpration of sulfoximine (**13**) enhances water solubility (logS = -5.01) andoral bioavalibility in addition to high gastrointestinal absorbtion. In molecular docking study compound **13** showed H-bonding interaction with CYS241 and has strong binding affinity (-7.5 Kcal/mol) ;higher than the colchicine.

2.2.5 Experimental Section

2.2.5.1 Chemistry

2.2.5.1.1 General Methods

The laboratory reagents were purchased from reputable suppliers such as Sigma-Aldich, Alfa Aesar and Spectrochem India Pvt. Ltd and used without further purification. The reactions were monitored by thin layer chromatography and conducted on Merck pre-coated plates (silica gel 60 F_{254}, 0.2mm). Column chromatographic purification of products was carried out using silica gel (100-200 mesh) and ethyl acetate/hexane mixture was used for elution. ^1H NMR spectra and ^{13}C NMR spectra were recorded at 400 MHz and 100 MHz using CDCl$_3$ and DMSO-d_6. Chemical shifts are given in ppm relative to the residual solvent peak (^1H NMR: CDCl$_3$ δ 7.26; DMSO-d_6 δ 2.50; ^{13}C NMR: CDCl$_3$ δ 77.0; DMSO-d_6 δ 39.52) with multiplicity (s = singlet, d = doublet, t = triplet, q = quartet, m = multiplet), coupling constants (J, in Hz) and integration. Melting points were determined by using E-Z melting point apparatus and are uncorrected. High-resolution mass data (HRMS) were obtained *via* an Agilent 6545 Q-TOF LC/MS (ESI).

2.2.5.1.2 Procedure for the synthesis of thiocolchicine (12)

A mixture of colchicine **1** (200 mg, 1 mmol) and sodium methanethiolate in water was refluxed for 40 min. The reaction progress was monitored by TLC. After completion of the reaction, the entire mixture was extracted four times with chloroform. The combined organic layers was dried over anhydrous sodium sulphate and evaporated under reduced pressure. A bright yellow crystalline solid thiocolchicine **12** was obtained in 96% yield.

2.2.5.1.3 Procedure for the synthesis of colchicine sulfoximine (13)

To a methanolic solution of **12** (1 mmol) was added IBD (2.5 mmol), and ammonium carbamate (2 mmol) at 25 °C. The contents were stirred until completion of the reaction as monitored by the TLC. The solvent was evaporated under reduced pressure by using a rota evaporator. The residue thus obtained was purified by recrystallization to get the sulfoximine **13** (yellow solid) in 87% yield.

(S)-7-(acetoxyamino)-1,2,3-trimethoxy-10-(methylthio)-6,7-dihydrobenzo[*a*]heptalen-9(5*H*)-one (12)
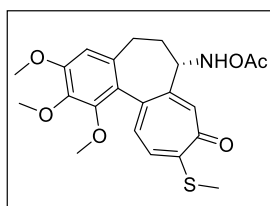
Yellow solid, 96% yield. ^1H NMR (400 MHz, DMSO) δ 8.63 (d, J = 7.5 Hz, 1H), 7.27 (d, J = 10.5 Hz, 1H), 7.16 (d, J = 10.3 Hz, 1H), 7.03 (s, 1H), 6.79 (s, 1H), 4.33 (dt, J = 13.7, 6.8 Hz, 1H), 3.84 (s, 3H), 3.79

(s, 3H), 3.54 (s, 3H), 2.61 (dd, J = 13.6, 6.2 Hz, 1H), 2.41 (s, 3H), 2.23 (td, J = 13.4, 7.3 Hz, 1H), 2.09 – 1.97 (m, 2H), 1.85 (s, 3H); ^{13}C NMR (100 MHz, CDCl$_3$) δ 181.65, 169.16, 157.79, 153.63, 151.63, 150.89, 141.20, 137.99, 134.86, 134.58, 128.29, 127.12, 125.78, 108.27, 61.39, 61.19, 60.25, 56.33, 51.83, 36.12, 29.62, 22.89, 14.82.

((S)-7-(acetoxyamino)-1,2,3-trimethoxy-9-oxo-5,6,7,9-tetrahydrobenzo[*a*]heptalen-10-yl)(imino)(methyl)-l6-sulfanone (13)
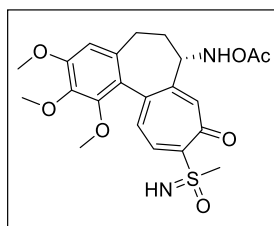
Yellow solid, 87% yield, ^{1}H NMR (400 MHz, DMSO) δ 8.31 (d, J = 11.7 Hz, 1H), 7.48–7.35 (m, 2H), 6.71 (s, 1H), 6.55 (s, 1H), 4.60 (p, J = 6.0 Hz, 1H), 3.96 (s, 3H), 3.93 (s, 3H), 3.72 (d, J = 1.3 Hz, 3H), 3.41 (d, J = 13.7 Hz, 3H), 2.64 – 2.55 (m, 1H), 2.29 – 2.14 (m, 2H), 2.02 (s, 3H); ^{13}C NMR (100 MHz, DMSO) δ 181.65, 169.16, 157.79, 153.63, 151.63, 150.89, 141.20, 137.99, 134.86, 134.58, 128.29, 127.12, 125.78, 108.27, 61.39, 61.19, 60.25, 56.33, 51.83, 36.12, 29.62, 22.89, 14.82; MS (ESI) *m/z* calcd. for C$_{22}$H$_{26}$N$_2$O$_6$S: 447.1545 [M + H]$^+$, found: 447.1615; HPLC: tR = 5.45 min (98 % purity).

2.2.6 References

1. Bray, F.; Ferlay, J.; Soerjomataram, I.; Siegel, R. L.; Torre, L. A.; Jemal, A., Global cancer statistics 2018: GLOBOCAN estimates of incidence and mortality worldwide for 36 cancers in 185 countries. *CA: a Cancer Journal for Clinicians* **2018,** *68* (6), 394-424.

2. Boyle, P.; Levin, B., *World Cancer Report 2008*. 2008.

3. Pasquier, E.; Andre, N.; Braguer, D., Targeting microtubules to inhibit angiogenesis and disrupt tumour vasculature: implications for cancer treatment. *Current Cancer Drug Targets* **2007,** *7* (6), 566-581.

4. Pellegrini, F.; Budman, D. R., Tubulin function, action of antitubulin drugs, and new drug development. *Cancer Investigation* **2005,** *23* (3), 264-273.

5. Singh, H.; Kumar, M.; Nepali, K.; Gupta, M. K.; Saxena, A. K.; Sharma, S.; Bedi, P. M. S., Triazole tethered C5-curcuminoid-coumarin based molecular hybrids as novel antitubulin agents: Design, synthesis, biological investigation and docking studies. *European Journal of Medicinal Chemistry* **2016,** *116*, 102-115.

6. Li, L.; Jiang, S.; Li, X.; Liu, Y.; Su, J.; Chen, J., Recent advances in trimethoxyphenyl (TMP) based tubulin inhibitors targeting the colchicine binding site. *European Journal of Medicinal Chemistry* **2018,** *151*, 482-494.

7. Lai, Q.; Wang, Y.; Wang, R.; Lai, W.; Tang, L.; Tao, Y.; Liu, Y.; Zhang, R.; Huang, L.; Xiang, H., Design, synthesis and biological evaluation of a novel tubulin inhibitor 7a3 targeting the colchicine binding site. *European Journal of Medicinal Chemistry* **2018,** *156*, 162-179.

8. Sun, Y.; Pandit, B.; Chettiar, S. N.; Etter, J. P.; Lewis, A.; Johnsamuel, J.; Li, P.-K., Design, synthesis and biological studies of novel tubulin inhibitors. *Bioorganic & Medicinal Chemistry Letters* **2013,** *23* (15), 4465-4468.

9. Zhou, Y.; Yan, W.; Cao, D.; Shao, M.; Li, D.; Wang, F.; Yang, Z.; Chen, Y.; He, L.; Wang, T., Design, synthesis and biological evaluation of 4-anilinoquinoline derivatives as novel potent tubulin depolymerization agents. *European Journal of Medicinal Chemistry* **2017,** *138*, 1114-1125.

10. Beckers, T.; Reissmann, T.; Schmidt, M.; Burger, A. M.; Fiebig, H. H.; Vanhoefer, U.; Pongratz, H.; Hufsky, H.; Hockemeyer, J. r.; Frieser, M., 2-aroylindoles, a novel class of potent, orally active small molecule tubulin inhibitors. *Cancer Research* **2002,** *62* (11), 3113-3119.

11. Mirzaei, S.; Eisvand, F.; Hadizadeh, F.; Mosaffa, F.; Ghodsi, R., Design, synthesis, and biological evaluation of novel 5, 6, 7-trimethoxy quinolines as potential anticancer agents and tubulin polymerization inhibitors. *Iranian Journal of Basic Medical Sciences* **2020,** *23* (12), 1527.

12. Mirzaei, S.; Qayumov, M.; Gangi, F.; Behravan, J.; Ghodsi, R., Synthesis and biological evaluation of oxazinonaphthalene-3-one derivatives as potential anticancer agents and tubulin inhibitors. *Iranian Journal of Basic Medical Sciences* **2020,** *23* (11), 1388.

13. Behbahani, F. S.; Tabeshpour, J.; Mirzaei, S.; Golmakaniyoon, S.; Tayarani‐Najaran, Z.; Ghasemi, A.; Ghodsi, R., Synthesis and biological evaluation of novel benzo [c] acridine‐diones as potential anticancer agents and tubulin polymerization inhibitors. *Archiv der Pharmazie* **2019,** *352* (6), 1800307.

14. Tantak, M. P.; Klingler, L.; Arun, V.; Kumar, A.; Sadana, R.; Kumar, D., Design and synthesis of bis (indolyl) ketohydrazide-hydrazones: Identification of potent and selective novel tubulin inhibitors. *European Journal of Medicinal Chemistry* **2017,** *136*, 184-194.

15. Brossi, A.; Yeh, H. J.; Chrzanowska, M.; Wolff, J.; Hamel, E.; Lin, C. M.; Quin, F.; Suffness, M.; Silverton, J., Colchicine and its analogues: recent findings. *Medicinal Research Reviews* **1988,** *8* (1), 77-94.

16. McLoughlin, E. C.; O'Boyle, N. M., Colchicine-binding site inhibitors from chemistry to clinic: a review. *Pharmaceuticals* **2020,** *13* (1), 8.

17. Sapra, S.; Bhalla, Y.; Nandani; Sharma, S.; Singh, G.; Nepali, K.; Budhiraja, A.; Dhar, K. L., Colchicine and its various physicochemical and biological aspects. *Medicinal Chemistry Research* **2013,** *22*, 531-547.

18. Huczyński, A.; Rutkowski, J.; Popiel, K.; Maj, E.; Wietrzyk, J.; Stefańska, J.; Majcher, U.; Bartl, F., Synthesis, antiproliferative and antibacterial evaluation of C-ring modified colchicine analogues. *European Journal of Medicinal Chemistry* **2015,** *90*, 296-301.

19. Vilanova, C.; Diaz-Oltra, S.; Murga, J.; Falomir, E.; Carda, M.; Redondo-Horcajo, M.; Díaz, J. F.; Barasoain, I.; Marco, J. A., Design and synthesis of pironetin analogue/colchicine hybrids and study of their cytotoxic activity and mechanisms of interaction with tubulin. *Journal of Medicinal Chemistry* **2014,** *57* (24), 10391-10403.

20. Blakey, D. C.; Westwood, F. R.; Walker, M.; Hughes, G. D.; Davis, P. D.; Ashton, S. E.; Ryan, A. J., Antitumor activity of the novel vascular targeting agent ZD6126 in a panel of tumor models. *Clinical Cancer Research* **2002,** *8* (6), 1974-1983.

21. Varghese, H.; Mackenzie, L.; Groom, A.; Ellis, C.; Ryan, A.; Macdonald, I.; Chambers, A., In vivo videomicroscopy reveals differential effects of the vascular-targeting agent ZD6126 and the anti-angiogenic agent ZD6474 on vascular function in a liver metastasis model. *Angiogenesis* **2004,** *7*, 157-164.

22. Micheletti, G.; Poli, M.; Borsotti, P.; Martinelli, M.; Imberti, B.; Taraboletti, G.; Giavazzi, R., Vascular-targeting activity of ZD6126, a novel tubulin-binding agent. *Cancer Research* **2003,** *63* (7), 1534-1537.

23. Klejborowska, G.; Urbaniak, A.; Maj, E.; Wietrzyk, J.; Moshari, M.; Preto, J.; Tuszynski, J. A.; Chambers, T. C.; Huczyński, A., Synthesis, anticancer activity and molecular docking studies of N-deacetylthiocolchicine and 4-iodo-N-deacetylthiocolchicine derivatives. *Bioorganic & Medicinal Chemistry* **2021,** *32*, 116014.

24. Ghawanmeh, A. A.; Al-Bajalan, H. M.; Mackeen, M. M.; Alali, F. Q.; Chong, K. F., Recent developments on (−)-colchicine derivatives: Synthesis and structure-activity relationship. *European Journal of Medicinal Chemistry* **2020,** *185*, 111788.

25. Lücking, U., Sulfoximines: a neglected opportunity in medicinal chemistry. *Angewandte Chemie International Edition* **2013,** *52* (36), 9399-9408.

26. Lücking, U., Neglected sulfur (VI) pharmacophores in drug discovery: exploration of novel chemical space by the interplay of drug design and method development. *Organic Chemistry Frontiers* **2019,** *6* (8), 1319-1324.

27. Malik, M.; Kumar, D.; Lotana, H.; Shah, K.; Kumar, D., Design, synthesis and anticancer activity of N-aryl indolylsulfoximines: Identification of potent and selective anticancer agents. *Bioorganic & Medicinal Chemistry* **2023,** *93*, 117459.

28. Sreenivasulu, R.; Sujitha, P.; Jadav, S. S.; Ahsan, M. J.; Kumar, C. G.; Raju, R. R., Synthesis, antitumor evaluation, and molecular docking studies of indole–indazolyl hydrazide–hydrazone derivatives. *Monatshefte Für Chemie-chemical Monthly* **2017,** *148*, 305-314.

29. Daina, A.; Michielin, O.; Zoete, V., SwissADME: a free web tool to evaluate pharmacokinetics, drug-likeness and medicinal chemistry friendliness of small molecules. *Scientific Reports* **2017,** *7* (1), 1-13.

30. Cupp, M. J.; Tracy, T. S., Cytochrome P450: new nomenclature and clinical implications. *American Family Physician* **1998,** *57* (1), 107-116.

31. Shimada, T.; Yamazaki, H.; Mimura, M.; Inui, Y.; Guengerich, F. P., Interindividual variations in human liver cytochrome P-450 enzymes involved in the oxidation of drugs, carcinogens and toxic chemicals: studies with liver microsomes of 30 Japanese and 30 Caucasians. *Journal of Pharmacology and Experimental Therapeutics* **1994,** *270* (1), 414-423.

32. Bertz, R. J.; Granneman, G. R., Use of in vitro and in vivo data to estimate the likelihood of metabolic pharmacokinetic interactions. *Clinical Pharmacokinetics* **1997,** *32*, 210-258.

Chapter 3

Design and Synthesis of *N*-aryl indolylsulfoximines as CDK5/p25 Inhibitors
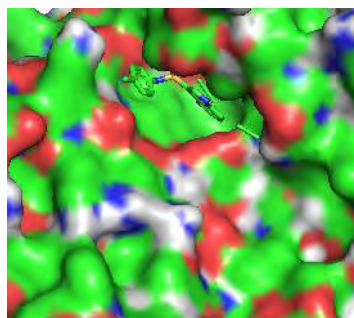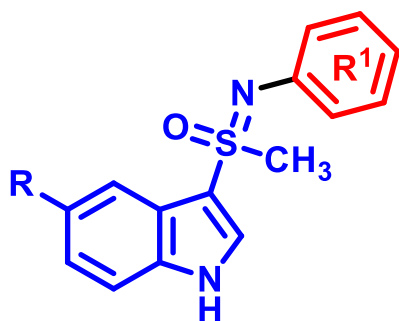
3.1 Introduction

3.1.1 Role of Cyclin-dependent kinases (CDKs) in Cancer

A growing body of knowledge in the field of oncology indicates that cyclin-dependent kinases (CDKs) are emerging as highly attractive molecular targets for the development of cancer therapies. Cancer is characterized by dysregulated cell cycle progression, with cyclin-dependent kinases (CDKs) playing crucial roles in driving tumorigenesis.[1] Dysfunctions in CDK/Cyclin complexes contribute to uncontrolled cell proliferation, a hallmark of cancer. Specifically, overexpression or hyperactivity of CDKs is associated with various cancers, highlighting their potential as therapeutic targets.[2, 3] The current prominence of kinases as drug targets is propelled by several converging factors. Firstly, the human genome encodes approximately 518 kinases, implicating their involvement in virtually every signal transduction process. This suggests that inhibiting kinase activity can provoke meaningful physiological responses. There exist over 2,000 other nucleotide-dependent enzymes, including polymerases, chaperones, motor proteins, reductases, and methyltransferases, each with potential binding sites.[4]

Achieving selectivity is a crucial aspect in developing new kinase inhibitors and this evaluation ideally occurs at the protein, cellular and whole organism levels.[5] Initially, kinase inhibitors undergo assessment at the protein level to gauge their potential to hinder kinase-catalyzed phosphotransfer from ATP to a substrate protein or peptide. Various service providers offer panels comprising more than 400 diverse kinase enzymatic or binding assays. This approach allows for an initial understanding of the compound's interaction with a diverse array of kinases, aiding in informed decision-making for further development and exploration as a kinase inhibitor. Specifically, Cyclin-dependent kinase 5 (CDK5) is overexpressed in many types of cancer and has been identified as a potential therapeutic target for cancer treatment. However, the development of CDK5 inhibitors has been challenging due to the high degree of structural similarity between CDK5 and other CDKs.

Recently, it has been reported that CDK5 plays important roles in regulating various biological and pathological processes, including cancer progression.[6] Concerning prostate cancer, the androgen receptor (AR) is majorly involved in tumorigenesis, while CDK5 can phosphorylate AR and promotes the proliferation of prostate cancer cells. Clinical evidence has also shown that the level of CDK5 is associated with the progression of prostate cancer. Interestingly, inhibition of CDK5 prevents prostate cancer cell growth, while drug-triggered CDK5 hyperactivation leads to apoptosis. The blocking of CDK5 activity by its small interfering RNAs (siRNA) or roscovitine, a pan-CDK inhibitor, reduces the cellular AR protein level and

triggers the death of prostate cancer cells. Thus, CDK5 plays a crucial role in the growth of prostate cancer cells and AR regulation is one of the important pathways.[7, 8]

(A)

(B)
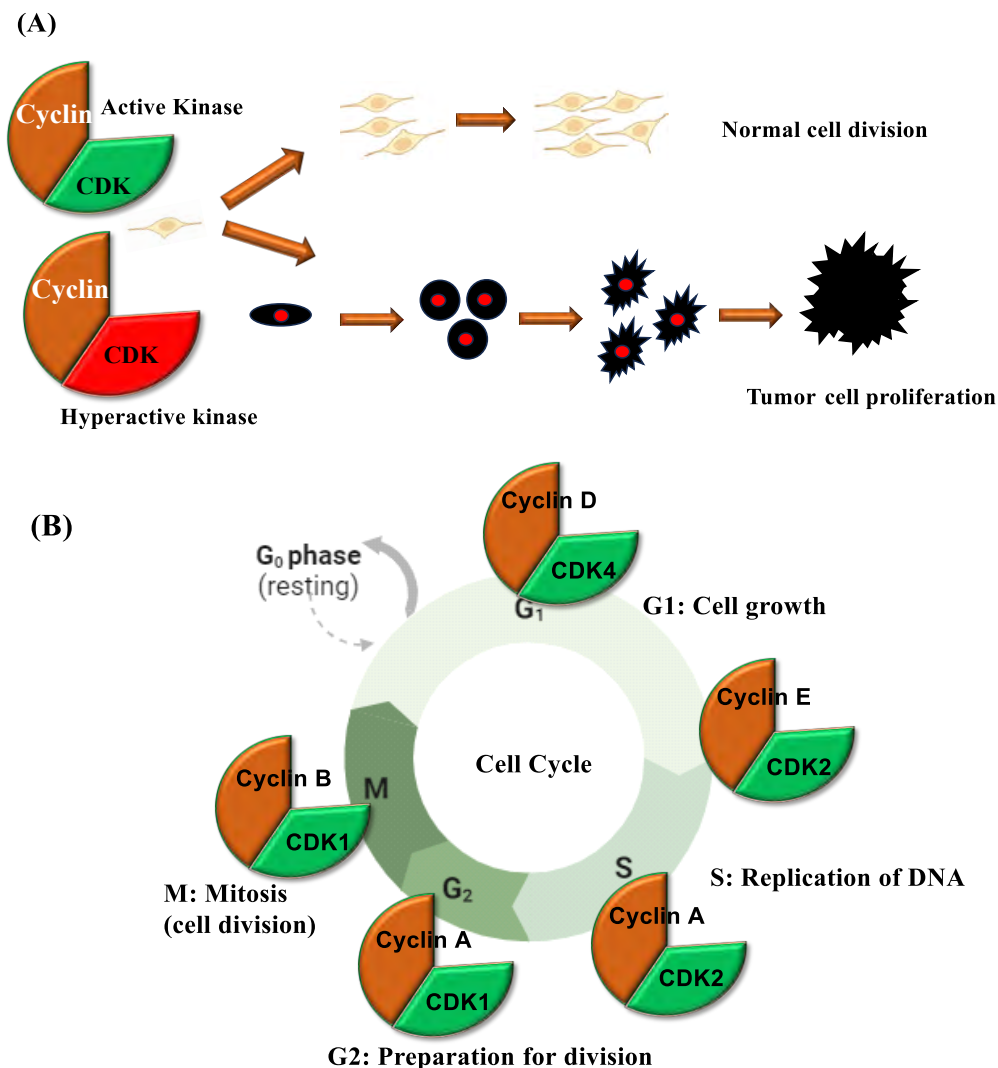
Figure 3.1 Role of CDKs in cancer. (**A**) Schematic representation of normal cell growth and division regulated by cyclin-dependent kinases. Hyperactivation of these kinases contributes to development of cancer cell proliferation. (**B**) Cell cycle regulation on CDK/cyclins.

In mammalian cells, approximately twenty different CDKs have been identified, alongside an equal number of cyclins, each contributing to a myriad of cellular functions beyond mere cell cycle regulation (Figure 3.1). The mitotic kinase CDK1/Cyclin B being essential for viability, and capable of recapitulating the functions of the other cyclin-dependent kinases in regulating cell cycle transitions in mammalian cells is not surprisingly one of the least mutated kinases in human cancers.[7] CDK1 overexpression has been documented in lymphoma, advanced melanoma and lung cancer, and loss of cytoplasmic CDK1 predicts poor survival and confers chemotherapeutic resistance in the latter.[8] CDK2 overexpression has been reported in laryngeal squamous cell cancer, advanced melanoma and breast cancer (Table 3.1).[9] Moreover, 33 simple

coding mutations have been reported in the COSMIC database for CDK2 in a wide variety of cancer tissues, most of which are missense mutations in the *N*-terminal lobe (amino acid 2, 13, 20, 34, 45, 68, 84), one silent mutation at amino acid 45 and one deletion frameshift at amino acid 79.[7] In addition to its involvement in neurodegenerative diseases, CDK5 has emerged as a significant target in oncology. Hyperactivation of CDK5 appears to contribute to the development of glioblastoma and neuroblastoma.[10] Furthermore, there is notable upregulation of CDK5 expression in various cancers, including head/neck, breast, lung, ovarian, lymphoma, prostate, sarcoma, myeloma, and bladder cancers, with well-documented evidence of its role in these malignancies (Table 3.1). Particularly, CDK5 plays a crucial role in regulating cell motility, migration, and metastasis in prostate cancer cells.[11]

CDK5 is distinct from other CDKs in that it is not typically involved in cell cycle processes and is not activated by cyclins, except cyclin 1. CDK5 is one member of the CDK family that is characterized by a highly conserved sequence and a basic structure with the ATP binding site clamped between the C-terminal and N-terminal lobes.[12] CDK5 can be activated by non-cyclin activators, including p35 and p39, as well as their respective fragments p25 and p29. These activators mainly accumulate in post-mitotic neurons. Emerging research has revealed specific CDK/Cyclin heterodimers whose roles extend to transcriptional processes, non-cell cycle functions and pathological conditions, expanding the scope of CDK involvement in cellular physiology and disease.[13]

Table 3.1 CDKs deregulation associated with different cancers

Target	Deregulation	Cancer
CDK5	Overexpression	Prostate cancer[11]
	Overexpression	Breast cancer[14]
	mRNA upregulation	Head/neck, breast, lung, ovarian and bladder cancer[13]
	Amplification/Overexpression	Pancreatic cancer[15]
CDK1	Overexpression	B lymphoma, advanced melanoma[8]
	Missense mutation (D73H)	Ovary carcinoma[7]
CDK2	Overexpression	Laryngeal squamous cell cancer, breast cancer[9]
	33 simple coding mutation	Wide variety of cancer tissues[7]

Kinases have emerged as a highly sought-after class of drug targets, with approximately 30 distinct kinase targets advancing to the Phase I clinical trial stage. The majority of these targets are primarily under investigation for cancer treatment. However, disruptions in kinase function have also been implicated in various other disorders, spanning immunological, neurological, metabolic, and infectious diseases. Consequently, there is significant interest in developing small molecule kinase inhibitors to address a broader spectrum of disorders.

3.1.2 CDK Inhibitors in Clinical Trial

As CDKs have become popular targets for cancer drug development,[16] many CDK inhibitors have entered early clinical trials for the therapy of various cancers (Figure 3.2). Roscovitine (**1**) is a trisubstituted purine initially found to be 10-fold more potent inhibitor of CDK1[17] and constitutes one of the first CDK inhibitors identified which successfully made it through the drug discovery pipeline to clinical trials. Roscovitine (**1**) is widely used to inhibit CDK5 in cell lines and mouse models. This purine analogue competes for ATP-binding to CDK5, but also inhibits CDK1 and 2 (Figure 3.2).[2]

In contrast dinaciclib (**2**), which has improved potency for CDK5 and CDK1, 2, 9 exhibits anti-proliferative effects on hematological cancers during clinical trials. Other small molecule inhibitors indolinone A (**3**) exhibit increased selectivity for Cdk5 and CDK2 over other CDKs and anti-cancer activity in cell lines,[18] but *in vivo* preclinical studies remain to be conducted. Several challenges persist in clinical studies of CDK inhibitors. Firstly, most pan-CDK inhibitors have demonstrated serious adverse effects during clinical trials. For instance, dinaciclib (**2**)[19] exhibited adverse reactions including diarrhea, nausea, fatigue, leukopenia, and thrombocytopenia in a phase II trial (NCT01096342), leading to treatment discontinuation in some patients.[20] Similarly, BAY 1000394 (**4**) resulted in bronchopulmonary hemorrhage and sepsis, leading to fatalities and premature termination of the trial (NCT02161419).[21] Flavopiridol (**5**) also induced adverse reactions such as diarrhea, fatigue, neutropenia, and transaminitis in over 90% of patients in a phase II trial (NCT00098371), prompting early termination of the study.[21] Secondly, some drugs demonstrated lower activity in clinical trials than expected based on preclinical studies. For example, compounds **5** and **6** despite showing promising antitumor activity in preclinical trials, exhibited unsatisfactory clinical efficacy as monotherapy in refractory multiple myeloma in a phase II trial.[22, 23] These challenges underscore the complexity of translating preclinical findings into clinical success and emphasize the need for further research to improve the safety and efficacy of CDK inhibitors in cancer treatment.

AT7519 (**7**) is a pyrazole-based multi CDK inhibitor, which has proven efficient towards several human cancer cell lines. The CDK inhibitor 7, is administered to patients with advanced solid tumours and currently it is in phase II trials for multiple myeloma. SU9516 (**8**), a 3-substituted indolinone, acts as an ATP-competitive inhibitor of CDK2 and CDK1 kinases. AZD5438, 4-(1-isopropyl-2-methylimidazol-5-yl)-2-(4-methylsulphonylanilino) pyrimidine (**9**), is a potent oral inhibitor of cyclin-dependent kinases 1, 2 and 9. Another promising compound, SNS-032 (**10**) by Sunesis Pharmaceuticals, is undergoing Phase I clinical trials for the treatment of B-lymphoid malignancies including chronic lymphocytic leukemia, mantle cell lymphoma, and multiple myeloma. Additionally, P1446A-05 (**11**) developed by Piramal Enterprises Limited is in Phase I trials targeting solid tumors and hematologic malignancies. Despite these advancements, challenges persist in translating preclinical findings into clinical success.[2]
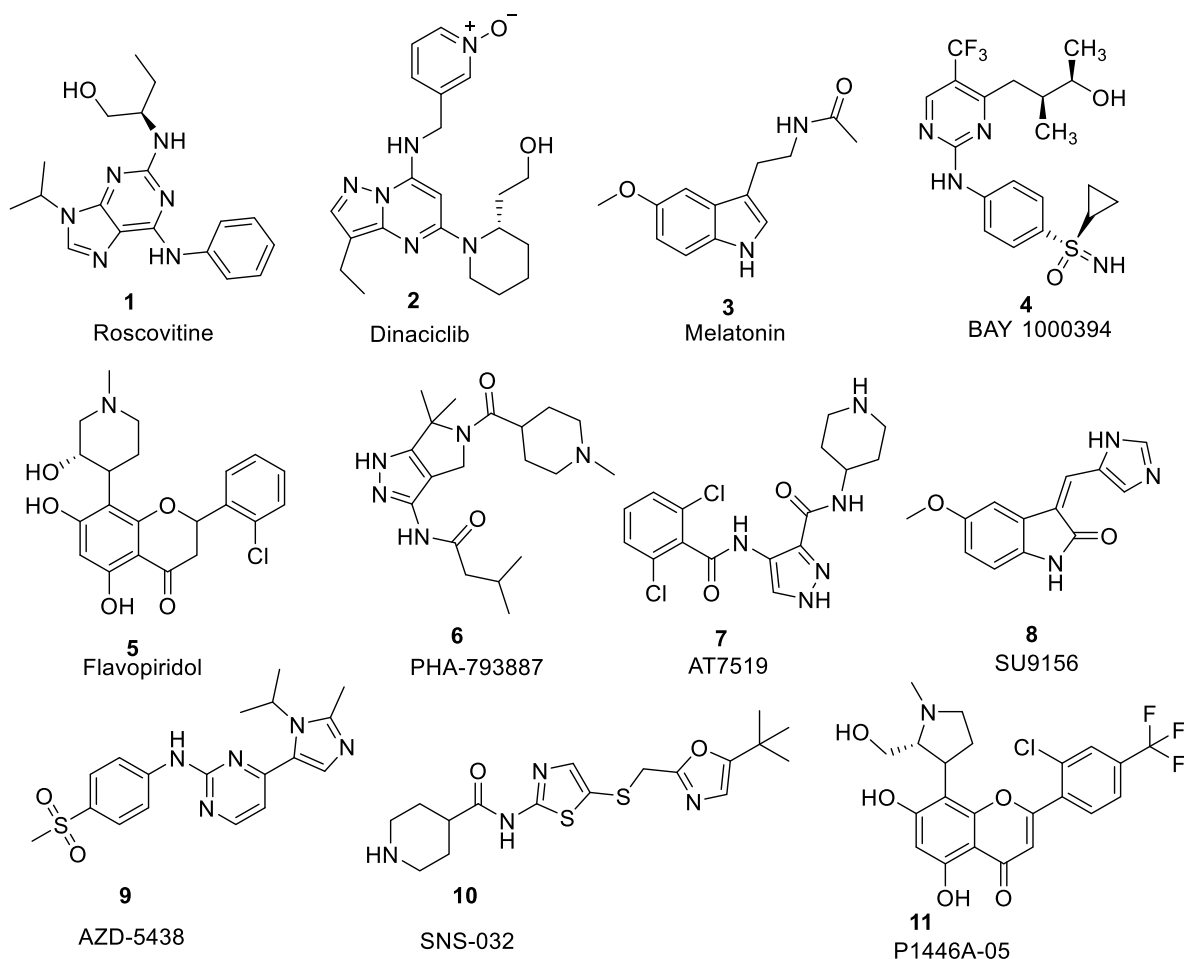
Figure 3.2 CDKs inhibitors in clinical trials

However, achieving therapeutic efficacy with CDK inhibitors necessitates selectivity, particularly in the context of structurally similar CDK isoforms. Among CDKs, CDK5 has

attracted significant attention as a therapeutic target in cancer due to its overexpression in various malignancies, including breast cancer, prostate cancer and glioblastoma, among others. Despite its potential as a therapeutic target, developing selective inhibitors for CDK5 has proven challenging owing to its structural resemblance to other CDK isoforms.

In this chapter, we designed and synthesized a series of novel CDK inhibitors targeting CDK5/p25, CDK2/CCNE, and CDK1/CCNB, with a focus on achieving interesting selectivity against CDK5. We performed molecular docking studies to investigate the binding interactions of the inhibitors with the target kinases and measured the kinase inhibition effects of the compounds.

Overall, our study underscores the importance of targeting specific CDK isoforms, particularly CDK5, in prostate cancer treatment. By delineating the molecular mechanisms underlying CDK dysregulation in cancer and developing selective inhibitors, we aim to advance precision medicine approaches for effective cancer therapy, ultimately improving patient outcomes and quality of life.

3.2 Structure and Biological Functions of CDK5

3.2.1 Structure of CDK5

CDK5 contains 292 amino acid stands hares high sequence homology with other CDKs, especially CDK2 (60%), whose substrate binding sites share 93% similarity (Figure 4.3A). CDK5 is composed of two main parts: a C-terminal domain (C-lobe) and an N-terminal domain (N-lobe) with the ATP binding site situated at the interface of these two domains (Figure 4.3B). The ATP binding site is typically a pocket or cleft located in the three-dimensional structure of the CDK5 protein. The N-lobe consists primarily of an α-helix and a β-sheet containing five antiparallel β-strands. The unique α-helix of CDK5 contains a PSSALRE sequence preceded by a 40s loop that interacts with activator proteins.[24]

The C-lobe is mainly composed of an α-helix containing a T-loop that regulates ATP and substrate binding at the interface of the N-lobe and C-lobe. While the activation of Thr160 in the T-loop of CDK2 requires phosphorylation of CDK activating kinase (CAK), CDK5 can be activated by p35 or p39 independent of CAK.[25, 26] Hydrogen bond interactions with active site inhibitors are commonly observed in the hinge region and the interface between the N and C-lobe scan bind ATP.[27] Unlike other CDKs that require cyclin for activation, CDK5 is typically activated by binding to p35 or p39, as well as their truncated products p25 and p29.[28] The ATP binding site is typically a pocket or cleft located in the three-dimensional structure of the CDK5 protein. It is a region specifically designed to accommodate ATP molecules, allowing them to interact with the kinase and participate in phosphorylation reactions.

(A)

10	16	45	51	81	84	144	147	
ATP-binding domain		Activators binding domain		Hinger region		T-loop		

CDK5/p25 complex

(B)
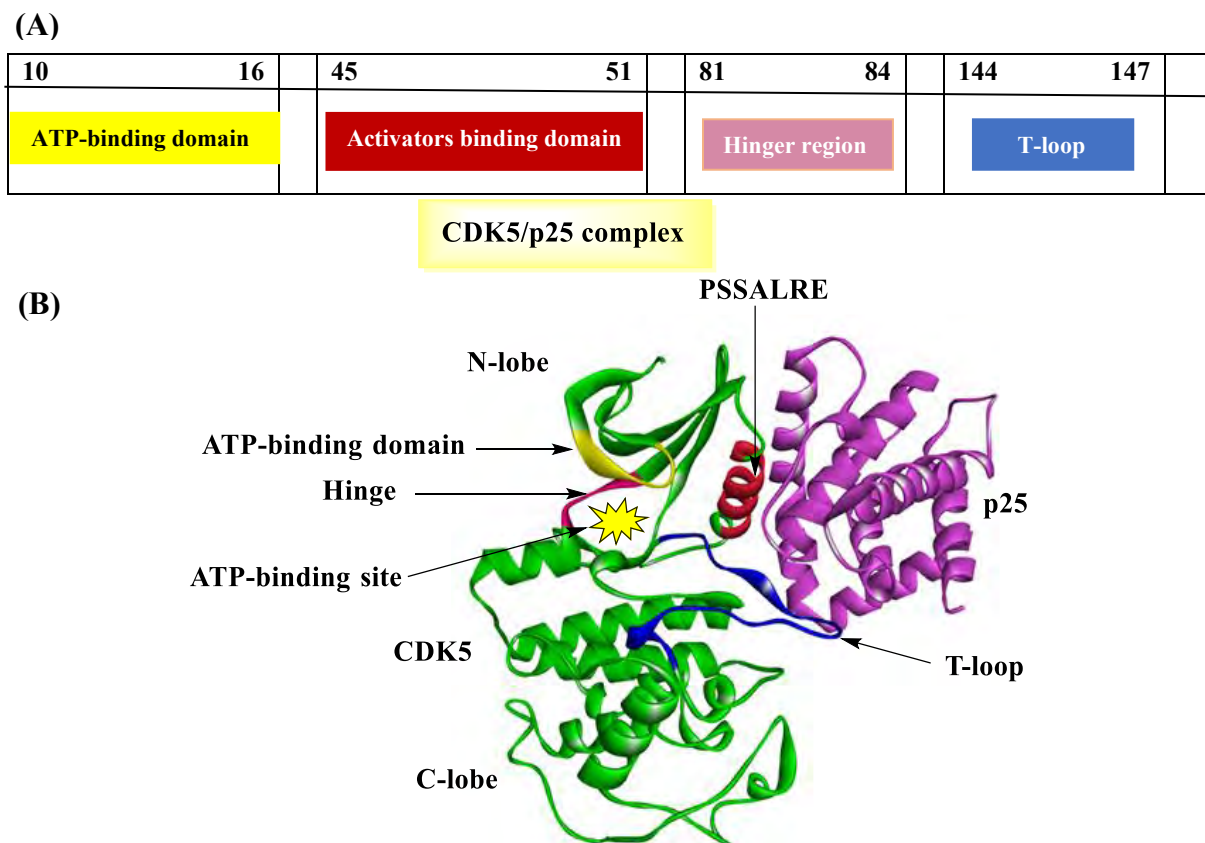
Figure 3.3 Structure of CDK5/p25 complex its binding site and interaction. (A) Modular domain of human CDK5. (B) The 3D structure of the CDK5/p25 complex depicts p25 (magenta) binding to CDK5 (green) around the PSSALRE helix (red) within the kinase's small lobe. This interaction involves extensive contacts with the activation loop or T-loop (dark blue).

3.2.2 Biological Function of CDK5

3.2.2.1 Role of CDK5 in Prostate Cancer

Abnormal expression of CDK5 has been found in prostate cancer. Unlike other CDKs, CDK5 is not primarily activated by cyclins. Prostate cancer, a prevalent malignancy in men, is a significant contributor to cancer-related mortality in the Western world. It progresses slowly and can metastasize, posing substantial challenges for diagnosis and treatment.[29] Prostate cancer, primarily affecting older men, progresses slowly and can metastasize. Age, with around 85% of cases diagnosed in individuals over 65, is a significant risk factor, while prostate-specific antigen (PSA) serves as a diagnostic marker.[30] CDK5, a protein complexed with p35, plays a pivotal role in prostate cancer progression by activating downstream signaling pathways that foster tumor growth. Moreover, CDK5 involvement extends beyond tumor growth regulation. It is implicated in angiogenesis through its influence on endothelial cell migration, highlighting its multifaceted role in cancer development.[31]

As previously mentioned, the CDK5 activator p25 is formed through cleavage of p35 by calpain. Under oxidative stress conditions, intracellular neuronal Ca^{2+} homeostasis is disrupted or met with death cells, calpain is activated and cuts p35 into p25 C-terminal fragment. Calpain cleaves p35 into p10 and p25, containing the binding domain to CDK5 (Figure 3.4). Compared with p35, p25 is resistant to ubiquitin-mediated degradation, so it is more stable and has a longer half-life. This results in an extended CDK5 activation period, inducing the hyperphosphorylation of CDK5 target molecules and neuronal toxicity.[32]
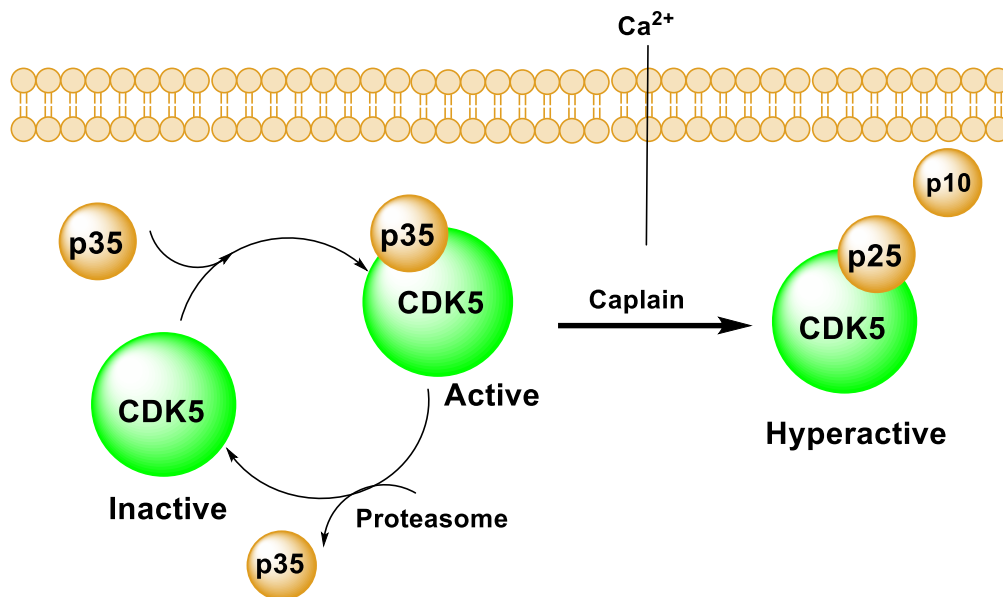
Figure 3.4 Activation of CDK5 by p35. CDK5 alone is an inactive catalyst subunit. CDK5 is activated by p35 CDK5 activator and move to the membrane as p35 binds to the membrane through myristorylation of the N-terminal region.

Additionally, recent studies have highlighted CDK5 significance in androgen production, particularly within the male reproductive system.[33] In Leydig cells responsible for testosterone production, CDK5 activity is modulated by human chorionic gonadotrophin (hCG), a crucial regulator of reproductive processes.[34] Inhibition of CDK5 activity results in decreased testosterone production, emphasizing its role in androgen steroidogenesis. Furthermore, CDK5 regulates the steroidogenic acute regulatory (StAR) protein, a key player in androgen production, by modulating its stability in Leydig cell mitochondria.[35] This regulatory mechanism ensures consistent androgen production, with implications for diseases like obesity and testicular cancer. These findings underscore the multifaceted role of CDK5 in prostate cancer and androgen production, suggesting potential avenues for targeted therapeutic interventions in this challenging disease.

3.2.2.2 Role of CDK5 in Tumor Angiogenesis

Angiogenesis is the process by which blood vessels form from pre-existing ones to ensure the delivery of oxygen and nutrients to growing tumor, allows removal of metabolic wastes and together with lymphatic vessels, provide an escape route for cancer cells migration to metastatic sites (Figure 3.5). Evidence is rapidly implicating CDK5 as a master regulator of angiogenesis at cancers.[36] In addition to tumor cells, CDK5 is expressed in endothelial cells lining of blood vessels that are usually quiescent and regulates their proliferative and migratory properties.[37]
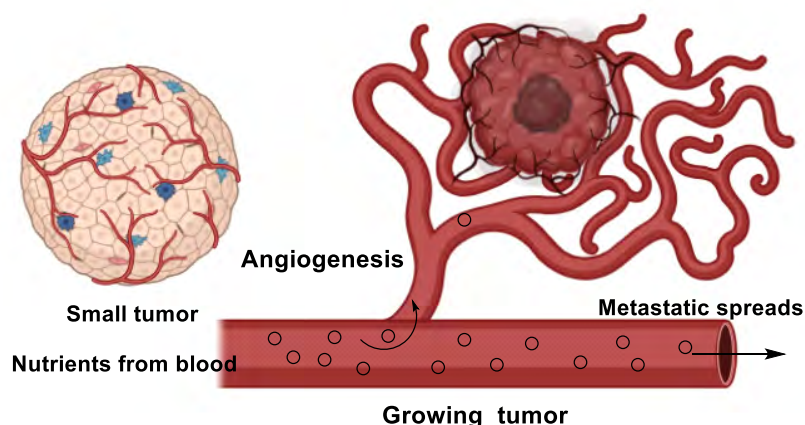
Figure 3.5 CDK5 in tumor angiogenesis

3.2.3 Rational Design

The high sequence homology between CDK5 and other kinases results in high similarity in inhibitor binding sites. Pan-CDK inhibitors lack selectivity for CDK5, causing unwanted adverse effects and ultimately reduced clinical efficacy. Selectively targeting CDK5 not only improves the clinical efficacy of inhibitors, but also reduces the incidence of adverse effects. In recent studies, a number of selective inhibitors with high efficiency in targeting CDK5 have been designed and synthesized through a series of approaches that includes high-throughput screening, fragment-based drug design, scaffold hopping and drug repurposing. In recent years, numerous indole-based anticancer agents have been identified from both natural and synthetic sources, exhibiting promising cytotoxic activities. For instance, compounds such as indirubin (**13**) which acts as an ATP competitive inhibitor, and BAY 1000394 (**14**) featuring a sulfoximine moiety, demonstrate noteworthy activity against CDK5 with an IC_{50} of 10 nM.[38] Additionally, molecules like GFB-12811 (**15**)[18] with an IC_{50} of 2.3 nM, along with compounds **16** (IC_{50} = 1 μM)[24] and **17** (IC_{50} = 4.3 μM), have shown potent kinase activity and have progressed to clinical trials (Figure 3.6).[39]
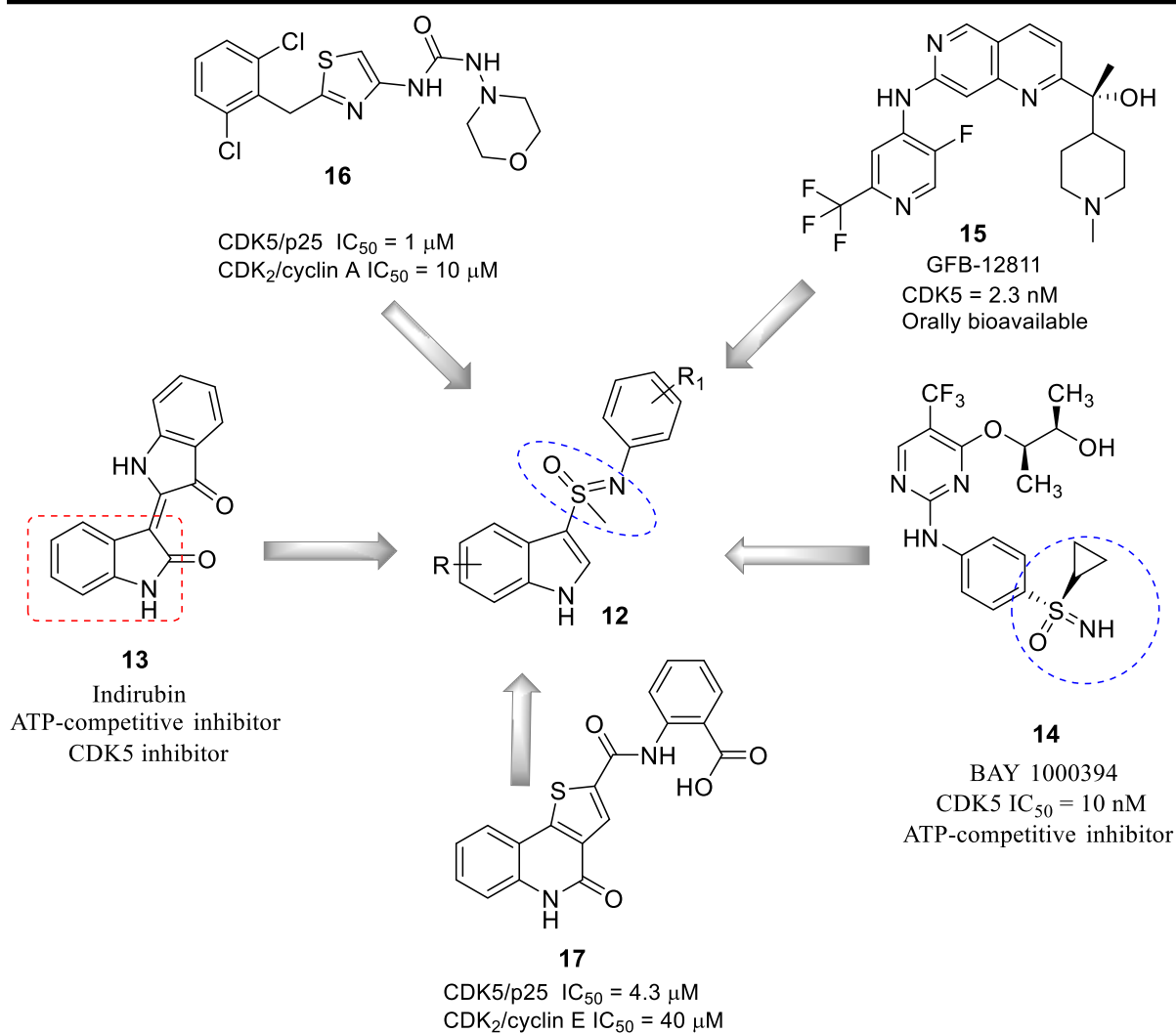
Figure 3.6 Rational Design of Indolylsulfoximines as CDK5 inhibitors

3.2.3.1 ATP competitive or Non-competitive Inhibitors
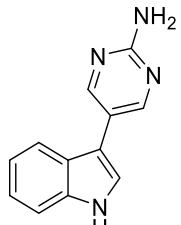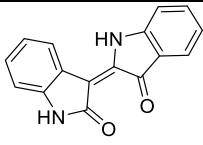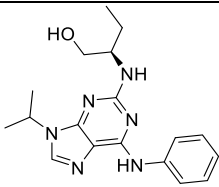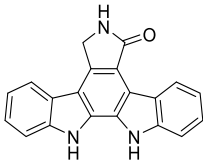
Efforts aimed at targeting cyclin-dependent kinase hyperactivity in human cancers began through compounds from natural sources. These first-generation ATP-competitive compounds served as templates for structure-guided, rational design of second-generation drugs that bind the ATP-binding pocket of CDKs (Table 3.2). Moreover, this class of drugs was implemented by compounds identified in activity-based screens of chemical libraries.[7] Over the more recent years, alternative strategies have been sought to develop compounds targeting pockets and patches which are distinct from the ATP pocket (Figure 3.7) which are thought to offer greater promises of selectivity and therefore circumvent some of the undesired side-effects of ATP-competitive inhibitors. They can be classified according to their specificity, as *pan*-specific or selective for one single CDK. Indirubin is a bis-indole and the active constituent of a Chinese antileukaemia medicine, Danggui Longhui Wan, that inhibits cyclin-dependent kinases, in

particular CDK1 and CDK5, as well as GSK-3β, and refrains cell proliferation by arresting cells at the G2/M transition.[40]
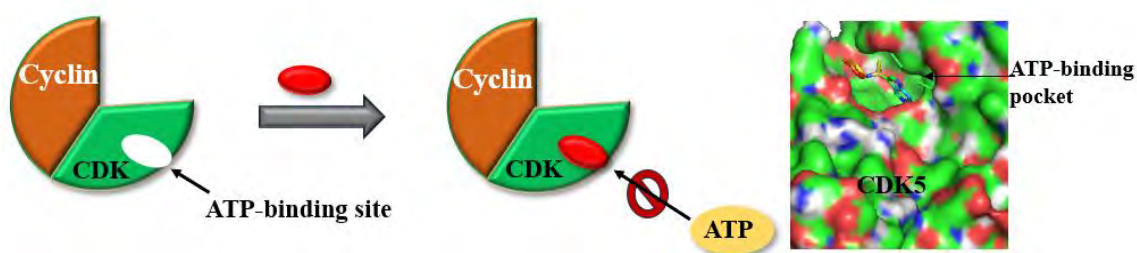
Figure 3.7 ATP-competitive inhibition of Cyclin-dependent Kinases

Table 3.2 Potent ATP-competitive inhibitors and their targets

Inhibitors	Type/Nature/Class	Target CDK
18 Merioline	ATP-competitive/ aminopyrimidine indole[41]	CDK1, CDK4
19 Indirubin	ATP-competitive inhibitor[42]	CDK1, CDK5
1 Roscovitine	ATP-competitive/ trisubstituted purine[43]	CDK5, CDK1 CDK2, CDK7
20 Staurosporine	ATP-competitive/alkaloid[44]	CDK1, CDK2, CDK4

3.3 Results and Discussion

3.3.1 Synthesis of *N*-aryl indolylsulfoximines (23a-k)

The synthesis and chacterization of *N*-arylindolyl sulfoximines (**23**) have been described inChapter 2a. The coupling of indolylsulfoximines (**21**) with aryl iodide **22** under MW involves the use of CuI (10 mol%), 1,10-phenanthroline (20 mol%), Cs$_2$CO$_3$ (2.5 equiv) in dry DMF at 130 °C for 35 min.
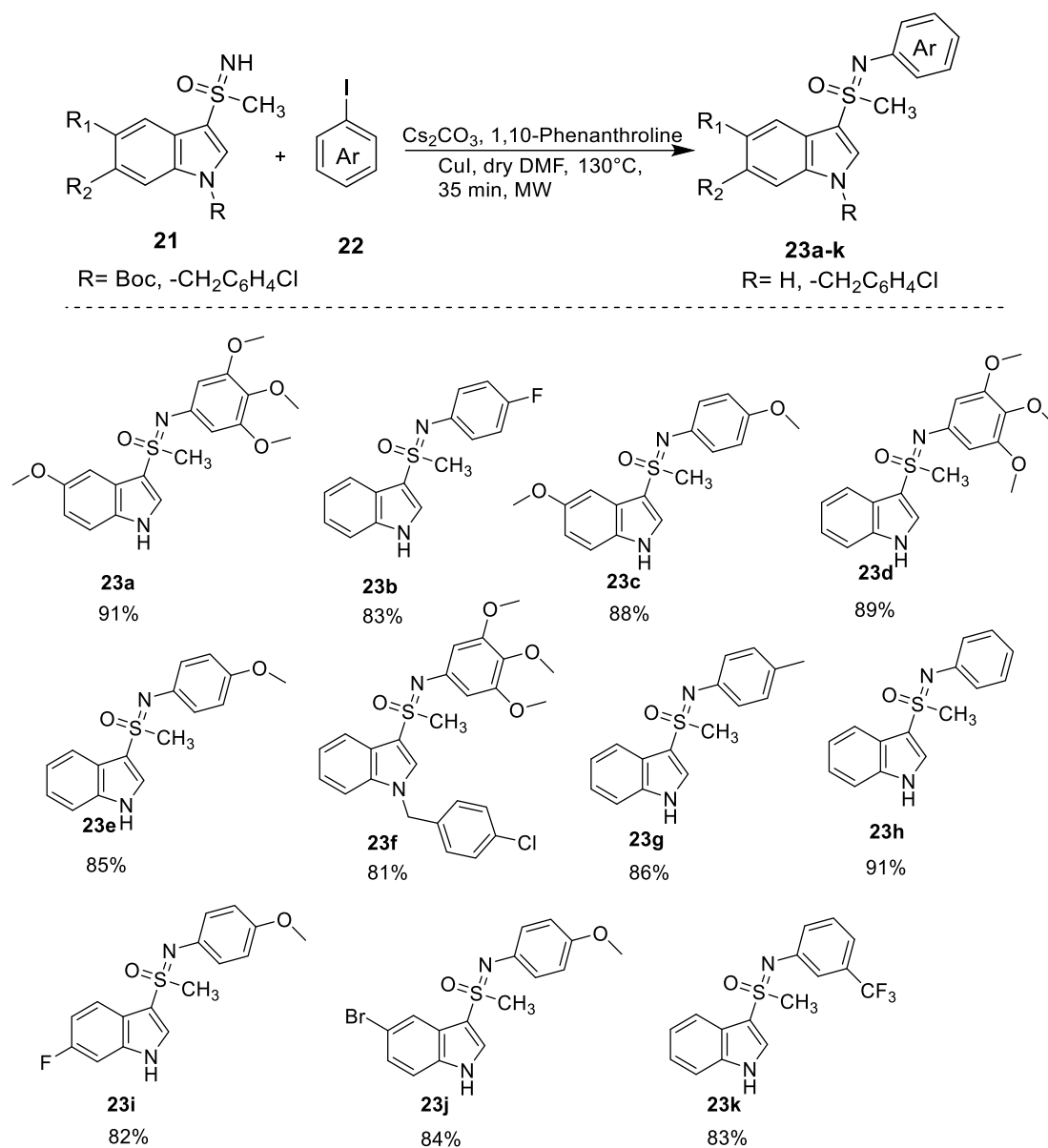
Scheme 3.1 Synthesis of *N*-arylindolylsulfoximines

3.3.2 Biological Evaluation

3.3.2.1 Anti-cancer Activity

The synthesized *N*-arylated indolylsulfoximine analogues **22a-k** were assessed *in vitro* for their cytotoxicity against a panel of cancer cell lines including 22Rv1, PC3 and C4-2 (human prostate cancer cells), MCF7 (human breast cancer cells) and HEK293 (normal human kidney cells) and the results are mentioned in previous chapter. The indolylsulfoximines **23c** (2.76 µM) showed selective cytotoxicity against 22Rv1 cells. The indolylsulfoximine derivatives **23b** (3.7 µM), **23e** (1.95 µM) and **23g** (2.3 µM) displayed good cytotoxicity against C4-2 cells. The introduction of electron-donating group, for example, sulfoximine derivatives **23g** (1.6 µM) and **23k** (1.28 µM) led to selective cytotoxicity against MCF7 cells. The indolylsulfoximines **23a-k** were found to be non-cytotoxic to normal HEK293 cells (>40 µM), indicating their potential selectivity towards cancer cells.

3.3.2.2 Cellular kinase activity of *N*-aryl indolylsulfoximines (22a-k)

The synthesized *N*-arylated indolylsulfoximine analogues **22a-k** tested for *in vitro* activity against various kinases including CDK5/p25, CDK1/CCNB, CDK2/CCNE, and AURKA. To validate the inhibition of CDKs in a cellular context, we evaluated the potency of these compounds using luciferase glow Kinase Assay. Our newly developed CDK inhibitors demonstrated potent cellular target engagement for CDK5/p25.

Table 3.3 Kinase activity for *N*-aryl indolylsulfoximines **23a-k** (IC_{50}, µM)

Compounds	CDK5/p25	CDK1/CCNB	CDK2/CCNE	AURKA
23a	15.9 ± 0.25	21.9 ± 0.93	27.6 ± 0.67	>40
23b	22 ± 1.83	19.8 ± 0.63	25 ± 0.25	>40
23c	$\mathbf{2.15 \pm 0.051}$	$\mathbf{16.45 \pm 0.38}$	$\mathbf{31 \pm 0.095}$	>40
23d	25 ± 0.098	26.2 ± 0.084	18.6 ± 0.12	>40
23e	$\mathbf{10.23 \pm 0.23}$	27 ± 0.61	23.5 ± 0.05	39
23f	16 ± 0.85	14 ± 0.92	18 ± 0.36	7.9
23g	$\mathbf{1.12 \pm 0.29}$	$\mathbf{20.8 \pm 0.16}$	$\mathbf{21.69 \pm 0.06}$	>40
23h	21 ± 0.59	31.8 ± 0.55	>40	>40
23i	17 ± 0.91	18.6 ± 0.24	19.96 ± 0.05	>40
23j	>40	>40	35 ± 0.23	14.3
23k	15.9 ± 0.26	11.6 ± 0.21	27.3 ± 0.56	>40
Roscovitine	0.16	0.65	0.70	-

The results for a subset of compounds are summarized in Table 3.3, with the pan CDK inhibitor roscovitine included as a control compound. Compound **23a** exhibited activity against different kinases, with IC_{50} values of 15.9 μM for CDK5/p25, 21.9 μM for CDK1/CCNB, and 27.6 μM for CDK2/CCNE. Interestingly, compound **23c** bearing 5-methoxyindole and *N*-aryl sulfoximine, displayed selectivity towards different kinase activities, with IC_{50} values of 2.15 μM (CDK5/p25), 16.45 μM (CDK1/CCNB), 31.0 μM (CDK2/CCNE), and >40 μM (AURKA). Compounds **23b**, **23f**, and **23i** exhibited activity against all tested kinases, with IC_{50} values ranging from 14.0 to 25.0 μM for CDK5, CDK1, and CDK2. Compound **23g** emerged as a potent CDK5/p25 inhibitor with an IC_{50} value of 1.12 μM, demonstrating selectivity over other kinases. And **23c** displayed 2.15 μM activity against CDk5/p25. Compound **23k** emerged as a dual inhibitor of CDK5 (15.9 μM) and CDK2 (11.6 μM) (Table 3.3). The selectivity of our compounds for CDK5 versus other CDKs was further evaluated using biochemical assays performed at the ATP site for each kinase. The results suggested that the shift in IC_{50} values was consistent with what would be expected for ATP-competitive inhibitors, confirming the selectivity of the compounds for CDK5 even in the presence of high ATP concentrations, such as in a cellular environment.

3.4 Molecular Docking Studies

3.4.1 Docking study of CDK5/p25 with *N*-aryl indolylsulfoximines (23g)

Many CDK inhibitors have been discovered, but only a few of them have demonstrated an appreciable selectivity for CDK5. However, achieving high selectivity for CDK5 over other members of CDK family is challenging due to their structural similarities of the ATP-binding sites; particularly CDK2, where only two of the 29 common residues of the ATP-binding pocket (Leu83 and His84) are different from those of CDK5 (Cys83 and Asp84). The ATP binding site is typically a pocket or cleft located in the three-dimensional structure of the CDK5 protein. Therefore, other factors such as differences in binding cavity volume and plasticity may be explored. The hinge region of CDK5 protein contains unique residues, in other words, Cys83 and Asp84, targeting which may favour CDK5 binding.

The newly synthesized indolylsulfoximines have been identified as potent CDK5 inhibitors, binding specifically to the ATP binding site within the CDK5 kinase. The ATP binding site is a critical region located in the active site of CDK5, responsible for the crucial process of ATP binding and hydrolysis, which is essential for CDK5 kinase activity and subsequent phosphorylation of target proteins. By selectively targeting this site, these indole-based molecules effectively compete with ATP, leading to the inhibition of CDK5 kinase activity. As a result, various cellular processes regulated by CDK5 are modulated, offering potential

therapeutic implications for diseases associated with CDK5 dysregulation. The crystal structure of the complex provides intricate details about the arrangement of atoms and amino acid residues within this binding site. It is a region specifically designed to accommodate ATP molecules, allowing them to interact with the kinase and participate in phosphorylation reactions. Molecular docking investigates the interaction between a compound (ligand) and its targeted protein. It investigates the binding affinity, nature and type of bonding and nonbonding interactions between the ligand and amino acid residues of the protein.
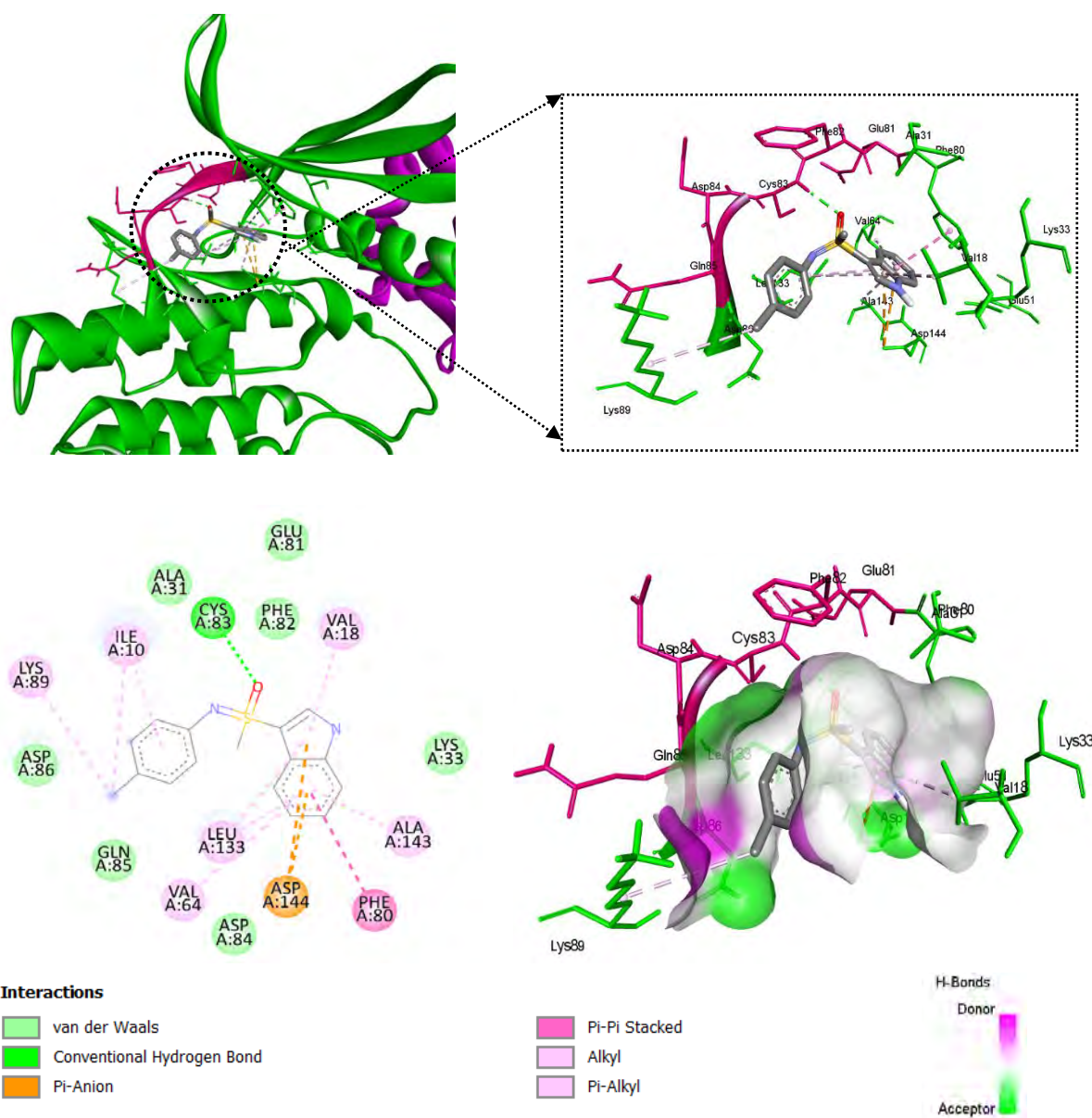
Figure 3.8 CDK5 binding modes by its inhibitor: Key interactions made by potent **23g** with CDK5/p25. CDK5 (green ribbon)/p25 (magenta ribbon) (PDB:1H4L). Hydrogen bonds are shown in green lines. Several types or interaction were shown by color with different amino acids residues.

Our docking studies revealed that roscovitine, a standard drug, interacts with the active site residues of the target kinases. Specifically, it engages in conventional hydrogen bonding with residues CYS:83 and ASP:144, forming stable interactions. Additionally, roscovitine exhibits Pi-Pi stacking with residue PHE:80 and hydrophobic interactions with residues ILE:10, ALA:31, VAL:64, LEU:133, and ALA:143. These interactions contribute to a binding affinity of -7.7 kcal/mol, indicating a strong affinity between roscovitine and CDK5 as shown in Figure 3.8.

In contrast, our molecular docking studies demonstrated that compound **23g**, a CDK5 inhibitor, binds specifically to the ATP binding active site of the target kinases with high binding affinity (-8.5 kcal/mol). **23g** forms a significant hydrogen bonding interaction with CYS:83, which is identified as the most potent interaction in CDK5. Furthermore, **23g** exhibits hydrophobic interactions with residues PHE:80, ILE:10, LEU:133, VAL:18, LYS:89, VAL:64, ASP:144, and ALA:143, contributing to the stability of the binding complex (Figure 3.8). Similarly, **23c** also engages in molecular interactions with the CDK5. It demonstrates two hydrogen bonding interactions with LYS:89 and ASP:144, as well as hydrophobic interactions involving residues PHE:82, ILE:10, LEU:133, and GLN:85 with binding affinity -7.3 Kcal/mol. These interactions collectively contribute to the binding affinity and specificity of **23c** towards the CDK5/p25 (Figure 3.9).
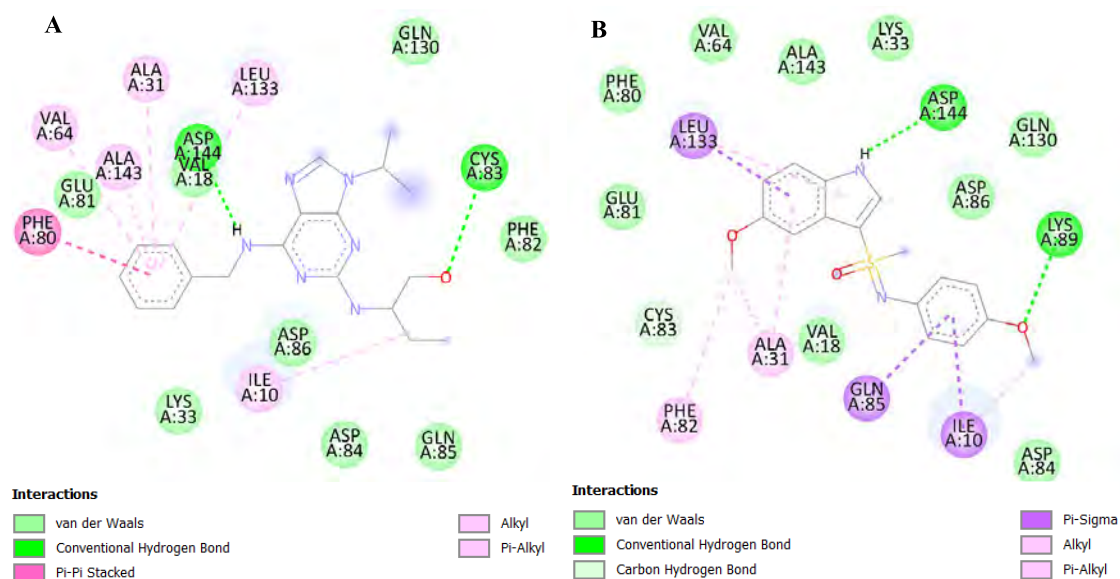
Figure 3.9 2D interactions: (A) between roscovitine and CDK5/p25 with binding affinity -7.7 Kcal/mol (PDB code: 1H4L), (B) between **23c** and CDK5/p25 with binding affinity -7.3 Kcal/mol.

3.4.2 Docking study of CDK2/CCNE with *N*-aryl indolylsulfoximine (23g)

Interactions between compound **23g** and the standard drug roscovitine with CDK2/CCNE are depicted in figure 3.9. The compound **23g** exhibited a lower binding affinity (-6.5 kcal/mol) when compared to roscovitine (-7.0 kcal/mol). Specifically, **23g** formed a hydrogen bonding interaction between its indolyl NH group and GLU:81, along with hydrophobic interactions with VAL:18, ILE:10, VAL:64, and ALA:131 (Figure 3.10). These findings suggested that **23g** is less potent as a CDK2 inhibitor compared to roscovitine. Consequently, **23g** and **23c** are not as effective as CDK2 inhibitors.
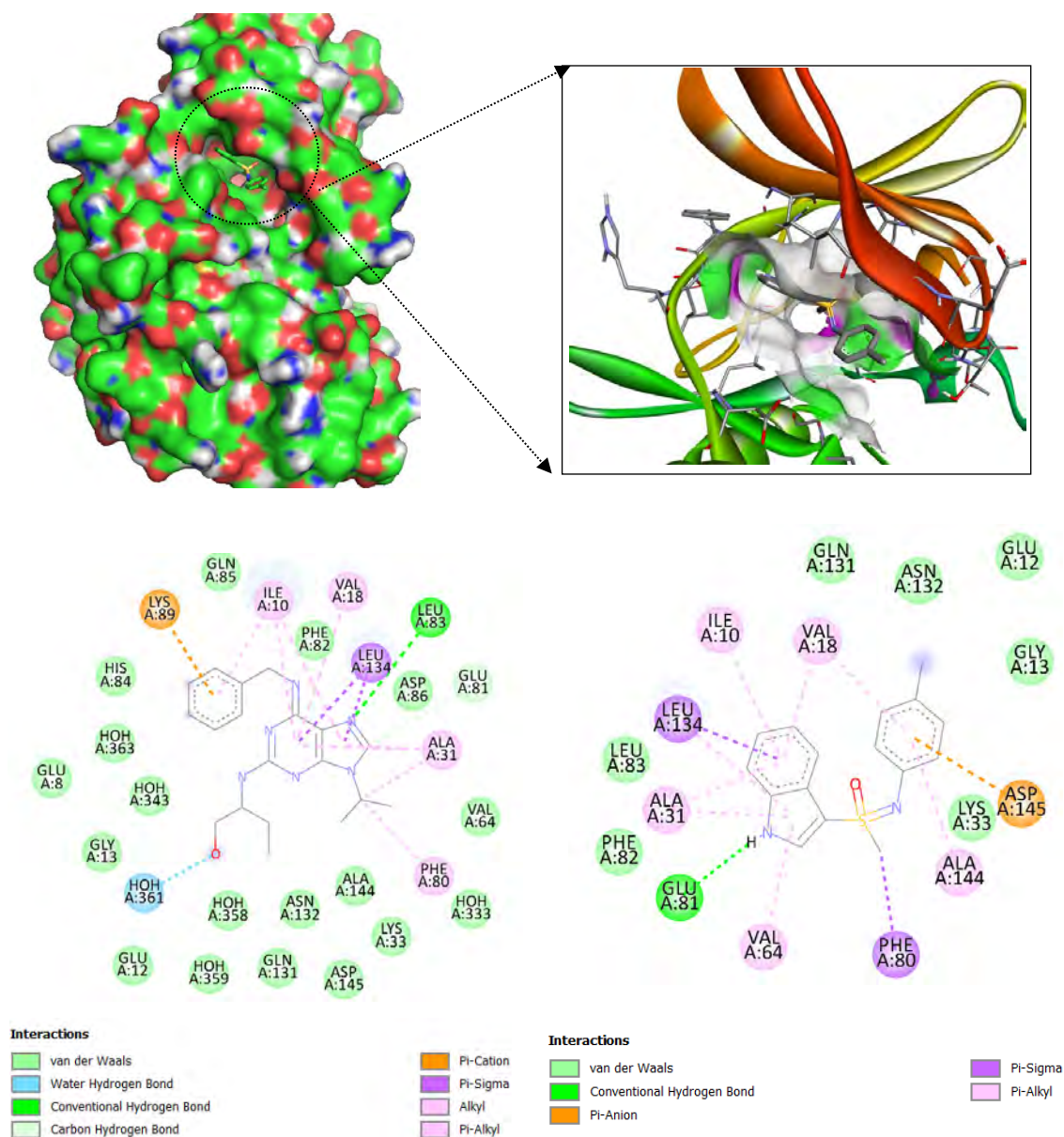
Figure 3.10 Roscovitine binding affinity in CDK2 -7.0 Kcal/mol and **23g** binding affinity -6.5 Kcal/mol. Key interactions made by **23g** and roscovitine with CDK2. Hydrogen bonds are shown in green lines.

3.4.3 Molecular docking study of CDK1/CCNB with *N*-aryl indolylsulfoximine (23g)

The compound **23g**, does not bind to the ATP binding site of the CDK1/CCNB complex but likely to interacts with other regions or sites on the protein (Figure 3.11). Roscovitine, a well-established CDK1 inhibitor, typically binds to the ATP binding site of CDK1, thereby inhibiting its activity. However, **23g** demonstrates a distinct interaction pattern compared to roscovitine. The inability of **23g** to bind to the ATP binding site suggests that it may operate *via* different mechanism of action or target site in comparison to roscovitine. Our docking study indicates that **23g** interacts with allosteric sites on CDK1/CCNB, suggesting a potential allosteric mechanism of inhibition. Moreover, kinase activity assay reveals that **23g** exhibits IC_{50} value of 30 µM, significantly higher than the IC_{50} value of roscovitine, which is 0.65 µM. This difference further supports the notion that **23g** operates through a distinct mechanism from roscovitine, likely targeting different sites or exerting its effects via different pathways within the CDK1/CCNB complex.
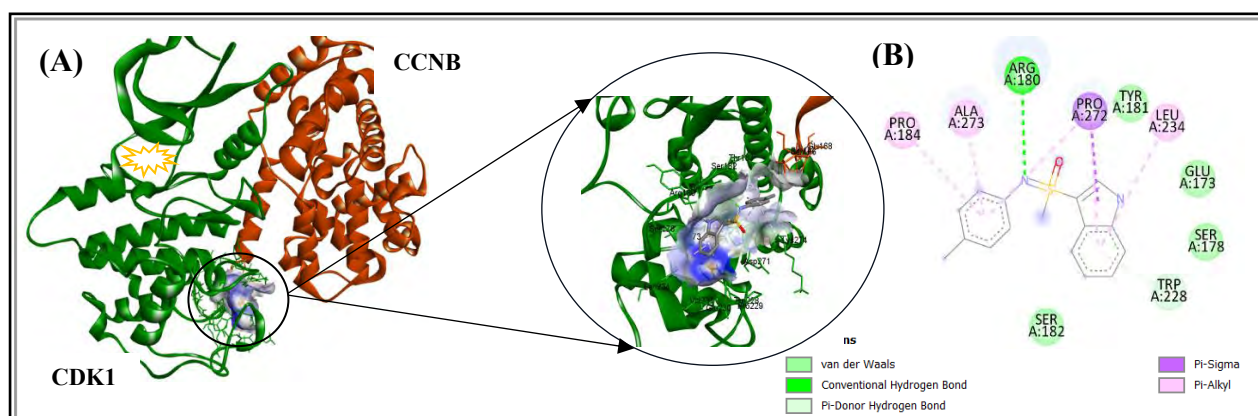
Figure 3.11 (A) 3D interaction between the protein–ligand complex CDK1/CCNB and **23g** after molecular docking. (B) 2D interaction between the protein–ligand complex.

3.4.4 Drug-likeness prediction and ADME properties

Following the molecular docking studies of **23c** and **23g**, an evaluation of ADME (absorption, distribution, metabolism, and excretion) properties was conducted, encompassing parameters such as size, solubility, lipophilicity, and other drug-likeness attributes for indolylsulfoximine analogues. The Swiss ADME web server was employed for these calculations, and the results are summarized in Table 3.4. In drug discovery, adherence to Lipinski's rule of five is crucial for a compound to be considered a potential lead.

After administration of the drug through any route to the human body or in the animal model, it undergoes the absorption, distribution, metabolism, excretion resulting active or passive transport to the target site. Interaction with the target biological macromolecules might produce

desirable or undesirable pharmacological effect. Drug design is a step-by-step evaluation process and lacking the evaluation my reason for rejection of the drug, which is costly for any companies. The bioavailability of a drug depends on the safety and efficacy, lack of safety and efficacy are the main cause of drug failure, which are mainly depend on the ADME properties. Here, we evaluate the ADME properties of the selected *N*-aryl indolylsulfoximines by using *in silico* SwissADME to see the pharmacokinetic properties.[25] The ADME properties of the selected compounds has shown in Table 3.4.

Table 3.4 List of pharmacokinetic properties (physico-chemical, lipophilicity, water solubility, drug likeness, and medicinal chemistry) of the selected potent *N*-aryl indolylsulfoximines with standard roscovitine.

Properties	Parameters	Roscovitine	23g	23c
Physico-chemical properties	MW (g/mol)	354.45	284.38	330.40
	Heavy atoms	26	20	23
	Arim. Heavy atoms	15	15	15
	Rotatable bonds	8	2	4
	H-bond acceptors	4	2	4
	H-bond donors	3	1	1
	Molar Refractivity	104.88	84.20	92.22
Lipophilicity	Log $P_{o/w}$	3.16	3.29	3.63
Water Solubility	Log S (ESOL)	-3.93	-4.58	-4.39
Pharmacokinetics	GI absorption	High	High	High
Drug likeness	Lipinski, Violation	0	0	0
Medic. chemistry	Synth. accessibility	3.58	3.64	3.85

BOILED-Egg model

The blood−brain barrier (BBB) penetration and gastointestinal (GI) absorption are found to be significant pharmacokinetic behaviors which need to be estimated in the process of drug development. The polarity and the lipophilicity of the molecules can be computed using the Brain Or IntestinaL EstimateD permeation method (BOILED-Egg) which provides datasets with accuracy, speed, and clear graphical outputs. In this model, the white region indicates greater probability of passive absorption of the GI tract, while the yellow area (yolk) signifies the high possibility of BBB penetration. The blue color indicator shows that the molecule is effluxed actively by P-glycoprotein, represented as (PGP+). Thus, the BOILED-Egg model

graph (Figure 3.12) predicted that our compound **23c** would undergo GI absorption not permeate through the BBB and its very close to cross blood-brain barrier.
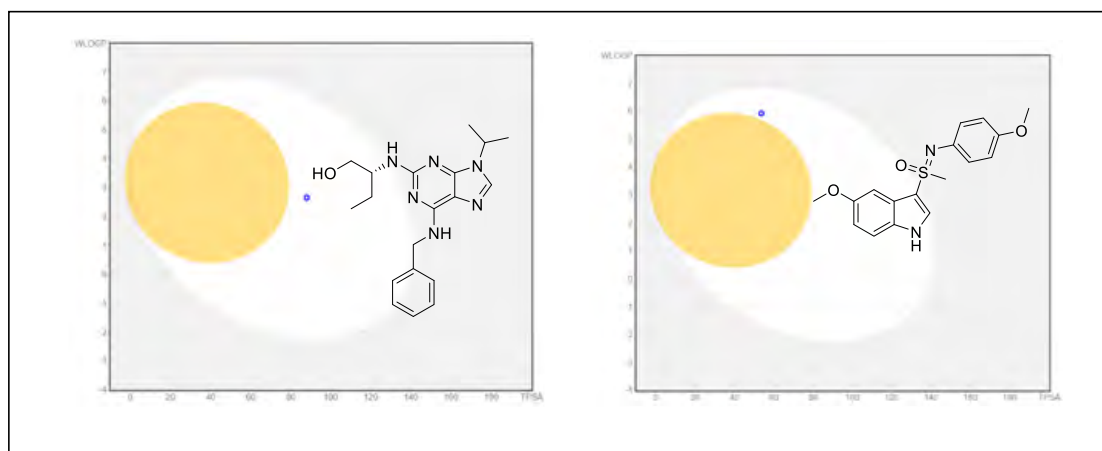
Figure 3.12 BOILED-Egg graph of roscovitine and indolylsulfoximine **23c**

3.5 Conclusions

Our synhesized indolylsulfoximines analogues displayed significant anticancer activity against PC3, C4-2, and MCF7 human cancer cell lines, bolstering their potential for cancer therapy. The dysregulation of CDK5 across various human cancers underscores its pivotal role in tumorigenesis and multiple cancer hallmarks, making it an attractive target for anticancer drug development. While the pursuit of pharmacological inhibitors with CDK5 specificity is essential for effective and low-toxicity treatment, the structural similarities between CDK5 and other family members, such as CDK2, present a challenge in designing mono-specific inhibitors. Our synthesis endeavors have yielded novel CDK inhibitors, *N*-aryl indolylsulfoximines (compounds **23a-k**), with compounds **23c** and **23g** demonstrating selectivity for CDK/p25 over other kinases. Notably, compound **23g** emerges as a potent CDK5/p25 inhibitor with an IC_{50} value of 1.12 μM, exhibiting selectivity over alternative kinases. And compound **23c** also shows promising selectivity with an IC_{50} value of 2.15 μM for CDK5/p25. The incorporation of the sulfoximine group not only enhances water solubility but also improves various pharmacokinetic and drug-like properties. Docking studies shed light on the interaction of compound **23g** with CYS83 of CDK5, and high binding affinity (-8.5 Kcal/mol) highlighting its potential as a therapeutic agent in cancer treatment. The docking results also showed a strong correlation with the *in vitro* study outcomes, indicating that the predicted binding modes and interactions between the **23g** and targeted proteins closely resembled the observed biological activities.

3.6 Biology Protocols

3.6.1 Transformation of CDKs DNA

In the process of transformation, BL21 cells were initially transformed with 1µL of DNA. Subsequently, colonies were inoculated in 30 mL and allowed to grow for 10 h. Following centrifugation, the cells were washed with LB media and then inoculated in 600 mL for further growth until the optical density (OD) reached 0.4-0.6. The addition of 60 µL of IPTG and a 3-h incubation induced protein expression, after which the cells were centrifuged, and the resulting pellets were stored at -20 °C.

3.6.2 Protein Purification

For protein purification, the pellets were treated with substrate lysis buffer containing 1mm PMSF. The cells were then subjected to French press treatment, followed by centrifugation to obtain the supernatant. The supernatant was transferred to a fresh tube, and beads prewashed with lysis buffer were added. Subsequent washing steps involved treating the beads with water, substrate lysis buffer, and different stringent buffers. The tube was left rotating at 4 °C for 1 h. Following centrifugation and removal of the supernatant, the beads underwent additional washing steps with low, medium, and high stringent buffers. The final step involved eluting the purified protein with elution buffer. This comprehensive process aims to efficiently transform cells, induce protein expression, and purify the target protein using a series of washing and elution steps with stringent buffers.

3.6.3 Kinase Assay

The Luciferase Kinase Assay is a widely used method for evaluating the activity of kinases, enzymes that play critical roles in cellular signaling pathways. In this assay, the activity of a specific kinase, such as CDK5/p25, CDK1/CCNE, CDK2/CCNB is assessed by measuring the phosphorylation of a target substrate peptide in the presence of ATP. The protocol involves setting up kinase reaction tubes containing the kinase, substrate, ATP, and test compounds, followed by incubation and subsequent addition of a luciferase reaction mixture. In the Luciferase Glow Kinase Assay protocol, following the incubation of the kinase reaction on a shaker at 25 °C for 30 min, the contents of the reaction tubes are centrifuged briefly to collect them at the bottom. Subsequently, the Luciferase buffer solution is prepared by combining 1 µL of luciferin with 1000 µL of luciferase buffer in a tube. Following this, 1 µL of luciferase enzyme, stored at -20 °C, is quickly added to the mixture. After the preparation of the Luciferase buffer solution, a 365-well white plate is utilized for the subsequent steps of the kinase glow protocol, facilitating the measurement of luminescence emitted   by the reaction

on plate reader. Relative inhibition was calculated as mean absorbance of treated cells/mean absorbance of DMSO treated cells (negative control). The IC_{50} values and dose response curve were obtained by nonlinear regression analysis [non-linear regression (sigmoidal dose response with variable slope)] using Graph Pad Prism, version 6.0 software (Graph Pad Software Inc., CA, USA).

3.6.4.1 Chemistry

Synthetic procedures and spectral data of *N*-aryl indolylsulfoximines (**23a-k**) are provided Chapter 2A of the thesis.

3.7 References

1. Tang, W.; Lin, C.; Yu, Q.; Zhang, D.; Liu, Y.; Zhang, L.; Zhou, Z.; Zhang, J.; Ouyang, L., Novel Medicinal Chemistry Strategies Targeting CDK5 for Drug Discovery. *Journal of Medicinal Chemistry* **2023**, *66* (11), 7140-7161.

2. Tang, W.; Lin, C.; Yu, Q.; Zhang, D.; Liu, Y.; Zhang, L.; Zhou, Z.; Zhang, J.; Ouyang, L., novel medicinal chemistry strategies targeting CDK5 for Drug Discovery. *Journal of Medicinal Chemistry* **2023,** *66* (11), 7140-7161.

3. Nikhil, K.; Shah, K., CDK5: an oncogene or an anti-oncogene: location location location. *Molecular Cancer* **2023,** *22* (1), 186.

4. Nakamura, S.; Kawamoto, Y.; Nakano, S.; Akiguchi, I.; Kimura, J., p35 nck5a and cyclin-dependent kinase 5 colocalize in Lewy bodies of brains with Parkinson's disease. *Acta Neuropathologica* **1997,** *94*, 153-157.

5. Lampropoulou, E.; Logoviti, I.; Koutsioumpa, M.; Hatziapostolou, M.; Polytarchou, C.; Skandalis, S. S.; Hellman, U.; Fousteris, M.; Nikolaropoulos, S.; Choleva, E., Cyclin-dependent kinase 5 mediates pleiotrophin-induced endothelial cell migration. *Scientific Reports* **2018,** *8* (1), 5893.

6. Liu, J.-L.; Wang, X.-Y.; Huang, B.-X.; Zhu, F.; Zhang, R.-G.; Wu, G., Expression of CDK5/p35 in resected patients with non-small cell lung cancer: relation to prognosis. *Medical Oncology* **2011,** *28*, 673-678.

7. Peyressatre, M.; Prével, C.; Pellerano, M.; Morris, M. C., Targeting cyclin-dependent kinases in human cancers: from small molecules to peptide inhibitors. *Cancers* **2015**, *7* (1), 179-237.

8. Zhao, M. Y.; Auerbach, A.; D'Costa, A. M.; Rapoport, A. P.; Burger, A. M.; Sausville, E. A.; Stass, S. A.; Jiang, F.; Sands, A. M.; Aguilera, N., Phospho-p70S6K/p85S6K and

cdc2/cdk1 are novel targets for diffuse large B-cell lymphoma combination therapy. *Clinical Cancer Research* **2009**, *15* (5), 1708-1720.

9. Abdullah, C.; Wang, X.; Becker, D., Expression analysis and molecular targeting of cyclin-dependent kinases in advanced melanoma: functional analysis and molecular targeting of cyclin-dependent kinase family members in advanced melanoma. *Cell Cycle* **2011**, *10* (6), 977-988.

10. Catania, A.; Urban, S.; Yan, E.; Hao, C.; Barron, G.; Allalunis-Turner, J., Expression and localization of cyclin-dependent kinase 5 in apoptotic human glioma cells. *Neuro-oncology* **2001**, *3* (2), 89-98.

11. Strock, C. J.; Park, J.-I.; Nakakura, E. K.; Bova, G. S.; Isaacs, J. T.; Ball, D. W.; Nelkin, B. D., Cyclin-dependent kinase 5 activity controls cell motility and metastatic potential of prostate cancer cells. *Cancer Research* **2006**, *66* (15), 7509-7515.

12. Tarricone, C.; Dhavan, R.; Peng, J.; Areces, L. B.; Tsai, L.-H.; Musacchio, A., Structure and regulation of the CDK5-p25nck5a complex. *Molecular Cell* **2001**, *8* (3), 657-669.

13. Otyepka, M.; Bártová, I.; Kříž, Z. k.; Koča, J., Different mechanisms of CDK5 and CDK2 activation as revealed by CDK5/p25 and CDK2/cyclin A dynamics. *Journal of Biological Chemistry* **2006,** *281* (11), 7271-7281.

14. Liang, Q.; Li, L.; Zhang, J.; Lei, Y.; Wang, L.; Liu, D.-X.; Feng, J.; Hou, P.; Yao, R.; Zhang, Y., CDK5 is essential for TGF-β1-induced epithelial-mesenchymal transition and breast cancer progression. *Scientific Reports* **2013**, *3* (1), 2932.

15. Eggers, J. P.; Grandgenett, P. M.; Collisson, E. C.; Lewallen, M. E.; Tremayne, J.; Singh, P. K.; Swanson, B. J.; Andersen, J. M.; Caffrey, T. C.; High, R. R., Cyclin-dependent kinase 5 is amplified and overexpressed in pancreatic cancer and activated by mutant K-Ras. *Clinical Cancer Research* **2011**, *17* (19), 6140-6150.

16. Banik, S. M.; Pedram, K.; Wisnovsky, S.; Ahn, G.; Riley, N. M.; Bertozzi, C. R., Lysosome-targeting chimaeras for degradation of extracellular proteins. *Nature* **2020**, *584* (7820), 291-297.

17. De Azevedo, W. F.; Leclerc, S.; Meijer, L.; Havlicek, L.; Strnad, M.; Kim, S. H., Inhibition of cyclin‐dependent kinases by purine analogues: crystal structure of human cdk2 complexed with roscovitine. *European Journal of Biochemistry* **1997**, *243* (1‐2), 518-526.

18. Daniels, M. H.; Malojcic, G.; Clugston, S. L.; Williams, B.; Coeffet-Le Gal, M.; Pan-Zhou, X.-R.; Venkatachalan, S.; Harmange, J.-C.; Ledeboer, M., Discovery and

optimization of highly selective inhibitors of CDK5. *Journal of Medicinal Chemistry* **2022**, *65* (4), 3575-3596.

19. Ghia, P.; Scarfò, L.; Perez, S.; Pathiraja, K.; Derosier, M.; Small, K.; McCrary Sisk, C.; Patton, N., Efficacy and safety of dinaciclib vs ofatumumab in patients with relapsed/refractory chronic lymphocytic leukemia. *The Journal of American Society of Hematology* **2017**, *129* (13), 1876-1878.

20. Kumar, S. K.; LaPlant, B.; Chng, W. J.; Zonder, J.; Callander, N.; Fonseca, R.; Fruth, B.; Roy, V.; Erlichman, C.; Stewart, A. K., Dinaciclib, a novel CDK inhibitor, demonstrates encouraging single-agent activity in patients with relapsed multiple myeloma. *The Journal of American Society of Hematology* **2015**, *125* (3), 443-448.

21. Lin, T. S.; Ruppert, A. S.; Johnson, A. J.; Fischer, B.; Heerema, N. A.; Andritsos, L. A.; Blum, K. A.; Flynn, J. M.; Jones, J. A.; Hu, W., Phase II study of flavopiridol in relapsed chronic lymphocytic leukemia demonstrating high response rates in genetically high-risk disease. *Journal of Clinical Oncology* **2009**, *27* (35), 6012.

22. Semenov, I.; Akyuz, C.; Roginskaya, V.; Chauhan, D.; Corey, S. J., Growth inhibition and apoptosis of myeloma cells by the CDK inhibitor flavopiridol. *Leukemia Research* **2002**, *26* (3), 271-280.

23. Dispenzieri, A.; Gertz, M. A.; Lacy, M. Q.; Geyer, S. M.; Fitch, T. R.; Fenton, R. G.; Fonseca, R.; Isham, C. R.; Ziesmer, S. C.; Erlichman, C., Flavopiridol in patients with relapsed or refractory multiple myeloma: a phase 2 trial with clinical and pharmacodynamic end-points. *Haematologica* **2006**, *91* (3), 390-393.

24. Lenjisa, J. L.; Tadesse, S.; Khair, N. Z.; Kumarasiri, M.; Yu, M.; Albrecht, H.; Milne, R.; Wang, S., CDK5 in oncology: recent advances and future prospects. *Future Medicinal Chemistry* **2017**, *9* (16), 1939-1962.

25. Demange, L.; Abdellah, F. N.; Lozach, O.; Ferandin, Y.; Gresh, N.; Meijer, L.; Galons, H., Potent inhibitors of CDK5 derived from roscovitine: Synthesis, biological evaluation and molecular modelling. *Bioorganic & Medicinal Chemistry Letters* **2013**, *23* (1), 125-131.

26. Malmström, J.; Viklund, J.; Slivo, C.; Costa, A.; Maudet, M.; Sandelin, C.; Hiller, G.; Olsson, L.-L.; Aagaard, A.; Geschwindner, S., Synthesis and structure-activity relationship of 4-(1, 3-benzothiazol-2-yl)-thiophene-2-sulfonamides as cyclin-dependent kinase 5 (cdk5)/p25 inhibitors. *Bioorganic & Medicinal Chemistry Letters* **2012**, *22* (18), 5919-5923.

27. Shukla, V.; Seo, J.; Binukumar, B.; Amin, N. D.; Reddy, P.; Grant, P.; Kuntz, S.; Kesavapany, S.; Steiner, J.; Mishra, S. K., TFP5, a peptide inhibitor of aberrant and hyperactive Cdk5/p25, attenuates pathological phenotypes and restores synaptic function in CK-p25Tg mice. *Journal of Alzheimer's Disease* **2017**, *56* (1), 335-349.

28. Ji, Y.-B.; Zhuang, P.-P.; Ji, Z.; Wu, Y.-M.; Gu, Y.; Gao, X.-Y.; Pan, S.-Y.; Hu, Y.-F., TFP5 peptide, derived from CDK5-activating cofactor p35, provides neuroprotection in early-stage of adult ischemic stroke. *Scientific Reports* **2017**, *7* (1), 40013.

29. Sasaki, Y.; Cheng, C.; Uchida, Y.; Nakajima, O.; Ohshima, T.; Yagi, T.; Taniguchi, M.; Nakayama, T.; Kishida, R.; Kudo, Y., Fyn and Cdk5 mediate semaphorin-3A signaling, which is involved in regulation of dendrite orientation in cerebral cortex. *Neuron* **2002**, *35* (5), 907-920.

30. Pollan, S. G.; Huang, F.; Sperger, J. M.; Lang, J. M.; Morrissey, C.; Cress, A. E.; Chu, C.; Bhowmick, N. A.; You, S.; Freeman, M. R., Regulation of inside-out β1-integrin activation by CDCP1. *Oncogene* **2018**, *37* (21), 2817-2836.

31. Do, P.; Lee, C., The Role of CDK5 in Tumours and Tumour Microenvironments. Cancers 2021, 13, 101. s Note: MDPI stays neu-tral with regard to jurisdictional clai-ms in : 2020.

32. Vosler, P.; Brennan, C.; Chen, J., Calpain-mediated signaling mechanisms in neuronal injury and neurodegeneration. *Molecular Neurobiology* **2008**, *38* (1), 78-100.

33. Oner, M.; Lin, E.; Chen, M.-C.; Hsu, F.-N.; Shazzad Hossain Prince, G.; Chiu, K.-Y.; Teng, C.-L. J.; Yang, T.-Y.; Wang, H.-Y.; Yue, C.-H., Future aspects of CDK5 in prostate cancer: from pathogenesis to therapeutic implications. *International Journal of Molecular Sciences* **2019**, *20* (16), 3881.

34. Musa, F. R. M.; Tokuda, M.; Kuwata, Y.; Ogawa, T.; TOMIZAWA, K.; Konishi, R.; Takenaka, I.; Hatase, O., Expression of Cydin‐Dependent Kinase 5 and Associated Cyclins in Leydig and Sertoli Cells of the Testis. *Journal of Andrology* **1998**, *19* (6), 657-666.

35. Lin, H.; Chen, M.-C.; Ku, C.-T., Cyclin-dependent kinase 5 regulates steroidogenic acute regulatory protein and androgen production in mouse Leydig cells. *Endocrinology* **2009**, *150* (1), 396-403.

36. Abdulghani, J.; Gu, L.; Dagvadorj, A.; Lutz, J.; Leiby, B.; Bonuccelli, G.; Lisanti, M. P.; Zellweger, T.; Alanen, K.; Mirtti, T., Stat3 promotes metastatic progression of prostate cancer. *The American Journal of Pathology* **2008**, *172* (6), 1717-1728.

37. Liebl, J.; Weitensteiner, S. B.; Vereb, G.; Takács, L.; Fürst, R.; Vollmar, A. M.; Zahler, S., Cyclin-dependent kinase 5 regulates endothelial cell migration and angiogenesis. *Journal of Biological Chemistry* **2010**, *285* (46), 35932-35943.

38. Reck, M.; Horn, L.; Novello, S.; Barlesi, F.; Albert, I.; Juhász, E.; Kowalski, D.; Robinet, G.; Cadranel, J.; Bidoli, P., Phase II study of roniciclib in combination with cisplatin/etoposide or carboplatin/etoposide as first-line therapy in patients with extensive-disease small cell lung cancer. *Journal of Thoracic Oncology* **2019**, *14* (4), 701-711.

39. Chatterjee, A.; Cutler, S. J.; Doerksen, R. J.; Khan, I. A.; Williamson, J. S., Discovery of thienoquinolone derivatives as selective and ATP non-competitive CDK5/p25 inhibitors by structure-based virtual screening. *Bioorganic & Medicinal Chemistry* **2014**, *22* (22), 6409-6421.

40. Hoessel, R.; Leclerc, S.; Endicott, J. A.; Nobel, M. E.; Lawrie, A.; Tunnah, P.; Leost, M.; Damiens, E.; Marie, D.; Marko, D., Indirubin, the active constituent of a Chinese antileukaemia medicine, inhibits cyclin-dependent kinases. *Nature Cell Biology* **1999**, *1* (1), 60-67.

41. Bettayeb, K.; Tirado, O. M.; Marionneau-Lambot, S.; Ferandin, Y.; Lozach, O.; Morris, J. C.; Mateo-Lozano, S.; Drueckes, P.; Schächtele, C.; Kubbutat, M. H., Meriolins, a new class of cell death–inducing kinase inhibitors with enhanced selectivity for cyclin-dependent kinases. *Cancer Research* **2007,** *67* (17), 8325-8334.

42. Malumbres, M., Cyclin-dependent kinases. *Genome Biology* **2014,** *15*, 1-10.

43. de Azevedo Jr, W. F.; Mueller-Dieckmann, H.-J.; Schulze-Gahmen, U.; Worland, P. J.; Sausville, E.; Kim, S.-H., Structural basis for specificity and potency of a flavonoid inhibitor of human CDK2, a cell cycle kinase. *Proceedings of the National Academy of Sciences* **1996,** *93* (7), 2735-2740.

44. Gadbois, D. M.; Hamaguchi, J. R.; Swank, R. A.; Bradbury, E. M., Staurosporine is a potent inhibitor of p34cdc2 and p34cdc2-like kinases. *Biochemical and Biophysical Research Communications* **1992,** *184* (1), 80-85.

Chapter 4

Design and Facile Synthesis of Indolyl-1,2,4-triazoles as Tubulin Interacting Anti-cancer Agents
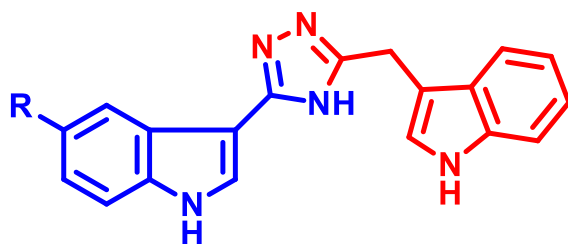
4.1 Introduction

Developing novel compounds that are both potent and selective towards tumors remains a major challenge for researchers. Despite technological advancements and progress in chemotherapy research, non-selectivity to cancerous tissue and multidrug resistance remain significant concerns.[1] In spite of the crucial advances in technology and chemotherapy research, the non-selectivity to cancerous tissue and multiple-drug resistance by cancer cells continues to be a grave concern for the medicinal chemists. Essential role in the growth and function of cells, microtubules are among the most important molecular targets for cancer chemotherapeutic agents.[2] Tubulin, a key constituent of the cytoskeleton, plays essential roles in cell formation, mitosis, signal transduction, and material transport. Consequently, targeting tubulin has been a successful strategy in anticancer drug discovery and cancer therapy . Established tubulin-targeting agents like paclitaxel/taxol, vincristine, and vinblastine have shown remarkable anticancer activity in clinical settings.[3] However, challenges such as poor water solubility, drug resistance, and side effects associated with identified tubulin inhibitors underscore the need for developing novel alternatives. However, owing to the poor water solubility, drug resistance or side effects of clinical used tubulin inhibitors,[4] it is necessary to develop novel tubulin inhibitors. The dynamic process of microtubule formation, involving polymerization and depolymerization of α,β tubulin heterodimers, can be disrupted by molecules binding to tubulins. This interference with microtubule dynamics leads to cell cycle arrest and eventual cell death, highlighting the potential of tubulin-targeting agents as effective anticancer therapies.[5]

In most therapeutic agents, the nitrogen-containing heterocycles are commonly found.[6] Triazoles are the five-membered heterocycles with three nitrogen atoms and two carbon atoms (Figure 4.1). While 1,2,4-triazole (**1**) is considered to be more signifcant isomer in pharmacology, due to their synthetic utility and a wide spectrum of biological activity,[7] the chemistry and fused heterocyclic structure of 1, 2, 4-triazoles has brought appreciable attention in the last few decades. The replacements in 1, 2, 4-triazole ring frameworks concentrated well among these heterocycles, and their subordinates have been recorded for an assortment of pharmacological exercises.[8] Triazole rings are part of a variety of antimicrobial,[9] antioxidant, anticancer,[10] antiviral, anti-infammatory,[11] antitubercular,[12] antihypertensive pharmaceutical drugs .[13] Due to their utilities as propellants, explosives, pyrotechnics and particularly, in chemotherapy,[14] the synthesis of high nitrogen-containing heterocyclic compounds has attracted increasing interests of synthetic and pharmaceutical researchers over the past decades.

Indole core (**2**) has been continuously attracting the attention of researchers and it has become a dynamic area of research due to its outstanding pharmacological properties.[15, 16] It is designated as "privileged scaffolds" which bind to multiple receptors with high affinity, leading to the development of novel bioactive drugs.[17, 18] It is used for the target-based design and development of anticancer agents. Heterocyclic compounds containing nitrogen atoms, especially heterocyclic rings with three nitrogen atoms, like 1,2,4-triazole ring (**2**), are one of the most important active pharmaceutical scaffolds. These scaffolds are able to form hydrogen bonds and other interactions with different targets, which leads to the improvement of pharmacokinetics, pharmacological and toxicological properties of compounds.[19] Indole is also an integral part of many clinical drugs such as indibulin (**4**), rizatriptan (**7**), etc., as displayed in figure 4.1.[20-22]

The triazole moiety is an elite building block in the discovery of potent anticancer agents, and some of its analogues have already been made up to healthcare and clinics or are under clinical trials for fighting against various cancer.[23]
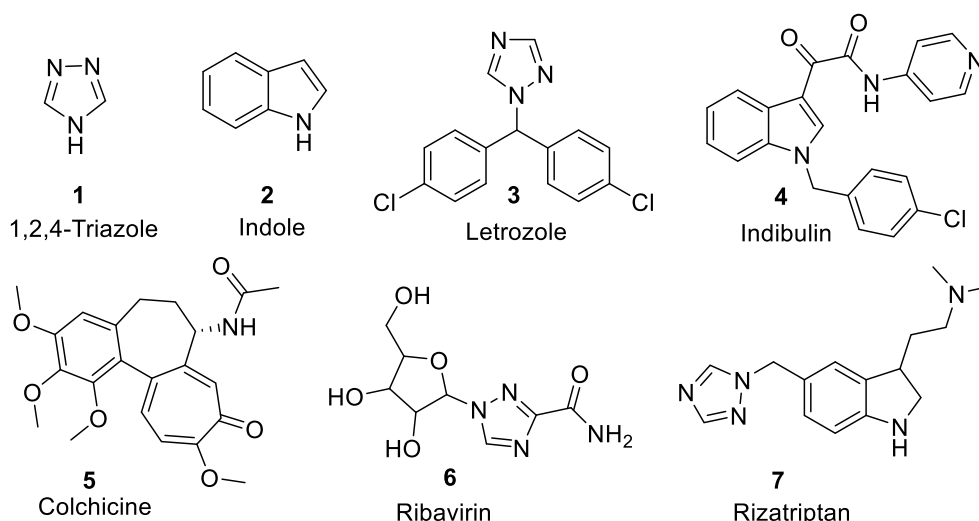
Figure 4.1 Representative drugs with indole and 1,2,4-triazole moieties

4.1.1 Rational Design

In recent years, several indole and triazole containing compounds have been isolated or synthesized with interesting activities. For example, Topsentins **8** and **9** (Figure 5.2) a class of *bis*indole alkaloid isolated from the marine sponge *Topsentina genitrix* as growth inhibitors of leukemia cells *in vitro*. Due to the interesting biological activities and unique chemical structures of the marine bisindole alkaloids, their usefulness as lead compounds in the identification of new chemical entities has pursued with increasing interest in medicinal chemistry.[24]

In 2023, Sherief *et al.* utilized 1,2,4-triazole scaffold to synthesize new Schiff base compounds as potential anticancer agents against various cancer cell lines. One such hybrid compound, denoted as compound **10**, demonstrated significant *in vitro* cytotoxicity against EGFR cells, with IC_{50} value of 0.13 µM. Additionally, compound **10** induced complete cell cycle arrest at the G1/S phase. Moreover, it led to 5.28% necrosis in the K562 cell line and triggered early apoptosis rather than late apoptosis.[14] A recent report from Li *et al.* described a series of 2-aryl-4-benzoylimidazoles where replacement of the aryl ring with an indole nucleus enhanced the antiproliferative activity. 1,2,4-Triazole core among the various heterocycles displayed a wide spectrum of biological properties and are well documented in the literature.[25] Similarly, a set of compounds bearing a 1,2,4-triazole core was synthesized and evaluated for their anticancer activity against a panel of cancer cell lines. The inhibitory activity of the most active compound, **11**, was examined in MTT assays against three known anticancer targets: EGFR, BRAF, and tubulin. The results revealed that compound **11** exhibited strong inhibition of tubulin as mentioned in figure 5.2. Additionally, **11** demonstrated the most potent inhibition of EGFR, with an IC_{50} value of 3.6 µM.[26] In 2023, Zaki *et.al*,[23] a novel series of indole–1,2,4-triazole-based *N*-phenyl acetamide structural motif **12** was synthesized and screened against the *in vitro* hepatocellular cancer Hep-G2 cell line. The excellent cytotoxicity efficacy against the liver cancer cell line Hep-G2 was displayed by the 3,4-dichloro moiety containing indole–triazole scaffold (**12**), which had the lowest cell viability (10.99-0.59) compared with the standard drug ellipticine (cell viability = 11.5-0.55) but displayed comparable potency in comparison with the standard drug doxorubicin (cell viability = 10.8-0.41).

In 2021,[27] we investigated the anticancer potential of synthesized indolyl-α-keto-1,3,4-oxadiazoles. Among them, compound **13**, demonstrated significant antiproliferative activity against a range of cell lines. Compound **13**, featuring a 3,4,5-trimethoxyphenyl motif, exhibited strong cytotoxicity against U937, Jurkat, BT474, and SB cancer cells, with IC_{50} values of 7.1 µM, 3.1 µM, 4.1 µM, and 0.8 µM, respectively. Molecular docking studies suggested a potential binding mode for **13** within the colchicine binding site of tubulin.

Hamedy and co-workwers,[28] conducted research to design and synthesize a series of 3-(benzylthio)-5-(1*H*-indol-3-yl)-4*H*-1,2,4-triazol-4-amines as potential anticancer agents targeting Bcl-2. Their efforts led to the discovery of several compounds exhibiting sub-micromolar activity in Bcl-2 expressing human cancer cell lines. Among these compounds, the 3-nitrobenzyl derivative **14a** demonstrated the highest activity. Further investigations revealed that compound **14a** binds within the BH3 domain of Bcl-2, as supported by molecular modeling and ELISA studies (Figure 4.2). These findings suggest that Bcl-2, an anti-apoptotic protein,

could serve as a mechanistic target underlying the *in vitro* anticancer activity of the synthesized compounds. Smillarly, the triazole **14b** was found to show activity against HepG-2 cells.[6, 8, 23]
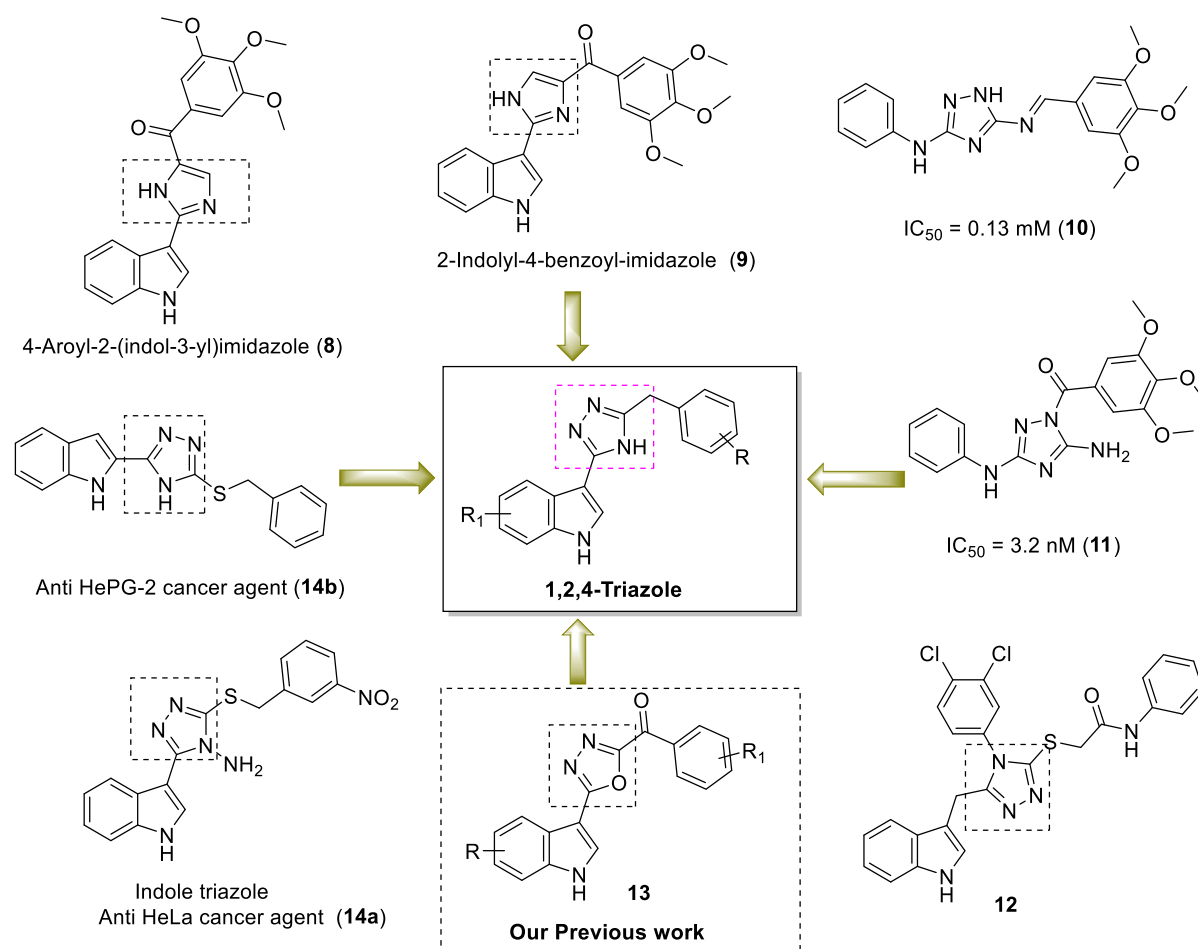
Figure 4.2 Design strategy of indolyl-1,2,4-triazoles as anti-cancer agents

The combination of two biological active moieties, indole and triazole has emerged as a promising strategy for developing new anticancer agents. Building upon previous research and our investigations into indole-based heterocycles as anticancer agents, we synthesized a series of novel indolyl-1,2,4-triazoles and evaluated their anticancer activities against human tumor cell lines. Our study aimed to design and synthesize novel 1,2,4-triazole derivatives, leveraging the bioavailability and chemical stability conferred by the 1,2,4-triazole ring. Furthermore, *in silico* approaches such as molecular docking and the ADMET pharmacological profile provided additional support for the anticancer potential of the synthesized compounds.

4.2 Results and Discussion

4.2.1 Synthesis and Characterization

Considering our interest in the design and synthesis of indolyl azoles, we prepared a newer library of indolyl-1,2,4-triazoles using both conventional and Microwave irradiation (MW) methods, and investigated their anticancer activity.

The developed efficient synthetic protocol to prepare the targeted indolyl–triazoles, is illustrated in Scheme 4.1. The different indole-3-carbonitriles **16** were prepared in good yields by reacting indole-3-carboxaldehydes with hydroxylamine hydrochloride and formic acid.[25] Next, the reaction of indole-3-carbonitriles **16** with sodium hydrosulfide and magnesium chloride in presence of dimethylformamide led to the formation of indole-3-thiocarboxamides **17a-e** as illustrated in Scheme 3. Reaction of thioamide **17** followed by S-methylation using methyliodide in THF afforded **18** in 94% yield. Indole derivatives **17c** and **17d** with bromine/fluorine substituent also successfully afforded **18c** (91%) and **18d** (94%) in good yields (Scheme 4.1). The *N*-(4-chlorobenzylchloride) protected indolethiocarboxamides **18e** reacted smoothly under similar conditions to provide **18e** in 95% yield. On the other hand, different hydrazides **21** were prepared from the corresponding carboxylic acids **19** *via* esterification and followed by tretament with hydrazine hydrate as shown in Scheme 4.1. Treatment of thioimidate **18** with the respective acylhydrazide **21**, provided indolyl triazoles (**22a-i**) in excellent yields (91-96%). (Table 4.2)
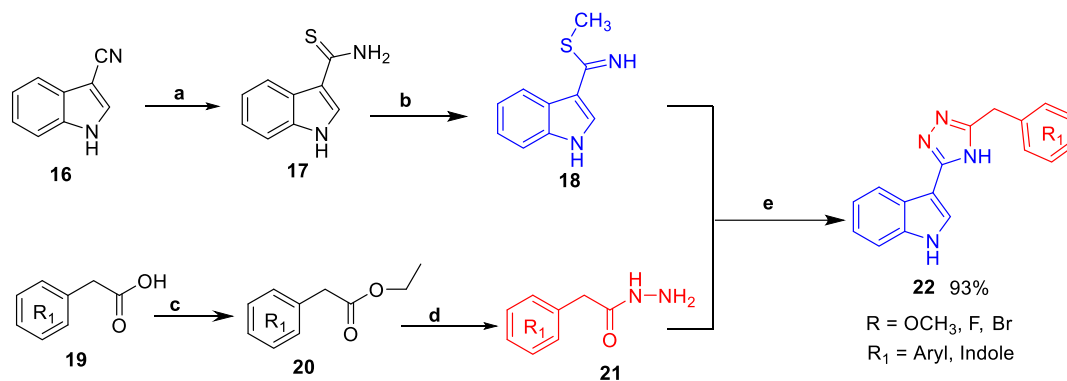
Scheme 4.1 Reagents and conditions: (a) 70% NaSH (4.0 equiv), $MgCl_2.6H_2O$ (2.0 equiv), DMF, 50 °C, 6 h; (b) MeI (2.5 equiv), THF, 25 °C, 2 h; (c) H_2SO_4 (0.2 equiv), ethanol 80 °C, 3 h; (d) hydrazine hydrate (2.0 equiv). (e) thioimidate **18**, (1.0 equiv), **21** (0.9 equiv), dry DMF, 35 min, MW, 130 °C.

Initially we treated **18a** with hydrazide (0.5 equiv) in dry DMF at 120 °C for 4 h to afford **22a** in 42% yield. When the same reaction was exposed to MW for 5 min, compound **22a** was formed in 36% yield (Table 4.1, entry 1). Next, by raising the reaction temperature to 130 °C both conventionally and MW yield of triazole was increased to 49% yield (Table 4.1, entry 2).

Reaction of **18a** with hydrazide afforded **22a** in 79% yield under conventional conditions and 83% yield in MW (Table 4.1, entry 4). With the increase in reaction time and use of 0.9 equivalents of hydrazide afforded **22a** in 86% and 91% yields, under heating and MW conditions (Table 4.1, entry 5). Further increase in reaction temperature, the reaction time was reduce to 15 min (MW) to furnish **22a** in 88% yield (Table 4.1, entry 7). Finally, we found that reaction of hydrazide (0.9 equiv) and indolyl-3-thioimidate (1.0 equiv) in dry DMF at 130 °C temperature for 35 min under MW is the optimum reaction conditions (Table 4.1, entry 6) for the preparation of indolyl-1,2,4-triazoles **22a**.

Table 4.1 Optimization of reaction conditions to prepared indolyl-1,2,4-triazole **22a**
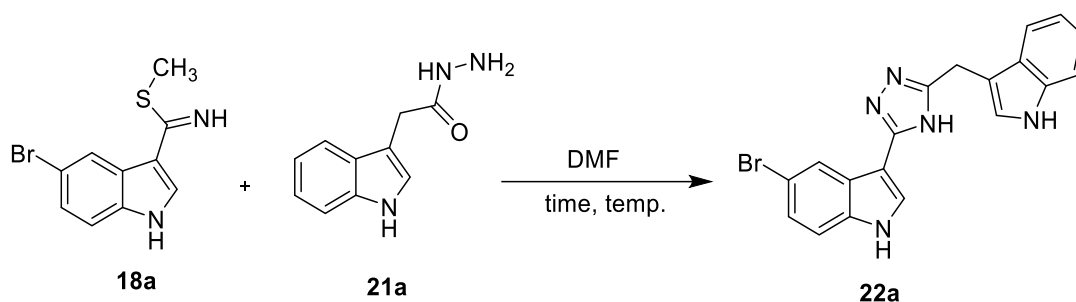
				Conventional heating		**Microwave (MW)**[a]	
Entry	Hydrazide	Temp(°C)	Time (h)	Yield[b] (%)		Time (min.)	Yield[b] (%)
1.	0.5	120	4	42		5	36
2.	0.5	130	4	49		5	42
3.	0.5	130	7	61		10	69
4.	0.9	130	7	79		15	83
5.	0.9	130	10	86		25	91
6.	**0.9**	**130**	**12**	**92**		**35**	**96**
7.	0.9	150	7	83		15	88

Reagents and conditions: [a]Thioimidate **18a**, (1.0 quiv), **21a** (0.9 equiv), dry DMF, 35 min, MW, 130 °C. [b]Isolated yield.

Intermediate **18a** was characterized through ^{1}H NMR analysis, revealing the presence of a peak corresponding to S-CH$_3$ at 2.86 ppm and a peak indicative of =NH at 10.85 ppm (Figure 4.3) The structure of **22a** was confirmed by detailed NMR (^{1}H & ^{13}C) and HRMS spectral analysis. Formation of analogues **22a** was indicative by appearance of singlets at 4.21 ppm and 7.91 ppm for -CH$_2$ protons and indole C$_2$-proton in its ^{1}H NMR spectrum. A distinct peak at 23.04 ppm corresponding to -CH$_2$ carbon in ^{13}C NMR spectrum also supports the formation of **22a**. The HRMS spectrum of **22a** displayed a molecular ion at 392.0433 and 394.0429 in agreement

with the expected mass for $C_{19}H_{14}BrN_5$ at 392.0485 and 394.0412 (Figure 4.6). Similarly, structural elucidation of other indolyltriazoles **22b-i** was carried out.

Table 4.2 Synthesis of indolyl-1,2,4-triazoles

18
R = OCH$_3$, F, Br
R$_1$ = Aryl, Indole

21

DMF
35 min, MW, 130 °C

22a-i

22a, 91%

22b, 93%

22c, 91%

22d, 96%

22e, 93%

22f, 95%

22g, 90%

22h, 92%

22i, 91%
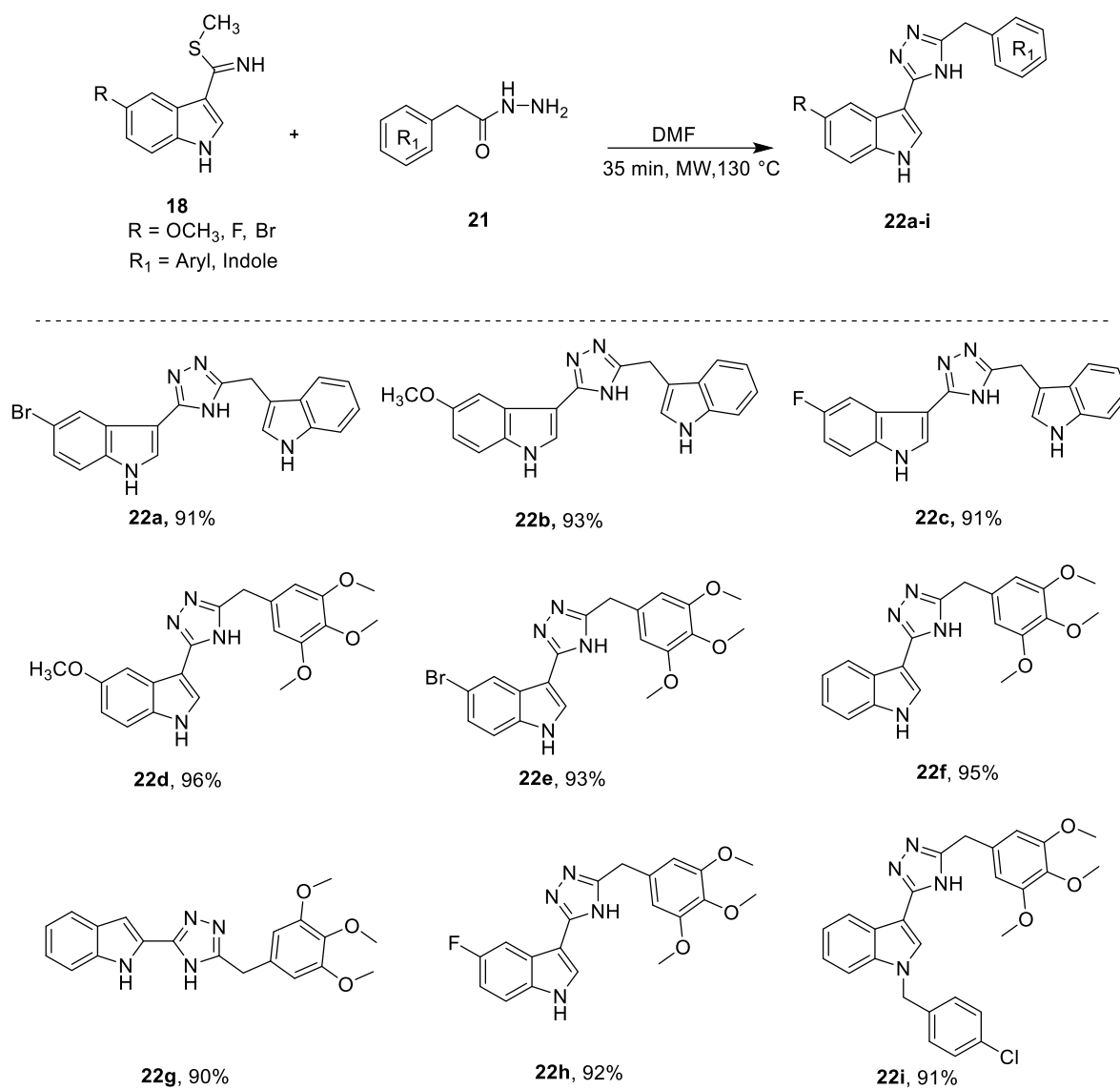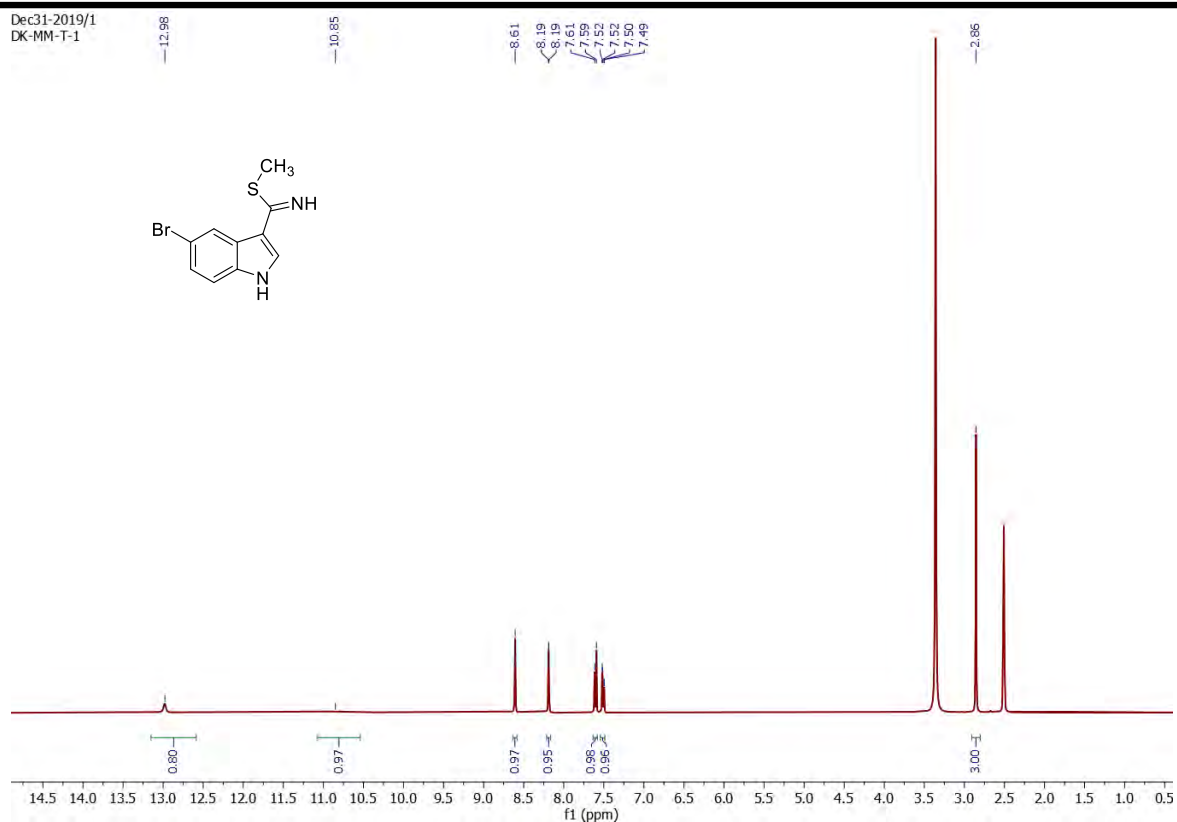
Figure 4.3 ^{1}H NMR spectrum of **18a**
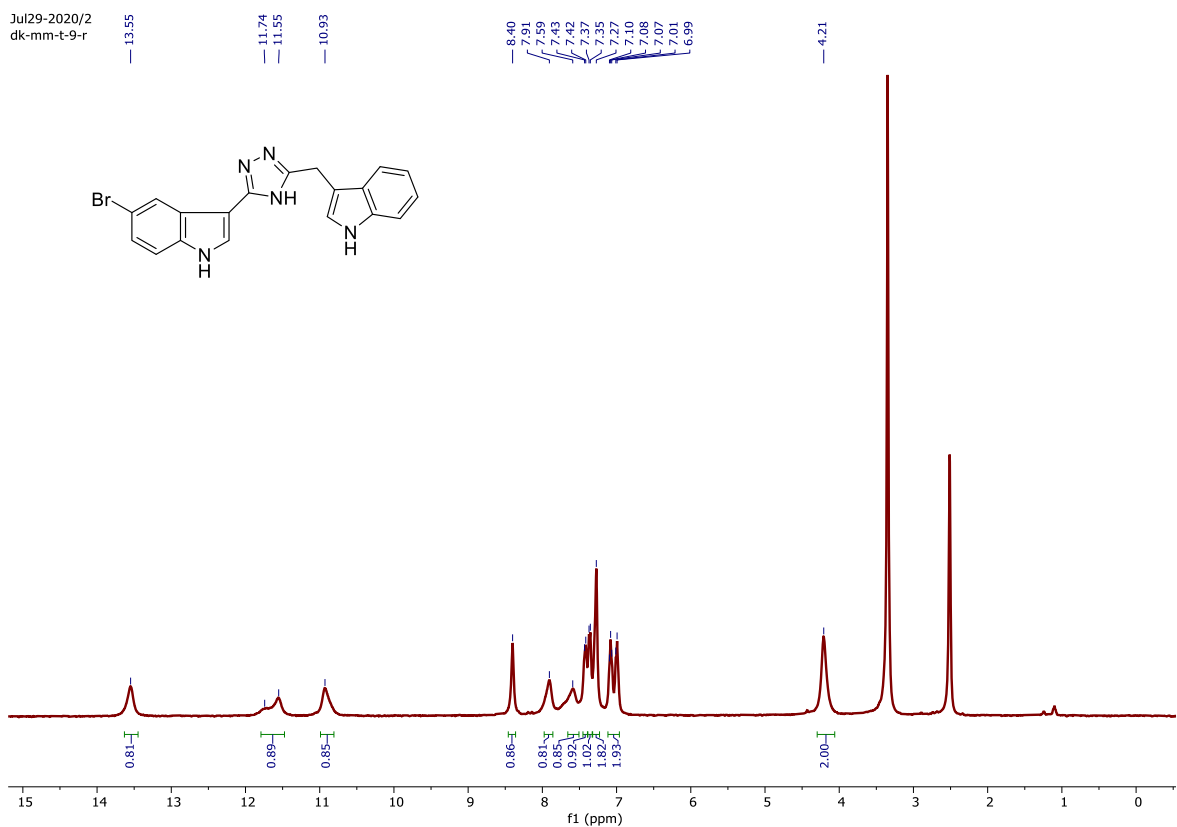
Figure 4.4 ^{1}H NMR spectrum of **22a**
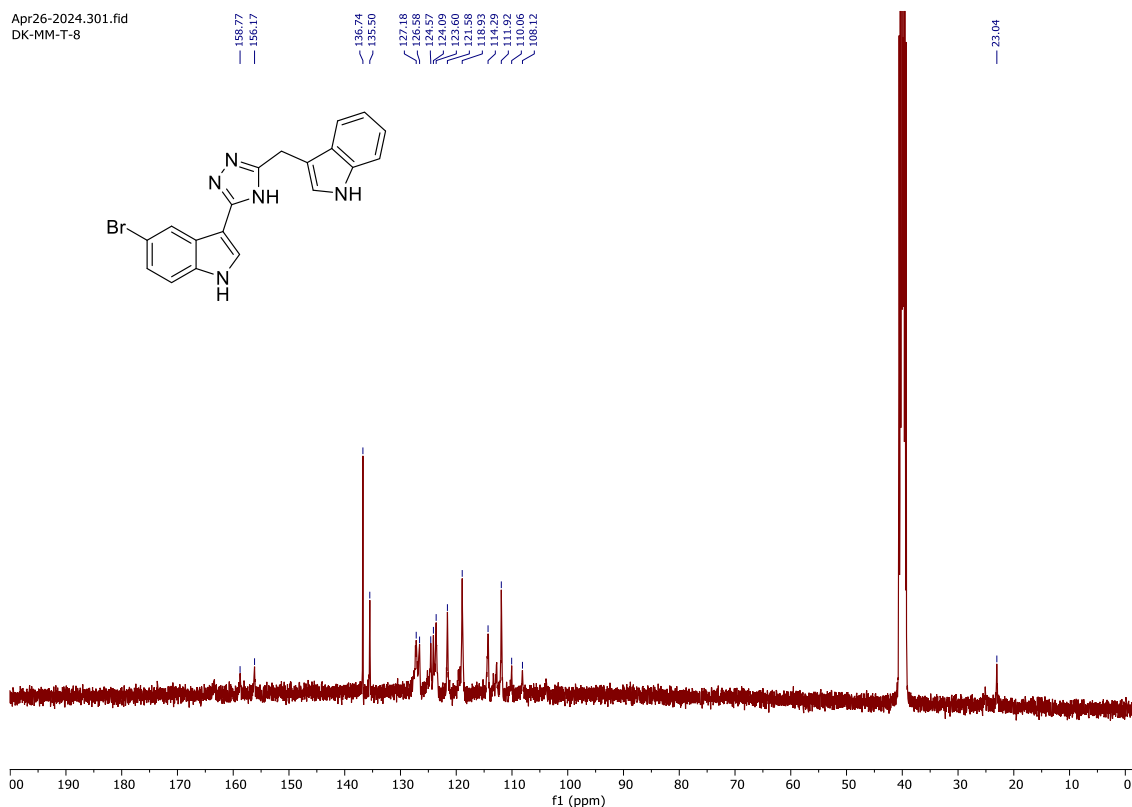
Figure 4.5 ^{13}C NMR spectrum of **22a**
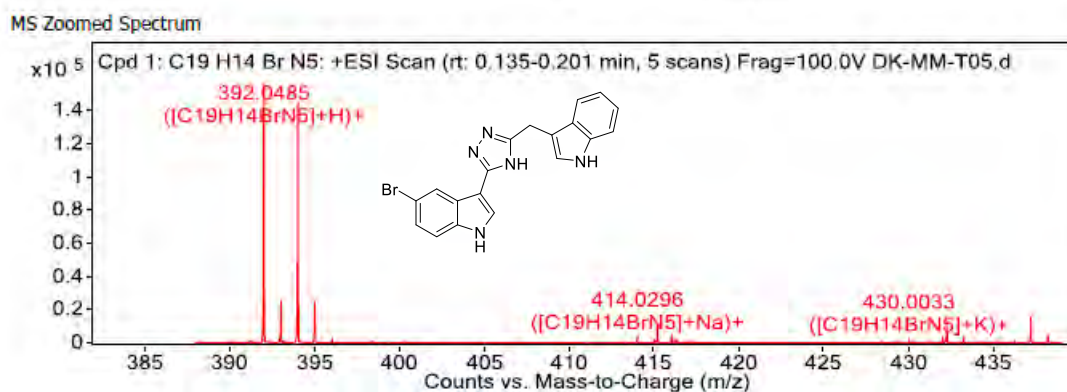
Figure 4.6 HRMS spectrum of **22a**

4.2.2 Biological Evaluation

4.2.2.1 Anti-cancer Activity

The cytotoxicity of synthesized indolyltriazole analogues **22a-i** was evaluated *in vitro* against a selected cancer cell lines, including HeLa (cervical cancer cells) and MCF-7 (breast cancer cells). Indolyltriazoles **22a** (IC$_{50}$ = 3.5 µM) and **22b** (IC$_{50}$ = 4.0 µM) exhibited selective cytotoxicity against HeLa cells. The presence of a bromo substituent on the indole moiety (compounds **22a**) was found to enhance the activity and selectivity towards the HeLa cancer

cell line. Introducing an electron-donating group into the C_5-indole (**22b**) also showed good anti-cancer activity. The compound **22d** with 5-methoxyindole was found to show moderate activity (IC$_{50}$ = 14.0 µM) against HeLa cancer cell line. The presence of a -CH$_2$ group was observed to be more advantageous when compared to a carbonyl group due to the former's ability to render the compound less hydrophobic.[6] This suggests that compounds containing a -CH$_2$ (benzyl) group may exhibit better water solubility, enhanced bioavailability and improved pharmacokinetic properties. Additionally, the introduction of a fluoro group, imparts moderate activity to compounds **22c** and **22h**. The presence of free-NH indole structure was found to confer greater cytotoxicity when compared to protected NH (compound **22i** vs **22a**). These findings underscore the importance of structural modifications and functional group substitutions in optimizing the cytotoxicity of indolyltriazole analogues for cancer therapy (Figure 4.7).
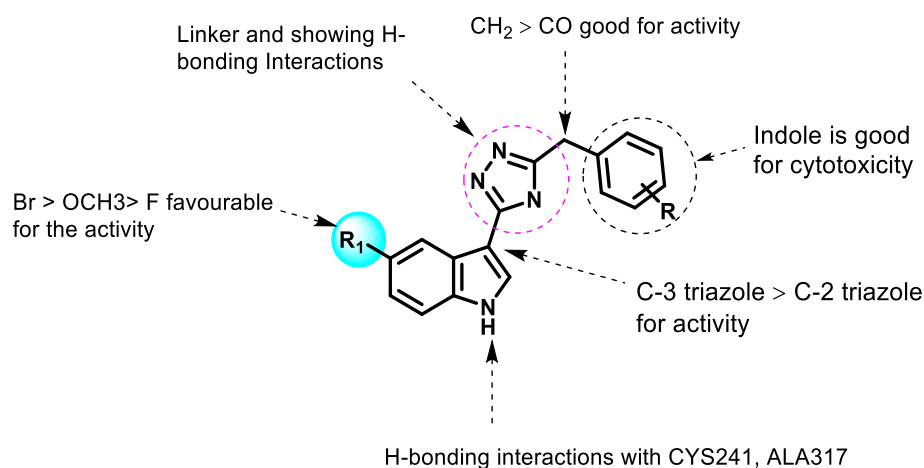
Figure 4.7 Structure-activity relationship analysis of compounds **22a-i**

4.2.3 Docking Studies

4.2.3.1 Molecular docking studies of indolyl-1,2,4-triazoles

To gain the potential binding features for the synthesized derivatives **22a-i** in the tubulin, a series of molecular docking simulations were carried out using the co-crystallized structure of tubulin with colchicine (PDB: 1SA0).[29] An overview of the binding site possessing the good binding affinity is shown in figure 4.3. Of interest is that **22** adopts a pretty similar location with colchicine (the inhibitor of the co-crystal) in the colchicine-binding site which is located on the interface between αβ-subunits and extended slightly out toward the β-subunit. The results of the molecular docking studies revealed that out of all the shortlisted possible tubulin

targets, these indolyltriazoles showed good binding affinities with the tubulin binding site. The analysis of their binding affinities showed that the indolyl-1,2,4-triazoles **22a**, **22b**, and **22c** were able to show higher affinities than colchicine in the molecular docking studies. Computational docking analysis was executed utilizing AutoDockVina. The minimum binding energy manifests that the target receptor (tubulin colchicine binding site) was successfully docked with our compounds.

The tubulin inhibitor DAMA colchicine was able to show a binding affinity of −6.8 Kcal/mol (Figure 4.9), while the newly synthesized compounds **22a**, **22b**, and **22c** were able to bind with the binding pocket with binding affinities of −8.8 Kcal/mol, −8.2 Kcal/mol, and −9.0 Kcal/mol, respectively. The conformational binding and interaction analysis of these indolyl–triazoles showed that these compounds show robust interactions of multiple types with the active site of the colchicine binding site. In compound **22a**, ligand–protein complex interacted *via* conventional hydrogen bonds by engaging the ASN258, ALA317 and LYS352 active site residues with NH-indole. The indole core of the **22a** showed Pi-sigma interactions with the LEU248 and ALA316, while the phenyl moiety presents on the triazole ring, as well as the bromo group attached to the C-5 position of indole, was also able to make multiple van der waal, π-cation and hydrophobic interactions with CYS241, LYS254, LEU255, ILE378, ALA354 and VAL318 receptor residues of the tubulin protein (Figure 4.8).

The NH-indole ring of **22b** went deep into the pocket, and the nitrogen atom formed a hydrogen-bonding interaction with residue CYS241. Meanwhile, the free amino group of the triazole core provided Pi-sigma interactions with the LEU248 and ALA250, respectively. Moreover, the oxygen atom of the 5-methoxylindole moiety established an additional Pi-alkyl (LEU258, LYS352, ALA354) and hydrophobic interactions (LYS254, LEU255). These docking studies indicated that **22b** was a novel potential tubulin inhibitor targeting at the colchicine-binding site shown in figure 4.10. The binding affinity of **22c** was -9.0 kcal/mol. **22c** also binds in the colchicine binding pocket and forms hydrogen bonds with the amino acid ALA317 as well as LYS352. Furthermore, the indole part fitted into the hydrophobic pocket of the colchicine active site and formed eight hydrophobic bonds with the surrounding amino acids (CYS241, LEU248, ALA316, ALA317, VAL318 and LYS352) and the tail formed two extra halogen bonds with the amino acid VAL 315 and ASN350 (Figure 4.11). Similarly, other compounds **22d, 22g** and **22h** also displayed interactions as shown in figures 4.12 to 4.14.
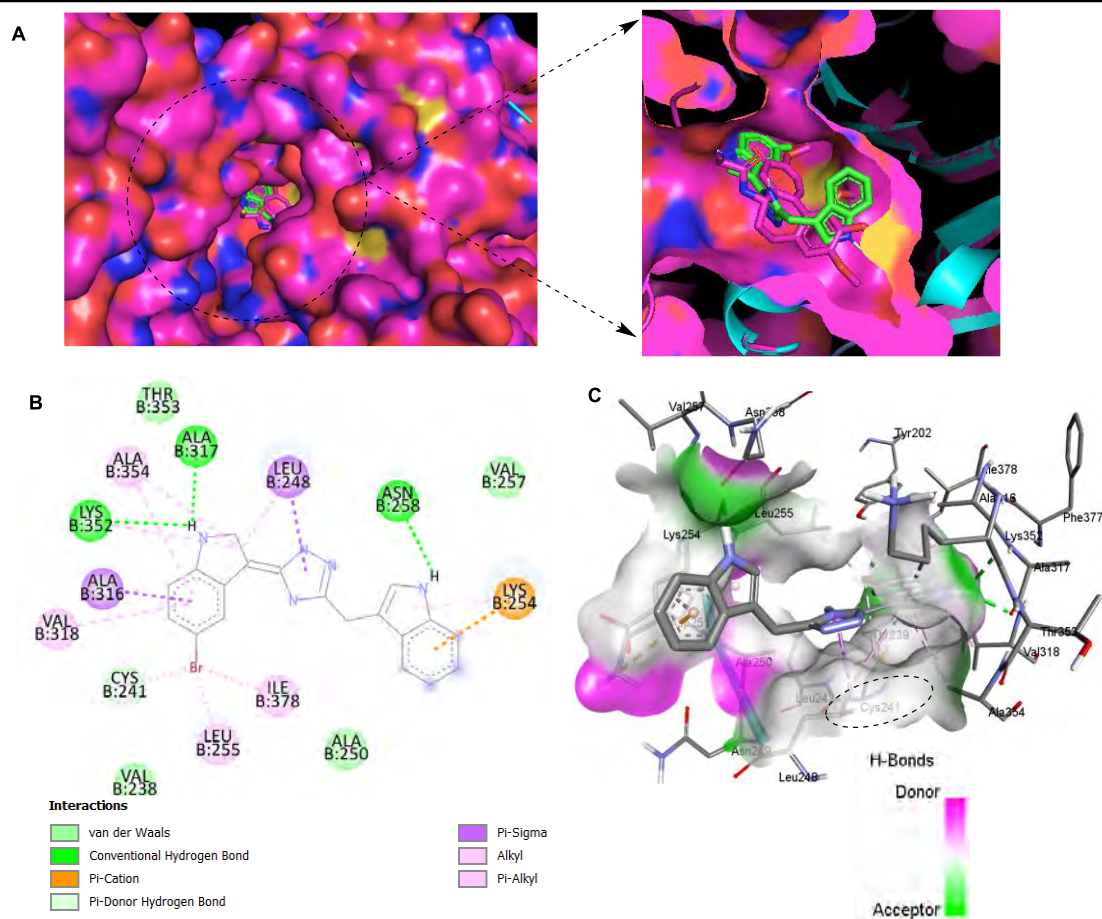
Figure 4.8 Binding Affinity = -8.8 Kcal/mol. Docking pose of compound **22a** in the active site of tubulin. Green dashed lines indicate hydrogen bonds with ASN258, ALA317 and LYS352.
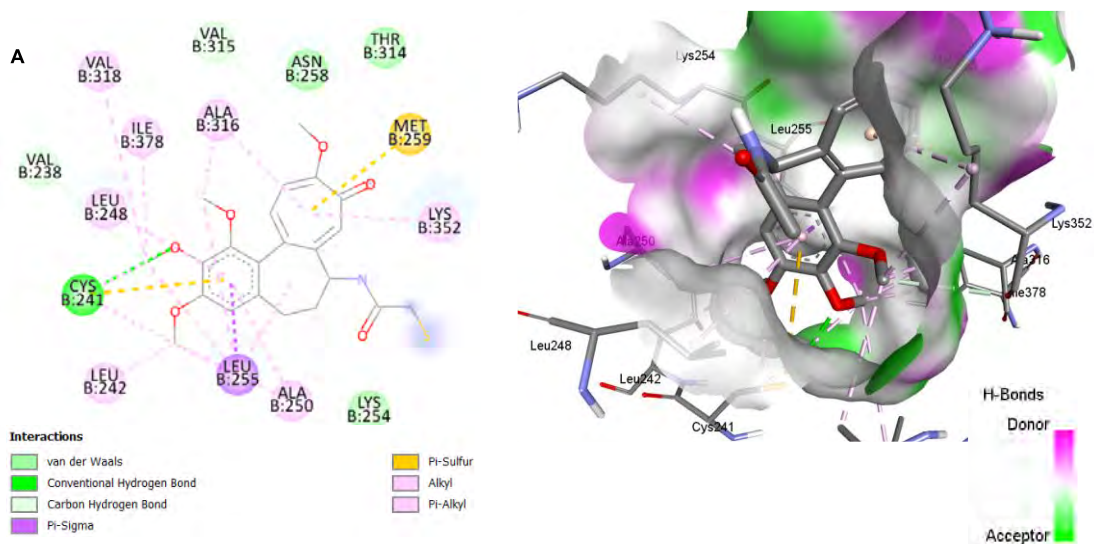
Figure 4.9 Docking pose of DAMA colchicine (Binding Affinity =-6.8 Kcal/mol) in the active site of tubulin. Green dashed lines indicate hydrogen bonds with CYS241.

Figure 4.10 Binding aSffinity of **22b** is -8.2 Kcal/mol. (a) Docking pose of compound **22b** in the active site of tubulin. (b) Overlay of colchicine and **22b**. (c) In 2D interactive conformations where green dashed lines indicate hydrogen bonds with CYS241. (d) 3D interactions with hydrophilic pocket.

Figure 4.11 Docking pose of compound **22c** in the active site of tubulin. Green dashed lines indicate hydrogen bonds. Binding Affinity =-9.0 Kcal/mol.
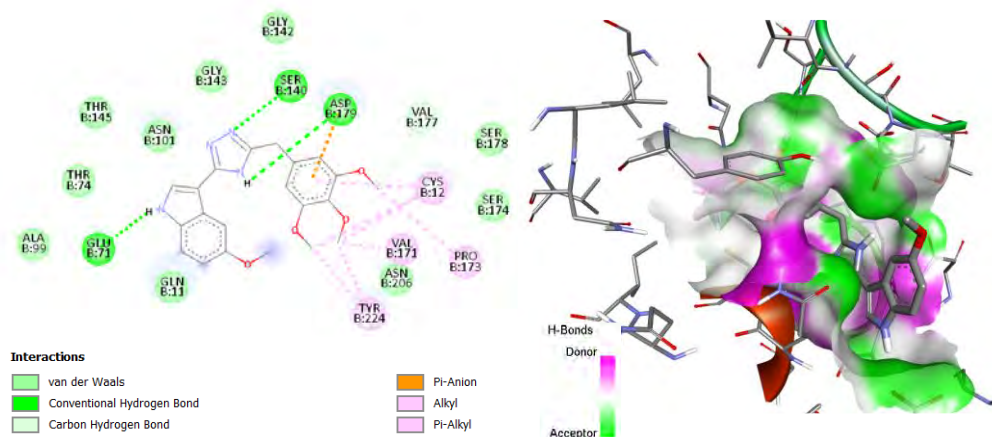
Figure 4.12 Binding Affinity = -7.7 Kcal/mol (**22d**)
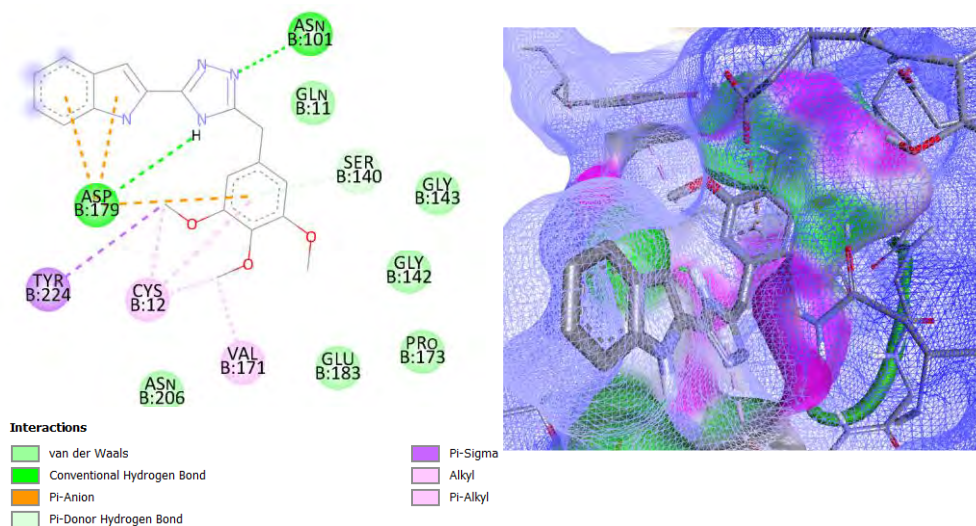
Figure 4.13 Binding Affinity = -7.3 Kcal/mol (**22g**)
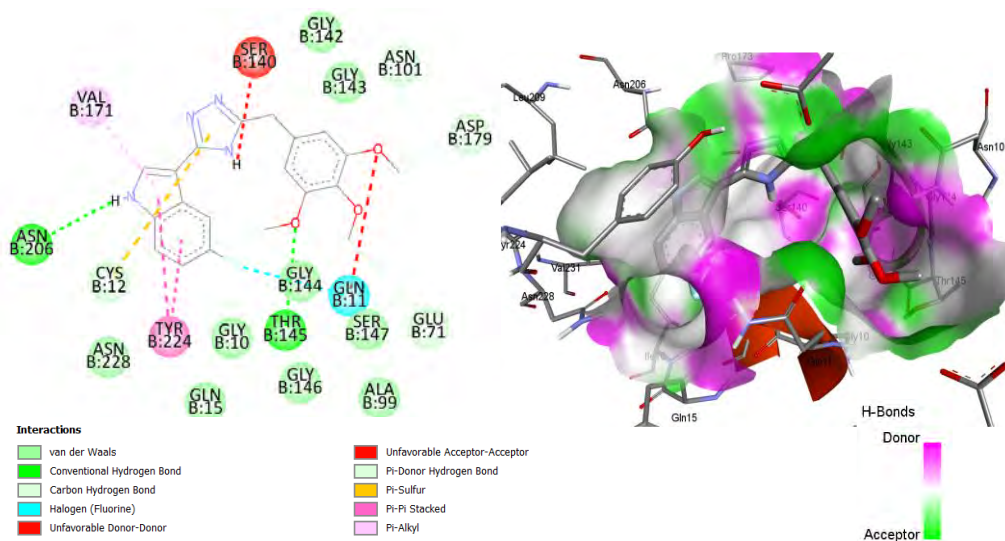
Figure 4.14 Binding Affinity = -8.7 Kcal/mol (**22h**)

4.2.4 *In silico* analysis of pharmacokinetic profile of indolyl triazole derivatives

In order for a chemical entity to qualify as a drug candidate, it must meet certain prerequisites encompassing physicochemical, pharmacodynamic, and pharmacokinetic parameters. Therefore, evaluating the potential of a prospective drug involves forecasting *in silico* physicochemical attributes, drug likeness, and absorption, distribution, metabolism, excretion, and toxicity (ADMET) traits.[13] In the past, the pharmacokinetic profile of promising compound was mainly determined on the basis of the results obtained in *in vivo* studies, but now, *in vitro* and in silico studies are more important in the early phase of development of new bioactive molecules, which can be carried out faster and at a lower cost.[30] In this study, *in silico* analysis was conducted of the synthesized compounds **22a-i**. Calculations were performed for various physicochemical characteristics, including the enumeration of specific atom classes, the hydrogen bond donor, hydrogen bond acceptor, lipophilicity and water solubility. Additionally, the topological polar surface area (TPSA), a parameter utilized to predict the passive molecular transport trait of drugs, was assessed. These physicochemical properties are summarized in Table 4.3, demonstrating that the attributes align well with the applied criteria and are anticipated to yield favourable bioavailability scores, as indicated by all compounds having TPSA values ≤ 140 Å.

Table 4.3 ADME properties of indolyl-1,2,4-triazoles **22a-i**

Compds.	Molecular weight	TPSA (20 to 130 Å2)	Water Solubility	Lipophilicity (-0.7to+5.5)	Lipinski Rule of five (Druglikeness property)	PAINS #alerts	HBD	HBA	Bioavalibility Score (0 to1)
22a	392.25	73.15	-7.28	3.91	Yes	0	3	2	0.55
22b	343.38	82.38	-8.10	3.29	Yes	0	2	2	0.55
22c	331.15	73.15	-8.02	3.66	Yes	0	3	3	0.55
22d	364.30	85.05	-7.50	3.06	Yes	0	2	5	0.55
22e	443.29	85.05	-8.10	3.72	Yes	0	2	5	0.55
22f	394.42	94.28	-7.63	3.13	Yes	0	2	6	0.55
22g	382.39	85.05	-7.79	3.42	Yes	0	2	6	0.55
22h	364.40	85.05	-7.52	3.12	Yes	0	1	5	0.55
22i	368.43	72.50	-6.74	2.96	Yes	0	1	3	0.55
Colchicine	399.44	83.9	-8.01	3.28	Yes	0	1	6	Low

Chemical toxicity poses significant risks to human health, potentially leading to various hazardous biological effects such as gene damage, carcinogenicity, or the induction of lethal diseases in both rodents and humans.[31] Given the potential impact on public health, it is imperative to evaluate the toxicity of synthesized compounds as shown in Table 4.4. According to the determined parameters related to the absorption of the drug substance, it can be said that

the synthesized compounds **22a-d** were characterized by good intestinal absorption (HIA) and bioavailability. Distribution analysis predicted the location of the tested compounds in the mitochondria and did not reveal permeability through the blood-brain barrier (BBB). In addition, the compounds were identified as P-glycoprotein substrates but not inhibitors. *In silico* toxicity and carcinogenicity are assessed and are given in Table 4.4. Furthermore, the computed rat acute toxicity, that is, LD_{50} in mol/kg seems to be sufficiently safe in the range 2.238−2.74 mol/kg. The LD_{50} of the potent compounds **22a-d** is similar to that of the standard colchicine drug shown in Table 4.4.

Table 4.4 *In silico*-predicted LD_{50}, toxicity, and carcinogenicity profiles and comparative probability of the toxicity of the selected compounds **22a-d**

Sr. No.	Toxicity target	Probability of compound toxicity				
		Colchicine	22a	22b	22c	22d
1.	Caco-2 Permeability	0.65	0.59	0.65	0.59	0.51
3.	Mitochondrial Membrane Potential (MMP)	1.0	0.83	0.80	0.83	0.71
4.	ATPase family AAA domain-containing protein 5 (ATAD5)	1.0	0.86	0.85	0.75	0.86
5.	Rat Acute toxicity (LD_{50})	2.37 mol/kg	2.47 mol/kg	2.36 mol/kg	2.61 mol/kg	2.51mol/kg
6.	Carcinogens	Non-Carcinogens (0.81)	Non-Carcinogens (0.83)	Non-Carcinogens (0.90)	Non-Carcinogens (0.81)	Non-Carcinogens (0.81)
	Distribution					
7.	Subcellular localization	Nucleus	Mitochondria	Mitochondria	Mitochondria	Mitochondria
8.	P-glycoprotein Substrate	0.59	0.51	0.66	0.52	0.63
	Absorption					
9.	Skin Permeability	1.17 LogPapp, cm/sec	0.58 LogPapp, cm/sec	0.64 LogPapp, cm/sec	0.56 LogPapp, cm/sec	1.35 LogPapp, cm/sec
10.	Human Intestine Absorption	0.98(High)	1.00 (High)	1.00 (High)	1.00 (High)	1.00 (High)

4.3 Conclusions

In conclusion, we have developed a facile, efficient, and high-yielding synthetic pathway for the synthesis of indolyl-1,2,4-triazoles **22a-i**. Formation of indolyl-1,2,4-triazoles involves reaction of readily available acetohydrazide and thioimidate. The reaction proceeded effectively under both conventional and microwave conditions yielding the desired compounds **22a-i** in good to excellent yields (up to 96%). The indolyl-1,2,4-triazoles were subjected to anticancer screening against a selected set of cancer cell lines, including HeLa and MCF-7. The findings revealed that compound **22a** emerged as the most potent among the tested compounds against the HeLa cancer cell line, exhibiting an IC_{50} value of 3.5 μM. Additionally, compound **22b** demonstrated good anticancer activity with an IC_{50} value of 4.0 μM and compound **22d** exhibited intermediate cytotoxicity against the HeLa cancer cell line, as indicated by its IC_{50} value of 14.10 μM. The inhibitory activity of compounds **22a**, **22b**, and **22d** can be attributed to two major factors: the minimum binding energy and hydrogen bond interactions of the ligand with the target tubulin protein. These results indicate that novel indolyl-1,2,4-triazoles hold promise as potential anti-cell proliferative agents for more effective cancer treatment.

4.4 Biology Protocols

4.4.1 MTT Assay

HeLa cancer cells were grown in RPMI 1640 media. All media were supplemented with 10% FBS, streptomycin (100 μg/mL) and penicillin (100 I.U./mL). For MTT assay, 5 x 10^3 cells/well were seeded in 96-well plates. After 12 h, cells were treated with different concentrations of **22a-i** in a range from 0.1 μM - 40 μM. 0.1% DMSO (vehicle control) was used as control. After 48 h, old media was removed, cells were washed with PBS followed by addition of 100 μl of serum free media and MTT (5mg/mL) cocktail (4:1 ratio) in each well. Cells were incubated for 4 h at 37 °C. MTT was then aspirated, cells were washed with PBS, and then 100 μL DMSO was added to dissolve the formazan crystals. The absorbance was measured at 570 nm using Tecan Spectrafluor Plus. Relative inhibition was calculated as mean absorbance of treated cells/mean absorbance of DMSO treated cells (negative control). The IC_{50} values and dose response curve were obtained by nonlinear regression analysis [non-linear regression (sigmoidal dose response with variable slope)] using Graph Pad Prism.

4.5 Experimental Section

4.5.1 General Remarks

The laboratory reagents were sourced from Sigma-Aldrich, TCI chemicals, Alfa Aesar, and Spectrochem India Pvt. Ltd. without additional purification. Reaction progress was tracked via thin-layer chromatography on Merck pre-coated plates (silica gel 60 F254, 0.2mm). NMR spectra (1H and 13C) were recorded at 400 MHz and 100 MHz, respectively, using $CDCl_3$ and DMSO-d_6 solutions. Chemical shifts were referenced to the residual solvent peaks (^{1}H NMR: $CDCl_3$ δ 7.26; DMSO-d_6 δ 2.50; ^{13}C NMR: $CDCl_3$ δ 77.0; DMSO-d_6 δ 39.52), with multiplicity (s = singlet, d = doublet, t = triplet, q = quartet, m = multiplet), coupling constants (J, in Hz), and integration values noted. Melting points were determined using an E-Z melting point apparatus, and HRMS data were obtained *via* an Agilent 6545 Q-TOF LC/MS (ESI).

4.5.1.1 General procedure for the synthesis of indole-3-carboxaldehyde

In a round-bottomed flask, freshly distilled dimethylformamide (DMF) (10 mL) was cooled in an ice-salt bath for approximately 30 min. Then, 90 mmol of freshly distilled phosphorus oxychloride was added gradually to the DMF with stirring over another 30 min. Subsequently, a solution of indole (2 g, 85.47 mmol) in 3 mL of DMF was added to the yellow solution over a period of 1 h. The resulting solution was stirred at 35 °C until it formed a yellow paste. After the reaction, 30 g of crushed ice was introduced to the paste while stirring, resulting in a clear cherry-red aqueous solution. A solution of sodium hydroxide (10 g, 94 mmol) in 100 mL of water was then added dropwise with stirring to the cherry-red solution. The resulting suspension was rapidly heated to 90 °C and allowed to cool to room temperature before being placed in a refrigerator overnight. The product was filtered, washed with water (2 × 100 mL), and air-dried to obtain pure **15** in yields ranging from 89-95%.

15a, yield 90%, mp 203-206 °C

15b, yield 95%, mp 179-182 °C

15c, yield 89%, mp 162-163 °C

15d, yield 93%, mp 195-197 °C

15e, yield 91%, mp 115-117 °C
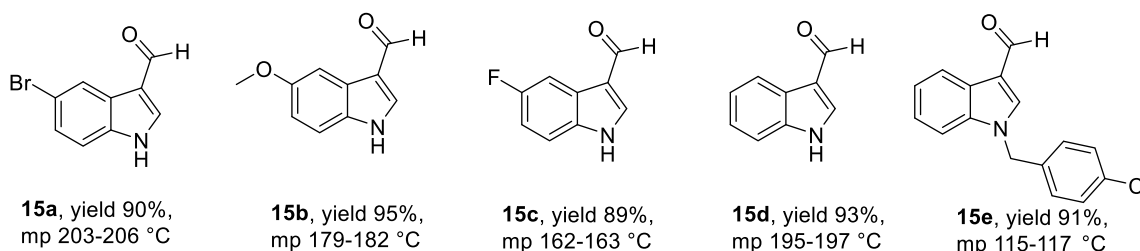
4.5.1.2 General procedure for the synthesis of indole-3-carbonitriles (16a-e)[32]

A round-bottom flask was successively charged with a mixture of **15** (13.78 mmol, 1.0 equiv), hydroxylamine hydrochloride (13.78 mmol, 1.0 equiv), and sodium formate (27.56 mmol, 2.0 equiv) dissolved in 15 mL of formic acid. The mixture was stirred for about 3 h at 130 °C (until TLC revealed the complete consumption of the starting material). The reaction mixture was

cooled to room temperature and poured into ice-cold water (150 mL) and organic layer was extracted in dichloromethane (2 × 40 mL). The extracted organic layer was washed with saturated sodium bicarbonate (50 mL) and brine (50 mL) solution. Evaporated the organic phase under reduced pressure and the residue obtained was purified by silica gel column chromatography (ethyl acetate: hexane as eluent) to obtain pure indole-3-carbonitriles **16a-e** (83-90% yields), mp. 177-180 °C.

4.5.1.3 General procedure for the synthesis of indole-3-thiocarboxamides (17a-e)[24]

A mixture of indole-3-carbonitrile (**16**, 0.02 mol), sodium hydrosulfide (0.04 mol) and magnesium chloride hexahydrate (0.02 mol) were taken in a round bottomed flask and stirred for 8 h at 50 °C. The progress of the reaction was monitored by TLC. After completion of the reaction, contents were poured into cold water (50 mL) and the solid obtained was filtered. The residue was re-suspended in 100 mL HCl solution (3N) and stirred for 10 min and then filtered-off the solid to obtain indole-3-thiocarboxamides **17a-e** yellow solid in 88-91% yields.

4.5.1.4 General procedure for the synthesis of indole-3-thioimidates (18)[33]

A mixture containing **17** (0.5 g, 3.65 mmol) and iodomethane (2 mL, 4.38 mmol) in THF (8 mL) was heated at reflux for 2 h. The solvent was removed to afford the **18a-e** aswhite solids in 88-94% yields.

18a, 92%	**18b**, 94%	**18c**, 91%	**18d**, 92%	**18e**, 88%
mp. 279-282 °C	mp. 291-293 °C	mp. 285-278 °C	mp. 268-272 °C	mp. 302-305 °C
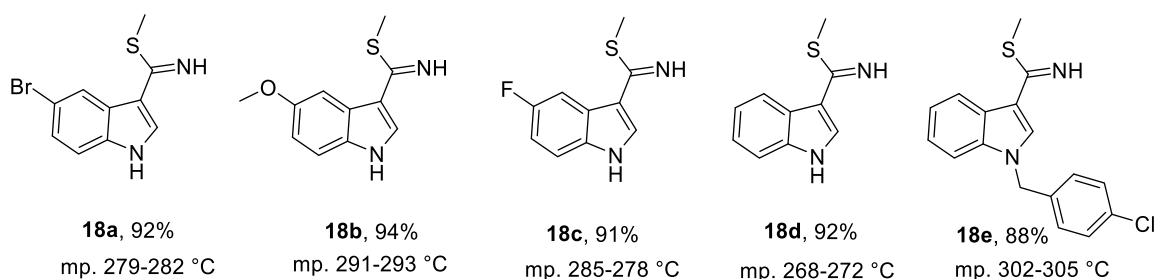
4.5.1.5 General procedure for the synthesis of ethyl 2-(1*H*-indol-3-yl) acetate (20a-e)

A solution of 2-(1*H*-indol-3-yl) acetic acid **19** (3 g, 17.1 mmol) in ethanol (20 mL) was cooled to 0 °C, to which a catalytic amount of H_2SO_4 was added and refluxed for 3 h. After completion of the reaction, monitored by TLC, the reaction contents were basified with a saturated solution of sodium carbonate. The organic phase was collected using ethyl acetate (50 mL × 3), dried with anhydrous Na_2SO_4, and concentrated in vacuo on a rotary evaporator. Crude solid was purified by column chromatography using silica gel to furnish pure acetate **20** with 91-92% yields.[34]

4.5.1.6 Procedure for the synthesis of 2-(1*H*-indol-3-yl) acetohydrazide (21)

To a solution of ethyl 2-(1*H*-indol-3-yl) acetate **20** (2 g, 0.98 mmol) in 20 mL ethanol, hydrazine hydrate (3.9 mmol) was added slowly at 0 °C and stirred 7 h at r.t. After completion of the reaction (indicated by TLC), ethanol was evaporated, and pure acetohydrazide[34] (**21**) was achieved in 91% yield.

4.5.1.7 General procedure for the synthesis of indolyl-1,2,4-triazoles (22a-i)

A mixture containing thioimidate (1.0 equiv) and the corresponding hydrazide (0.9 equiv) in dry DMF at 130 °C for 35 min. under microwave conditions. The progress of the reaction was monitored by TLC. After completion of the reaction, the mixture was quenched by adding it to ice-cold water. The resulting precipitate was filtered and subjected to recrystallization with ethanol. Compounds (**22a-i**) were obtained as white solid in 90-96% yields.

3-(5-((1*H*-indol-3-yl)methyl)-4*H*-1,2,4-triazol-3-yl)-5-bromo-1*H*-indole (22a)
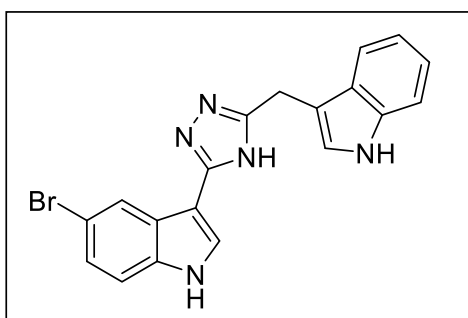
Off white solid, 91% yield, mp 282−283 °C. ^{1}H NMR (400 MHz, DMSO) δ 13.55 (s, 1H), 11.79 – 11.47 (m, 1H), 10.93 (s, 1H), 8.40 (s, 1H), 7.91 (s, 1H), 7.59 (s, 1H), 7.45– 7.39 (m, 1H), 7.36 (d, *J* = 7.1 Hz, 1H), 7.27 (s, 2H), 7.12 – 6.96 (m, 2H), 4.21 (s, 2H); ^{13}C NMR (100 MHz, DMSO-*d₆*) δ 180.75, 147.94, 146.94, 144.73, 137.32, 134.87, 132.28, 131.06, 128.29, 124.03, 122.69, 121.18, 119.86, 119.01, 114.96, 111.71, 109.88, 103.95, 101.75, 34.19. HRMS (ESI) *m/z* calcd for $C_{19}H_{14}BrN_5$: 392.0433 and 394.0412 (M + H)$^+$, found: 392.0485 and 394.0432.

3-(5-((1*H*-indol-3-yl)methyl)-4*H*-1,2,4-triazol-3-yl)-5-methoxy-1*H*-indole (22b)
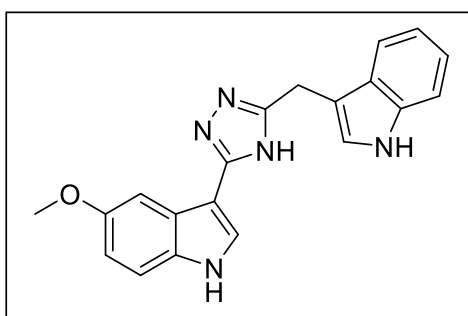
Off white solid, 93% yield, mp 275−276 °C. ^{1}H NMR (400 MHz, DMSO) δ 13.51 (s, 1H), 11.32 (s, 1H), 10.91 (s, 1H), 7.84 (s, 1H), 7.78 – 7.59 (m, 2H), 7.41 – 7.25 (m, 3H), 7.13 – 6.94 (m, 2H), 6.82 (s, 1H), 4.19 (s, 2H), 3.80 (s, 3H); ^{13}C NMR (100 MHz, DMSO-*d₆*) δ 154.51, 136.72, 131.84, 127.47, 125.98, 125.68, 123.90, 121.50, 119.15, 118.82, 112.96, 112.54, 111.85, 102.87, 55.78, 31.15.

3-(5-((1*H*-indol-3-yl)methyl)-4*H*-1,2,4-triazol-3-yl)-5-fluoro-1*H*-indole **(22c):** Brown-yellow solid, 91% yield, mp 269−271 °C. ^{1}H NMR (400 MHz, DMSO) δ 13.53 (s, 1H), 11.51 (s, 1H), 10.90 (s, 1H), 7.93 (s, 2H), 7.61 (s, 1H), 7.45 (s, 1H), 7.36 (d, *J* = 7.5 Hz, 1H), 7.27 (s, 1H), 7.10 – 7.04 (m, 1H), 7.02 – 6.95 (m, 2H), 4.19 (s, 2H); ^{13}C NMR (100 MHz, DMSO-*d6*) δ 154.51, 136.72, 131.84, 127.47, 125.98, 125.68, 123.90, 121.50, 119.15, 118.82, 112.96, 112.54, 111.85, 102.87, 31.15. HRMS (ESI) *m/z* calcd for C$_{19}$H$_{14}$FN$_5$: 332.1267 (M+H)$^+$, found: 332.1290.
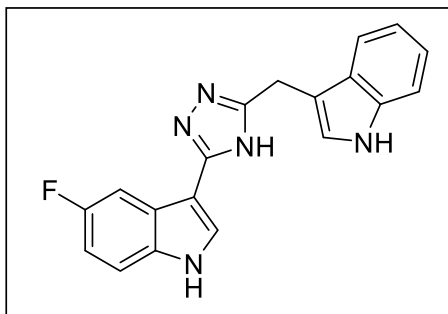
5-methoxy-3-(5-(3,4,5-trimethoxybenzyl)-4*H*-1,2,4-triazol-3-yl)-1*H*-indole (22d)
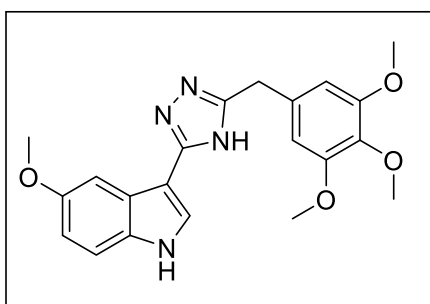
Off white solid, 96% yield, mp 250-253 °C. ^{1}H NMR (400 MHz, DMSO) δ 13.65 – 13.44 (m, 1H), 11.48 (s, 1H), 7.73 (s, 2H), 7.35 (s, 1H), 6.82 (s, 1H), 6.71 (d, *J* = 15.3 Hz, 2H), 4.08 – 3.96 (m, 2H), 3.79 (s, 3H), 3.76 (s, 6H), 3.63 (s, 3H); ^{13}C NMR (100 MHz, DMSO-*d6*) δ 162.46, 154.51, 136.72, 131.84, 127.47, 125.98, 125.68, 123.90, 121.50, 119.15, 118.82, 112.96, 106.59, 102.80, 60.43, 56.27, 55.72, 32.15.

(5-(3,4,5-trimethoxybenzyl)-4*H*-1,2,4-triazol-3-yl)-1*H*-indole (22e)
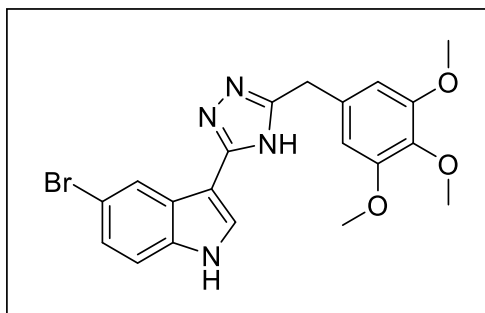
Brownish-white solid, 93% yield, mp 255−257°C. ^{1}H NMR (400 MHz, DMSO) δ 13.65–13.50 (m, 1H), 11.63 – 11.30 (m, 1H), 8.24 (t, *J* = 8.7 Hz, 1H), 7.98 – 7.80 (m, 1H), 7.50 – 7.40 (m, 1H), 7.23 – 7.07 (m, 2H), 6.72 (d, *J* = 15.3 Hz, 2H), 4.09 – 3.97 (m, 2H), 3.77 (s, 6H), 3.63 (s, 3H); ^{13}C NMR (100 MHz, DMSO-*d6*) δ 162.46, 154.51, 136.72, 131.84, 127.47, 125.98, 125.68, 123.90, 121.50, 119.15, 118.82, 112.96, 106.59, 102.80, 60.43, 56.27, 55.72, 34.15.

3-(5-(3,4,5-trimethoxybenzyl)-4*H*-1,2,4-triazol-3-yl)-1*H*-indole (22f)
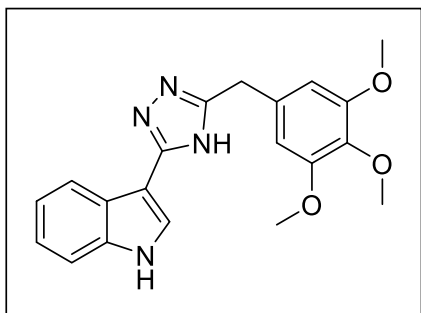
White solid, 95% yield, mp 276-278 °C. ^{1}H NMR (400 MHz, DMSO) δ 13.65 – 13.50 (m, 1H), 11.63 – 11.30 (m, 1H), 8.24 (t, *J* = 8.7 Hz, 1H), 7.98 – 7.80 (m, 1H), 7.50 – 7.40 (m, 1H), 7.23 – 7.07 (m, 2H), 6.72 (d, *J* = 15.3 Hz, 2H), 4.09 – 3.97 (m, 2H), 3.77 (s, 6H), 3.63 (s, 3H); ^{13}C NMR (100 MHz, DMSO-*d6*) δ 162.46, 154.51, 136.72, 131.84, 127.47, 125.98, 125.68, 123.90, 121.50, 119.15, 118.82, 112.96, 106.59, 102.80, 60.43, 56.27, 55.72, 34.15.

2-(5-(3,4,5-trimethoxybenzyl)-4*H*-1,2,4-triazol-3-yl)-1*H*-indole (22g)
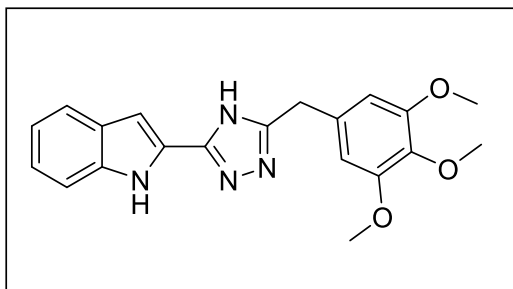
Off white solid, 90% yield, mp 286−289 °C. ^{1}H NMR (400 MHz, DMSO) δ 13.89 (s, 1H), 11.60 (s, 1H), 7.61 – 7.52 (m, 1H), 7.42 (d, *J* = 7.7 Hz, 1H), 7.13 – 6.85 (m, 3H), 6.67 (s, 2H), 4.11 (s, 2H), 3.77 (s, 6H), 3.64 (s, 3H); ^{13}C NMR (100 MHz, DMSO-*d₆*) δ 154.51, 136.72, 131.84, 127.47, 125.98, 125.68, 123.90, 121.50, 119.15, 118.82, 112.96, 112.54, 111.85, 102.87, , 56.29, 56.25, 31.15.

5-fluoro-3-(5-(3,4,5-trimethoxybenzyl)-4*H*-1,2,4-triazol-3-yl)-1*H*-indole (22h)
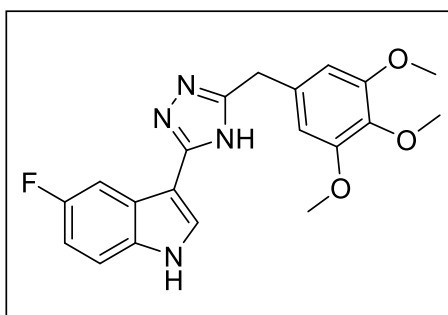
Yellowish-white solid, 92% yield, mp 259−260 °C. ^{1}H NMR (400 MHz, DMSO) δ 13.90 – 13.49 (m, 1H), 12.03 – 11.43 (m, 1H), 8.42 (s, 1H), 8.06 – 7.83 (m, 1H), 7.52 – 7.20 (m, 2H), 6.82 – 6.63 (m, 2H), 4.12 – 3.95 (m, 2H), 3.78 (s, 6H), 3.63 (s, 3H); ^{13}C NMR (100 MHz, DMSO-*d₆*) δ 154.51, 136.72, 131.84, 127.47, 125.98, 125.68, 123.90, 121.50, 119.15, 118.82, 112.96, 112.54, 111.85, 102.87, , 56.29, 56.25, 31.15. HRMS (ESI) *m/z* calcd for $C_{20}H_{19}FN_4O_3$: 383.1475 (M+H)$^+$, found: 383.1503.

1-(4-chlorobenzyl)-3-(5-(3,4,5-trimethoxybenzyl)-4*H*-1,2,4-triazol-3-yl)-1*H*-indole (22i)
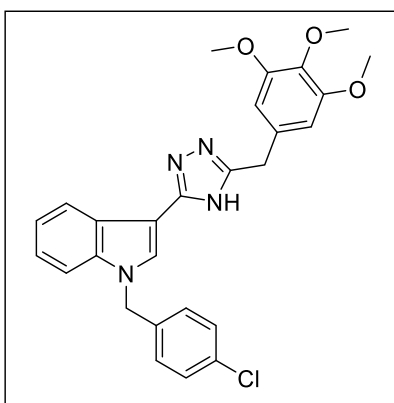
Off white solid, 91% yield, mp 287−289 °C. ^{1}H NMR (400 MHz, DMSO) δ 13.63 (s, 1H), 8.27 (d, *J* = 6.8 Hz, 1H), 8.05 (s, 1H), 7.53 – 7.36 (m, 3H), 7.31 – 7.14 (m, 4H), 6.71 (s, 2H), 5.50 (s, 2H), 4.04 (s, 2H), 3.77 (s, 6H), 3.63 (s, 3H); ^{13}C NMR (100 MHz, DMSO-*d₆*) δ172.63 153.26, 153.05, 136.59, 110.99, 106.89, 106.59, 65.38, 60.43, 56.29, 56.25, 48.97, 29.46.

4.6 References

1. Liu, X.; Pang, X.-J.; Liu, Y.; Liu, W.-B.; Li, Y.-R.; Yu, G.-X.; Zhang, Y.-B.; Song, J.; Zhang, S.-Y., Discovery of novel diarylamide n-containing heterocyclic derivatives as new tubulin polymerization inhibitors with anti-cancer activity. *Molecules* **2021,** *26* (13), 4047.

2. Sachdeva, H.; Mathur, J.; Guleria, A., Indole derivatives as potential anticancer agents: A review. *Journal of the Chilean Chemical Society* **2020,** *65* (3), 4900-4907.

3. Binarová, P.; Tuszynski, J., Tubulin: structure, functions and roles in disease. MDPI: 2019; Vol. 8, p 1294.

4. Bumbaca, B.; Li, W., Taxane resistance in castration-resistant prostate cancer: mechanisms and therapeutic strategies. *Acta Pharmaceutica Sinica B* **2018,** *8* (4), 518-529.

5. Podolak, M.; Holota, S.; Deyak, Y.; Dziduch, K.; Dudchak, R.; Wujec, M.; Bielawski, K.; Lesyk, R.; Bielawska, A., Tubulin inhibitors. Selected scaffolds and main trends in the design of novel anticancer and antiparasitic agents. *Bioorganic Chemistry* **2023,** 107076.

6. Kerru, N.; Gummidi, L.; Maddila, S.; Gangu, K. K.; Jonnalagadda, S. B., A review on recent advances in nitrogen-containing molecules and their biological applications. *Molecules* **2020,** *25* (8), 1909.

7. Song, J.; Gao, Q.-L.; Wu, B.-W.; Zhu, T.; Cui, X.-X.; Jin, C.-J.; Wang, S.-Y.; Wang, S.-H.; Fu, D.-J.; Liu, H.-M., Discovery of tertiary amide derivatives incorporating benzothiazole moiety as anti-gastric cancer agents in vitro via inhibiting tubulin polymerization and activating the Hippo signaling pathway. *European Journal of Medicinal Chemistry* **2020,** *203*, 112618.

8. Othman, E. M.; Fayed, E. A.; Husseiny, E. M.; Abulkhair, H. S., The effect of novel synthetic semicarbazone-and thiosemicarbazone-linked 1, 2, 3-triazoles on the apoptotic markers, VEGFR-2, and cell cycle of myeloid leukemia. *Bioorganic Chemistry* **2022,** *127*, 105968.

9. Phatak, P. S.; Bakale, R. D.; Dhumal, S. T.; Dahiwade, L. K.; Choudhari, P. B.; Siva Krishna, V.; Sriram, D.; Haval, K. P., Synthesis, antitubercular evaluation and molecular docking studies of phthalimide bearing 1, 2, 3-triazoles. *Synthetic Communications* **2019,** *49* (16), 2017-2028.

10. Al-Karmalawy, A. A.; Rashed, M.; Sharaky, M.; Abulkhair, H. S.; Hammouda, M. M.; Tawfik, H. O.; Shaldam, M. A., Novel fused imidazotriazines acting as promising top. II inhibitors and apoptotic inducers with greater selectivity against head and neck tumors: Design, synthesis, and biological assessments. *European Journal of Medicinal Chemistry* **2023,** *259*, 115661.

11. Abuo-Rahma, G. E.-D. A.; Abdel-Aziz, M.; Beshr, E. A.; Ali, T. F., 1, 2, 4-Triazole/oxime hybrids as new strategy for nitric oxide donors: Synthesis, anti-

inflammatory, ulceroginicity and antiproliferative activities. *European Journal of Medicinal Chemistry* **2014,** *71*, 185-198.

12. Goher, S. S.; Griffett, K.; Hegazy, L.; Elagawany, M.; Arief, M. M.; Avdagic, A.; Banerjee, S.; Burris, T. P.; Elgendy, B., Development of novel liver X receptor modulators based on a 1, 2, 4-triazole scaffold. *Bioorganic & Medicinal Chemistry Letters* **2019,** *29* (3), 449-453.

13. Al Sheikh Ali, A.; Khan, D.; Naqvi, A.; Al-Blewi, F. F.; Rezki, N.; Aouad, M. R.; Hagar, M., Design, synthesis, molecular modeling, anticancer studies, and density functional theory calculations of 4-(1, 2, 4-triazol-3-ylsulfanylmethyl)-1, 2, 3-triazole derivatives. *ACS Omega* **2020,** *6* (1), 301-316.

14. Mohamed, M. S.; Ibrahim, N. A.; Gouda, A. M.; El-Sherief, H. A., Design, synthesis and molecular docking of 1, 2, 4-triazole schiff base hybrids as tubulin, EGFR inhibitors and apoptosis-inducers. *Journal of Molecular Structure* **2023,** *1286*, 135621.

15. Kumari, A.; Singh, R. K., Medicinal chemistry of indole derivatives: Current to future therapeutic prospectives. *Bioorganic Chemistry* **2019,** *89*, 103021.

16. Zhang, M.-Z.; Chen, Q.; Yang, G.-F., A review on recent developments of indole-containing antiviral agents. *European Journal of Medicinal Chemistry* **2015,** *89*, 421-441.

17. Sravanthi, T.; Manju, S., Indoles—A promising scaffold for drug development. *European Journal of Pharmaceutical Sciences* **2016,** *91*, 1-10.

18. Dadashpour, S.; Emami, S., Indole in the target-based design of anticancer agents: A versatile scaffold with diverse mechanisms. *European Journal of Medicinal Chemistry* **2018,** *150*, 9-29.

19. Maddila, S.; Pagadala, R.; B Jonnalagadda, S., 1, 2, 4-Triazoles: A review of synthetic approaches and the biological activity. *Letters in Organic Chemistry* **2013,** *10* (10), 693-714.

20. İbiş, K.; Nalbat, E.; Çalışkan, B.; Kahraman, D. C.; Cetin-Atalay, R.; Banoglu, E., Synthesis and biological evaluation of novel isoxazole-piperazine hybrids as potential anti-cancer agents with inhibitory effect on liver cancer stem cells. *European Journal of Medicinal Chemistry* **2021,** *221*, 113489.

21. Man, S.; Luo, C.; Yan, M.; Zhao, G.; Ma, L.; Gao, W., Treatment for liver cancer: From sorafenib to natural products. *European Journal of Medicinal Chemistry* **2021,** *224*, 113690.

22. Khedr, F.; Ibrahim, M. K.; Eissa, I. H.; Abulkhair, H. S.; El‑Adl, K., Phthalazine‑based VEGFR‑2 inhibitors: Rationale, design, synthesis, *in silico*, ADMET profile, docking, and anticancer evaluations. *Archiv Der Pharmazie* **2021,** *354* (11), 2100201.

23. Zahoor, A. F.; Saeed, S.; Rasul, A.; Noreen, R.; Irfan, A.; Ahmad, S.; Faisal, S.; Al-Hussain, S. A.; Saeed, M. A.; Muhammed, M. T., Synthesis, Cytotoxic, and Computational Screening of Some Novel Indole–1, 2, 4-Triazole-Based S-Alkylated N-Aryl Acetamides. *Biomedicines* **2023,** *11* (11), 3078.

24. Guo, J.; Hao, Y.; Ji, X.; Wang, Z.; Liu, Y.; Ma, D.; Li, Y.; Pang, H.; Ni, J.; Wang, Q., Optimization, structure–activity relationship, and mode of action of nortopsentin analogues containing thiazole and oxazole moieties. *Journal of Agricultural and Food Chemistry* **2019,** *67* (36), 10018-10031.

25. El-Sherief, H. A.; Youssif, B. G.; Bukhari, S. N. A.; Abdel-Aziz, M.; Abdel-Rahman, H. M., Novel 1, 2, 4-triazole derivatives as potential anticancer agents: Design, synthesis, molecular docking and mechanistic studies. *Bioorganic Chemistry* **2018,** *76*, 314-325.

26. Dixit, D.; Verma, P. K.; Marwaha, R. K., A review on 'triazoles': Their chemistry, synthesis and pharmacological potentials. *Journal of the Iranian Chemical Society* **2021,** *18* (10), 2535-2565.

27. Tantak, M. P.; Malik, M.; Klingler, L.; Olson, Z.; Kumar, A.; Sadana, R.; Kumar, D., Indolyl-α-keto-1, 3, 4-oxadiazoles: Synthesis, anti-cell proliferation activity, and inhibition of tubulin polymerization. *Bioorganic & Medicinal Chemistry Ltters* **2021,** *37*, 127842.

28. Hamdy, R.; Ziedan, N.; Ali, S.; El-Sadek, M.; Lashin, E.; Brancale, A.; Jones, A. T.; Westwell, A. D., Synthesis and evaluation of 3-(benzylthio)-5-(1H-indol-3-yl)-1, 2, 4-triazol-4-amines as Bcl-2 inhibitory anticancer agents. *Bioorganic & Medicinal Chemistry Letters* **2013,** *23* (8), 2391-2394.

29. Sreenivasulu, R.; Sujitha, P.; Jadav, S. S.; Ahsan, M. J.; Kumar, C. G.; Raju, R. R., Synthesis, antitumor evaluation, and molecular docking studies of indole–indazolyl hydrazide–hydrazone derivatives. *Monatshefte Für Chemie-chemical Monthly* **2017,** *148*, 305-314.

30. Wu, F.; Zhou, Y.; Li, L.; Shen, X.; Chen, G.; Wang, X.; Liang, X.; Tan, M.; Huang, Z., Computational approaches in preclinical studies on drug discovery and development. *Frontiers in Chemistry* **2020,** *8*, 726.

31. Zhu, H.; Martin, T. M.; Ye, L.; Sedykh, A.; Young, D. M.; Tropsha, A., Quantitative structure− activity relationship modeling of rat acute toxicity by oral exposure. *Chemical Research in Toxicology* **2009,** *22* (12), 1913-1921.

32. Kumar, D.; Kumar, N. M.; Chang, K.-H.; Gupta, R.; Shah, K., Synthesis and in-vitro anticancer activity of 3, 5-bis (indolyl)-1, 2, 4-thiadiazoles. *Bioorganic & Medicinal Chemistry Letters* **2011,** *21* (19), 5897-5900.

33. Scott, F. J.; Khalaf, A. I.; Giordani, F.; Wong, P. E.; Duffy, S.; Barrett, M.; Avery, V. M.; Suckling, C. J., An evaluation of Minor Groove Binders as anti-Trypanosoma brucei brucei therapeutics. *European Journal of Medicinal Chemistry* **2016,** *116*, 116-125.

34. Shahzadi, I.; Zahoor, A. F.; Rasul, A.; Mansha, A.; Ahmad, S.; Raza, Z., Synthesis, hemolytic studies, and in silico modeling of novel acefylline–1, 2, 4-triazole hybrids as potential anti-cancer agents against MCF-7 and A549. *ACS Omega* **2021,** *6* (18), 11943-11953.

Chapter 5

Design, Synthesis and Anti-cancer Activity of Novel α-cyano bis(indolyl) chalcones

Part 5A: L-Proline Catalysed Synthesis and *in-silico* Studies of Novel α-cyano bis(indolyl)chalcones as Potential Anti-cancer Agents
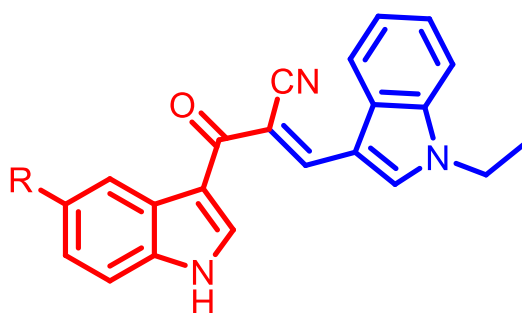
5.1.1 Introduction

Indole motif is a key building block of many naturally occurring and synthetic compounds endowed with different biological and pharmacological activities. With wider presence among a large number of heterocyclic compounds having medicinal properties, indole and derived compounds are pursued with greater interest.[1] Particular attention has been paid to bisindole containing compounds known to exhibit interesting anticancer activities by affecting numerous biological targets.[2] Additionally, bisindole alkaloids, isolated from marine sources, continue to inspire the development of novel anticancer agents. Most of the bisindole alkaloids possess two indole units connecting through a linear or heterocyclic ring spacer as shown in figure 5.1.1. Isolated from marin sponges Topsentia genitrix and Spongosorites, bisindole alkaloids, Topsentin (**1**) and Nortopsentin (**2**) with an imidazole linker, have been reported to display potent cytotoxicity towards diverse cancers.[3] Another emerging class of marine alkaloid, Dragmacidin B (**3**) with a piperazine linker, was isolated from the deep-water marine sponge Hexadella sp. and found to display good anticancer activity (IC_{50} = 15 μg/mL, P388; 1-10 μg/mL, A-549, HCT-8 and MDA-MB-231).[4]
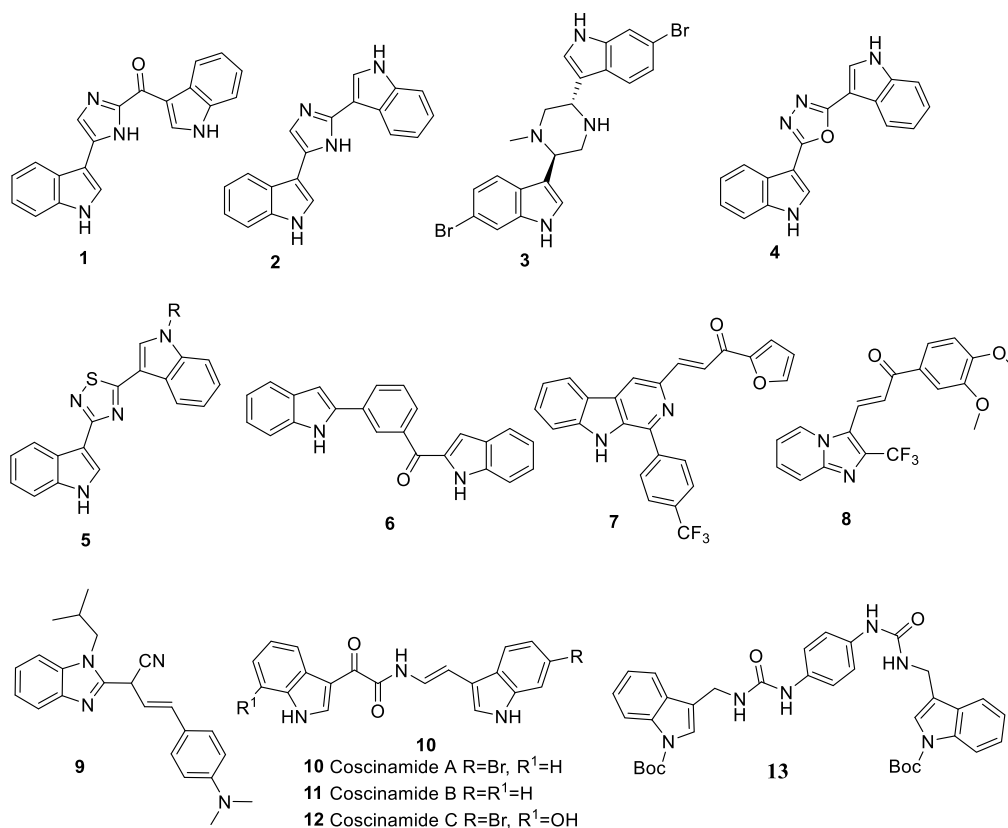
Figure 5.1.1 Indole analogues as anticancer agents

Despite the interesting anticancer activity exerted by bisindole alkaloids, in the recent past, researchers have identified several synthetic analogues of bisindole alkaloids with improved anticancer properties.[5] Kumar *et al.* identified bis(indolyl)-1,3,4-oxadiazoles (**4**) as apoptosis inducing cytotoxic agents (IC$_{50}$ = 20 nM; HeLa).[8] Several synthetic analogues of bisindole alkaloids with variety of cyclic spacers such as thiazole **5**, have been reported for their cytotoxic properties (Figure 5.1.1).[9] Many bisindole alkaloids with linear spacers have been reported to exhibit interesting anticancer activities.[6] For examples; bisindole with 1,2-diketo linker, Coscinamides A-C (**5**) with a linear α-keto enamide spacer from the extract of marine sponge *Coscinoderma* sp., were reported to exhibit antitumor activity against human prostate cancer cell line (IC$_{50}$ = 7.6 µg/mL).[7] The inhibition of tubulin polymerization is a well-established strategy for anticancer drug development, as microtubules play an essential role in cellular processes such as mitosis, intracellular transport, and cell motility.[10] Tubulin targeting substances are broadly categorized into microtubule stabilizing (taxanes, epothilones and discodermolide) and destabilizing (colchicine, vinca alkaloids, and CA-4P) agents. Microtubules targeting agents (MTAs) that bind to the colchicine binding site (also called CBSI) have the potential to overcome the drawbacks associated with taxanes and vinca alkaloids, owing to their structural simplicity, non-substrate nature for the multidrug resistance protein 1 (P-glycoprotein) and reasonable physicochemical properties. Duke *et al.* explored chalcone linked β-carboline hybrids (**7**) as anti-topoisomerase-I, DNA-interactive, and apoptosis inducing anticancer agents.[13] Ikeda *et al.* disclosed a series of α-methylated chalcones with 10-folds enhanced activity when compared to their parent derivatives.[14] Natural and synthetic chalcones have been reported to show diverse biological activities such as antiinflammatory,[15] antimalarial,[16] antiviral, antifungal, antibacterial and anticancer.[17] The *N,N*-dimethylamino substituted acrylonitrile bearing *N*-isobutyl and cyano substituents placed on the benzimidazole nuclei (**9**), showed strong and selective antiproliferative activity in submicromolar range of inhibitory concentrations (IC$_{50}$= 0.2-0.6 µM), while being significantly less toxic than reference systems docetaxel and staurosporine, thus promoting them as lead compounds.[18]

Coscinamides A-C (**10-12**) with a linear α-keto enamide spacer from the extract of marine sponge *Coscinoderma* sp., were reported to exhibit antitumor activity against human prostate cancer cell line (IC$_{50}$ = 7.6 µg/mL).[19] Isolated from a red alga *Chondria* sp. two cytotoxic bisindole amides, Chondriamides A-B, were found to be cytotoxic against KB and LOVO cell lines (IC$_{50}$ = 0.5-10 µg/mL).[20] In 2023, Jan *et al.* conducted a study focused on synthesizing novel bis-indole analogues containing a phenyl linker derived from indole phytoalexins. The

synthesis involved the reaction of [1-(tert-butoxycarbonyl)indol-3-yl]methylisothiocyanate with *p*-phenylenediamine to obtain the target bis-indole thiourea (**13**) linked with a phenyl linker.[7] Literature reports show that the indole scaffold frequently encounters in anticancer drug discovery research as illustrated in figure 5.1.1.

5.1.1.2 Rational Design

On the other hand, the αβ-unsaturated ketones also known as chalcones are reported to play a vital role in the identification of bioactive molecules. Indolyl chalcones (**14**) as potential cytotoxic agents.[21] Edwards *et al.* first reported that *α*-substituted chalcones are more potent than their unsubstituted analogs.[22] Li and Huang group reported **15**, exhibited most potent activity, with IC_{50} values of 3−9 nM and also displayed excellent tubulin polymerization inhibitory activity with an IC_{50} of 2.68 μM.[22]
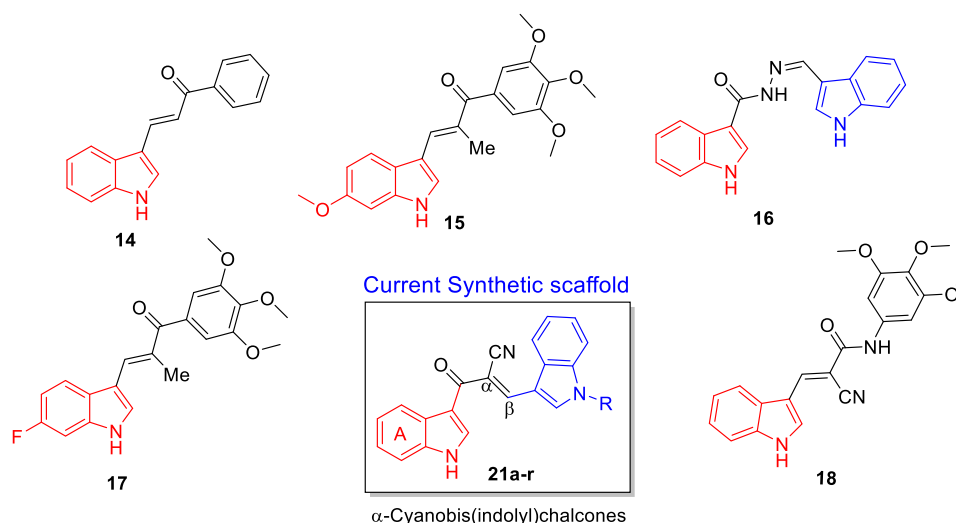
Figure 5.1.2 Rational design of **21**

Inspired from the interesting anticancer activities of naturally occurring bisindoles with linear chain spacers, Kumar *et al.* report ed bis(indolyl)hydrazide–hydrazones (**16**) as potent cytotoxic agents (IC_{50} = 1 μM; MDA-MB-231).[23] Over a period of time, several chalcones have been reported with structural modifications around the basic enone template. Ikeda *et al.* disclosed a series of *α*-methylated chalcones with 10-folds enhanced activity when compared to their parent derivatives.[14] Liu X *et al.* reported the synthesis of hybrid molecules containing indole and 3,4,5-trimethoxy-phenyl moieties as tubulin targeting agents. Among them, a fluorine-containing derivative **17** (Figure 5.1. 2) exhibited significant inhibitory activity toward HCT116 and CT26 cells.[24] Additionally, the presence of a α-cyano moiety in enone framework likely to plays an important role in view of its several advantageous properties, including enhanced binding affinity, improved pharmacokinetic profiles and reduced drug resistance.[25]

Trans-indol-3-ylacrylamide (**18**) exhibited antiproliferative activity, with an IC$_{50}$ value of 5 μM in Huh7 cells.[24] The heterocyclic pharmacophores in medicinal chemistry plays a crucial role in developing potent moieties towards successful cancer drug design. Among them all bisindole derivatives are the leading structural fragments which play an important role in synthetic and medicinal chemistry as well as various other fields.

With the observed side effects and high resistance rate against available drugs; identification of new and potent chemical entities is desirable to tackle the increasing disease problem.[9, 26] In order to further improve the anticancer efficacy of indole-based analogs, herein we designed, synthesized and evaluated cytotoxicity of a series of novel α-cyano bis(indolyl)chalcones.

5.1.2 Results and Discussion

5.1.2.1 Synthesis and Characterization

Synthesis of α-cyano bis(indolyl)chalcone (**21a**) involves the reaction of 3-cyanoacetyl indole (**19a**) with *N*-methyl indole-3-carboxaldehyde **20a** in presence of a base as described in Table 5.1.1. Initially, the reaction of **19a** with **20a** in presence of either piperidine or triethylamine resulted in lower product yield (Table 5.1.1, entries 1-2).

Table 5.1.1 Optimization of α-cyano bis(indolyl)chalcone **21a**
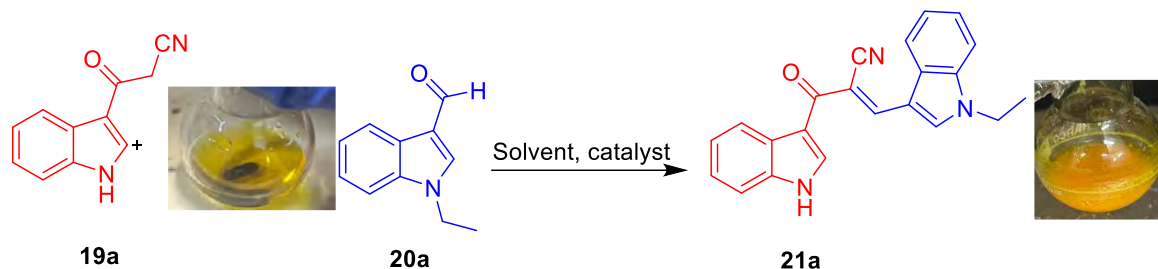
Entry	Solvent	Base	Temp.	Time (h)	Yield[b] (%)
1.	EtOH	piperidine	25 °C	2.5	48
2.	EtOH	Et$_3$N	25 °C	2.5	45
3.	EtOH	KOH	25 °C	2.5	80
4.	EtOH	KOH	25 °C	3.0	93
5.	-	KOH	25 °C (grinding)	0.5	88
6.	EtOH	-	25 °C	2.5	NR[c]
7.	EtOH	L-proline	25 °C	2.5	67
8.	**EtOH**	**L-proline**	**25 °C**	5.5	**95**
9.	EtOH:H$_2$O(1:1)	L-proline	25 °C	5.5	78
10.	**EtOH**	-	**25 °C**	5.5	NR[c]

[a]Reagents and conditions: **19a** (1.0 mmol, 1.0 equiv), **20a** (1.0 equiv), L-proline (0.1 equiv), EtOH (3 mL) at 25 °C. [b]Isolated yield. [c]NR; No reaction

Next, with the use of KOH as a base at 25 °C produced the expected *α*-cyano bis(indolyl)chalcone **21a** in 80% yield (Table 5.1.1, entry 3). With the increase in reaction time from 1.5 h to 3 h, the product yieldwas increased to 93% (Table 5.1.1, entry 4). When a neat mixture of 3-cyanoacetylindole **19a** and *N*-ethylindole-3-carboxyaldehyde (**20a**) in the presence of KOH was grinded at room temperature for 0.5 h, bisindole **21a** was formed in 88% yield (Table 5.1.1, entry 5). No product was obtained when the same reaction was performed in absence of base (Table 5.1.1, entry 6).

In the recent past, the natural and inexpensive L-proline has been widely used as a prominent organocatalyst for carbon-carbon bond formation in various organic transformations.[29] In view of success of proline catalysed transformations along with its inexpensive and environmentally benign nature, next we performed the reaction of 3-cyanoacetylindole **19a** and *N*-ethyl indole-3-carboxyaldehyde in the presence of readily available and metal-free catalytic L-proline, in ethanol at 25 ºC, to obtain **21a** in 95% yield (Table 5.1.1, entry 8). However, in absence of L-proline, the reaction was failed to produce **21a** (Table 5.1.1, entry 10).
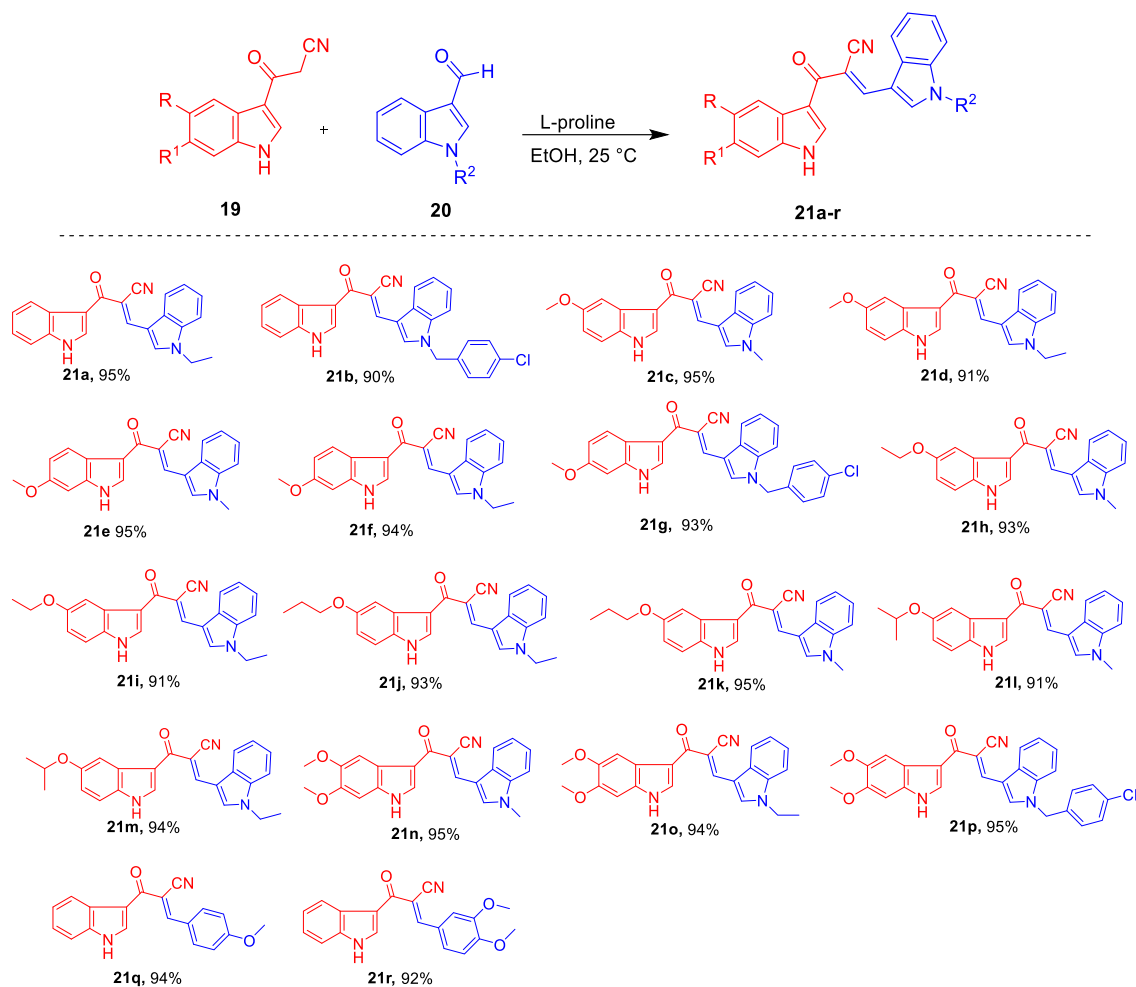
Scheme 5.1.1 Synthesized *α*-cyano bis(indolyl)chalcones (**21a-r**)

The structure of **21a** was confirmed by the NMR (^{1}H & ^{13}C) analysis. The proton NMR of **21a** displayed characteristic singlets at 8.50 ppm (alkenyl proton, =CH), 4.44 ppm (CH$_2$) while CH$_3$ protons resonated at 1.46 ppm. In ^{13}C NMR spectrum signals due to carbonyl, nitrile carbon, alkenyl (=CH), CH$_3$ and CH$_2$ carbons were observed at about 181.26, 121.07, 144.96, 42.18 and 15.60 ppm, respectively. In IR spectra, a characteristic sharp peak at ~ 2200 cm^{-1} was observed due to the presence of a nitrile functional group. Similarly, using the optimized reaction conditions, compounds **21b-r** were prepared in high yields (90-95%) and characterized the products by their NMR spectral data. (Figure 5.1.3 and 5.1.4)
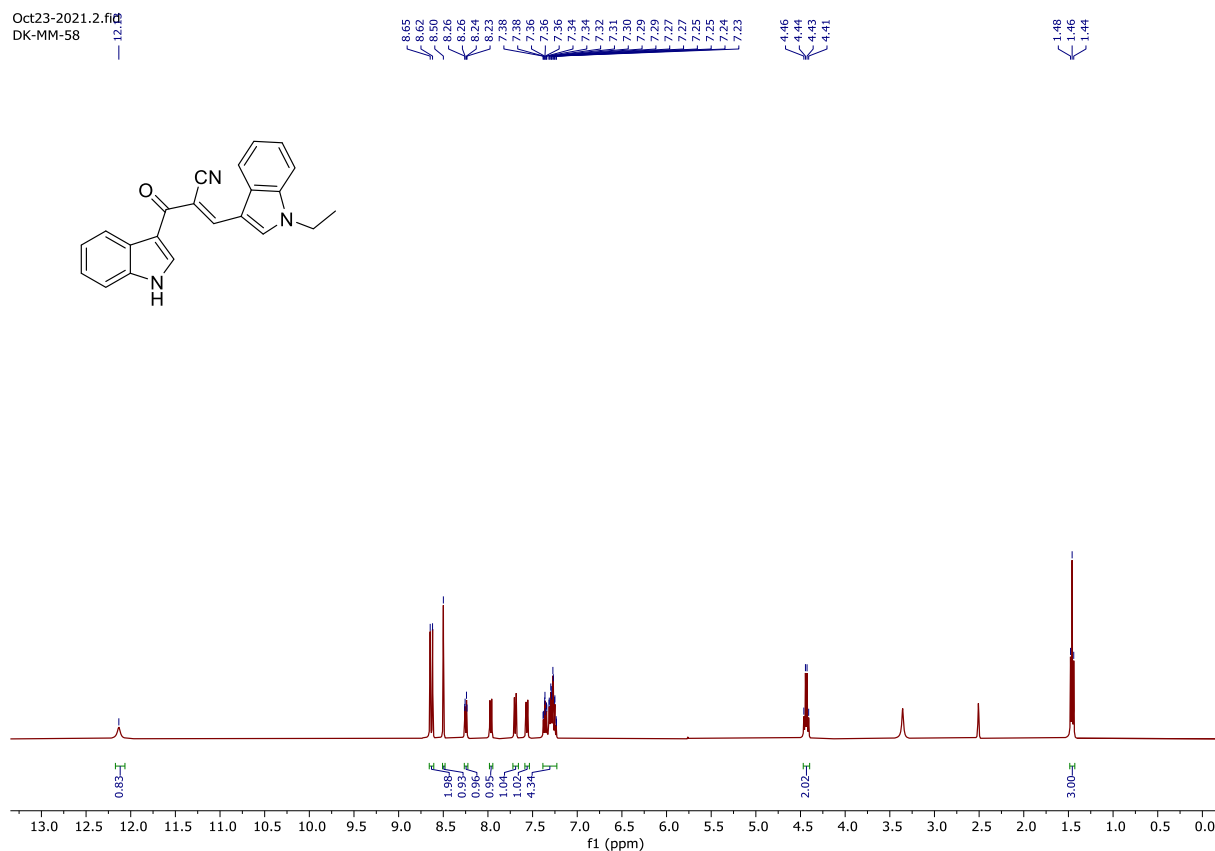
Figure 5.1.3 ^{1}H NMR spectrum of **21a**

Oct23-2021.31.fid
DK-MM-58
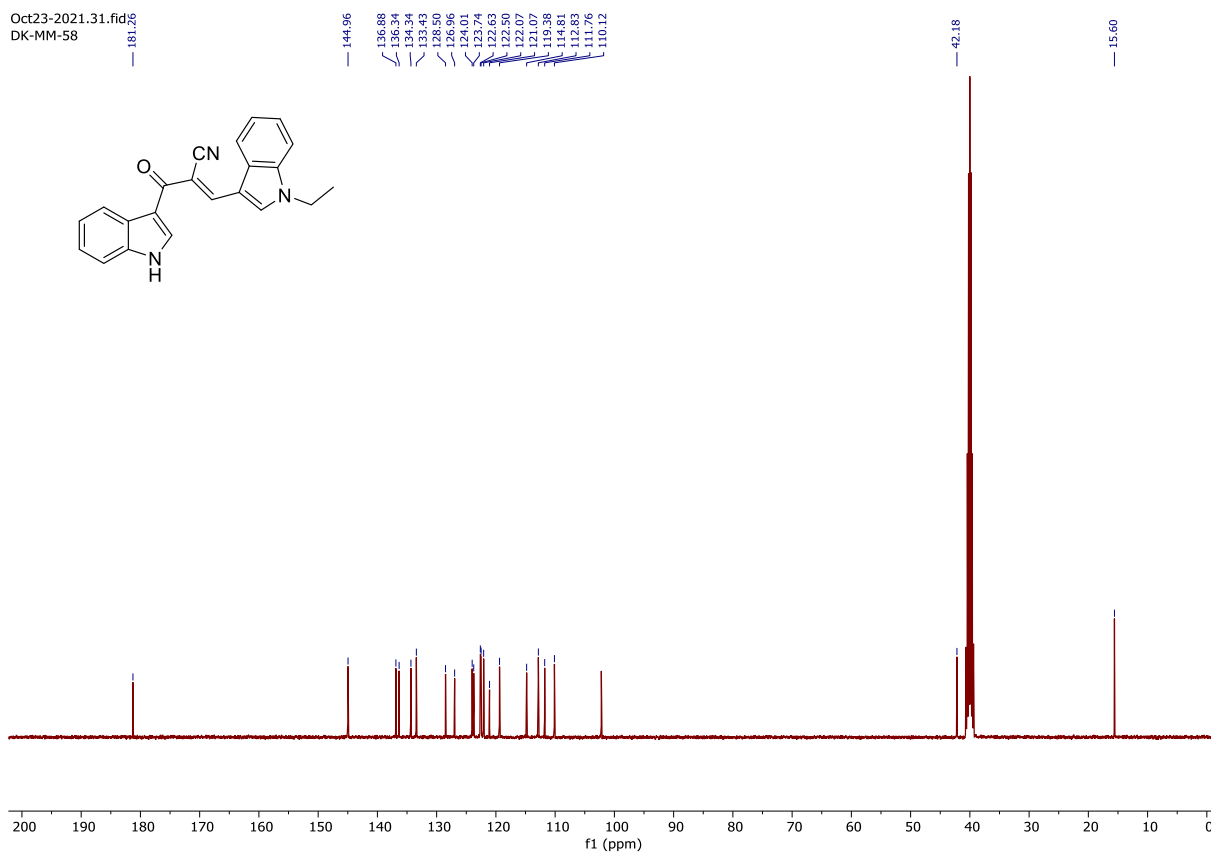
Figure 5.1.4 ^{13}C NMR spectrum of **21a**

The formation of **21** may be rationalized by the *in-situ* generation of enamine intermediate **I** by the condensation of 3-cyanoacetylindole **19a** and L-proline. Further, the nucleophilic addition of enamine **I** to the carbonyl group of indole-3-carboxaldehyde (**20**) and followed by dehydration is likely to produce **21** as illustrated in Scheme 5.1.2.
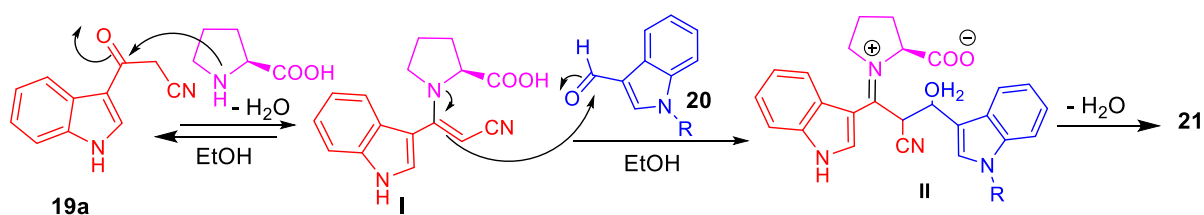
Scheme 5.1.2 Plausible mechanistic pathway for of *α*-cyano bis(indolyl)chalcones.

5.1.2.2 Biological Evaluation

5.1.2.2.1 Anti-cancer Activity

The cytotoxicity of the synthesized α-cyano bis(indolyl)chalcones derivatives **21a-r** were evaluated against five human cancer cell lines; prostate (C4-2, PC3 and 22Rv1), breast

(MCF7), epithelial cancer (MIAPACA) and normal human kidney (HEK293) cell lines by using MTT assay. The anticancer activity is expressed in terms of IC_{50} values for inhibition of tumor cell growth as provided in Table 5.1.2. A structure-activity relationship (SAR) study was conducted by synthesizing a diverse set of α-cyano bis(indolyl)chalcones with various substituents on both indole rings. Most of the synthesized compounds are not inhibiting the normal cells (HEK 293). Initial Bisindole **21a** was found to be selectively cytotoxic against C4-2 ($IC_{50} = 3.9$ μM).

Table 5.1.2 IC_{50} (μM) values of α-cyano bis(indolyl)chalcones (**21a-r**)

Compounds	MCF7	PC3	C4-2	22Rv1	MIAPACA	HEK293
21a	10.2	13	**3.9**	>40	>40	>40
21b	**6.9**	10.6	13.5	21.5	**4.9**	40
21c	25.3	15.45	**7.5**	**1.23**	**4.5**	>40
21d	10.9	>40	8	25	15.5	39.2
21e	12.47	**7.61**	15.7	28	>40	>40
21f	37	24	12.5	>40	>40	40
21g	10.5	14.3	13.3	34	**7.9**	>40
21h	16.75	27.3	10	**5.23**	**1.35**	40
21i	**7.38**	**2.63**	**2.2**	**8.9**	**5.8**	>40
21j	**1.2**	**5.6**	**0.98**	**2.9**	**5.3**	>40
21k	18.6	16.1	13.8	28	28.9	39.8
21l	7.95	4.6	26.4	**2.5**	37.6	37.9
21m	**2.98**	11.7	17.6	16.4	**1.6**	>40
21n	**5.61**	**7.1**	**1.02**	20.5	15.6	>40
21o	31.5	19	**5.9**	26	12.95	>40
21p	>40	>40	31	>40	>40	>40
21q	25	37	>40	28	15.4	>40
21r	>40	25	>40	34	37	31

Next, protection of indole-NH with *p*-chlorobenzyl moiety produced **21b** with moderate activity. Incorporation of a C5-methoxy group in indole moiety led to compounds **21c** and **21d**. Particularly, compound **21c** with 5-methoxyindole and *N*-methylated indole displayed selective cytotoxicity against **22Rv1** (1.23 μM). With the change in position of methoxy group in indole ring from C-5 to C-6 and protection of indole NH with *p*-chlorobenzyl group led to compounds

21e, **21f** and **21g** with reduced activity. To optimize the size of C5-alkoxy group, ethoxy and propyloxy derivatives **21h**, **21i** and **21j** were prepared with significantly enhanced cytotoxicity against the tested cancer cells. By the introduction of 5-isopropyloxy group led to **21l** with improved selectivity against prostate cancer cells (2.5 μM, 22Rv1 cells). The presence of an additional methoxy group in indole ring and protection of indole NH as *N*-Me/*N*-Et (compounds **21n** and **21o** with 5,6-dimethoxyindole moiety) improved the selectivity against prostate cancer cell lines. The protection of indole nitrogen with *p*-chlorobenzyl moiety (compounds **21p**) or replacement of the indole ring with a phenyl group (compounds **21q** and **21r**) or was found to be detrimental for the activity. These activity results suggest that both the indole rings are necessary for the potency of α-cyano bis(indolyl)chalcones. Protection of second indole ring as *N*-Et (**21j**) instead of *N*-Me (**21k**) or *N*-chlorobenzyl (**21p**) is also beneficial for the activity. Particularly, **21j** with C-5 propyloxy substituent and N-ethylindole was found to be the best compound of series with an IC$_{50}$ value of 0.98 μM against C4-2 (prostate) cancer cells.
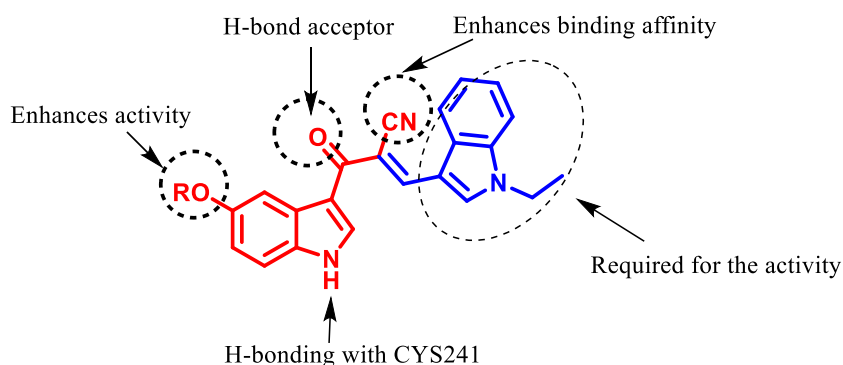
Figure 5.1.5 SAR for the *α*-cyano bis(indolyl)chalcones (**21a-r**)

5.1.2.2.2 Acridine Orange (AO)/Ethidium Bromide (EB) staining

Our data revealed **21j** as the most effective compound, as it showed broad selectivity. Thus, to explore the mechanism of cell death, we initially used acridine orange (AO)/ethidium bromide (EB) staining to differentiate the percentage of live and dead cells. While AO stain both live and dead cells, ethidium bromide (EB) stain only dead cells. Incubation of compound **21j** in C4-2 cells for 48 h resulted in red fluorescence, indicating that **21j** causes cell death in C4-2 cells (Figure 5.1.6).
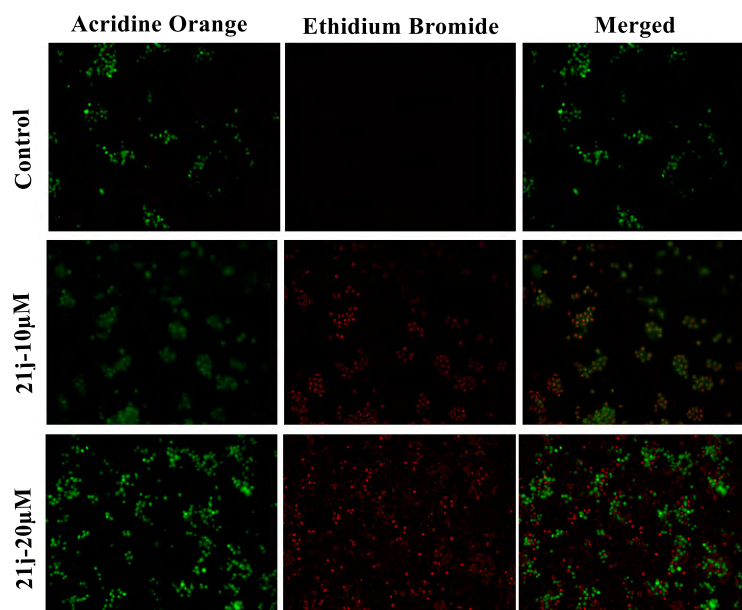
Figure 5.1.6 Fluorescent microscopic images of C4-2 prostate cancer lines treated with DMSO, **21j** and puromycin at 48 h by AO-EB staining. Control cells show green fluorescence confirming their viability. Puromycin showed considerable red fluorescence representing significant apoptosis. **21j** showed substantial apoptosis as majority of cells displayed red fluorescence.

5.1.2.2.3 Induces Mitochondrial Dysfunction in C4-2 cells

Increased oxidative stress is often linked to mitochondrial dysfunction, which prompted us to investigate whether **21j** treatment could cause mitochondrial depolarization. C4-2 cells were treated with either **21j** (10 µM and 20 µM) or positive control puromycin for 48 h, both of which induced significant mitochondrial depolarization, thereby revealing that **21j** toxicity at least partly arises due to mitochondrial damage (Figure 5.1.7).
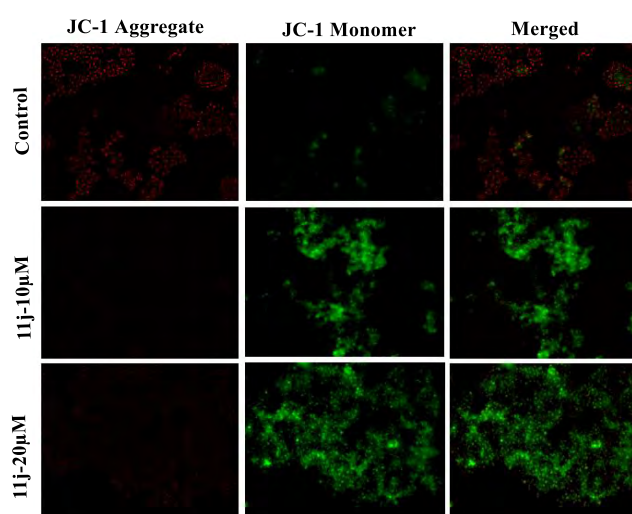
Figure 5.1.7 21j increases mitochondrial depolarization in C4-2 cells. Cells were treated with DMSO, **21j** (10 µM and 20 µM) and Puromycin for 48 h and stained with JC-1. Photographs were taken in FITC (green) and TRITC (red) channel at 20X objective with the fluorescence microscope (Nikon).

5.1.2.2.4 Tubulin Depolymerization and Cytokinesis Defects

While physiological ROS levels promote cytoskeleton polymerization, oxidation stress induces the F-actin severing and impedes microtubule polymerization. As **21j** promotes oxidative stress, we next analysed whether **21j** has an impact on tubulin polymerization in C4-2 cells. Briefly, C4-2 cells were treated with **21j** for 48 h and then stained for β-tubulin antibody. The images were captured and processed in fluorescent microscope at low and high magnifications. The low magnification images show more cells displaying cytokinesis defects (Figure 5.1.8) in **21j** treated group. In parallel, high magnification images revealed clear loss of tubulin assembly in **21j** treated group.
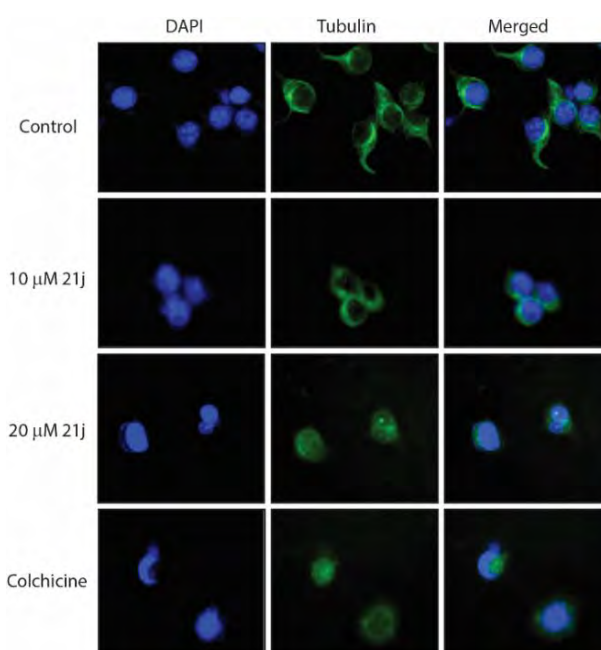
Figure 5.1.8 21j Increases depolymerization of tubulin in C4-2 cells. C4-2 cells were treated with DMSO or compound **21j** (10 μM and 20 μM) for 48 h. The fluorescence images were captured in FITC secondary antibody (green) to visualise tubulin. Nucleus were visualised by DAPI (blue). Fluorescence images captured at 20X showing a greater number of cells with incomplete cytokinesis in **21j** group.

To further validate a potential impact of **21j** on tubulin dynamics, we measured the relative concentrations of polymerized versus depolymerized tubulin in control and **21j**-treated C4-2 cells. As a positive control, colchicine was employed. While colchicine treatment significantly decreased the levels of polymerized tubulin by ~30% as compared to control. **21j** treatment also resulted in ~20% less polymerized tubulin. These results suggest that at least some percentage of **21j**'s anti-cancer effect stems from its tubulin-depolymerizing activity (Figure 5.1.9).
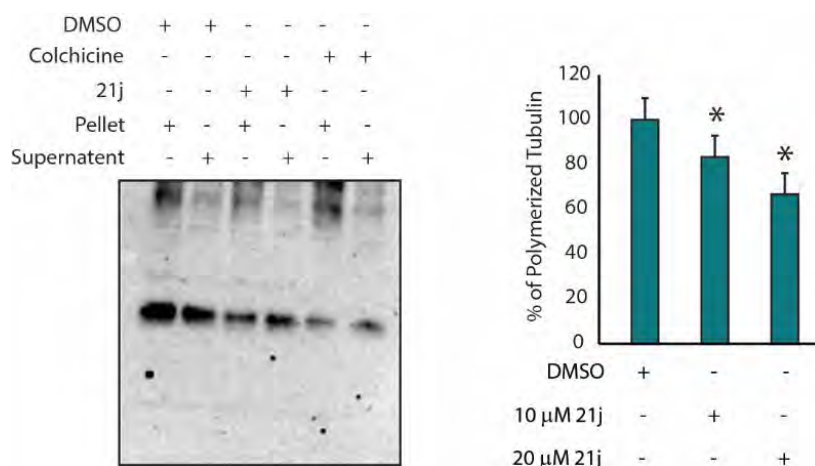
Figure 5.1.9 21j increases tubulin depolymerization in C4-2 cells. (A) C4-2 cells were treated with DMSO, colchicine (100 nM) or compound **21j** (20 µM) for 24 h. Following cell lysis in hypotonic buffer, pellet and supernatant were separated using ultracentrifugation. Equal amounts of proteins were loaded in each lane. (B) Data analysis was performed using 3 independent replicates, and statistical significance between DMSO (control), Colchicine, and **21j**-treated cells was determined using Student T-test. *P < 0.05.

5.1.2.2.5 Induces Reactive Oxygen Species (ROS) Accumulation

Increased oxidative stress induces cell death. Therefore, we examined whether compound **21j** promotes ROS using DCFDA staining in C4-2 cells. Both 10 µM and 20 µM concentrations of **21j** induced robust increase in ROS levels (Figure 5.1.10). These results confirm that **21j** induces cytotoxicity at least in part by increasing oxidative stress.
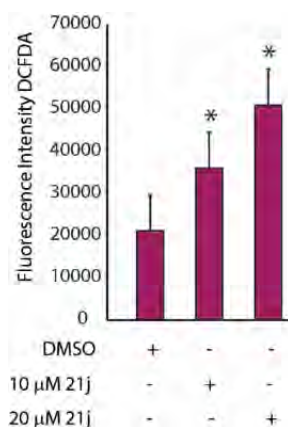
Figure 5.1.10 21j increases ROS levels in C4-2 cells. C4-2 cells were treated with DMSO vehicle control, or 10 µM and 20 µM of compound **21j** for 48 h and stained with H2-DCFDA. The bar graph shows arbitrary intensity of ROS level (green signal) using control and 10 µM and 20 µM **21j**-treated cells. Data analysis was performed using three independent replicates, and statistical significance between DMSO (control), 10 and 20 µM **21j**-treated cells were performed using Student T-test. *P < 0.05.

5.1.2.2.6 21j Inhibits Colony Formation

Clonogenic assay is an *in vitro* cell based technique that is often used to determine the tumorigenic potential of cells *in vivo*. Therefore, we determined the effect of **21j** on colony forming ability of C4-2 cells. **21j** treatment significantly inhibited the number and size of colonies as compared to the control group (Figure 5.1.11) indicating that **21j** should serve as an effective anti-cancer agent.
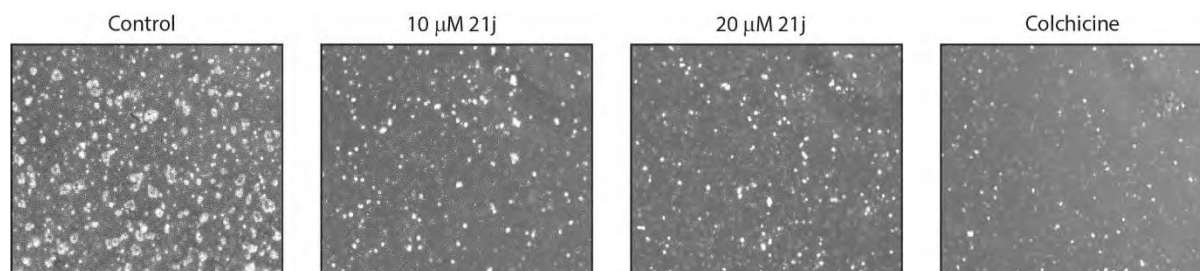
Figure 5.1.11 21j inhibits colony formation in C4-2 cells. (A) Equal number of cells (1000 cells /well) were plated in a 6-well plate. They were treated with 0.05% DMSO (control) or compound **21j** at 10 μM or 20 μM. 200 nM Colchicine was used as a positive control. After 10 days cells were fixed and photographed.

5.1.2.3 Molecular docking studies

Tubulin-colchicine complex (PDB code: 1SA0) structure was provided by the Protein Data Bank (rcsb.org).[27] Possible interactions between tubulin and the α-cyano bis(indolyl)chalcones were investigated, and orientations were compared with the reference drug colchicine. To gain better understanding on the potency of **21j** and guide further SAR studies, we proceeded to examine the interaction of **21j** with tubulin crystal structure (PDB code: 1SA0) using AutoDock 1.5.6 software (The Scripps Research Institute, USA). The X-ray crystallographic enzyme tubulin complex with colchicine shows an essential hydrogen bonding interaction with CYS241 in addition to hydrophobic interaction. The selected pose of the **21j** out of eight poses that showed similarity to the binding mode of DAMA colchicine is considered the best pose with binding energy is -7.7 Kcal/mol (Figure. 5.1.12). As shown in figure 10, C_5-propyloxy and NH moieties of indole in **21j** form hydrogen bonding interactions with CYS241 and LEU255, respectively, in addition to hydrophobic interactions (ALA250, ALA354, LEU248, ALA316, LYS352). Molecular docking results further highlight that **21j** as a novel tubulin polymerization inhibitor that displayed interactions in the colchicine binding site of the tubulin. The structures were visualised and analysed in Discovery studio 2021 software.
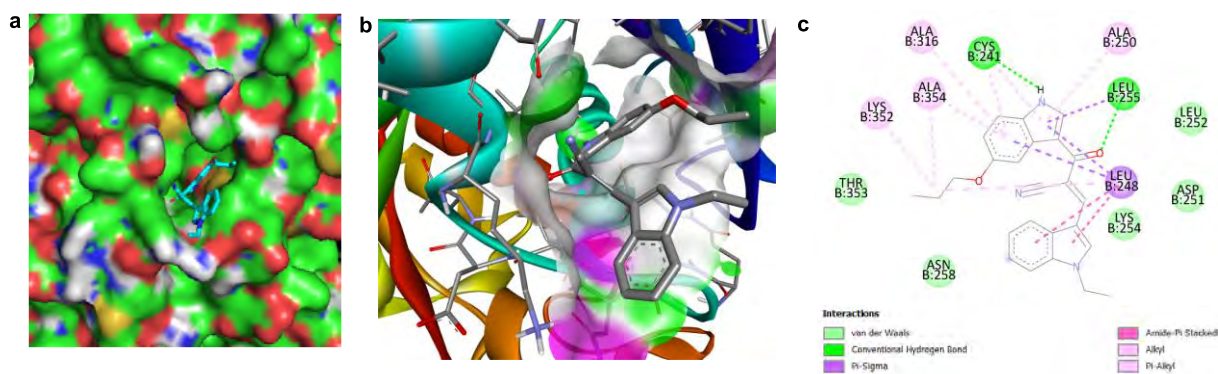
Figure. 5.1.12 Molecular interactions of **21j** in colchicine binding site

5.1.2.4 *In silico* ADME evaluation of compounds 21a-r

As a result, many *in silico* models for predicting chemical ADMET properties have been created and it has become advantageous as it reveals a pharmacokinetics-related failure of drugs before proceeding to the clinical phase.[27] Lipophilicity is generally considered a key determinant of permeability across tissue membranes, while water solubility is another physicochemical property that determines a drug's ADMET behaviours. Orally administered drugs usually have a high lipophilic value, indicating easy passage and absorption through the intestinal lining, penetration of the membrane of the target cells, and travel in the blood. There is a direct relationship between the logP value and lipophilicity, but this negatively correlates with water solubility.[28] Hence, the test compounds (**21a-r**) with log P values between 3.3 and 5.5. Drug-likeness is established based on chemical structures and physicochemical properties and is a qualitative assessment of oral bioavailability.[29] Moreover, Lipinski's Rule states that for an orally active drug, the following conditions must be obeyed: ≤ 5 H-bond donors, ≤ 10 H-bond acceptors, a molecular weight ≤ 500 g/mol, and a log p ≤ 5.43; a ligand is considered orally inactive if it violates two or more of Lipinski's rules.[30]

Moreover, none of the test compounds violated Veber's rule, whose criteria are the presence of rotatable bonds ≤ 10 and polar surface (TPSA) area ≤ 140 Å2.[30] Moreover, evident from the bioavailability score of 0.55%, all the selected test compounds **21a-r** will be good oral drugs.

Table 5.1.3 Physicochemical properties of **21a-r**

Comp.	MW[a](g/mol)	ClogP$_{o/w}$[b]	nHBA[c]	nHBD[d]	nRB[e]	TPSA(A^2)[f]	logS[g]	druglikeness
21a	339.39	3.70	2	1	4	61.58	-4.97	Yes
21b	435.90	5.16	2	1	5	61.58	-6.58	Yes
21c	355.39	2.91	3	1	4	70.81	-4.67	Yes
21d	369.42	3.17	3	1	5	70.81	-4.86	Yes
21e	355.29	3.36	3	1	4	70.81	-4.67	Yes
21f	369.42	3.68	3	1	5	70.81	-4.86	Yes
21g	465.93	5.14	3	1	6	70.81	-6.65	Yes
21h	399.44	3.68	4	1	6	80.04	-4.93	Yes
21i	383.44	4.03	3	1	6	70.81	-5.09	Yes
21j	**397.47**	**4.40**	**3**	**1**	**7**	**70.81**	**-5.43**	**Yes**
21k	383.44	3.37	3	1	6	70.81	-5.24	Yes
21l	354.40	3.92	2	1	4	47.02	-4.86	Yes
21r	332.35	3.18	4	1	5	75.11	-4.34	Yes

[a] Molecular weight; [b] Lipophilicity; [c] No. of H-bond acceptors; [d] No. of H-bond donor
[e] No. of rotatable bonds; [f] Topological surface area; [g] water solubility

As highlighted in the table, the skin permeation values (log Kp in cm/s) of the test compounds ranged from -5.54 (more permeant) to -5.07 (most permeant). Compounds **21c** and **21j** are the most skin permeant among the prepared compounds; however, the range of values of each test compound suggested that they are permeable compared to the values from the standard ligand. All the test compounds possess high gastrointestinal (GI) absorption potential, and the compounds (**21b**, **21c**, **21d**, **21k** and **21r**) displayed the ability to penetrate the blood-brain barrier (BBB).

According to the pharmacokinetic predictions, except for **21a**, all the test compounds were predicted to be inhibitors of CYP1A2, CYP2C19, CYP2C9, CYP2D6, and CYP3A4 (Table 4). Cytochrome P450 (CYP) is an isoenzyme superfamily that catalyzes various biochemical processes in phase I of drug metabolism (Hollenberg, 2002). The inhibition of the five main isoforms CYP1A2, CYP2C19, CYP2C9, CYP2D6, and CYP3A4 from eventually becoming the substrates of medications is a primary cause of pharmacokinetics-related drug interactions.[31]

Table 5.1.4 Selected pharmacokinetic parameters **21a-r**

Comp.	GI absorption	BBB permeant	LogKp (cm/s)	CYP1A2	CYP2C19	CYP2C9	CYP2D6	CYP3A4
21a	Low	No	-5.07	No	Yes	Yes	No	Yes
21b	High	Yes	-5.45	Yes	Yes	Yes	No	Yes
21c	High	Yes	-5.54	Yes	Yes	Yes	No	Yes
21d	High	Yes	-5.45	Yes	Yes	Yes	No	Yes
21e	High	No	-5.25	Yes	Yes	Yes	No	Yes
21f	High	No	-5.25	Yes	Yes	Yes	No	Yes
21g	High	No	-5.25	Yes	Yes	Yes	No	Yes
21h	High	No	-5.38	Yes	Yes	Yes	No	Yes
21i	High	No	-5.47	Yes	Yes	Yes	No	Yes
21j	**High**	**No**	**-5.18**	**Yes**	**Yes**	**Yes**	**No**	**Yes**
21k	High	Yes	-5.07	Yes	Yes	Yes	No	Yes
21l	High	No	-5.25	Yes	Yes	Yes	No	Yes
21r	High	Yes	-5.45	Yes	Yes	Yes	No	Yes

Moreover, according to Table 5.1.4, the bioavailable radar charts in Figure 5.1.13, and the BOILED-Egg plot in Figure 5.1.14, the investigated compounds were predicted to possess high gastrointestinal tract (GI) absorption and blood–brain barrier (BBB) permeability.
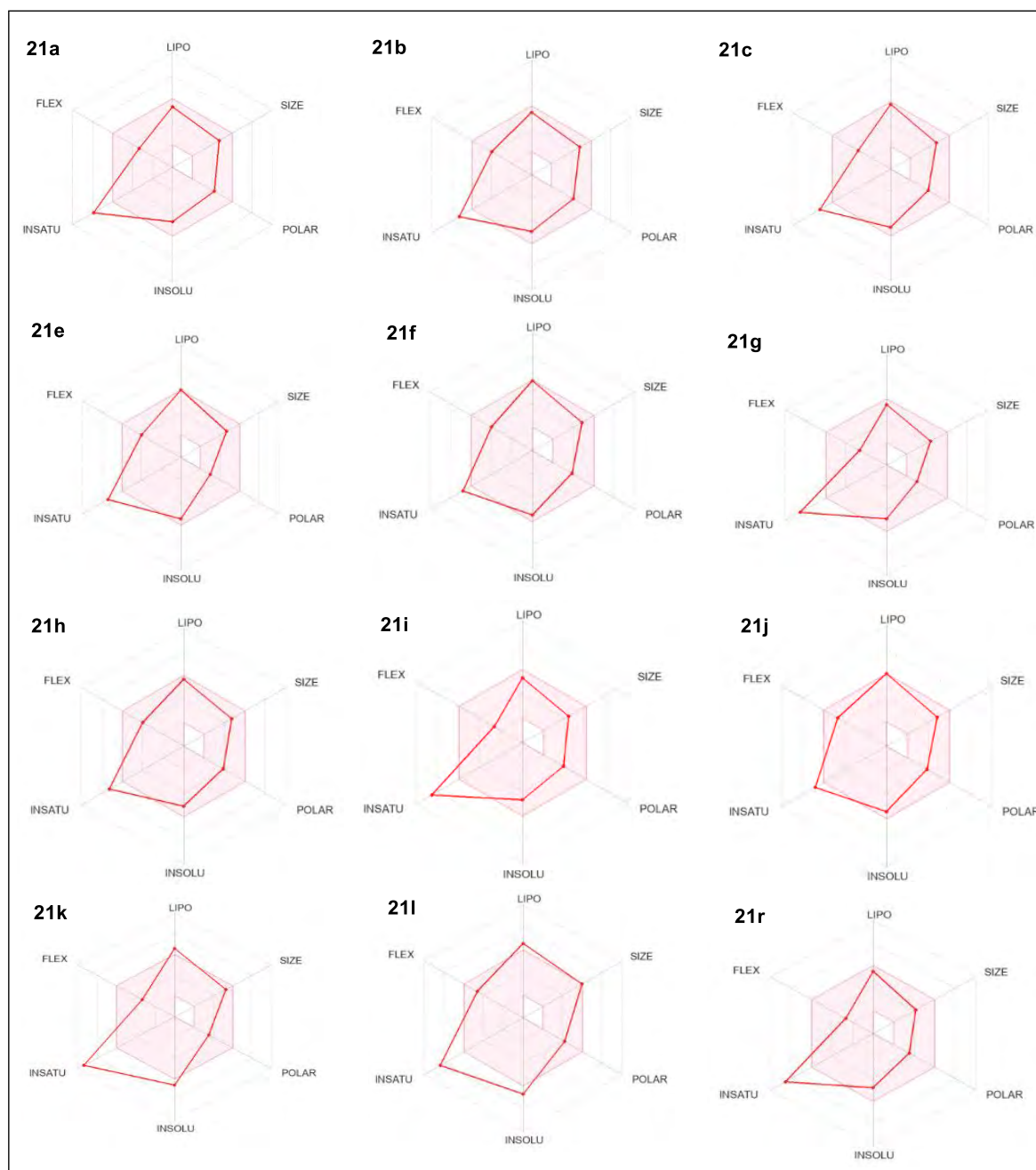
Figure 5.1.13 Oral bioavailability radar charts for the studied potent compounds **21a-r**. In bioavailability radar, the pink area represents the optimal range for each physicochemical property of oral bioavailability (LIPO-lipophilicity, SIZE-size, POLAR-polarity, INSOLU-solubility, INSATU-saturation and FLEX-flexibility), while the red lines represent compounds: **21a-r**

The BOILED-Egg is of great support for lead optimization

The BOILED-Egg model offers a rapid, intuitive, and easily reproducible yet statistically robust method for predicting the passive gastrointestinal absorption and brain access of small molecules, which is valuable for drug discovery and development. Illustrated in figure 5.1.14, the BOILED-Egg model delineates the physicochemical space of molecules: the white region

represents the highest probability of absorption by the gastrointestinal tract, while the yellow region (yolk) indicates the highest probability of permeating to the brain. It's important to note that the yolk and white areas are not mutually exclusive.
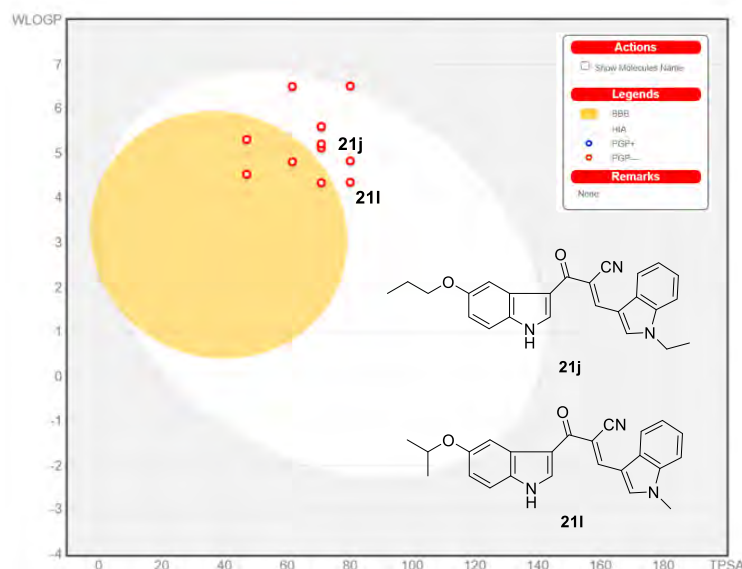
Figure 5.1.14 BOILED-Egg plot for the studied compounds **21a-r**

According to the determined parameters related to the absorption of the drug substance, it can be said that the synthesized compounds **21a-r** were characterized by good intestinal absorption (HIA) and bioavailability.

Table 5.1.5 Physiochemical and ADME parameters with bioactivity scores

Toxicity target	Toxicity probability of compounds				
	Colchicine	21i	21j	21m	21n
Caco-2 Permeability	0.65	0.53	0.53	0.58	0.51
Rat Acute toxicity (LD$_{50}$) mol/kg	2.37	2.63	2.61	2.56	2.66
Carcinogens	Non-carcinogens				
	0.81	0.88	0.91	0.91	0.93
Distribution					
Subcellular localization	Nucleus	Mitochondria			
P-glycoprotein Substrate	0.59	0.52	0.55	0.62	0.60
Absorption	LogP app, cm/sec				
Caco-2 Permeability	1.17	1.29	1.20	1.29	1.64
Human Intestine Absorption	0.98 (High)	1.00 (High)	1.00 (High)	1.00 (High)	1.00 (High)

Distribution analysis predicted the location of the tested compounds in the mitochondria and did not reveal permeability through the blood-brain barrier (BBB). In addition, the compounds were identified as P-glycoprotein substrates but not inhibitors. *In silico* toxicity and carcinogenicity are assessed and are given in Table 5.1.5. Furthermore, the computed rat acute toxicity, that is, LD_{50} in mol/kg seems to be sufficiently safe in the range 2.23−2.66 mol/kg. The LD_{50} and other bioactivity score of **21j** is similar to that of the standard colchicine drug shown in Table 5.1.5.

5.1.3 Conclusions

The high yielding synthesis of indolyl α-cyano bis(indolyl)chalcones was achieved from the L-proline catalysed reaction of appropriate aldehydes with 3-cyanoacetylindoles. Of the prepared eighteen α-cyano bis(indolyl)chalcones, compound **21j** demonstrated remarkable potency against the C4-2 prostate cancer cell line (IC_{50} = 0.9 μM). With broad spectrum of activity (0.98-5.6 μM), the compound **21j** was found to increase the endogenous level of ROS, upregulate the level of p-53 and c-jun besides mitochondrial dysfunction, causes apoptosis. Additionally, moderate tubulin activity of **21j** suggest that at least some percentage of **21j**'s anti-cancer effect stems from its tubulin de-polymerization. The molecular docking study of **21j** displayed important interactions in the colchicine binding site of the tubulin which supports its observed tubulin activity.

5.1.4 Biology Protocols
5.1.4.1 MTT Assay

C4-2, PC-3 and 22Rv1 prostate cancer cells were grown in RPMI 1640 media. HEK293 (human kidney cells) and MCF7 (human breast cancer cells) were maintained in Dulbecco's modified Eagle's media (DMEM). All media were supplemented with 10% FBS, streptomycin (100 μg/mL) and penicillin (100 I.U./mL). For MTT assay, 5 x 10^3 cells/well were seeded in 96-well plates. After 12h, cells were treated with different concentrations of **21a-r** in a range from 0.1 μM - 40 μM. 0.1% DMSO (vehicle control) was used as control. After 48 h, old media was removed, cells were washed with PBS followed by addition of 100 μL of serum free media and MTT (5mg/ml) cocktail (4:1 ratio) in each well. Cells were incubated for 4 h at 37 °C. MTT was then aspirated, cells were washed with PBS, and then 100 μL DMSO was added to dissolve the formazan crystals. The absorbance was measured at 570 nm using Tecan Spectrafluor Plus. Relative inhibition was calculated as mean absorbance of treated cells/mean absorbance of DMSO treated cells (negative control). The IC_{50} values and dose response curve

were obtained by nonlinear regression analysis [non-linear regression (sigmoidal dose response with variable slope)] using Graph Pad Prism, version 6.0 software (Graph Pad Software Inc., CA, USA).

5.1.4.2 JC-1 staining

JC-1 staining was employed to investigate the effect of **21j** compound on mitochondrial health and apoptosis. Briefly, 0.25×10^5 C4-2 cells were seeded on 12 mm coverslips. After 12 h, the cells were treated with DMSO or 21j (10 µM & 20µM) for 48 h. The cells were washed with PBS and incubated with JC-1 dye in PBS (2 µM) for 20 min. Cells were washed with PBS and images were captured in a BZ-X810 Keyence fluorescence microscope using FITC (green) and TRITC (red) channels. The healthy mitochondria exhibit more J-aggregates and emit orange fluorescence in the TRITC channel, whereas unhealthy or mitochondrial depolarization (a hallmark of cellular death) results in a decrease of JC-1 accumulation and a shift in fluorescence more towards green.

5.1.4.3 Acridine Orange-Ethidium Bromide staining

Acridine orange (AO) /Ethidium bromide (EB) staining was performed to determine the effect of **21j** compound on the permeability of plasma membrane, chromatin condensation and nuclear morphology. Briefly, 0.25×10^5 C4-2 cells were seeded on 12 mm coverslip in 24-well plates. 12 h later, the cells were treated with DMSO or **21j** (10 µM & 20µM) for 48 h. The old media was removed, cells were washed with PBS followed by incubation with the AO/EB (100 µg/mL AO and 100 µg/mL EB) dye mixture in PBS for 20 min. Cells were washed with PBS and imaged in a fluorescent microscope (Nikon) using FITC (green) and TRITC (red) channels. The nucleus appears green because AO permeates all cells, whereas EB only appears red when the integrity of the cytoplasmic membrane is compromised (as in necrosis or late apoptosis).

5.1.4.4 Tubulin polymerization assay

C4-2 cells were plated 16 h prior to the treatment with the corresponding drugs. The cells were treated with either 20 µM of **21j** or 100 nM of colchicine for 48 h at 37 °C. Colchicine was used as a positive control. The cells were lysed using hypotonic buffer (1 mM $MgCl_2$, 2 mM EGTA, 0.5% NP40, 2 mM phenylmethylsulfonyl fluoride, 20 mM Tris HCl pH 6.8). Ultracentrifugation was used to separate the pellet and supernatant containing the polymerized and depolymerized tubulin respectively. The lysis buffer was used to resuspend the pellet followed by a Bradford assay for protein quantification. Equal amounts of the pellet and supernatant fractions were loaded onto a 12% SDS-PAGE gel, and immunoblotting was used for tubulin detection.

5.1.4.5 Western blot analysis

C4-2 cells were treated with DMSO, 20 μM of **21j** or 100 nM of colchicine for 48 h at 37 °C. Cells were washed with PBS and lysed in hypotonic buffer. The proteins were resolved by 12% SDS-PAGE gel electrophoresis, and transferred at polyvinylidene difluoride (PVDF) membrane, followed by blocking in 5% skim milk (0.1% TBST). The membrane was incubated overnight at 4 °C with tubulin (1:5000) primary antibodies. Tubulin hybridoma was purchased from Developmental Studies Hybridoma Bank (DHSB). PVDF membrane was washed with 0.1% TBST and incubated with secondary antibody (HRP-conjugated) for 1h at room temperature. The proteins were visualized using chemiluminescence detection reagent (Pierce Biotechnology) in GeneGnomeXRQ chemiluminescence imager.

5.1.4.6 Immunofluorescence

C4-2 cells were plated in on poly-lysine -coated cover slips. After 16 h, the cells were treated with DMSO or **21j** (10 μM & 20μM). After 24 h of treatment, the cells were fixed and permeabilized with ice cold methanol. A blocking solution (2% BSA and 1% Triton X-100 in 1X PBS) was used for non-specific blocking for one hour. The poly-lysine-coated cover slips containing cells were subsequently incubated with tubulin primary antibody overnight at 4 °C. The conjugated secondary antibody goat anti-mouse-FITC was used for 3 h in the dark, and images were captured using a BZ-X810 Keyence fluorescence microscope.

5.1.5 Experimental Section
5.1.5.1 General Remarks

The required laboratory reagents were purchased from Sigma-Aldich, Alfa Aesar and Spectrochem India Pvt. Ltd and used without further purification. The reactions were monitored by thin layer chromatography and performed on Merck pre-coated plates (silica gel 60 F_{254}, 0.2mm). Column chromatographic purification of products was carried out using silica gel (100-200 mesh) and ethyl acetate/hexane mixture was used for elution. ^{1}H NMR spectra and ^{13}C NMR spectra were recorded at 400 MHz and 100 MHz using $CDCl_3$ and DMSO-d_6 solutions. Chemical shifts are given in ppm relative to the residual solvent peak (^{1}H NMR: $CDCl_3$ δ 7.26; DMSO-d_6 δ 2.50; ^{13}C NMR: $CDCl_3$ δ 77.0; DMSO-d_6 δ 39.52) with multiplicity (s = singlet, d = doublet, t = triplet, q = quartet, m = multiplet), coupling constants (*J*, in Hz) and integration. Melting points were determined by using E-Z melting point apparatus and are uncorrected. High-resolution mass data (HRMS) were obtained on an Agilent 6545 Q-TOF LC/MS (ESI).

5.1.5.2 General procedure for the synthesis of 3-cyanoacetyl indoles (19):[54]

Methane sulfonyl chloride (0.13 ml, 0.17 mmol) and corresponding indoles (0.20g, 0.17mmol) were added to a stirred solution of potassium cyanoacetate (0.42g, 0.34 mmol) in acetonitrile (3 mL). The resulting solution was stirred at room temperature for 1h. The progress of the reaction was monitored by TLC. After the consumption of the starting material, contents were allowed to cool and a white solid thus obtained was collected by filtration, washed with methanol and dried to obtain pure products (**19a-g**) as mentioned below:

| **19a**, 91% | **19b**, 91% | **19c**, 92% | **19d**, 95% | **19e**, 93% | **19f**, 93% | **19g**, 92% |
| mp 241-243 °C | mp 269-272°C | mp 248-250 °C | mp 251-253 °C | mp 260-261 °C | mp 227-230 °C | mp 279-280 °C |
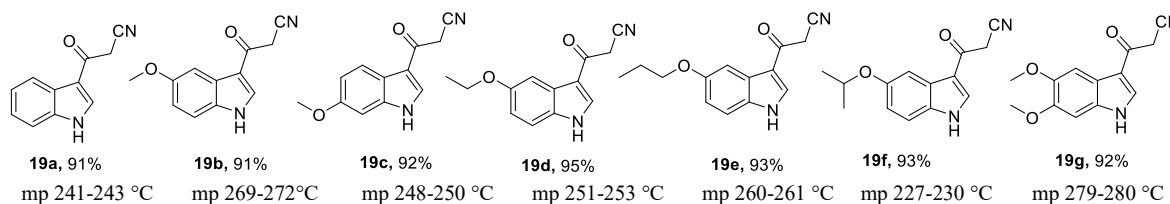
5.1.5.3 Procedure for the synthesis of 5-ethoxyindole and 5,6-dimethoxyindole

A mixture of 5-hydroxyindole/5,6-hydroxyindole (0.50 g, 3.8 mmol) and K_2CO_3 (1.52 g, 11.0 mmol), dissolved in 5 mL ethanol and heated to reflux. The ethyliodide/ propylbromide/ isopropylbromide (0.77 g, 4.9 mmol) was added and the reaction mixture was allowed to reflux for 1h and then concentrated the mixture at reduce pressure. Water (20 mL) was added and the aqueous layer was extracted with ethyl acetate (3×30 mL). The combined organic layer was dried with $MgSO_4$ and concentrated. The crude product was purified by flash column chromatography using 5% ethyl acetate/hexane (v/v) as eluent.

| 95% | 93% | 91% | 92% |
| mp 38-40 °C | mp 57-59 °C | mp 51-53 °C | mp 157-159 °C |
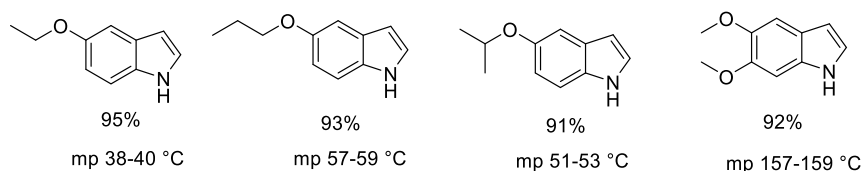
5.1.5.4 General procedure for the synthesis of indole-3-carboxaldehyde (20):[56]

A round bottomed flask containing freshly distilled dimethylformamide (DMF) (10 mL) was cooled in an ice-salt bath for about 0.5 h and freshly distilled phosphorus oxychloride (POCl₃) was added with stirring to the DMF over a period of 0.5 h. A solution of indole (**18**, 2g, 85.47 mmol) in DMF (130 mmol) was added to the yellow solution over a period of 1 h. The solution was stirred at 35 °C till it became a yellow paste. At the end of the reaction, 30 g of crushed ice was added to the paste with stirring to obtain a clear cherry-red aqueous solution. To this cherry-red solution, sodium hydroxide (10 g, 94 mmol) in 100 mL of water was added dropwise with stirring. The resulting suspension was heated rapidly to 90 °C and allowed to cool at room temperature, after which it was placed in refrigerator for overnight. The product was filtered,

washed with water (2 × 100 mL) and air dried to afford the pure indole-3-carboxaldehyde derivatives **20** in 91-93% yields.

5.1.5.5 Procedure for alkylation of indole-3-carboxaldehydes

In a reaction flask, indole-3-carboxaldehyde (1 g, 1.0 equiv.) was dissolved in THF (15 mL), followed by the addition of sodium hydride (0.3 g, 2.5 equiv.) and methyl/ethyl iodide (3.0 equiv) at 0 °C to room temperature. Reaction was monitored by the TLC. After the completion of reaction, organic phase was washed twice with aqueous NaHCO$_3$ (50 mL), water and saturated brine (100 mL), and then dried over anhydrous Na$_2$SO$_4$. The solvent was evaporated under vacuum and residue was purified by the column chromatography with ethylacetate and hexane led to pure *N*-alkylated 3-carboxaldehydes (93-96% yields). *N*-methyl-3-carboxaldehyde (mp. 68-70 °C) and *N*-ethyl-3-carboxaldehyde (mp. 99-102 °C).

5.1.5.6 General procedure for the preparation of *α*-cyano bis(indolyl)chalcones (21a-r)

A mixture containing 3-cyanoacetylindole derivative **19** (0.1 g, 1 mmol) and appropriate aldehyde **20** (0.065g, 1 mmol) in ethanol (10 mL) was stirred at 25 °C. Catalytic amount of L-proline (10 mol%) was added to reaction mixture and it was stirred for 5 h at 25 °C. The reaction progress was monitored *via* TLC using a developing solvent system of n-hexane: ethyl acetate. The resulting yellow solid was then recrystallized from ethanol to obtain pure *α*-cyano bis(indolyl)chalcones **21a-r** in 91-95% yields.

(E)-3-(1-ethyl-1*H*-indol-3-yl)-2-(1*H*-indole-3-carbonyl)acrylonitrile (21a):
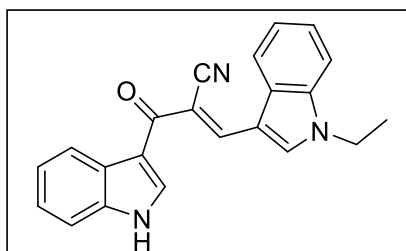
Pale Yellow solid, 94% yield, mp 221−222 °C; ^{1}H NMR (400 MHz, DMSO-*d$_6$*) δ 12.13 (s, 1H), 8.63 (d, *J* = 10.5 Hz, 2H), 8.50 (s, 1H), 8.26 – 8.22 (m, 1H), 7.97 (dt, *J* = 7.7, 1.0 Hz, 1H), 7.69 (dt, *J* = 8.2, 0.9 Hz, 1H), 7.59 – 7.54 (m, 1H), 7.38 – 7.23 (m, 4H), 4.44 (q, *J* = 7.2 Hz, 2H), 1.46 (t, *J* = 7.2 Hz, 3H); ^{13}C NMR (100 MHz, DMSO-*d$_6$*) δ 181.26, 144.96, 136.88, 136.34, 134.34, 133.43, 128.50, 126.96, 124.01, 123.74, 122.63, 122.50, 122.07, 121.08, 119.38, 114.81, 112.83, 111.76, 110.12, 102.20, 42.18, 15.60.

3-(1-(4-chlorobenzyl)-1H-indol-3-yl)-2-(1H-indole-3-carbonyl)acrylonitrile (21b):
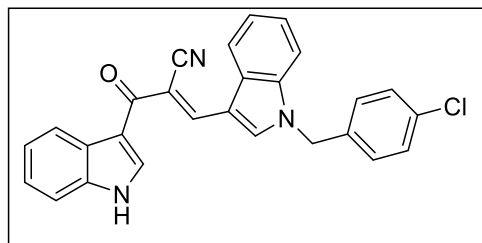
Yellow solid, 90% yield, mp 222−225 °C ; ^{1}H NMR (400 MHz, DMSO-*d$_6$*) δ 12.17 (s, 1H), 8.75 (s, 1H), 8.63 (s, 1H), 8.51 (s, 1H), 8.26 (d, *J* = 6.5 Hz, 1H), 7.97 (d, *J* = 7.9 Hz, 1H), 7.59 (d, *J* = 14.8 Hz, 2H), 7.42 (s, 2H), 7.31 (d, *J* = 10.0 Hz, 6H), 5.68 (s, 2H); ^{13}C NMR (100 MHz, DMSO-

d_6) δ 181.31, 144.92, 136.82, 136.44, 135.84, 134.45, 134.10, 133.09, 129.62, 129.22, 128.41, 126.78, 124.33, 123.95, 122.89, 122.71, 122.01, 120.86, 119.31, 114.75, 112.88, 111.96, 110.51, 102.80, 49.87.

2-(5-methoxy-1H-indole-3-carbonyl)-3-(1-methyl-1H-indol-3-yl)acrylonitrile (21c):
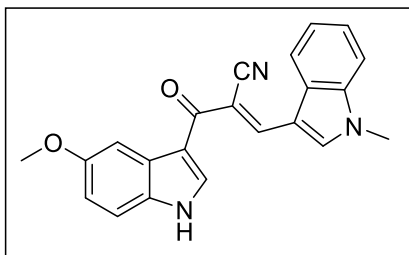
Yellow solid, 95% yield, mp 220−221 °C; ^{1}H NMR (400 MHz, DMSO-d_6) δ 12.03 (s, 1H), 8.62 (s, 1H), 8.59 (s, 1H), 8.45 (d, J = 3.3 Hz, 1H), 7.96 (d, J = 7.8 Hz, 1H), 7.77 (d, J = 2.8 Hz, 1H), 7.65 (d, J = 8.3 Hz, 1H), 7.45 (d, J = 8.8 Hz, 1H), 7.40 – 7.28 (m, 2H), 6.91 (dd, J = 8.7, 2.6 Hz, 1H), 4.01 (s, 3H), 3.81 (s, 3H); ^{13}C NMR (100 MHz, DMSO-d_6) δ 180.90, 156.10, 144.84, 137.34, 134.92, 134.35, 131.66, 128.31, 127.83, 124.03, 122.68, 121.10, 119.11, 114.65, 113.64, 113.59, 111.75, 109.89, 103.84, 101.87, 55.74, 34.22.

3-(1-ethyl-1H-indol-3-yl)-2-(5-methoxy-1H-indole-3-carbonyl)acrylonitrile (21d):
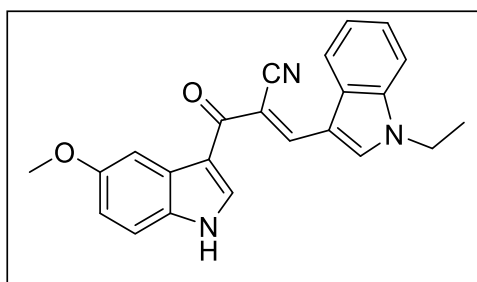
Yellow solid, 91% yield, mp 214−215 °C; ^{1}H NMR (400 MHz, DMSO-d_6) δ 8.63 (d, J = 3.8 Hz, 2H), 8.47 (s, 1H), 7.96 (d, J = 7.7 Hz, 1H), 7.80 (d, J = 2.6 Hz, 1H), 7.67 (d, J = 8.1 Hz, 1H), 7.46 (d, J = 8.8 Hz, 1H), 7.38 – 7.26 (m, 2H), 6.92 (dd, J = 8.7, 2.6 Hz, 1H), 4.42 (q, J = 7.2 Hz, 2H), 3.82 (s, 3H), 1.45 (t, J = 7.2 Hz, 3H); ^{13}C NMR (100 MHz, DMSO-d_6) δ 180.87, 156.10, 144.81, 136.31, 134.43, 133.30, 131.73, 128.52, 127.88, 123.99, 122.62, 121.18, 119.30, 114.69, 113.62, 113.58, 111.73, 110.12, 103.87, 102.04, 55.73, 42.17, 15.57.

2-(6-methoxy-1H-indole-3-carbonyl)-3-(1-methyl-1H-indol-3-yl)acrylonitrile(21e):
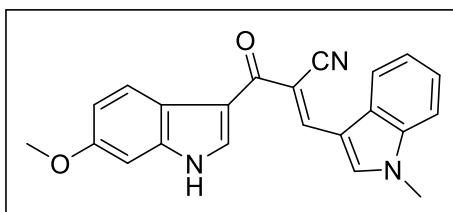
Yellow solid, 95% yield, mp 217−220 °C; ^{1}H NMR (400 MHz, DMSO-d_6) δ 11.92 (s, 1H), 8.59 (d, J = 6.2 Hz, 2H), 8.37 (d, J = 3.1 Hz, 1H), 8.09 (d, J = 8.8 Hz, 1H), 7.96 (d, J = 7.9 Hz, 1H), 7.65 (d, J = 8.1 Hz, 1H), 7.41 – 7.27 (m, 2H), 7.04 (d, J = 2.4 Hz, 1H), 6.89 (dd, J = 8.8, 2.3 Hz, 1H), 4.00 (s, 3H), 3.82 (s, 3H); ^{13}C NMR (100 MHz, DMSO-d_6) δ ^{13}C NMR (101 MHz, DMSO) δ 180.94, 157.16, 144.81, 137.77, 137.34, 134.95, 133.34, 128.29, 124.02, 122.75, 122.67, 121.08, 120.87, 119.13, 114.92, 112.33, 111.74, 109.88, 101.88, 95.81, 55.74, 34.22.

3-(1-ethyl-1H-indol-3-yl)-2-(6-methoxy-1H-indole-3-carbonyl)acrylonitrile (21f):
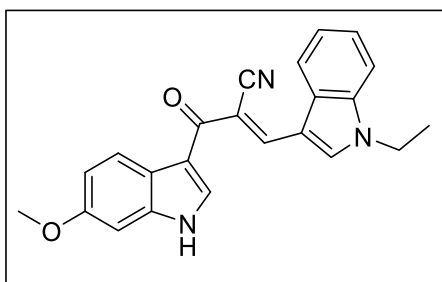
Yellow solid, 94% yield, mp 228−230 °C. ^{1}H NMR (400 MHz, DMSO-d_6) δ 11.93 (s, 1H), 8.62 (d, J = 8.3 Hz, 2H), 8.40 (s, 1H), 8.12 (d, J = 8.7 Hz, 1H), 7.95 (d, J = 7.8 Hz, 1H), 7.67 (d, J = 8.2 Hz, 1H), 7.39 – 7.25 (m, 2H), 7.05 (s, 1H), 6.90 (d, J = 11.1 Hz, 1H), 4.41 (q, J = 7.3 Hz, 2H), 3.82 (s, 3H), 1.45 (t, J = 7.2 Hz, 3H); ^{13}C NMR (100 MHz, DMSO-d_6) δ 180.92, 157.17, 144.79, 137.80, 136.31, 133.34, 128.51, 123.98, 122.78, 122.61, 121.15, 120.91, 119.32, 114.96, 112.31, 111.72, 110.12, 102.05, 95.81, 55.73, 42.16, 15.56.

3-(1-(4-chlorobenzyl)-1*H*-indol-3-yl)-2-(6-methoxy-1*H*-indole-3-carbonyl)acrylonitrile
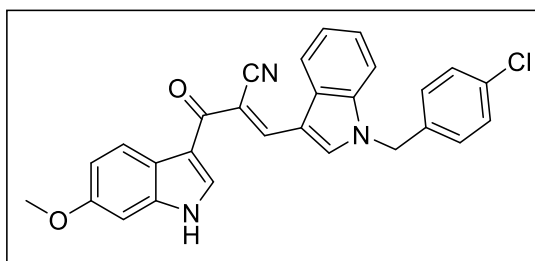
(21g): Yellowish solid, 93% yield, mp 215−217 °C.[33] ^{1}H NMR (400 MHz DMSO-d_6) δ 12.07 (s, 1H), 8.74 (s, 1H), 8.63 (s, 1H), 8.48 (s, 1H), 7.97 (d, J = 7.8 Hz, 1H), 7.80 (s, 1H), 7.61 (d, J = 7.9 Hz, 1H), 7.45 (dd, J = 17.1, 8.4 Hz, 3H), 7.31 (dd, J = 15.3, 7.8 Hz, 4H), 6.93 (d, J = 9.0 Hz, 1H), 5.68 (s, 2H), 3.81 (s, 3H); ^{13}C NMR (100 MHz, DMSO-d_6) δ 180.91, 156.15, 144.65, 136.52, 136.16, 134.61, 133.96, 133.01, 131.72, 129.67, 129.26, 128.56, 127.84, 124.20, 122.74, 120.88, 119.39, 114.64, 113.67, 113.61, 112.06, 110.57, 103.87, 103.01, 55.74, 49.80.

2-(5-ethoxy-1H-indole-3-carbonyl)-3-(1-methyl-1H-indol-3-yl)acrylonitrile (21h):
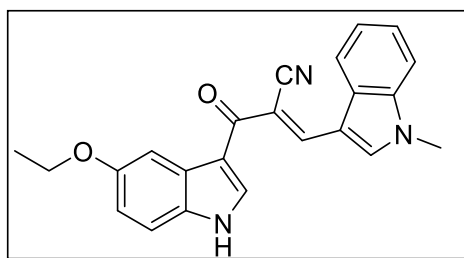
Yellow solid, 93% yield, mp 217−220 °C. ^{1}H NMR (400 MHz, DMSO-d_6) δ 12.02 (s, 1H), 8.61 (s, 1H), 8.57 (s, 1H), 8.45 (s, 1H), 7.94 (d, J = 7.7 Hz, 1H), 7.78 (d, J = 2.6 Hz, 1H), 7.62 (d, J = 8.1 Hz, 1H), 7.45 (d, J = 8.8 Hz, 1H), 7.38 – 7.26 (m, 2H), 6.90 (dd, J = 8.8, 2.6 Hz, 1H), 4.06 (q, J = 7.0 Hz, 2H), 3.99 (s, 3H), 1.37 (t, J = 7.0 Hz, 3H); ^{13}C NMR (100 MHz, DMSO-d_6) δ 180.79, 155.31, 144.76, 137.31, 134.84, 134.32, 131.65, 128.33, 127.89, 123.97, 122.62, 121.16, 119.08, 114.69, 114.05, 113.54, 111.69, 109.92, 104.72, 101.88, 63.75, 34.18, 15.31.

2-(5-ethoxy-1H-indole-3-carbonyl)-3-(1-ethyl-1H-indol-3-yl)acrylonitrile (21i):

Yellow solid, 91% yield, mp 272−273 °C; ^{1}H NMR (400 MHz, DMSO-d_6) δ 12.06 (s, 1H), 8.62 (d, J = 11.4 Hz, 2H), 8.44 (s, 1H), 7.97 (d, J = 7.8 Hz, 1H), 7.76 (d, J = 2.6 Hz, 1H), 7.70 (d, J = 8.1 Hz, 1H), 7.44 (d, J = 8.8 Hz, 1H), 7.39 – 7.27 (m, 2H), 6.90 (dd, J = 8.8, 2.4 Hz, 1H), 4.44 (q, J = 7.2 Hz, 2H), 4.06 (q, J = 7.0 Hz, 2H), 1.46 (t, J = 7.2 Hz, 3H), 1.38 (t, J = 7.0 Hz, 3H); ^{13}C NMR (100 MHz, DMSO-d_6) δ 180.91, 155.29, 144.80, 136.32, 134.46, 133.33, 131.69, 128.50, 127.86, 124.00, 122.62, 121.13, 119.34, 114.63, 114.05, 113.57, 111.77, 110.10, 104.66, 102.10, 63.75, 42.17, 15.61, 15.32.

3-(1-ethyl-1H-indol-3-yl)-2-(5-propoxy-1H-indole-3-carbonyl)acrylonitrile (21j):
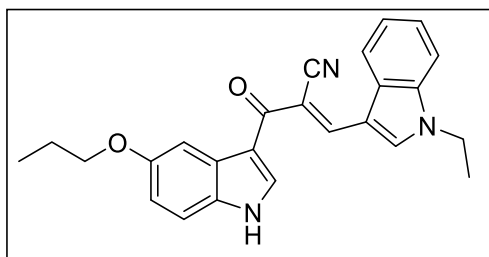
Yellow solid, 93% yield, mp 294-295 °C. ^{1}H NMR (400 MHz, DMSO-d_6) δ 12.02 (s, 1H), 8.63 (s, 1H), 8.62 (s, 1H), 8.45 (s, 1H), 7.96 (d, J = 7.7 Hz, 1H), 7.78 (d, J = 2.4 Hz, 1H), 7.69 (d, J = 9.2 Hz, 1H), 7.45 (d, J = 8.8 Hz, 1H), 7.38 – 7.27 (m, 2H), 6.91 (dd, J = 8.8, 2.4 Hz, 1H), 4.43 (q, J = 7.2 Hz, 2H), 3.96 (t, J = 6.6 Hz, 2H), 1.77 (h, J = 7.4 Hz, 2H), 1.45 (t, J = 7.2 Hz, 3H), 1.01 (t, J = 7.4 Hz, 3H); ^{13}C NMR (100 MHz, DMSO-d_6) δ 180.90, 155.47, 144.80, 136.31, 134.38, 133.31, 131.65, 128.52, 127.86, 123.99, 122.62, 121.15, 119.30, 114.66, 114.09, 113.53, 111.75, 110.11, 104.77, 102.06, 69.83, 42.17, 22.67, 15.58, 10.94.

3-(1-methyl-1H-indol-3-yl)-2-(5-propoxy-1H-indole-3-carbonyl)acrylonitrile (21k):
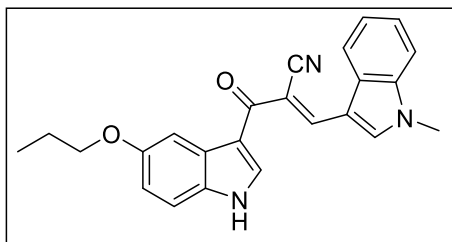
Yellow solid, 95% yield, mp 224−225 °C. ^{1}H NMR (400 MHz, DMSO-d_6) δ 8.56 (s, 1H), 8.50 (s, 1H), 8.39 (s, 1H), 7.88 (d, J = 7.7 Hz, 1H), 7.72 (d, J = 2.6 Hz, 1H), 7.59 (d, J = 8.1 Hz, 1H), 7.43 (d, J = 8.8 Hz, 1H), 7.38 – 7.26 (m, 2H), 6.89 (dd, J = 8.8, 2.6 Hz, 1H), 3.93 (s, 3H), 3.74 (s, 3H), 1.73 (h, J = 7.2 Hz, 2H), 0.97 (t, J = 7.4 Hz, 3H); ^{13}C NMR (100 MHz, DMSO-d_6) δ 181.11, 155.47, 145.00, 137.33, 135.06, 134.19, 131.45, 128.20, 127.69, 124.17, 122.82, 121.12, 119.02, 114.57, 113.59, 111.74, 109.85, 104.80, 101.63, 69.94, 34.20, 22.57, 10.88.

3-(1-ethyl-1H-indol-3-yl)-2-(5-isopropoxy-1H-indole-3-carbonyl)acrylonitrile (21l):
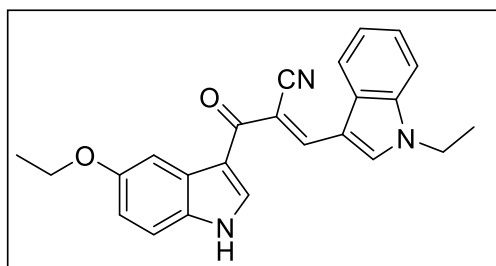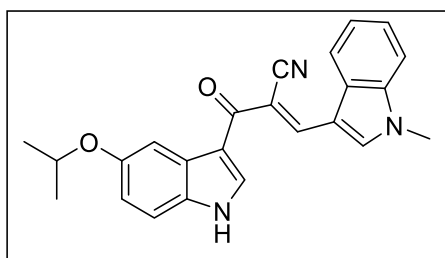
Yellow solid, 91% yield, mp 196−197 °C. ^{1}H NMR (400 MHz, DMSO-d_6) δ 12.01 (s, 1H), 8.64 (s, 1H), 8.61 (s, 1H), 8.45 (s, 1H), 7.97 (d, J = 7.7 Hz, 1H), 7.78 (d, J = 2.6 Hz, 1H), 7.69 (d, J = 8.1 Hz, 1H), 7.44 (d, J = 8.8 Hz, 1H), 7.39 – 7.27 (m, 2H), 6.89 (dd, J = 8.8, 2.4 Hz, 1H), 4.57 (hept, J = 6.0 Hz, 1H), 4.43 (q, J = 7.2 Hz, 2H), 1.45 (t, J = 7.2 Hz, 3H), 1.31 (s, 3H), 1.30 (s, 3H); ^{13}C NMR (100 MHz, DMSO-d_6) δ 180.92, 154.07, 144.83, 136.32, 134.49, 133.32, 131.77, 127.90, 123.99, 122.62, 121.15, 119.34, 115.32, 114.60, 113.56, 111.75, 110.12, 106.97, 102.08, 70.46, 42.17, 22.44, 15.59.

2-(5-isopropoxy-1H-indole-3-carbonyl)-3-(1-methyl-1H-indol-3-yl)acrylonitrile (21m):
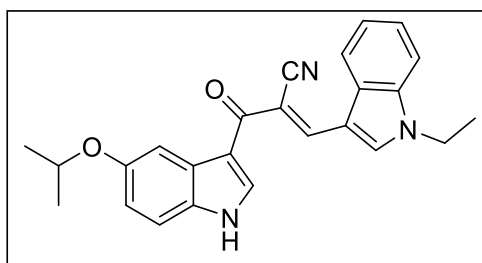
Yellow solid, 94% yield, mp 220−221 °C. ^{1}H NMR (400 MHz, DMSO-d_6) δ 8.60 (d, J = 11.1 Hz, 2H), 8.44 (s, 1H), 7.96 (d, J = 7.8 Hz, 1H), 7.78 (d, J = 2.6 Hz, 1H), 7.64 (d, J = 8.2 Hz, 1H), 7.44 (d, J = 8.7 Hz, 1H), 7.39 – 7.27 (m, 2H), 6.89 (dd, J = 8.7, 2.5 Hz, 1H), 4.57 (p, J = 6.1 Hz, 1H), 4.00 (s, 3H), 1.31 (d, J = 6.1 Hz, 6H). ^{13}C NMR (100 MHz, DMSO-d_6) ^{13}C NMR (101 MHz, DMSO) δ 184.84, 180.89, 154.06, 144.82, 137.34, 134.88, 134.45, 131.75, 128.32, 127.89, 124.00, 122.65, 121.11, 119.14, 115.32, 114.58, 113.57, 111.74, 109.91, 106.95, 101.91, 70.46, 34.22, 22.44, 22.40.

2-(5,6-dimethoxy-1H-indole-3-carbonyl)-3-(1-methyl-1H-indol-3-yl)acrylonitrile (21n)

Yellow solid, 95% yield, mp 286−289 °C. ^{1}H NMR (400 MHz, DMSO-d_6) δ 8.60 (s, 1H), 8.56 (s, 1H), 8.33 (s, 1H), 7.93 (d, J = 7.6 Hz, 1H), 7.76 (s, 1H), 7.63 (d, J = 8.1 Hz, 1H), 7.40 – 7.26 (m, 2H), 7.08 (s, 1H), 3.98 (s, 3H), 3.82 (s, 3H), 3.81 (s, 3H); ^{13}C NMR (100 MHz, DMSO-d_6) δ 180.75, 147.94, 146.94, 144.73, 137.32, 134.87, 132.28, 131.06, 128.29, 124.03, 122.69, 121.18, 119.86, 119.01, 114.96, 111.71, 109.88, 103.95, 101.75, 96.05, 6.15, 34.19. HRMS (ESI) m/z calcd for $C_{23}H_{19}N_3O_3$: 386.1460 (M+H)$^+$, found: 386.1480.

2-(5,6-dimethoxy-1H-indole-3-carbonyl)-3-(1-ethyl-1H-indol-3-yl)acrylonitrile (21o)
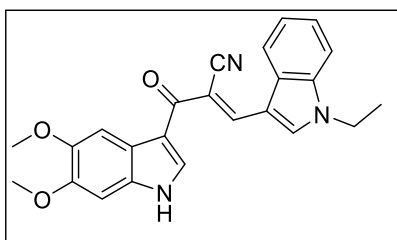
Yellow solid, 94% yield, mp 250−251 °C. ^{1}H NMR (400 MHz, DMSO) δ 8.54 (d, J = 7.0 Hz, 2H), 8.30 (s, 1H), 7.87 (d, J = 7.7 Hz, 1H), 7.72 (s, 1H), 7.60 (d, J = 8.1 Hz, 1H), 7.35 – 7.24 (m, 2H), 7.07 (s, 1H), 4.33 (q, J = 7.2 Hz, 2H), 3.79 (s, 9H), 1.41 (t, J = 7.3 Hz, 3H).^{13}C NMR (100 MHz,

DMSO-*d₆*) δ 180.84, 147.86, 146.86, 144.84, 136.24, 133.27, 132.10, 130.84, 128.40, 122.73, 121.27, 119.71, 119.09, 114.90, 111.66, 110.03, 103.78, 101.56, 95.88, 56.04, 42.18, 15.38. HRMS (ESI) *m/z* calcd for $C_{24}H_{21}N_3O_3$: 400.1616 (M+H)⁺, found: 400.1651.

3-(1-(4-chlorobenzyl)-1H-indol-3-yl)-2-(5,6-dimethoxy-1H-indole-3-carbonyl)-acrylonitrile (21p):
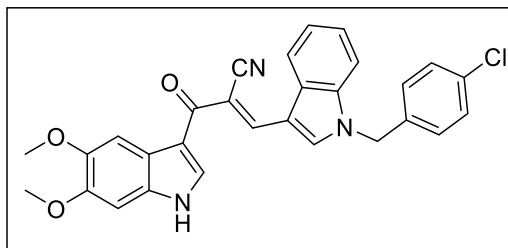
Yellow solid, 95% yield, mp 294-295 °C. ¹H NMR (400 MHz, DMSO-*d₆*) δ 11.90 (s, 1H), 8.74 (s, 1H), 8.62 (s, 1H), 8.36 (s, 1H), 7.97 (d, *J* = 7.2 Hz, 1H), 7.77 (s, 1H), 7.63 (d, *J* = 7.7 Hz, 1H), 7.44 (d, *J* = 8.4 Hz, 3H), 7.32 (dd, *J* = 15.9, 8.3 Hz, 5H), 7.08 (s, 1H), 5.69 (s, 2H), 3.83 (s, 3H), 3.82 (s, 3H); ¹³C NMR (100 MHz, DMSO-*d₆*) δ 180.73, 147.95, 146.97, 144.51, 136.51, 136.23, 133.90, 132.98, 132.58, 131.11, 129.68, 129.26, 128.57, 124.18, 122.72, 120.91, 114.90, 112.08, 110.55, 103.93, 102.96, 96.05, 56.13, 49.77.

3-(3,4-dimethoxyphenyl)-2-(1H-indole-3-carbonyl)acrylonitrile (21q):

Yellow solid, 94% yield, mp 287−288 °C. ¹H NMR (400 MHz, DMSO-*d₆*) δ 12.27 (s, 1H), 8.47 (s, 1H), 8.22 (d, *J* = 9.5 Hz, 2H), 7.80 (s, 1H), 7.57 (d, *J* = 6.8 Hz, 1H), 7.32 – 7.24 (m, 2H), 7.15 (d, *J* = 8.6 Hz, 1H), 3.87 (s, 3H), 3.84 (s, 3H); ¹³C NMR (100 MHz, DMSO-*d₆*) δ 181.87, 153.14, 152.88, 149.12, 137.08, 135.74, 126.74, 126.38, 125.45, 123.94, 122.76, 121.93, 119.14, 114.24, 113.20, 112.91, 112.22, 108.33, 56.26, 55.96.

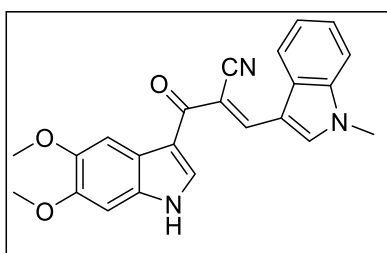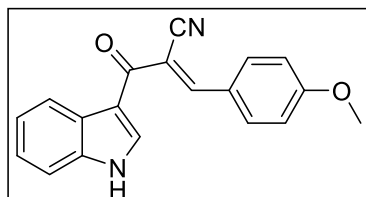### 2-(5,6-dimethoxy-1*H*-indole-3-carbonyl)-3-(1-methyl-1*H*-indol-3-yl)acrylonitrile (21r)
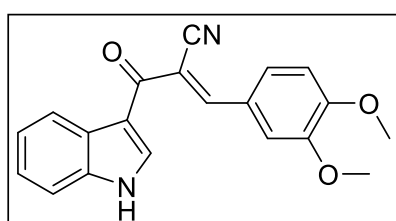
Yellow solid, 95% yield, mp 286−289 °C. ¹H NMR (400 MHz, DMSO-*d₆*) δ 8.60 (s, 1H), 8.56 (s, 1H), 8.33 (s, 1H), 7.93 (d, *J* = 7.6 Hz, 1H), 7.76 (s, 1H), 7.63 (d, *J* = 8.1 Hz, 1H), 7.40 – 7.26 (m, 2H), 7.08 (s, 1H), 3.98 (s, 3H), 3.82 (s, 3H), 3.81 (s, 3H); ¹³C NMR (100 MHz, DMSO-*d₆*) δ 180.75, 147.94, 146.94, 144.73, 137.32, 134.87, 132.28, 131.06, 128.29, 124.03, 122.69, 121.18, 119.86, 119.01, 114.96, 111.71, 109.88, 103.95, 101.75, 96.05, 56.15, 34.19.

5.1.6 References

1. Wan, Y.; Li, Y.; Yan, C.; Yan, M.; Tang, Z., Indole: A privileged scaffold for the design of anti-cancer agents. *European Journal of Medicinal Chemistry* **2019,** *183*, 111691.

2. Mehra, A.; Sharma, V.; Verma, A.; Venugopal, S.; Mittal, A.; Singh, G.; Kaur, B., Indole derived anticancer agents. *ChemistrySelect* **2022,** *7* (34), e202202361.

3. Carbone, A.; Pennati, M.; Parrino, B.; Lopergolo, A.; Barraja, P.; Montalbano, A.; Spanò, V.; Sbarra, S.; Doldi, V.; De Cesare, M., Novel 1 H-pyrrolo [2, 3-b] pyridine

derivative nortopsentin analogues: Synthesis and antitumor activity in peritoneal mesothelioma experimental models. *Journal of Medicinal Chemistry* **2013,** *56* (17), 7060-7072.

4. Miyake, F. Y.; Yakushijin, K.; Horne, D. A., A Facile Synthesis of Dragmacidin B and 2, 5-Bis (6 '-bromo-3 '-indolyl) piperazine. *Organic Letters* **2000,** *2* (20), 3185-3187.

5. Al-Karmalawy, A. A.; Rashed, M.; Sharaky, M.; Abulkhair, H. S.; Hammouda, M. M.; Tawfik, H. O.; Shaldam, M. A., Novel fused imidazotriazines acting as promising top. II inhibitors and apoptotic inducers with greater selectivity against head and neck tumors: Design, synthesis, and biological assessments. *European Journal of Medicinal Chemistry* **2023,** *259*, 115661.

6. Budovska, M.; Michalkova, R.; Kello, M.; Vaskova, J.; Mojzis, J., Design, Synthesis and Antiproliferative Evaluation of Bis-Indole Derivatives with a Phenyl Linker: Focus on Autophagy. *Molecules* **2022,** *28* (1), 251.

7. Ma, Y.; Yakushijin, K.; Miyake, F.; Horne, D., A concise synthesis of indolic enamides: Coscinamide A, coscinamide B, and igzamide. *Tetrahedron Letters* **2009,** *50* (30), 4343-4345.

8. Kumar, D.; Arun, V.; Maruthi Kumar, N.; Acosta, G.; Noel, B.; Shah, K., A Facile Synthesis of Novel Bis‐(indolyl)‐1, 3, 4‐oxadiazoles as Potent Cytotoxic Agents. *ChemMedChem* **2012,** *7* (11), 1915-1920.

9. Gupta, L.; Talwar, A.; Chauhan, P. M., Bis and tris indole alkaloids from marine organisms: new leads for drug discovery. *Current Medicinal Chemistry* **2007,** *14* (16), 1789-1803.

10. Kumar, D.; Kumar, N. M.; Ghosh, S.; Shah, K., Novel bis (indolyl) hydrazide–hydrazones as potent cytotoxic agents. *Bioorganic & Medicinal Chemistry Letters* **2012,** *22* (1), 212-215.

11. Boumendjel, A.; Ronot, X.; Boutonnat, J., Chalcones derivatives acting as cell cycle blockers: potential anti cancer drugs? *Current Drug Targets* **2009,** *10* (4), 363-371.

12. Kontogiorgis, C.; Mantzanidou, M.; Hadjipavlou-Litina, D., Chalcones and their potential role in inflammation. *Mini Reviews in Medicinal Chemistry* **2008,** *8* (12), 1224-1242.

13. Agarwal, A.; Srivastava, K.; Puri, S.; Chauhan, P. M., Synthesis of substituted indole derivatives as a new class of antimalarial agents. *Bioorganic & Medicinal Chemistry Letters* **2005,** *15* (12), 3133-3136.

14. Liu, X.-F.; Zheng, C.-J.; Sun, L.-P.; Liu, X.-K.; Piao, H.-R., Synthesis of new chalcone derivatives bearing 2, 4-thiazolidinedione and benzoic acid moieties as potential anti-bacterial agents. *European Jurnal of Medicinal Chemistry* **2011,** *46* (8), 3469-3473.

15. Perin, N.; Hok, L.; Bec̆, A.; Persoons, L.; Vanstreels, E.; Daelemans, D.; Vianello, R.; Hranjec, M., N-substituted benzimidazole acrylonitriles as in vitro tubulin polymerization inhibitors: Synthesis, biological activity and computational analysis. *European Journal of Medicinal Chemistry* **2021,** *211*, 113003.

16. Ullah, H.; Khan, N. N.; Ullah, S.; Rahim, F.; Hussain, A., Synthesis, molecular docking, and bioactivity study of bis-indole-sulfonamide analogues as acetylcholinesterase and butyrylcholinesterase inhibitors. *Chemical Data Collections* **2023,** *47*, 101063.

17. Kamal, A.; Reddy, J. S.; Ramaiah, M. J.; Dastagiri, D.; Bharathi, E. V.; Sagar, M. V. P.; Pushpavalli, S.; Ray, P.; Pal-Bhadra, M., Design, synthesis and biological evaluation of imidazopyridine/pyrimidine-chalcone derivatives as potential anticancer agents. *MedChemComm* **2010,** *1* (5), 355-360.

18. Kamal, A.; Srinivasulu, V.; Nayak, V. L.; Sathish, M.; Shankaraiah, N.; Bagul, C.; Reddy, N. S.; Rangaraj, N.; Nagesh, N., Design and synthesis of C3‐pyrazole/chalcone‐linked beta‐carboline hybrids: antitopoisomerase I, DNA‐interactive, and apoptosis‐inducing anticancer agents. *ChemMedChem* **2014,** *9* (9), 2084-2098.

19. Kumar, D.; Kumar, N. M.; Akamatsu, K.; Kusaka, E.; Harada, H.; Ito, T., Synthesis and biological evaluation of indolyl chalcones as antitumor agents. *Bioorganic & Medicinal Chemistry Letters* **2010,** *20* (13), 3916-3919.

20. Robichaud, B. A.; Liu, K. G., Titanium isopropoxide/pyridine mediated Knoevenagel reactions. *Tetrahedron Letters* **2011,** *52* (51), 6935-6938.

21. Jiang, B.; Gu, X.-H., Syntheses and cytotoxicity evaluation of bis (indolyl) thiazole, bis (indolyl) pyrazinone and bis (indolyl) pyrazine: Analogues of cytotoxic marine bis (indole) alkaloid. *Bioorganic & Medicinal Chemistry* **2000,** *8* (2), 363-371.

22. Kumar, D.; Kumar, N. M.; Chang, K.-H.; Gupta, R.; Shah, K., Synthesis and in-vitro anticancer activity of 3, 5-bis (indolyl)-1, 2, 4-thiadiazoles. *Bioorganic & Medicinal Chemistry Letters* **2011,** *21* (19), 5897-5900.

23. Kemnitzer, W.; Kuemmerle, J.; Jiang, S.; Zhang, H.-Z.; Sirisoma, N.; Kasibhatla, S.; Crogan-Grundy, C.; Tseng, B.; Drewe, J.; Cai, S. X., Discovery of 1-benzoyl-3-cyanopyrrolo [1, 2-a] quinolines as a new series of apoptosis inducers using a cell-and

caspase-based high-throughput screening assay. Part 1: Structure–activity relationships of the 1-and 3-positions. *Bioorganic &Medicinal Chemistry Letters* **2008,** *18* (23), 6259-6264.

24. Bartoli, G.; Beleggia, R.; Giuli, S.; Giuliani, A.; Marcantoni, E.; Massaccesi, M.; Paoletti, M., The CeCl3· 7H2O–NaI system as promoter in the synthesis of functionalized trisubstituted alkenes via Knoevenagel condensation. *Tetrahedron Letters* **2006,** *47* (37), 6501-6504.

25. Coelho, A.; El-Maatougui, A.; Ravina, E.; Cavaleiro, J. A.; Silva, A. M., Efficient consecutive alkylation-Knoevenagel functionalisations in formyl aza-heterocycles using supported organic bases. *Synlett* **2006,** *2006* (19), 3324-3328.

26. Kumar, D.; Kumar, N. M.; Tantak, M. P.; Ogura, M.; Kusaka, E.; Ito, T., Synthesis and identification of α -cyano bis (indolyl) chalcones as novel anticancer agents. *Bioorganic & Medicinal Chemistry Letters* **2014,** *24* (22), 5170-5174.

27. Slaett, J.; Romero, I.; Bergman, J., Cyanoacetylation of indoles, pyrroles and aromatic amines with the combination cyanoacetic acid and acetic anhydride. *Synthesis* **2004,** *2004* (16), 2760-2765.

28. Guan, L.; Yang, H.; Cai, Y.; Sun, L.; Di, P.; Li, W.; Liu, G.; Tang, Y., ADMET-score– a comprehensive scoring function for evaluation of chemical drug-likeness. *MedChemComm* **2019,** *10* (1), 148-157.

29. Ursu, O.; Rayan, A.; Goldblum, A.; Oprea, T. I., Understanding drug‐likeness. *Wiley Interdisciplinary Reviews: Computational Molecular Science* **2011,** *1* (5), 760-781.

30. Lipinski, C. A.; Lombardo, F.; Dominy, B. W.; Feeney, P. J., Experimental and computational approaches to estimate solubility and permeability in drug discovery and development settings. *Advanced Drug Delivery Reviews* **1997,** *23* (1-3), 3-25.

31. Huang, S. M.; Strong, J. M.; Zhang, L.; Reynolds, K. S.; Nallani, S.; Temple, R.; Abraham, S.; Habet, S. A.; Baweja, R. K.; Burckart, G. J., New era in drug interaction evaluation: US Food and Drug Administration update on CYP enzymes, transporters, and the guidance process. *The Journal of Clinical Pharmacology* **2008,** *48* (6), 662-670.

32. Wu, Q.; Luo, Y.; Lei, A.; You, J., Aerobic copper-promoted radical-type cleavage of coordinated cyanide anion: nitrogen transfer to aldehydes to form nitriles. *Journal of American Chemical Society* **2016,** *138* (9), 2885-2888.

Chapter 5

Design, Synthesis and Anti-cancer Activity of Novel α-cyano bis(indolyl) chalcones

Part 5B: Design and Synthesis of FICD Inhibitors
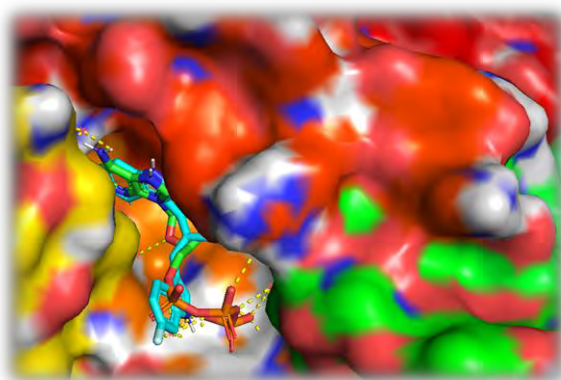
5.2 Introduction

FICD (Filamentation induced by cAMP domain) is a conserved protein found in many eukaryotes, including humans, and plays a crucial role in regulating the activity of several key proteins involved in various cellular processes.[1] FICD-mediated ampylation of proteins, which involves the transfer of AMP from ATP to specific amino acid residues, is essential for the proper functioning of several pathways, including ion channel activity, endocytosis, and cell signaling.[2] Dysregulation of FICD-mediated AMPylation has been linked to various human diseases, including cancer and neurodegenerative disorders. In recent years, the discovery of FICD inhibitors has gained significant attention as a potential therapeutic strategy for the treatment of these diseases. Post-translational modifications (PTMs) play critical roles in regulating protein function and cellular processes. Among the PTMs, AMPylation, the transfer of adenosine monophosphate (AMP) from ATP to target proteins, is a relatively newly discovered modification that has been found to regulate a diverse range of cellular processes, including cell growth, proliferation, and metabolism. FICD, a conserved protein that inhibits the hypoxia-inducible factor (HIF)-1α, has been identified as a key regulator of AMPylation.[3] Inhibiting FICD has potential implications, as it can lead to the dysregulation of AMPylation and therefore impact multiple cellular processes. The current understanding of FICD-mediated AMPylation and the potential therapeutic benefits of targeting FICD as a novel approach for drug development. FICD inhibitors are small molecules that block the enzymatic activity of FICD, thus preventing it from modifying its substrate BiP. FICD inhibitors bind to the active site of FICD and prevent it from carrying out its catalytic function, which is to add an AMP molecule to a conserved histidine residue in the substrate BiP.[3]

5.2.1 Rational Design

FICD aka HYPE, a newly identified bifunctional enzyme, which is capable of both AMPylation and DeAMPylation.[4] While several prokaryotic AMPylators are known, FICD and SELO are the only known AMPylators in metazoans. AMPylation is an emerging post-translational modification, which is predominantly linked to endoplasmic reticulum stress.[5, 6] A role of FICD or AMPylation and DeAMPylation is largely unknown in human health and disease.[3] Recently uncovered that FICD AMPylase activity is deregulated in highly aggressive castration-resistant prostate cancer (CRPC). Deregulation of the AMPylase activity of FICD in turn promotes highly oncogenic phenotypes in CRPC, highlighting it as a potential target for CRPC. In contrast, FICD's DeAMPylase activity does not contribute to oncogenesis. Instead, it is

required for normal physiological functions of the cells. In agreement with these findings, knockdown of FICD is highly toxic for both normal and cancer cells, as it eliminates both its AMPylase and DeAMPylase functions. These findings therefore suggest that inhibitors of FICD AMPylase activity should be highly effective in reversing oncogenic phenotypes in cells and *in vivo*. There is the only report that identified FICD inhibitors, (Figure 5.2.1) but their specificity was not rigorously tested.[7]
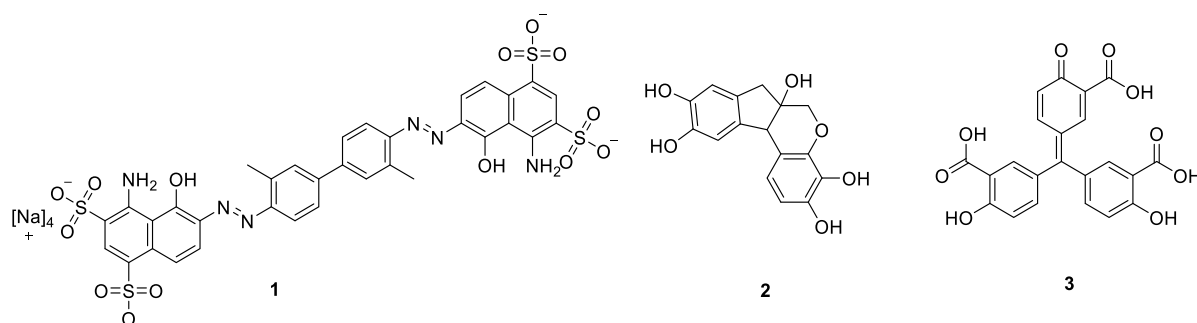
Figure 5.2.1 Chemical structures of selected E234G FICD inhibitors

5.2.2 Results and Discussion

Initially we screened a focused library of 20 cyanobis(indoyl)chalcones (MM-series), which revealed a potent inhibitor **MM-2** with AMPylase inhibition activity (IC_{50} = 10 μM). (Figure 5.2.2). Based on the structure activity relationship (SAR) obtained from these 20 compounds, as well as docking of the hit compound **MM-2** into FICD crystal structure, we identified a hydrophobic tunnel unique to FICD that could be potentially exploited to generate second generation FICD inhibitors (Figure 5.2.2).
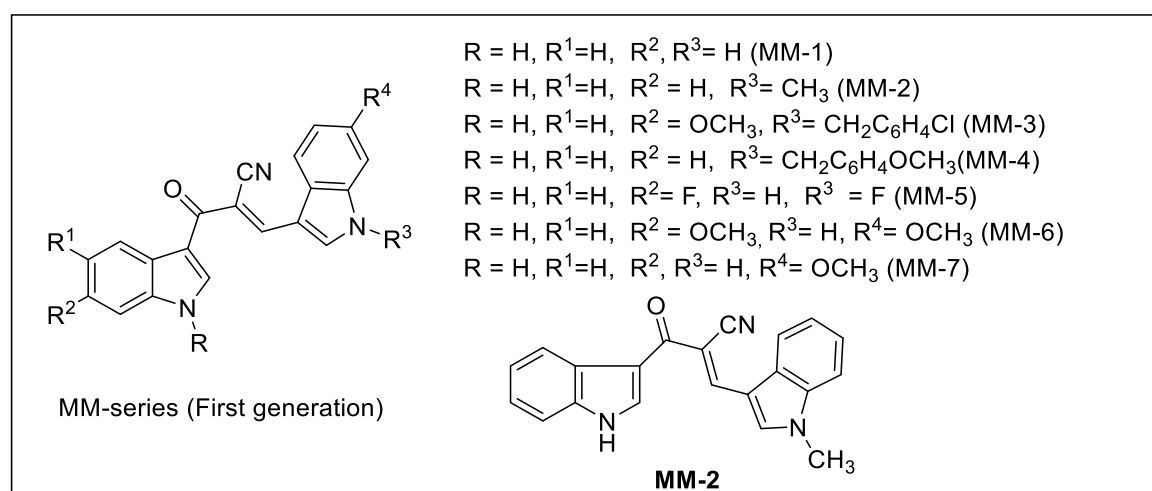
Figure 5.2.2 FICD inhibitor, **MM-2** (IC_{50} = 10 μM)
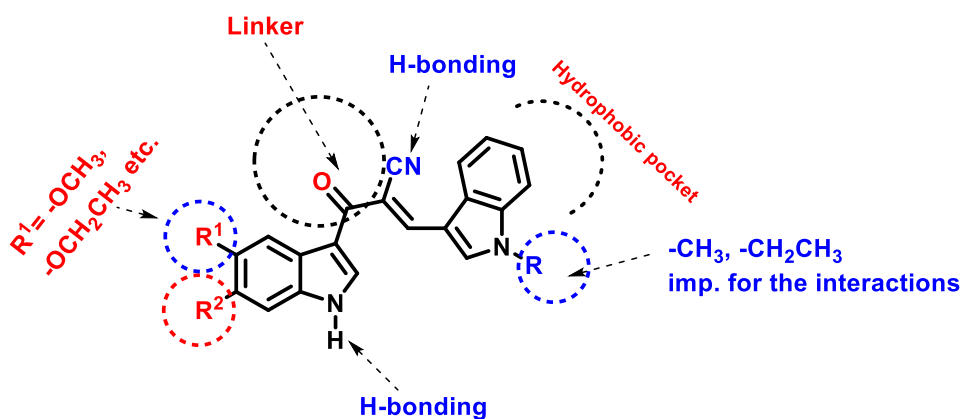
Figure 5.2.3 SAR of a-cyano bis(indolyl)chalcones
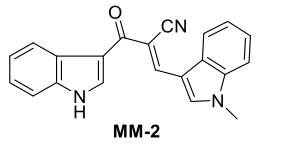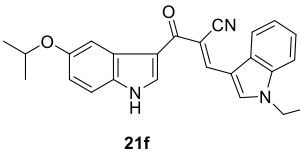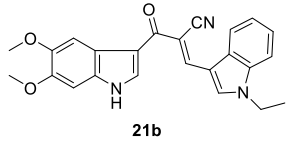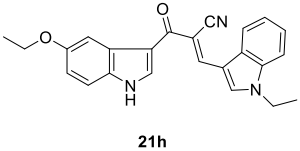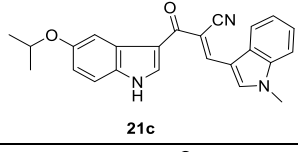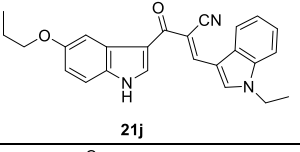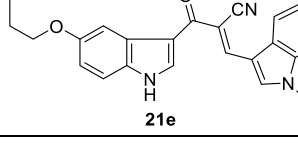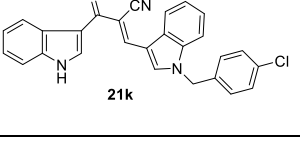
The docking studies further revealed that substituents R^1 and R^2 are most likely to be highly effective in accessing this hole. Based on these criteria, we designed a virtual library of 50 compounds varying at R^1 and R^2. These compounds were virtually screened using FICD crystal structure with AutoDock Vina program. These studies have led to the identification of **21a-r** compounds that show potentially very high binding with FICD. A few of these structures modified at R^1 position with their AutoDock Vina scores are listed in figure 5.2.3.

5.2.2.1 Biological Evaluation

5.2.2.1.1 FICD AMPylation inhibition activity (µM) of potent compounds

The synthesized α-cyano bis(indolyl)chalcones **21a-r** were subjected to evaluation for their cytotoxicity against five human cancer cell lines: prostate (C4-2, PC3, and 22Rv1), breast (MCF7), epithelial cancer (MIAPACA), and normal human kidney (HEK293) cell lines, using the MTT assay. As outlined in our previous discussion in Chapter 5a, compound **21c** exhibited anticancer activity with an IC$_{50}$ value of 1.23 µM against 22Rv1 (prostate cancer cell line). Interestingly, compound **21e** demonstrated potent anticancer activity with IC$_{50}$ values of 1.28 µM and 2.3 µM against 22RV1 and C4-2 (prostate cancer cell lines), respectively. Among the **21a-r** compounds evaluated, three demonstrated notable potency in inhibiting FICD activity. Specifically, compounds **MM-2**, **21b**, **21c**, and **21e** exhibited significant inhibitory activity against FICD, with IC$_{50}$ values of 10.1 µM, 12.9 µM, 7.9 µM and 11.9 µM, respectively, as depicted in Table 5.2.1 and figure 5.2.4. Their potency highlights their potential as promising candidates for further investigation and development as anticancer agents.

Table 5.2.1 Potent α-cyano bis(indolyl)chalcones (**21a-r**) FICD inhibitors (μM)

Comp.	FICD-WT inhibitors (IC$_{50}$, μM)	Comp.	FICD-WT inhibitors (IC$_{50}$, μM)
MM-2	10.1	**21f**	35.8
21b	12.9	**21h**	12.84
21c	7.9	**21j**	20.2
21e	11.9	**21k**	39.2
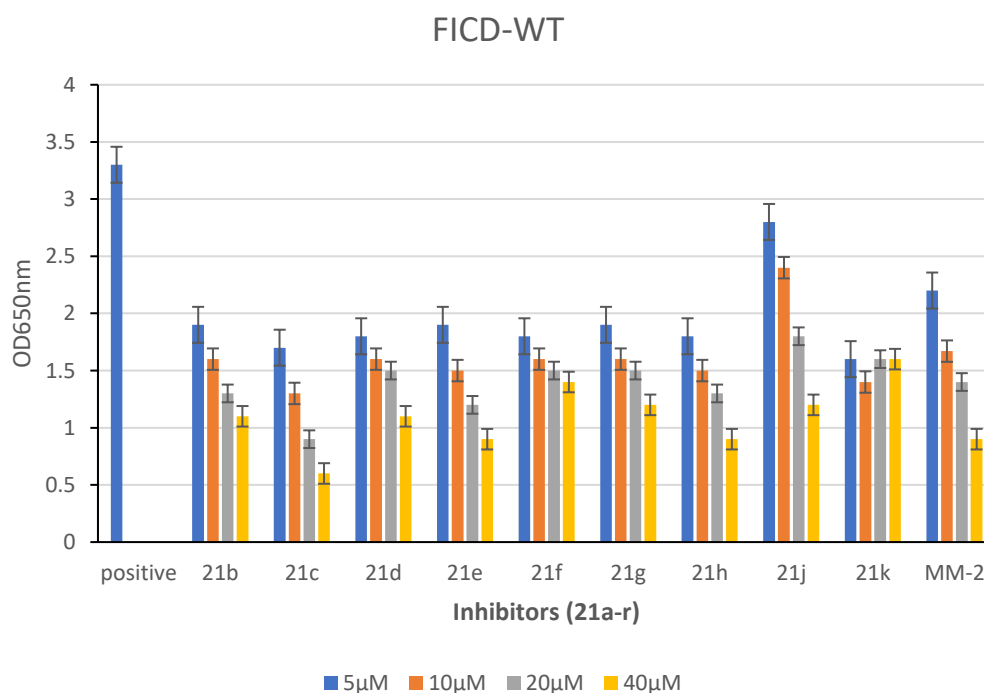
Figure 5.2.4 Potent (**21a-r**) FICD AMPylation inhibitors

5.2.3 Molecular Docking

Molecular docking simulation is one of the most frequently used methods to aid in modern drug designing. The prediction power of docking programs helps to find out suitable conformation of ligands within the binding site. In the present study, to predict the inhibitory mechanism, we employed molecular docking analysis on the newly synthesized indole acrylonitriles that displayed significant inhibitory effect for *in vitro* assay on FICD inhibitor.

The structure of FICD is composed of an N-terminal domain, a central domain, and a C-terminal domain. The central domain of FICD contains the conserved FIC domain, which is responsible for catalyzing the AMPylation process. The N-terminal domain of FICD is responsible for substrate recognition, while the C-terminal domain is involved in FICD dimerization.
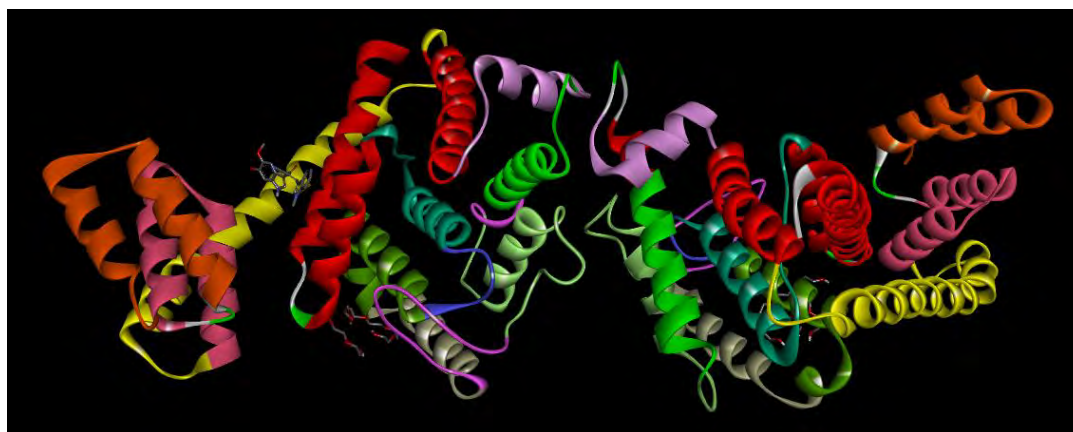
Figure 5.2.5 Crystal structure of FICD protein. (a) 3D Representation of FICD (b) domain of FICD protein

FICD recognizes its substrate proteins through a specific consensus sequence, which consists of a hydrophobic residue followed by a negatively charged residue. Once FICD binds to its substrate, it catalyzes the transfer of AMP from ATP to a conserved histidine residue on the substrate protein, resulting in AMPylation.[1]

Compounds **MM-2, 21c** and **21j** are FICD AMPylation inhibitors that has been shown to bind to the ATP binding site of FICD and block its enzymatic activity. This leads to the accumulation of misfolded proteins in the ER and the activation of the UPR.
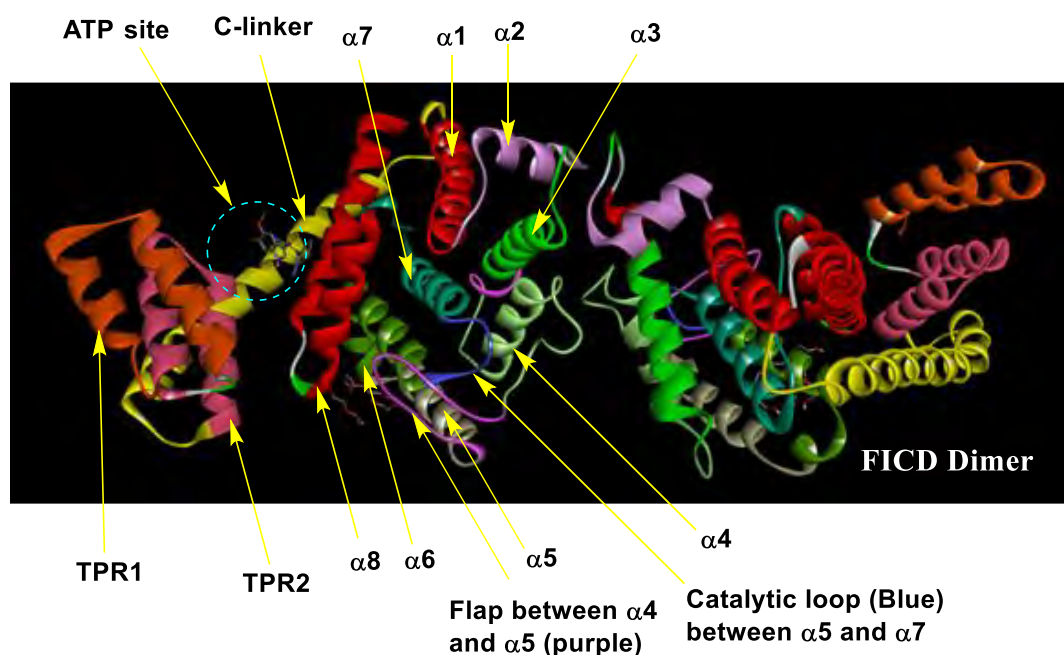
Figure 5.2.6 3D representation of FICD dimer

The ATP binding site in FICD is crucial for its enzymatic activity, facilitating essential interactions necessary for this process. Within this binding site, specific amino acid residues play pivotal roles in forming hydrogen bonds with ATP molecules, as highlighted in figure 5.2.7. Notably, residues GLY368, HIS363, ILE366, ARG371, TYR399, and ASN407 are actively involved in establishing these critical hydrogen bonding interactions.

Compound **21c** exhibits significant interactions within the ATP binding site. It forms hydrogen bonds with amino acid residues GLY368, ARG371, and ASN369, indicating a strong affinity for these regions. Additionally, hydrophobic interactions are observed with residues LEU403, HIS319, TYR400, and VAL360, further enhancing the binding affinity of the compound at the ATP binding site. Interestingly, the potent compound (**21c**) perfectly overlays with the ATP molecule, suggesting a close structural resemblance and optimal binding geometry (Figure 5.2.8). These interactions between the potent compound and the ATP binding site are crucial for its inhibitory activity against FICD. By precisely targeting key residues and mimicking the binding mode of ATP, the compound effectively disrupts the enzymatic function of FICD, ultimately inhibiting the AMPylation process.
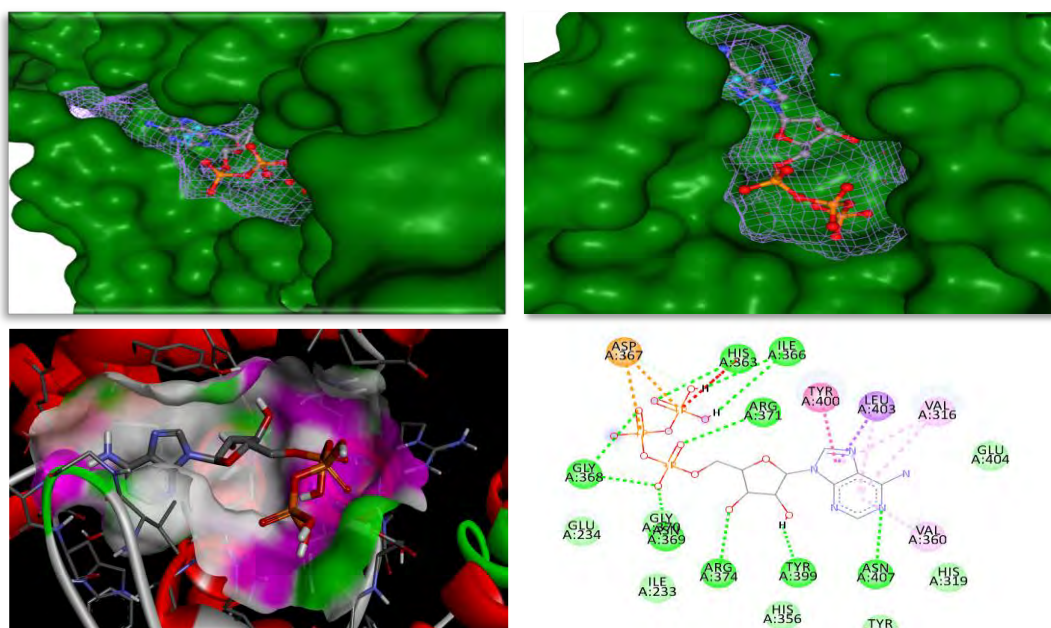
Figure 5.2.7 (a) ATP binding active site in FICD (b) 2D interaction of ATP with different amino acids.
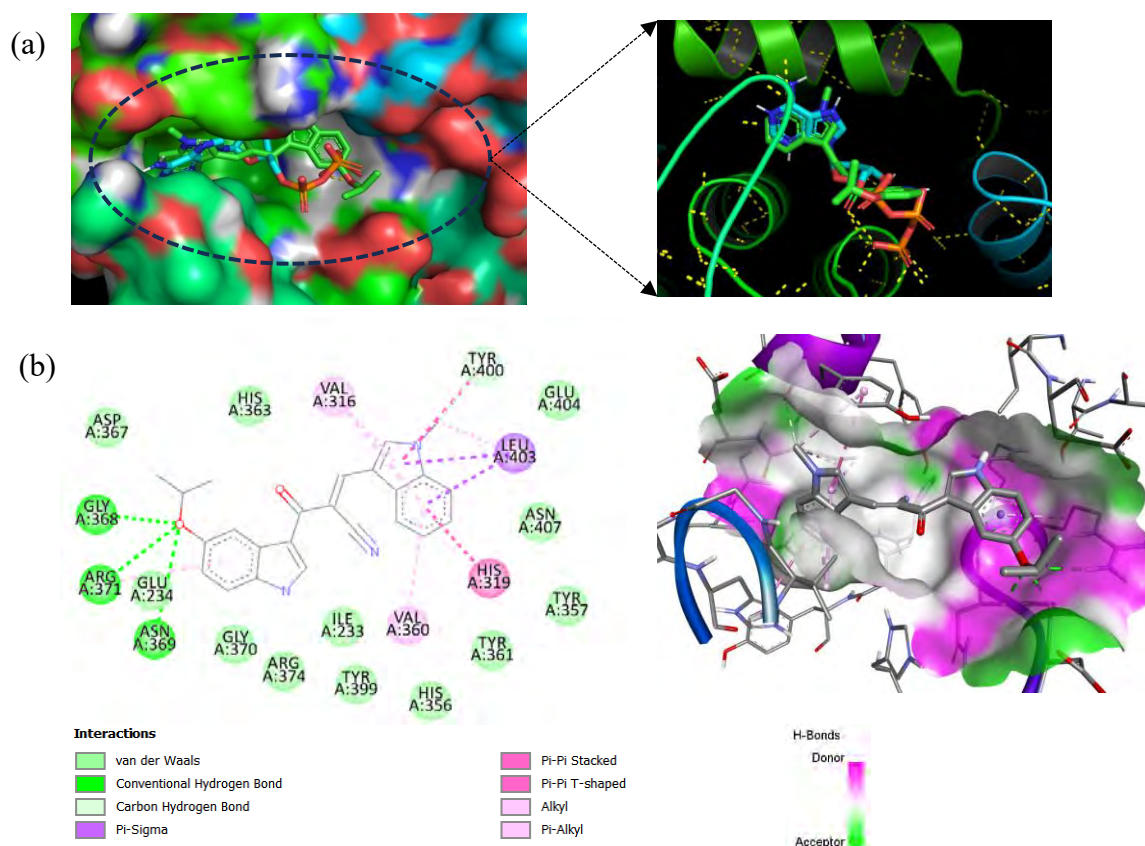
Figure 5.2.8 Binding affinity of potent compound **21c** = -9.3 Kcal/mol. **21c** bind at ATP binding site and exactly overlay on ATP. (b) 2D interactions with H-bonding (green dotted line)
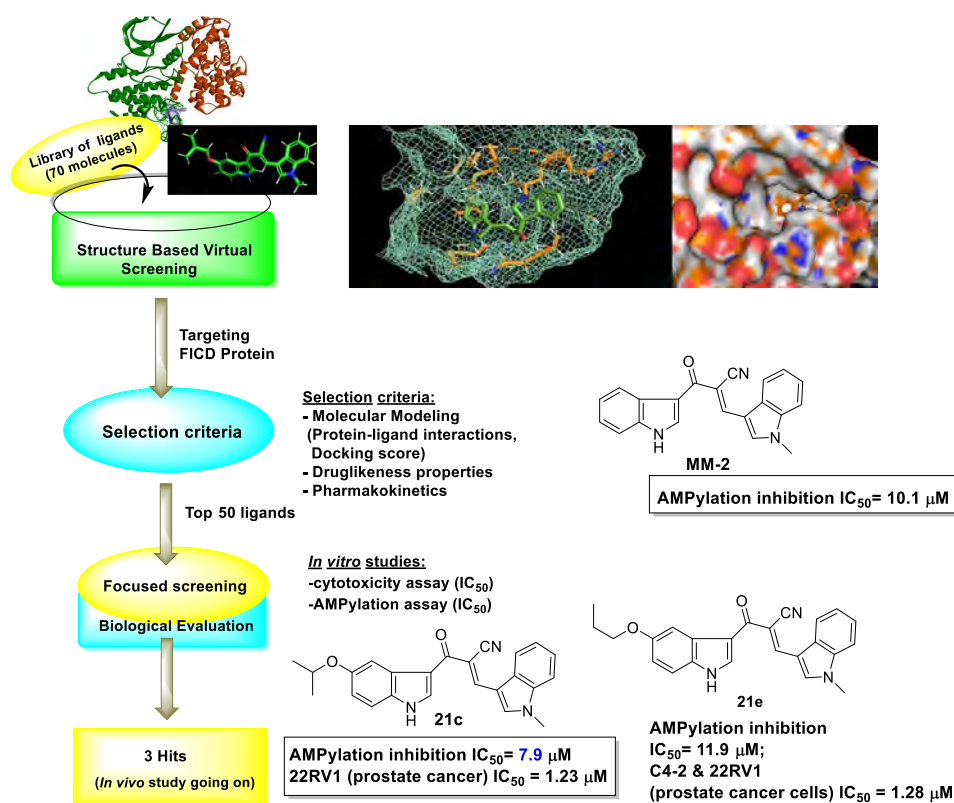
Figure 5.2.9 Identification of potent FICD inhibitors

5.2.4 Conclusions

In this chapter, the development of α-cyano bis(indolyl)chalcones (**21a-r**) as FICD inhibitors in a novel strategy for treating prostate cancer has been reported. Through an AMPylation assay, we identified **21c** as a potent FICD inhibitor, demonstrating an IC_{50} value of 7.9 μM, while **MM-2** and **21e** also exhibited promising activity at 10.1 and 11.98 μM, respectively. Furthermore, we conducted computational analyses, including molecular docking and pharmacokinetic studies, on the synthesized indolyl chalcones. Our findings unveiled specific molecules with remarkable binding affinity at the ATP binding site. Crucially, our *in vitro* experiments validated these computational predictions, underscoring the reliability and significance of our computational modeling strategies in drug discovery.

5.2.5 Biological Protocols

5.2.5.1 Protein Purification

To begin the protein purification process, the FICD pellet is taken and combined with substrate lysis buffer (8 mL) containing 1 mM PMSF (80 μL). The mixture is subjected to three cycles of French press treatment, with escalating pressures (medium, high, high), followed by

centrifugation at 10,000 rpm for 20 min. at 4 °C. The resulting supernatant is transferred to a fresh 15 mL tube, where prewashed beads (washed with 2X water and 2X substrate lysis buffer) are added (80 µL). The beads are then washed twice with 1 mL of water and twice with 1 mL of substrate lysis buffer. Subsequently, the 15 mL tube containing the mixture is placed in a cold room and rotated at 4 °C for 1 h. After rotation, the tube is centrifuged at 10,000 rpm for 10 min., and the supernatant is discarded. The beads are then subjected to sequential washes with 1X low stringent buffer, 2X medium stringent buffer, 1X high stringent buffer, and finally 1X low stringent buffer. Finally, the purified protein is eluted from the beads using FICD elution buffer, completing the protein purification process.

5.2.5.2 AMPylation Assay (Malachite Green Assay)

To prepare Reagent A, start by diluting 34.5 mL of concentrated HCl with distilled water to make a total volume of 90 mL. Then, dissolve 4.2 g of ammonium molybdate in this solution and dilute it further to a final volume of 100 mL. This solution, containing 4.2% (w/v) of ammonium molybdate in 4N HCl, remains stable at room temperature for extended periods. For Reagent B, dissolve 45 mg of malachite green-HCl in 100 mL of distilled water. Alternatively, 150 µL of liquid malachite green can be dissolved in 10 mL of distilled water to achieve the same concentration of 0.045% (w/v). Reagent C is prepared by mixing Reagent A and Reagent B in a ratio of 1:3. Lastly, Reagent D is a 2% (w/v) solution of NP-40, which can be prepared by dissolving NP-40 in distilled water to achieve the desired concentration.

To initiate the AMPylation reaction, a 30 µL reaction volume is prepared in an eppendorf tube, following a specific order of component addition. Firstly, distilled water was added, followed by the 10X AMP buffer, compounds from a 200 µM stock concentration, histone substrate at a concentration of 1 mg/mL, FICD protein, and ATP to achieve a final concentration of 30 µM. The tubes were then spin to ensure thorough mixing. Subsequently, the reaction tubes was set up for a 2 h incubation period at room temperature to allow the AMPylation reaction to proceed. Once the reaction is complete, pyrophosphatase enzyme (0.5-1 µL) was added to each tube containing the reaction mixture. This enzyme facilitates the breakdown of any remaining pyrophosphate. The reaction mixture, now containing the AMPylated substrate, was then transferred into wells of a 96-well plate. To each well, 1 µL of reagent D is added, followed by the addition of 30 µL of freshly prepared reagent C. Finally, the readings on the plate reader was measured according to the appropriate settings, allowing for the quantification and analysis of the AMPylated substrate.

5.2.6 Experimental Section

5.2.6.1 Chemistry

In our previous Chapter 5A, we provided detailed procedures and spectral data for synthesizing α-cyano bis(indolyl)chalcones (**21a-r**). A mixture containing 3-cyanoacetylindoles (0.1 g, 1 mmol) and appropriate aldehyde 20 (0.065g, 1 mmol) in ethanol (10 mL) was stirred at 25 °C. Catalytic amount of L-proline (10 mol%) was added to reaction mixture and it was stirred for 5 h at 25 °C. The reaction progress was monitored via TLC using a developing solvent system of n-hexane: ethyl acetate. The resulting yellow solid was then recrystallized from ethanol to obtain pure α-cyano bis(indolyl)chalcones in 91-95% yields.

5.2.7 References

1. Roy, C. R.; Cherfils, J., Structure and function of Fic proteins. *Nature Reviews Microbiology* **2015,** *13* (10), 631-640.

2. Goepfert, A.; Stanger, F. V.; Dehio, C.; Schirmer, T., Conserved inhibitory mechanism and competent ATP binding mode for adenylyltransferases with Fic fold. *PloS one* **2013,** *8* (5), e64901.

3. Liu, M.; Li, L.; Wang, Z.; Wang, S.; Tang, X., Catalytic deAMPylation in AMPylation-inhibitory/assistant forms of FICD protein. *Frontiers in Chemistry* **2023,** *11*, 1077188.

4. Truttmann, M. C.; Zheng, X.; Hanke, L.; Damon, J. R.; Grootveld, M.; Krakowiak, J.; Pincus, D.; Ploegh, H. L., Unrestrained AMPylation targets cytosolic chaperones and activates the heat shock response. *Proceedings of the National Academy of Sciences* **2017,** *114* (2), E152-E160.

5. Truttmann, M. C.; Ploegh, H. L., rAMPing up stress signaling: Protein AMPylation in metazoans. *Trends in Cell Biology* **2017,** *27* (8), 608-620.

6. Aghaei, M.; Dastghaib, S.; Aftabi, S.; Aghanoori, M.-R.; Alizadeh, J.; Mokarram, P.; Mehrbod, P.; Ashrafizadeh, M.; Zarrabi, A.; McAlinden, K. D., The ER stress/UPR axis in chronic obstructive pulmonary disease and idiopathic pulmonary fibrosis. *Life* **2020,** *11* (1), 1.

7. Camara, A.; George, A.; Hebner, E.; Mahmood, A.; Paluru, J.; Mattoo, S., A fluorescence polarization-based high-throughput screen to identify the first small-molecule modulators of the human adenylyltransferase hype/ficd. *International Journal of Molecular Sciences* **2020,** *21* (19), 7128.

Chapter 6

Diaryliodonium Salts Promoted Versatile Approach to Diverse β-Oxo Amides and Potent Benzo[a]carbazoles
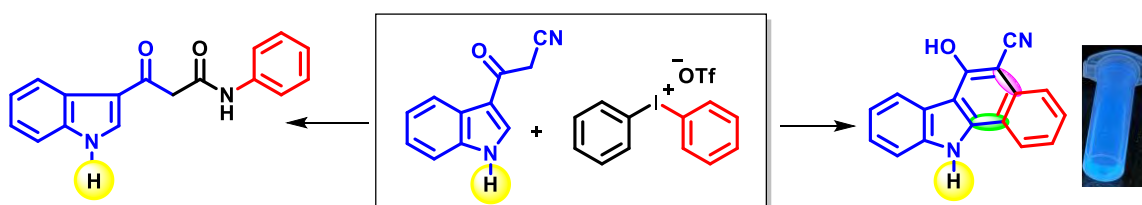
6.1 Introduction

Formation of amide linkages is among the important chemical connections for development of various pharmaceutical drugs, proteins, natural products, and synthetic polymers. Among the amides, β-oxo amides represent a valuable structural unit in medicinal and synthetic organic chemistry.[1-4] Recently, extensive research efforts have been directed towards the synthesis of β-oxo amides for being potential precursors to achieve a variety of bioactive heterocyclic compounds[5-8], *i.e.*, pyridones,[9] quinolones,[10] and chromones.[11, 12] But, most of the existing methods to prepare β-oxo amides suffer from the disadvantages such as formation of undesirable side products in stoichiometric amounts, high reaction temperatures, and less substrate scopes.[13-17] Therefore it is desirable to develop a simple and efficient approach to prepare β-oxo amides. Apart from these applications, β-oxo amide motifs are commonly found in various natural compounds and therapeutic agents For example, several metabolites Myxothiazol S1,[18] possess intriguing biological activities, Verticilactam (**1**),[19] Niizalactam C (**2**),[20] and 3-oxo-C12-HSL (**3**).[21] Teriflunomide (**4**), a medication that modulates the immune system, is actually the enol form of alpha-cyano β-oxo amide Piptidyl difluoro β-ketoamides (PDBKA) belong to a class of effective elastase inhibitors.[22] (Figure 6.1) The chiral β-ketoamide 4-Odemethylbarbamide (**5**) is a natural product derived from marine cyanobacteria.[23]
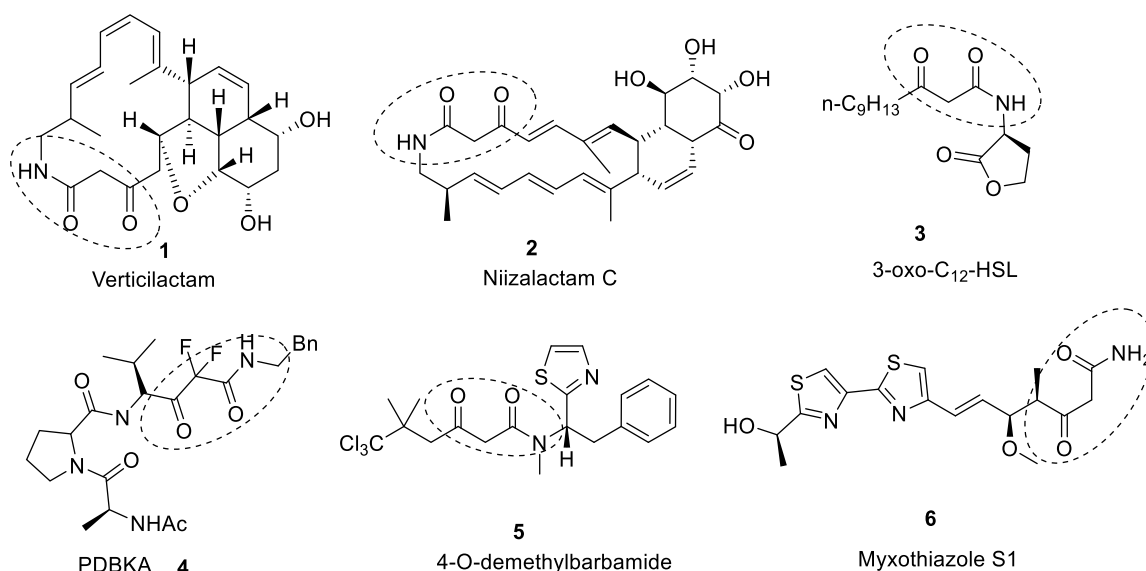
Figure 6.1 Biological active β-oxo amides

During the past years a broad spectrum of novel and simple strategies have been developed for the preparation of *N*-substituted β-oxo amides.[24-28] The most prevalent methods for the synthesis of β-oxo amides involve esters and amines in a stoichiometric amount of base at

elevated temperature[14, 29] Other synthetic strategies involve the utilization of dia-zonium salts,[30] diketenes or diketene–acetone adducts and isoxazolium salts (Scheme 6.1) at high temperatures.[16, 28] The well-known synthetic protocols for their synthesis includes acylation of amide enolates or their synthetic equivalents.[27]
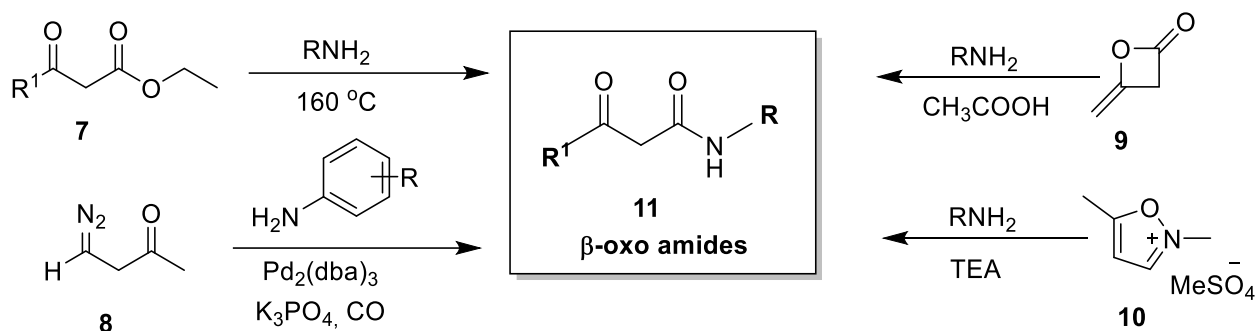
Scheme 6.1 General synthesis of β-oxo amides

In 2020, Malakar *et al.* presented a cost-effective synthesis protocol for β-oxo amides. They introduced a straightforward and economical method mediated by 1,1,1,3,3,3-hexafluoro-2-propanol (HFIP) to synthesize β-oxo amides, utilizing amines and β-keto esters as substrates. The reaction conditions displayed high efficiency in cleaving the carbon-oxygen (C-O) bond, facilitating consecutive site-selective C-N bond formation under these conditions.[31] In 2016, Yang and co-workers have developed a protocol for the amidation involving the reaction of aryl boronic acids with various arylnitriles under copper-catalyzed conditions.[32]

On the other hand, diaryliodonium salts have been widely employed as highly electrophilic arylating agents in many coupling reactions and in the construction of valuable heterocycles with five- and six-membered ring systems.[33-35] Due to unique advantageous properties, such as high reactivity, easy handling, less toxic nature, the application of diaryliodonium salts are rapidly growing for the synthesis and functionalization of medicinally potent heterocycles. Olofsson *et al.* developed a facile, high yielding direct synthesis of diaryliodonium triflates.[36] This convenient one-pot protocol involves aryl iodides **12** and arenes **13** in the presence of *m*-chloroperbenzoic acid (*m*-CPBA) and triflic acid. Use of mild oxidant *m*-CPBA is beneficial due to its low solubility in organic solvents which simplifies its removal from the reaction mixture. The method is applicable for the synthesis of a variety of diaryliodonium salts bearing various substitution on the aryl rings (Scheme 6.2).
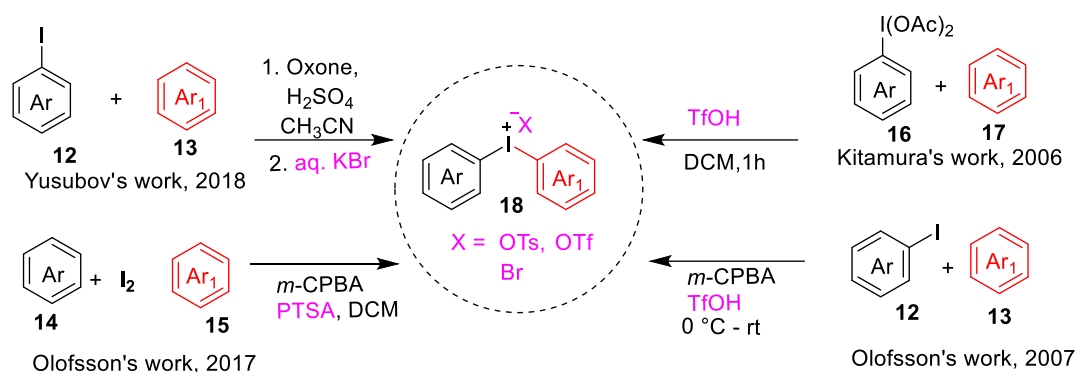
Scheme 6.2 Most common routes for the preparation of diaryliodonium salts

Symmetrical diaryliodonium salts have two identical aryl rings. But if the aryl rings of iodonium salts are not identical then it's called unsymmetrical diaryliodonium salts. The chemoselectivity become important when the arylation reaction was carried out with unsymmetrical diaryliodonium salts because both aryl rings have opportunity to enter the transition state. Chemoselectively transfer of an aryl ring in unsymmetrical diaryliodonium salts is depicted in figure 6.2.[37]
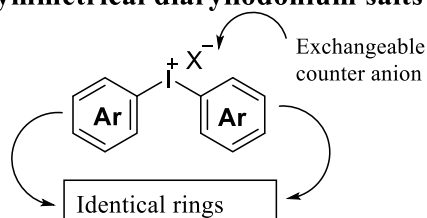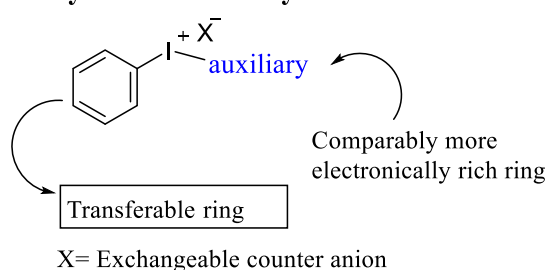
Figure 6.2 (A) Selective aryl transfer from symmetrical and unsymmetrical iodonium salts (B) Advantageous features of iodonium salts
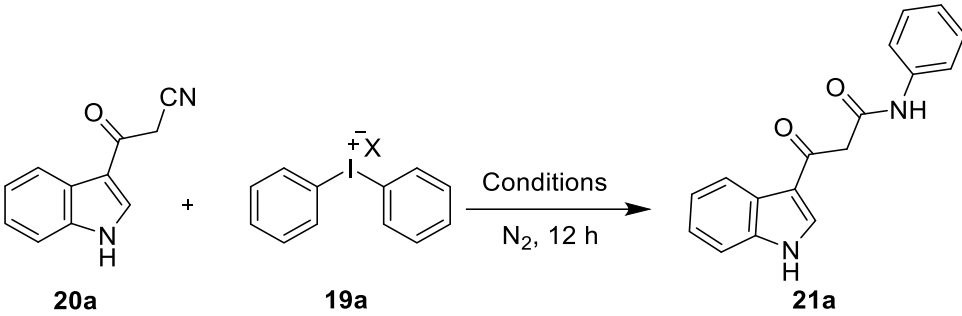
6.2 Results and Discussion

6.2.1 Synthesis and Characterization

Literature methods for the preparation of β-oxo amides involve the reaction of esters and amines in a stoichiometric amount of base at an elevated temperature.[14, 29] But, there is no report to access β-oxo amides by the reaction of readily available α-cyano ketones and diaryliodonium salts. Easy preparation of α-cyano ketones prompted us to explore the reaction of α-cyano ketones and the relatively benign diaryliodonium salts to achieve bioactive β-oxo amides under mild reaction conditions. The 3-cyanoacetyl indole (**20**) can be easily prepared in one synthetic step without column-chromatography purification from the reaction of commercially available indoles and cyanoacetic acid.[38]

We chosen α-cyano ketone (**20a**) and diphenyliodonium triflate (**19a**) as model substrates to investigate the reaction conditions (Table 6.1). Firstly, the reaction of **20a** with **19a** using 10 mol% of CuCl as the catalyst and 1,2-dichloroethane (DCE) as solvent at 80 °C resulted in expected **21a** in 20% yield (Table 6.1, entry 1). Use of CuI instead of CuCl as a catalyst decreased the yield of **21a** (Table 6.1, entry 2). Gratifyingly, changing the catalyst from CuI to Cu(OTf)$_2$ produced **21a** in 91% yield (Table 6.1, entry 3). Use of Cu(OAc)$_2$H$_2$O instead of Cu(OTf)$_2$ afforded **21a** in trace amount (Table 6.1, entry 4). When reaction of **20a** and **19a** was performed in absence of the catalyst, no product formation was observed (Table 6.1, entry 5). This control experiment revealed the essential role of copper catalyst. Next, we focused to optimize the catalyst loading. No significant improvement in the yield of **21a** was observed with the increased amount of Cu(OTf)$_2$ from 10 mol% to 20 mol% (Table 6.1, entry 6). Notably, lower product yield (**21a)** was observed with reduced catalyst loading (5 mol%) (Table 6.1, entry 7). Further, variation in reaction temperatures also did not improve the yield of **21a** significantly (Table 6.1, entries 8-9).

Use of solvents such as toluene, DMF and THF resulted in lower product yields (Table 6.1, entries 10-12). To study the reactivity of diphenyliodonium salts with different counterions, we subjected diphenyliodonium salts with counter ions such as OTs, Br and PF$_6$ (Table 6.1, entries 13-15). Reaction of **20a** with diphenyliodonium salt **19a** having OTs and Br counterions afforded **21a** in poor yields while **19a** with PF$_6$ counterion provided **21a** in 85% yield.

Table 6.1 Optimization of reaction conditions[a]

Entry	X	Catalyst (10 mol%)	Solvent	Temp. (^{0}C)	Yield[b] (%)
1.	OTf	CuCl	DCE	80	20
2.	OTf	CuI	DCE	80	10
3.	**OTf**	**Cu(OTf)$_2$**	**DCE**	**80**	**91**
4.	OTf	Cu(OAc)$_2$ .H$_2$O	DCE	80	trace
5.	OTf	-	DCE	80	NR[c]
6.	OTf	Cu(OTf)$_2$	DCE	80	92[d]
7.	OTf	Cu(OTf)$_2$	DCE	80	80[e]
8.	OTf	Cu(OTf)$_2$	DCE	100	91
9.	OTf	Cu(OTf)$_2$	DCE	60	75
10.	OTf	Cu(OTf)$_2$	Toluene	80	79
11.	OTf	Cu(OTf)$_2$	DMF	80	10
12.	OTf	Cu(OTf)$_2$	THF	80	78
13.	OTs	Cu(OTf)$_2$	DCE	80	55
14.	Br	Cu(OTf)$_2$	DCE	80	45
15.	PF$_6$	Cu(OTf)$_2$	DCE	80	85

[a]Reaction conditions: **20a** (0.70 mmol, 1.0 equiv), **19a** (0.84 mmol, 1.2 equiv), catalyst (0.07 mmol, 0.1 equiv.) in DCE (2.5 mL) at 80 °C (min). [b]Isolated yield of the product. [c]NR = no reaction, [d]20 mol% catalyst was used. [e]5 mol% catalyst was used.

Under the developed reaction conditions, by employing 5-methoxy/bromoindolyl α-cyano ketones (**20b-c**) and diphenyliodonium salt **19a** afforded the desired β-oxo amides **21b** (70% yield) and **21c** (64% yield).

Table 6.2 Synthesis of various β-oxo amides 21a-c[a,b]

21, 75%   **21b, 70%**   **21c, 64%**
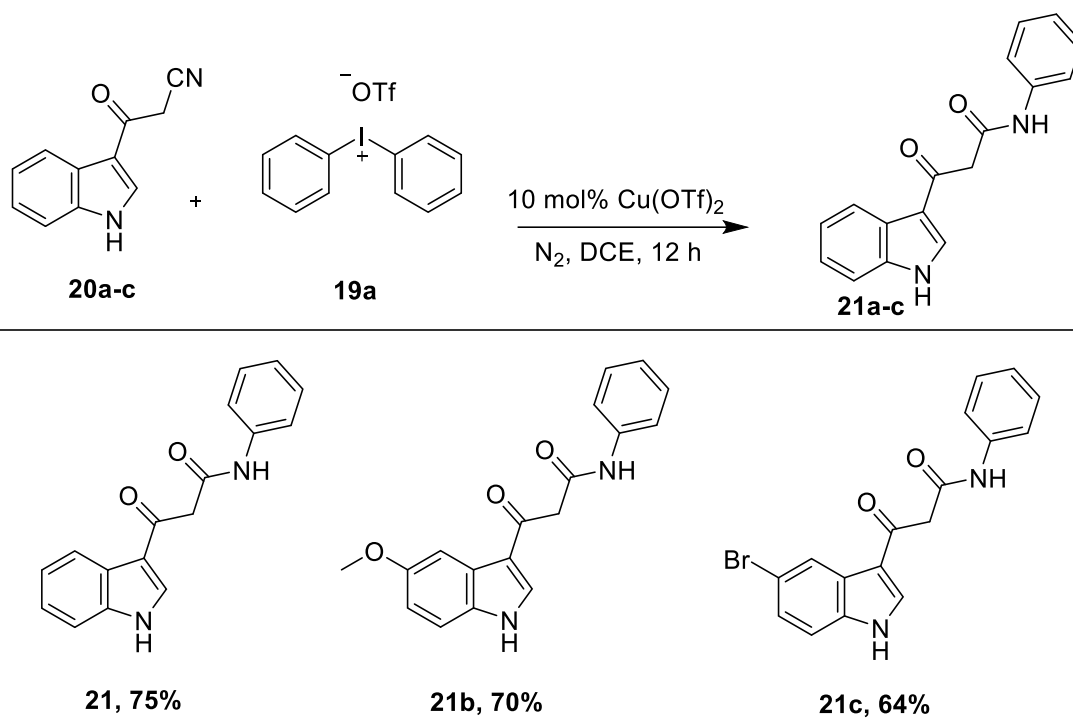
[a]Reaction conditions: **20a-d** (0.70 mmol, 1.0 equiv), **19a** (0.84 mmol, 1.2 equiv), Cu(OTf)$_2$ (0.07 mmol, 0.1 equiv.), DCE (2.5 mL) under N$_2$ atmosphere at 80 °C for 12 h. [b]Isolated yield.

All the synthesized compounds (**21a-c**) were isolated by column chromatography and characterized by their ^{1}H and ^{13}C NMR spectral data. The proton NMR of **21b** displayed two characteristic singlets at 3.96 ppm (-CH$_2$ protons) and 3.78 ppm (OCH$_3$) (Figure 6.3). Its ^{13}C NMR spectrum also showed characteristic peaks at 49.27 (methylene carbon), 55.73 (OCH$_3$) and 156.01 ppm (amidic carbon) as shown in figure 6.4.

Figure 6.3 ^{1}H NMR spectrum of compound **21b**

Figure 6.4 ^{13}C NMR spectrum of compound **21b**

In view of recent reports on the C-2 arylation of indole using diaryliodonium salts, we explored the reaction of 3-cyanoacetyl indole **20a** with iodonium salts in an efforts to prepare C-2-arylated 3-cyanoacetyl indole. To our surprise, the reaction of **20a** with diaryliodonium salt (**19a**) in the presence of palladium catalyst led to the formation of benzocarbazole **23a** as a major product (75% yield) instead of C-2 arylated 3-cyanoacetyl indole **22** (Scheme 6.3).

Scheme 6.3 Synthesis of C-2 arylated 3-cyanoacetyl indole and benzo[*a*]carbazoles

Over the past few years, a subclass of carbazoles, benzo[*a*]carbazoles, have captured the attention of both synthetic and medicinal chemists because of their broad range of properties in medicinal and material chemistry. In this context, benzo[*a*]carbazole derivatives have been prepared by Gu and co-workers from the reaction of acetol and 2-arylindoles by using a zwitterion based on TfOH as the catalyst.[39] Likewise, in 2016, Pelkey and colleagues developed a two-step synthetic route for the preparation of 3-pyrrolin-2-one-fused benzo[*a*]carbazoles through the formation of indole-substituted 3-pyrrolin-2-one by a BF₃-mediated reaction of indole and *N*-alkyl-substituted 3-aryltetramic acids and followed by Scholl-type oxidative-cyclization.[40] Similarly, as depicted in Scheme 6.4, Pi and Sha groups independently achieved the synthesis of functionalized benzo[*a*]carbazoles through Diels-Alder reaction of vinylindoles (**26**) and in situ generated arynes from 2- (trimethylsily)aryl triflate) in the presence of CsF and oxygen gas.[41, 42] Moreover, many transition-metal-catalyzed reactions of pre-functionalized indole substrates have been reported to afford efficiently and diversely substituted benzo[*a*]carbazoles. For instance, a novel synthetic methodology has been reported by Li *et al.* to prepare benzo[*a*]carbazoles or 6-amino benzo[*a*]carbazoles from the cascade reaction of 2-arylindoles or 2-arylindole-3-carbonitriles (**27**) with a diazo carbonyl compounds using Rh(III)-catalyzed conditions (Scheme 6.4).[43]

Likewise, Huang and co-workers accomplished the synthesis of 11*H*-benzo[*a*]carbazole derivatives through sequential cross-dehydrogenative coupling reaction of 2-arylindoles (**28**) and alkenes in presence of Rh-catalyzed conditions at 140 °C (Scheme 6.4).[44] In 2018, Fan *et al.* discovered an approach for the selective synthesis of benzo[*a*]carbazole derivatives *via*

Rh(III)-catalyzed cascade reaction of 2-arylindoles (**29**) with sulfoxonium ylides which involved inert C-H bond alkylation and followed by intramolecular condensation (Scheme 6.4).[45]

Scheme 6.4 Reported methodologies for the construction of benzo[*a*]carbazoles

In our efforts to develop efficient synthesis of benzocarbazoles, we further optimized the reaction conditions involving readily available cyano ketones **20a** and diphenyliodonium triflate (**19a**) as model substrates (Table 6.3). Initial reaction of **20a** with 1.0 equiv. of **19a** using 10 mol% Pd(OAc)$_2$ as catalyst and DMF (1.5 mL) as solvent at 100 °C afforded the expected 6-hydroxy-11*H*-benzo[*a*]carbazole-5-carbonitrile (**23a**) in 60% yield after 24 h (Table 6.3, entry 1). Next, changing the equivalent of **19a** from 1.0 to 1.5 equivalents significantly improved the yield (up to 82%) of **23a**, but further increasing the iodonium salt **23a** to 2.0 equivalents resulted in a relatively low product yield (72%) of **23a** (Table 6.3, entries 2-4). Reducing the catalyst loading from 10 mol% to 5 mol% led to a slightly improved product yield (**23a**, 85%) (Table 6.3, entry 5). It is noticeable that the use of an elevated reaction temperature (120 °C) completed this reaction within 16 h only and further enhanced the yield to 91% when the reaction temperature was increased to 140 °C (Table 6.3, entries 6 and 7). We then focused our investigation on screening the different polar and non-polar solvents. However, when this reaction was performed in non-polar solvents such as toluene or THF, no formation of **23a** was detected even after refluxing for 24 h (Table 6.3, entries 8 and 9), highlighting the need for a polar solvent. Moreover, the use of other solvents like DMSO and AcOH was also futile, resulting in low yield of the expected product **23a** (Table 6.3, entries 10 and 11). Experiments using other catalysts [Cu(OTf)$_2$, CuI] were disappointing (Table 6.3,

entries 12 and 13), as the starting materials remained intact (TLC). Finally, the reaction conditions of entry 6 of Table 6.3 appeared to be the optimized.

Table 6.3 Optimization of the Reaction Conditions for the Preparation of **23a**[a,b]
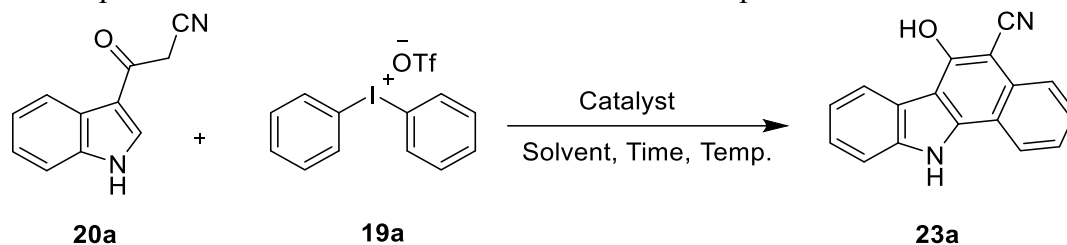
Entry	Catalyst (mol%)	19a (equiv.)	Solvent	Temp (°C)	Time (h)	Yield[b] (%)
1.	Pd(OAc)₂ (10)	1.0	DMF	100	24	60
2.	Pd(OAc)₂ (10)	1.2	DMF	100	24	68
3.	Pd(OAc)₂ (10)	1.5	DMF	100	24	82
4.	Pd(OAc)₂ (10)	2.0	DMF	100	24	72
5.	Pd(OAc)₂ (5)	1.5	DMF	100	24	85
6.	**Pd(OAc)₂ (5)**	**1.5**	**DMF**	**120**	**16**	**91**
7.	Pd(OAc)₂ (5)	1.5	DMF	140	16	89
8.	Pd(OAc)₂ (5)	1.5	toluene	reflux	24	ND[c]
9.	Pd(OAc)₂ (5)	1.5	THF	reflux	24	ND[c]
10.	Pd(OAc)₂ (5)	1.5	DMSO	120	24	71
11.	Pd(OAc)₂ (5)	1.5	AcOH	reflux	24	65
12.	Cu(OTf)₂ (5)	1.5	DMF	120	24	ND[c]
13.	CuI (5)	1.5	DMF	120	24	ND[c]

[a] Reaction conditions: **20a** (0.54 mmol, 1.0 equiv.), **19a** (0.81 mmol, 1.5 equiv.), catalyst (0.027 mmol, 0.05 equiv.), solvent (1.5 mL), 16 h. [b] Isolated yield. [c] ND = not determined

To test the general usefulness of our developed protocol, a variety of diaryliodonium salts (**19a-e**) and 3-cyanoacetyl indole derivatives (**20a-h**) were examined (Scheme 6.2). Initially, the study was conducted with the variation of diaryliodonium salt derivatives.

Table 6.4 Synthesis of 6-hydroxy-11*H*-benzo[*a*]carbazole-5-carbonitriles
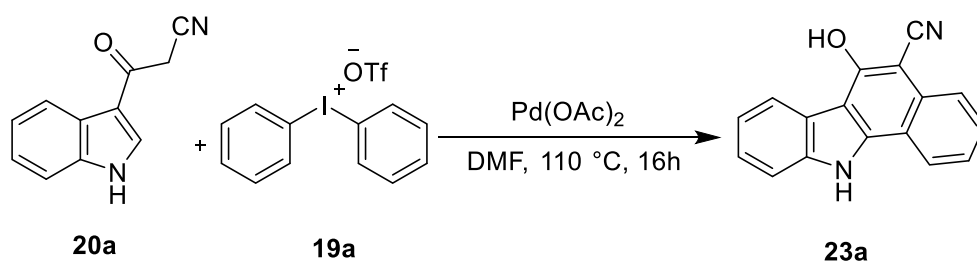
a) Substrate scope of diaryliodonium salts

23a, 91%   **23b, 89%**   **23c, 86%**

23d, 84%   **23e, 70%**   **23f, 85%**
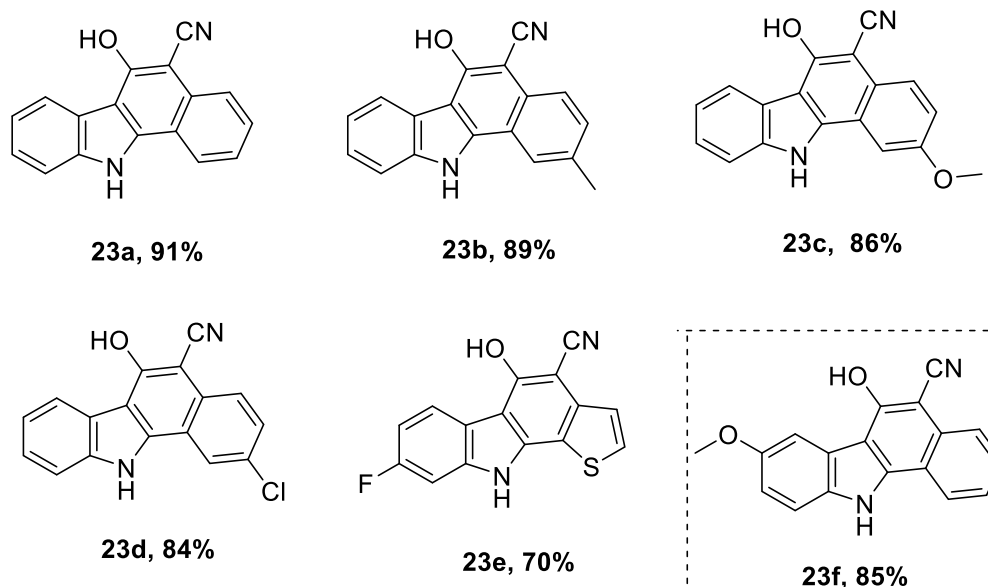
b) Substrate scope of keto cyanoindole

23g, 82%   **23h, 81%**   **22** Intermediate
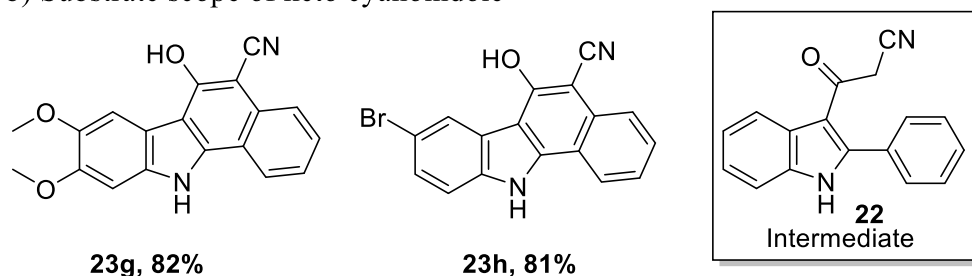
Reaction conditions: **20** (0.54 mmol), **19** (0.81 mmol), Pd(OAc)$_2$ (0.027 mmol), DMF (1.5 mL), 16 h.

The reaction of **20a** with diaryliodonium salts having different electronic nature substituents afforded the products **23b** (methyl; 89%), **23c** (methoxy; 86%) and **23d** (chloro; 85%) in excellent yields under optimized conditions (Scheme 6.2a). Pleasingly, the reaction of mesityl(thiophen-2-yl)iodonium triflate (**19e**) with **20a** worked smoothly to afford the desired product **23e** in 70 % yield. Furthermore, we investigated the substrate scope by using substituted 3-cyanoacetyl indoles (**20a-d**). 3-Cyanoacetyl indole derivatives with methoxy

(**20b**), dimethoxy (**20c**) and bromo (**20d**) substituents reacted well, affording the corresponding products **23f**, **23g** and **23h** in good yields of 85%, 80% and 81%, respectively (Table 6.4).

The ^{1}H NMR spectra of the intermediate (**22**) revealed characteristic peaks, appearing at 3.93 ppm, indicating the presence of the methylene group (Figure 6.5). Additionally, the ^{13}C NMR spectra (Figure 6.6) displayed a distinct signal at 32.20 ppm, for the methylene carbon of **22**. These spectroscopic data confirm the successful formation of the desired intermediates. In NMR spectrum of compound **23a**, peak corresponding to the -CH$_2$ proton and carbon were absent (Figures 6.7 and 6.8).
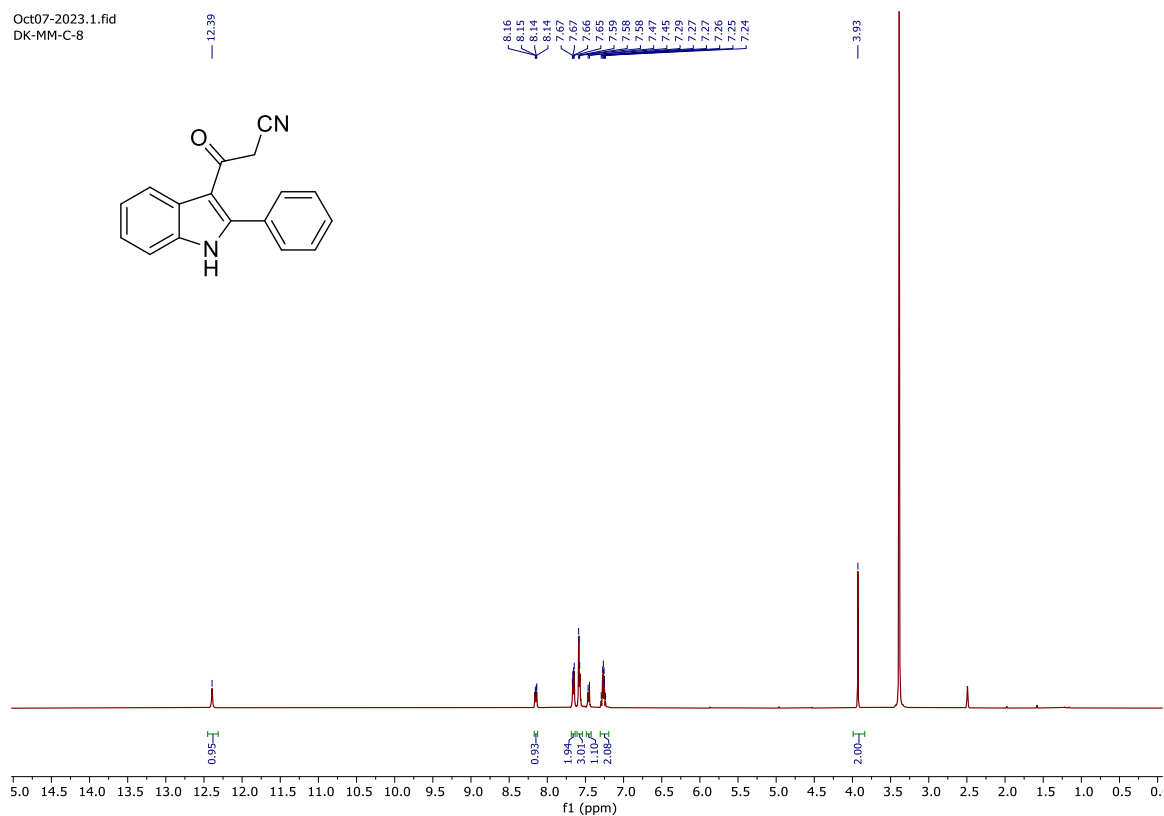
Figure 6.5 ^{1}H NMR spectrum of compound **22**
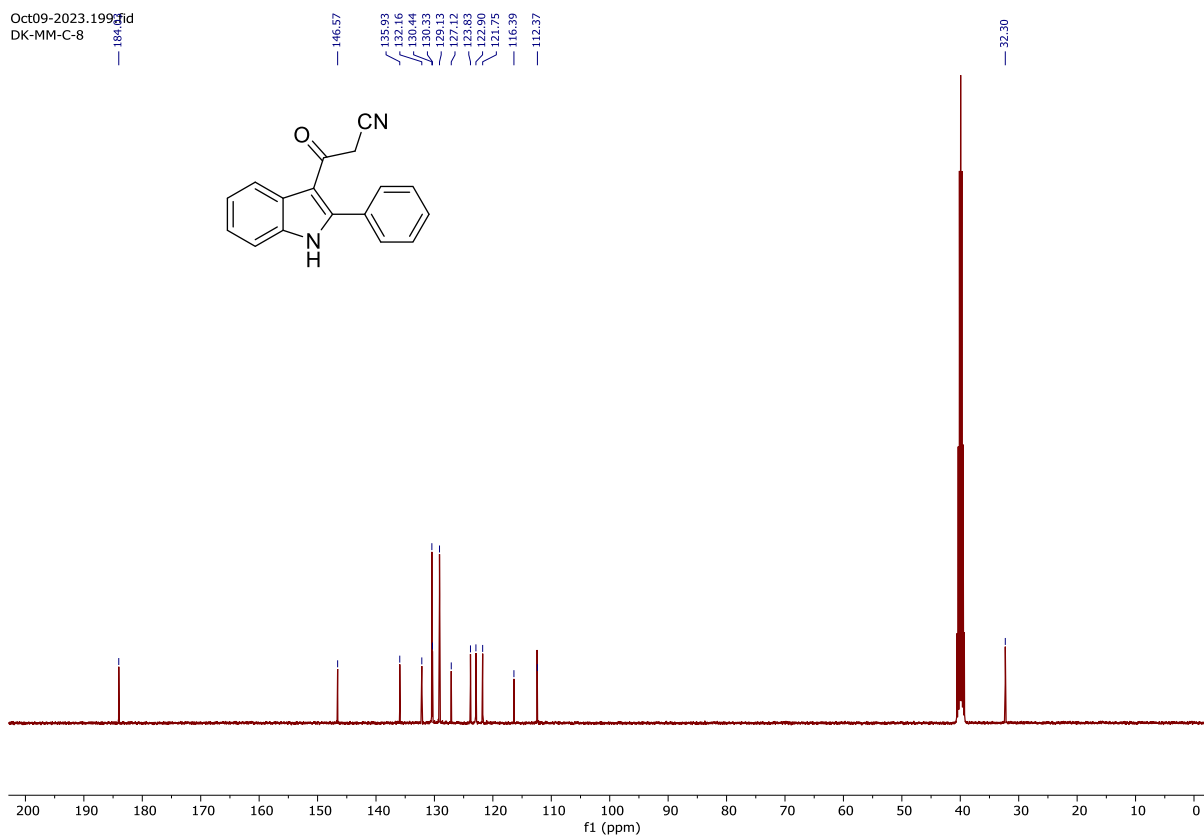
Figure 6.6 ^{13}C NMR spectrum of compound **22**
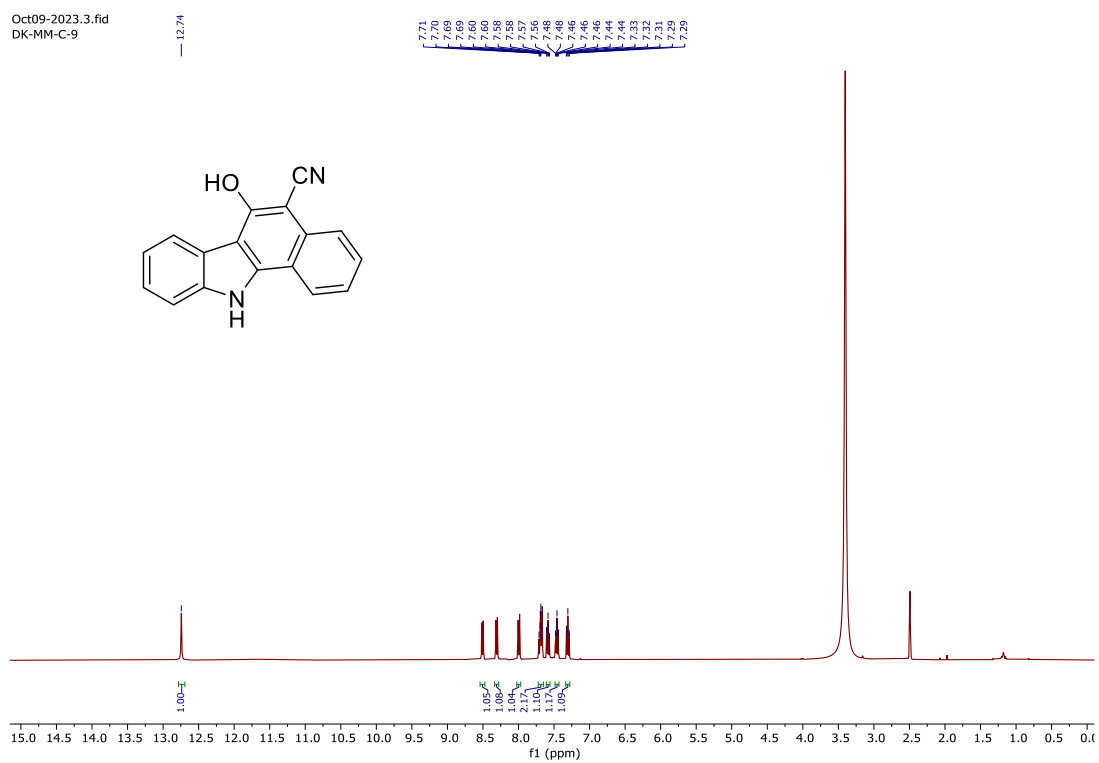
Figure 6.7 ^{1}H NMR spectrum of compound **23a**
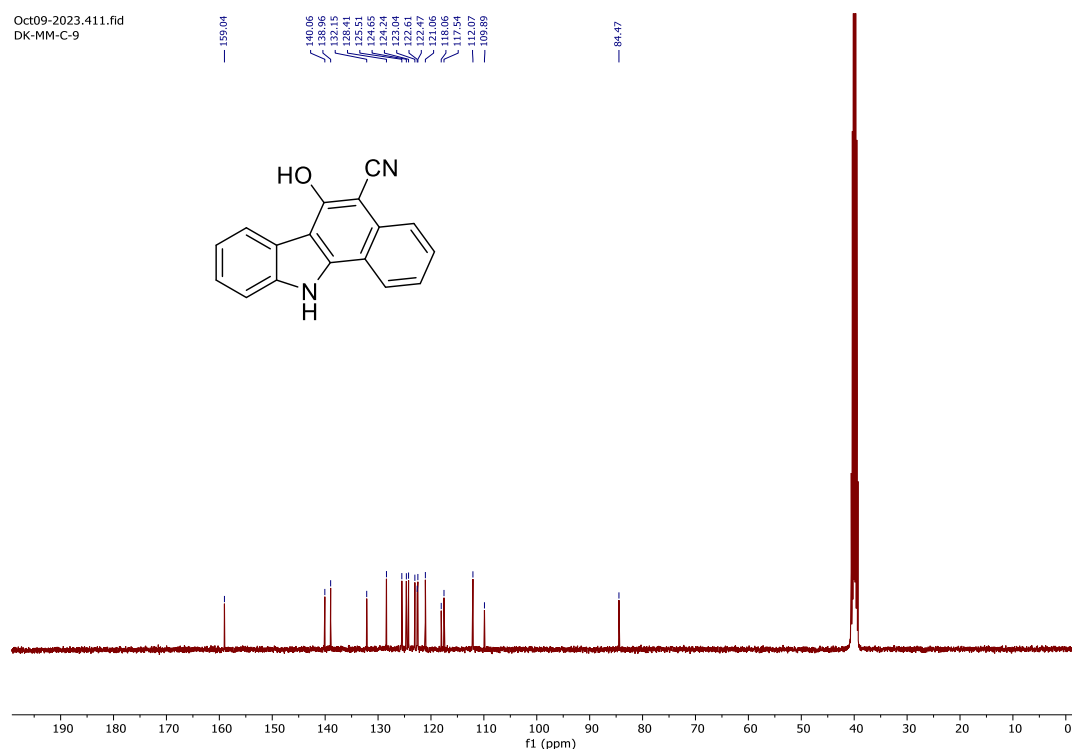
Figure 6.8 ^{13}C NMR spectrum of compound **23a**

In 2014, Gulia *et al.* reported a (5+2) cycloaddition reaction involving o-vinylphenol and an alkyne, catalyzed by rhodium, to produce annulated oxepino.[49] Under similar conditions, using the reaction of **23a** and diphenylacetylene (**24**) we successfully prepared 4H-oxepino carbazole **25** in 75% yield (Scheme 6.5).
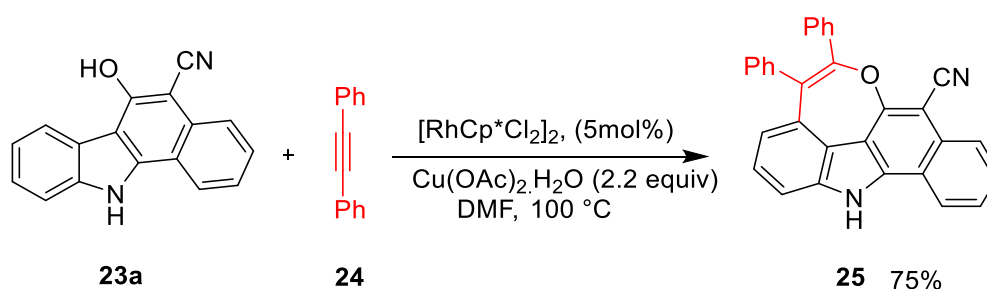
Scheme 6.5 Synthesis of oxepino carbazole **25**

6.3.2 Photophysical Studies

Absorption and emission spectra of the prepared indolyl carbazoles **23a-h** were recorded in UV grade acetonitrile solvent at 25 °C. The absorption spectra of **23a-h** displayed characteristic absorption bands (279-304 nm) and emission bands (381-418 nm) excited at their respective absorption bands with 100-150 nm Stokes shift was observed (Table 6.5, Figure 6.9).

Changing the chemical functionalities on indolyl carbazoles effectively modulated absorption and emission maxima. Introduction of an electron donating C5-OMe group (compound **23f**) led to showed absorption at 280 nm and emission at 396 nm, respectively.
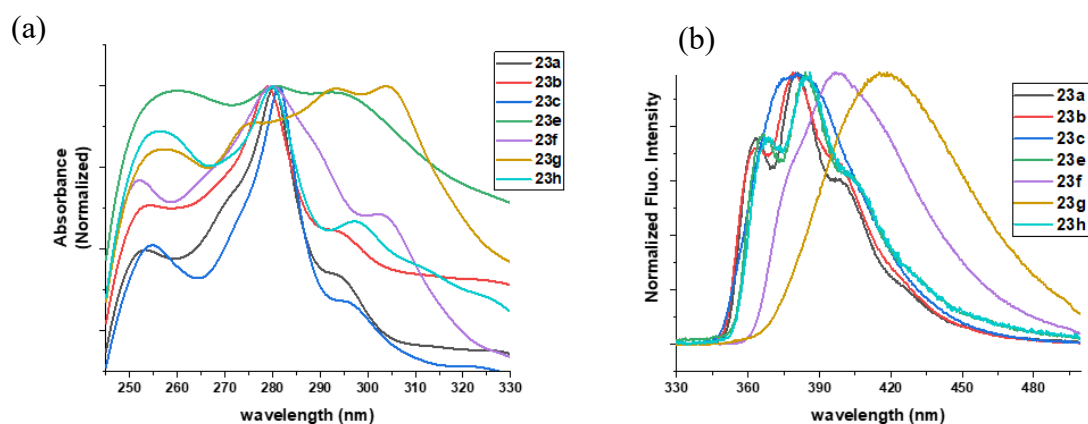
Figure 6.9 UV-Visible (a) Normalized absorption spectra (b) Normalized emission spectra of **23a-h** (2 μM) in UV grade acetonitrile (λ_{ex}: 300 nm; slit width: 4 nm)

Table 6.5 Photophysical properties of **23a-h** in UV-grade acetonitrile (2×10^{-6} M)

Compd.	λ_{abs} (nm)	ε (M^{-1}cm^{-1})	λ_{em} (nm)	Stokes shift (nm)
23a	280	962945	381	101
23b	279	581875	379	100
23c	281	1141130	380	99
23e	281	272640	384	103
23f	280	934315	396	116
23g	304	564985	418	114
23h	280	625090	386	106

Thereafter, photophysical properties of **23a-h** were checked in six different solvents namely dichloromethane (DCM), chloroform (CHCl₃), tetrahydrofuran (THF), methanol (MeOH), dimethyl formamide (DMF) and dimethyl sulfoxide (DMSO). Solvatochromism could be considered as experimental evidence for the intramolecular charge transfer (ICT) effect occurs due to donor (methoxy)-acceptor (cyano) system. A bathochromic shift of 10 nm was observed for the longer-wavelength peak of **23f** with the change in solvent from DCM (279 nm) to DMSO (289 nm) as shown in figure 6.10 (Table 6.6); illustrates a remarkable ICT effect. To get insight into the electronic structures, DFT calculations were performed at the B3LYP/6-31G(d,p) level (Figure 6.11). The LUMO lobes are largely localized on the cyano moiety in

23f, while the HOMO and HOMO−1 lobes are distributed more on the methoxy moiety in **23f**; explains the more significant ICT effect observed in the solvatochromism experiment.
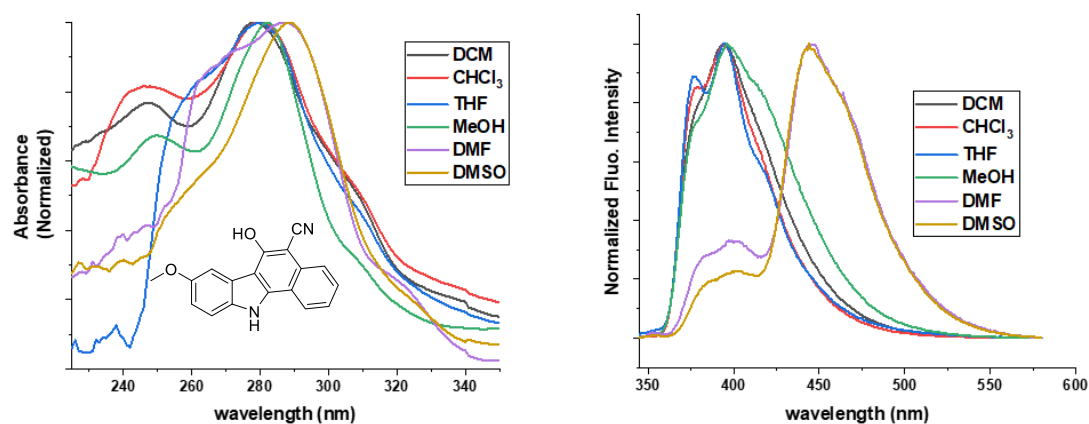
Figure 6.10 UV-Visible (a) Normalized absorption spectra (b) Normalized emission spectra of **23f** (10 µM) in different solvents (λ_{ex}: 300 nm; slit width: 4 nm)

Table 6.6 Photophysical properties of **23f** (10 µM) in different solvents

Solvent	λ_{abs}/nm	λ_{em}/nm	Stoke's shift/nm
DCM	279	394	115
CHCl$_3$	280	394	114
THF	280	394	114
MeOH	282	396	114
DMF	287	444	157
DMSO	289	444	155
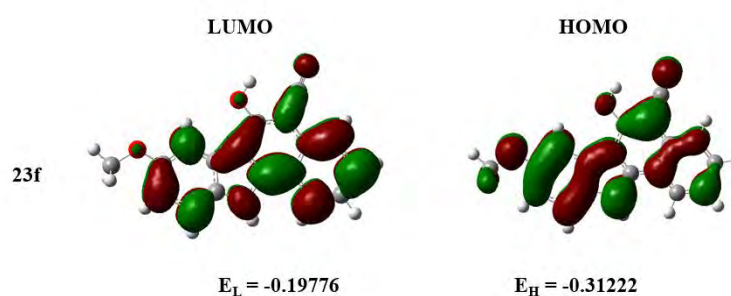
Figure 6.11 DFT calculated frontier molecular orbitals

6.3.3 Plausible Mechanisms for Pd-catalyzed Reaction

Based on our experimental results and previous literature reports, a plausible mechanism pathway is proposed in Scheme 6.6. Firstly, for C-2 arylation, the enol form of **20a** is believed to coordinate with Pd(II) catalyst to activate the Csp^2-H bond of C-2 position to produce five-membered cyclopalladated species **A**. Further, oxidative addition of diaryliodonium salt **19a** is

expected to result in the formation of diaryl Pd(IV) species **B**. Species **B** then undergoes reductive elimination and reinsertion of Pd(II) between the Csp^2-H bond of the phenyl ring to afford species **C**. We then speculated that Pd(II) forms C-Pd(II)-C bonds through 1,3-rearrangement to generate species **D**. Finally, reductive elimination of **D** provides desired product **23a** and release the active Pd(II) species to complete the catalytic cycle.
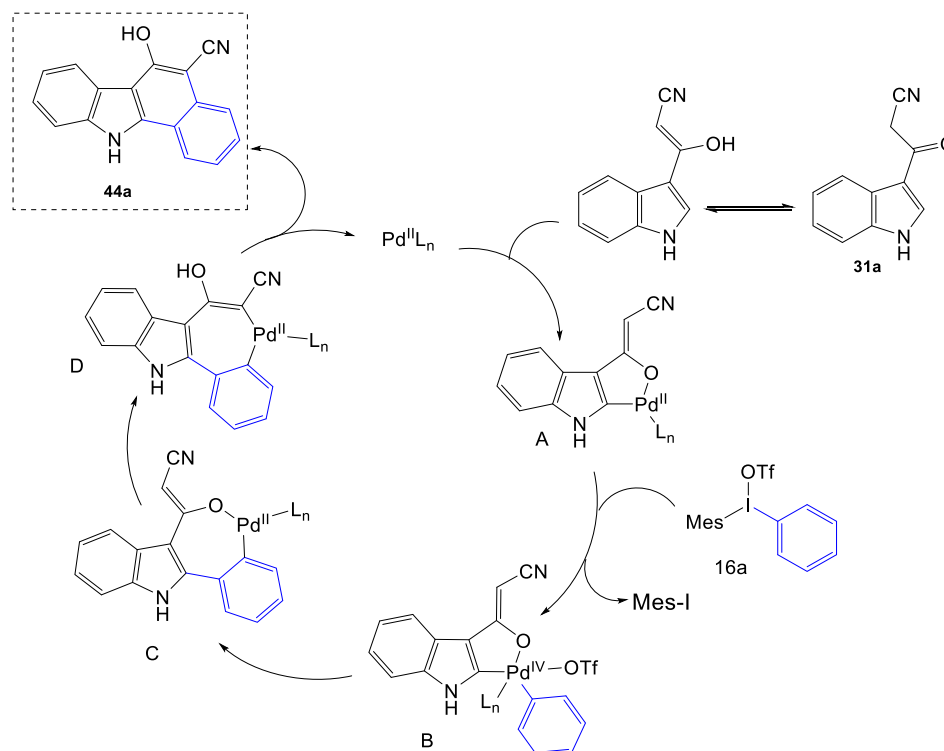
Scheme 6.6 Plausible reaction mechanism of Pd-catalyze reactions

6.4 Conclusions

In conclusion, we have successfully developed two efficient synthetic methodologies for the preparation of diverse and biologically relevant compounds. Our copper-catalyzed strategy enables the synthesis of β-oxo amides using iodonium salts under milder reaction conditions. However, Pd-catalyzed reaction of α-cyano ketone and diaryliodonium salts afforded the substituted benzo[a]carbazoles in high yields. The developed conditions were found to be advantegeous in term of high product yield, use of readily available starting materials and short synthesis of bioactive compounds.

6.5 Experimental Section

6.5.1 General Materials and Methods

All the laboratory reagents were purchased from Sigma-Aldrich, Alfa Aesar, and Spectrochem India Pvt. Ltd and used without further purification. The reactions were monitored by thin layer

chromatography and performed on Merck pre-coated plates (silica gel 60 F$_{254}$, 0.2mm). Column chromatographic purification of products was carried out using silica gel (100~200 mesh) and ethyl acetate/hexane mixture was used for elution. ^{1}H NMR spectra was recorded at 400 MHz, ^{13}C NMR spectra was recorded at 100 MHz, and in CDCl$_3$ and DMSO-d_6 solutions. Chemical shifts are given in ppm relative to the residual solvent peak (^{1}H NMR: CDCl$_3$ δ 7.28; DMSO-d_6 2.50; ^{13}C NMR: CDCl$_3$ δ 77.0; DMSO-d_6 39.52) with multiplicity (s = singlet, d = doublet, t = triplet, q = quartet, m = multiplet), coupling constants (in Hz) and integration. Melting points were determined by E-Z melting point apparatus. Used 3-cyanoacetylindole derivative was prepared according to literature reported method.[46]

6.5.1.1 General procedure for the preparation of diaryliodonium salts (21a-f)[47, 48]

19a-e
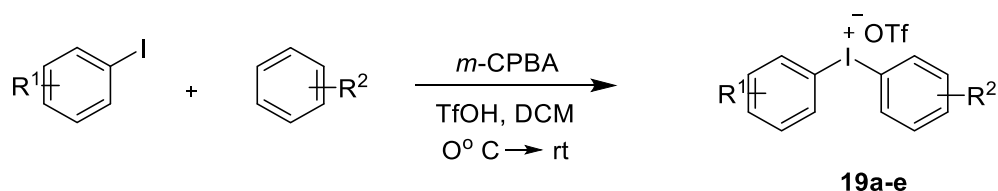
To a solution of iodoarene (2.5 mmol, 1.0 equiv), *m*-chloroperbenzoic acid (*m*-CPBA, 2.7 mmol, 1.1 equiv) in dichloromethane (8 mL) was added. The resulting mixture was stirred at room temperature for 10 min then arene (2.7 mmol, 1.1 equiv)) was added. Reaction mixture was cooled to 0 °C and then trifluoromethanesulfonic acid (TfOH, 5.0 mmol, 2.0 equiv)) was added dropwise. After the addition of TfOH, mixture was allowed to stir at room temperature for 0.5 h. The solvent was evaporated under vaccum and the residue was dissolved in cold diethyl ether (4 mL) under cooling (0 °C) conditions. The obtained solid was collected by filtration, washed with cold diethyl ether and dried under vacuum to give diaryliodonium triflates **19a-e** as white solids in 88-95% yields.

| **19a**, 95% | **19b**, 93% | **19c**, 92% | **19d**, 92% | **19e**, 88% |
| mp 178-179 °C | mp 122-124 °C | mp 129-132 °C | mp 175-176 °C | mp 132-134 °C |
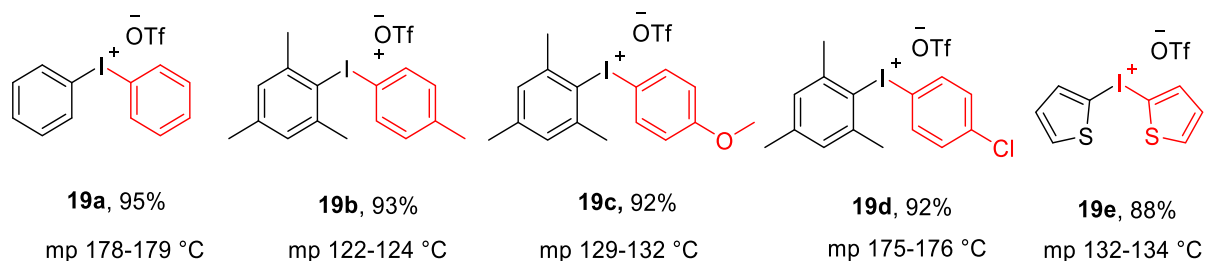
6.5.1.2 General procedure for the synthesis of 3-cyanoacetyl indoles (20a-r):[54]

Indole (10 mmol) **17** was added to a stirred solution of cyanoacetic acid (10 mmol) in acetic anhydride (10 mL) at 50 °C. The solution was heated at 85 °C for 20 min. During that period 3-cyanoacetyl indole started to crystallize. After completion of the reaction as indicated by

TLC, the mixture was allowed to cool and the solid was collected, washed with Hexane:EtOAc and dried to afford pure 3-cyanoacetyl indoles (**20a-h**) in 87-95 % yields.

6.5.1.3 General experimental procedure for *N*-phenyl-β-ketoamides (21a-c):

To the mixture α-cyano ketones **20** (0.70 mmol, 1.0 equiv), copper(II)triflate (0.07 mmol) and diaryliodonium salts (**19**, 0.84 mmol, 1.2 equiv) were dissolved in DCE (2.5 mL, contains 0.1% v/v H$_2$O) under N$_2$ atmosphere. The resulting reaction mixture was stirred at 80 °C for 12 h. After completion of the reaction as indicated by TLC, the contents were cooled to room temperature and evaporated the solvent under reduced pressure. The obtained crude residue was purified by column chromatography using ethyl acetate and hexane as an eluent to obtain pure products **21a-c** in 65-75% yields.

6.5.1.4 General experimental procedure for the synthesis of benzo[*a*]carbazole derivatives (23a-h):

The reaction was initiated by dissolving α-cyano ketones **20** (1.0 equiv) and diaryliodonium salts (**19**, 1.5 equiv) in DMF, followed by the addition of Pd(OAc)$_2$ (5 mol%). The resulting mixture was stirred at 120 °C for 16 h under a N$_2$ atmosphere. Upon completion of the reaction, indicated by TLC analysis, the reaction mixture was cooled to room temperature and poured into crushed ice. The resulting crude residue was purified by column chromatography using ethyl acetate and hexane as eluents, yielding pure products **23a-h** in 88-91% yields.

3-(1*H*-Indol-3-yl)-3-oxo-*N*-phenylpropanamide(21a):
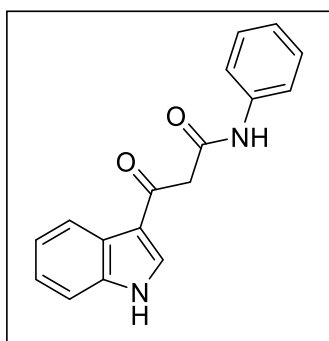
Light brown solid, 75% yield, mp 214−215 °C; ^{1}H NMR (400 MHz, DMSO-d_6) δ 12.06 (s, 1H), 10.20 (s, 1H), 8.43 (d, J = 3.1 Hz, 1H), 8.19 (d, J = 7.0 Hz, 1H), 7.62 (d, J = 7.7 Hz, 2H), 7.50 (d, J = 8.1 Hz, 1H), 7.32 (t, J = 7.9 Hz, 2H), 7.26 – 7.19 (m, 2H), 7.06 (t, J = 7.4 Hz, 1H), 3.99 (s, 2H); ^{13}C NMR (100 MHz, DMSO-d_6) δ 189.2, 166.3, 139.6, 137.1, 135.7, 129.2, 125.8, 123.7, 123.5, 122.4, 121.7, 119.5, 116.8, 112.7, 49.3; IR (neat, cm^{-1}): 3310, 1667, 1601, 1420, 1339, 1173; HRMS (ESI) *m/z* calcd for C$_{17}$H$_{15}$N$_2$O$_2$: 279.1128 (M + H)$^+$, found: 279.1126.

3-(5-Methoxy-1*H*-indol-3-yl)-3-oxo-*N*-phenylpropanamide (21b): Off white solid, 70% yield; mp 221-224°C; ^{1}H NMR (400 MHz, DMSO-d_6) δ 11.96 (s, 1H), 10.19 (s, 1H), 8.37 (d, J = 3.2 Hz, 1H), 7.70 (d, J = 2.4 Hz, 1H), 7.62 (d, J = 7.7 Hz, 2H), 7.39 (d, J = 8.8 Hz, 1H), 7.32 (t, J = 7.9 Hz, 2H), 7.06 (t, J = 7.4 Hz, 1H), 6.87 (dd, J = 8.8, 2.5 Hz, 1H), 3.96 (s, 2H), 3.78 (s, 3H); ^{13}C NMR (100 MHz, DMSO-d_6) δ 189.1, 166.3, 156.0 , 139.6, 135.8 , 131.9, 129.2, 126.7, 123.7, 119.5, 116.7, 113.4, 103.3, 55.7, 49.3.
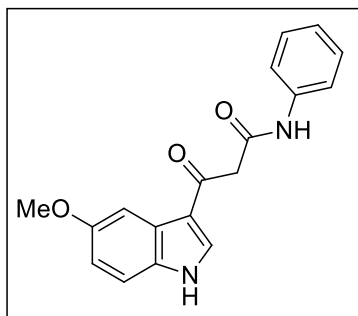
3-(5-Bromo-1*H*-indol-3-yl)-3-oxo-*N*-phenylpropanamide (21c): Light brown solid, 64% yield, mp 227−228 °C; ^{1}H NMR (400 MHz, DMSO-d_6) δ 12.27 (s, 1H), 10.22 (s, 1H), 8.49 (d, J = 3.1 Hz, 1H), 8.32 (d, J = 1.9 Hz, 1H), 7.61 (d, J = 7.6 Hz, 2H), 7.49 (d, J = 8.6 Hz, 1H), 7.38 (dd, J = 8.6, 2.0 Hz, 1H), 7.32 (t, J = 7.9 Hz, 2H), 7.06 (t, J = 7.4 Hz, 1H), 3.99 (s, 2H); ^{13}C NMR (100 MHz, DMSO-d_6) δ 189.4, 166.1, 139.5, 136.8, 135.9, 129.2, 127.6, 126.1, 123.8, 123.8, 119.5, 116.3, 115.2, 114.9, 49.3; IR (neat, cm^{-1}): 3395, 3294, 1670, 995; HRMS (ESI) *m/z* calcd for $C_{17}H_{14}BrN_2O_2$: 357.0233 (M + H)$^+$, found: 357.0196.
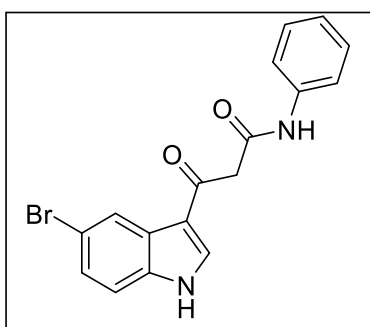
6-hydroxy-11*H*-benzo[a]carbazole-5-carbonitrile (23a): Brown solid, 91% yield, mp 156−158 °C. ^{1}H NMR (400 MHz, DMSO) δ 12.74 (s, 1H), 8.54 – 8.47 (m, 1H), 8.31 (d, J = 7.9 Hz, 1H), 8.00 (dd, J = 8.3, 1.0 Hz, 1H), 7.70 (dd, J = 5.8, 4.3 Hz, 2H), 7.58 (td, J = 7.6, 1.3 Hz, 1H), 7.46 (ddd, J = 8.2, 7.2, 1.3 Hz, 1H), 7.34 – 7.28 (m, 1H); ^{13}C NMR (100 MHz, DMSO-d_6) 159.04, 140.06, 138.96, 132.15, 128.41, 125.51, 124.65, 124.24, 123.04, 122.61, 122.47, 121.06, 118.06, 117.54, 112.07, 109.89, 84.47.
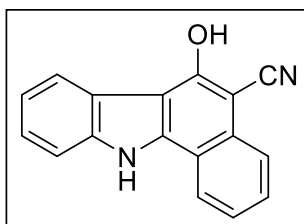
6-hydroxy-3-methyl-11*H*-benzo[a]carbazole-5-carbonitrile (23b): Off-white solid, 89% yield, mp 156-158 °C. ^{1}H NMR (400 MHz, DMSO-d_6) δ 12.64 (s, 1H), 11.54 (s, 1H), 8.41 (d, J = 8.3 Hz, 1H), 8.30 (d, J = 7.9 Hz, 1H), 7.79 (s, 1H), 7.66 (d, J = 8.1 Hz, 1H), 7.48 – 7.40 (m, 2H), 7.33 – 7.28 (m, 1H), 2.56 (s, 3H); ^{13}C NMR (100 MHz, DMSO-d_6) δ 158.98, 140.22, 138.92, 138.08, 132.47, 130.89, 130.22,
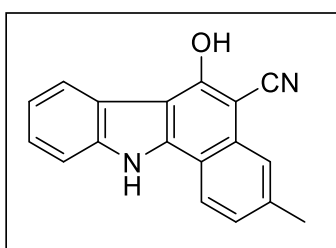
126.45, 125.30, 123.62, 123.00, 122.69, 122.36, 120.96, 118.14, 115.58, 111.96, 109.37, 84.19, 22.04.

6-hydroxy-3-methoxy-11*H*-benzo[a]carbazole-5-carbonitrile (23c): Off-white solid, 89% yield, mp 185-186 °C; ^{1}H NMR (400 MHz, DMSO-d_6) δ 12.58 (s, 1H), 11.55 (s, 1H), 8.44 (d, J = 9.0 Hz, 1H), 8.28 (d, J = 7.8 Hz, 1H), 7.64 (d, J = 8.1 Hz, 1H), 7.46 – 7.41 (m, 1H), 7.35 (d, J = 2.4 Hz, 1H), 7.32 – 7.24 (m, 2H), 3.95 (s, 3H); ^{13}C NMR (100 MHz, DMSO-d_6) δ 159.64, 159.33, 140.55, 138.89, 134.20, 125.10, 124.88, 122.76, 122.19, 120.92, 118.20, 115.37, 112.04, 111.85, 108.44, 104.68, 84.17, 55.75.
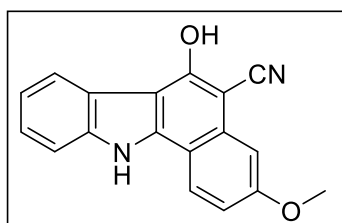
6-hydroxy-3-chloro-11*H*-benzo[a]carbazole-5-carbonitrile (23d): Off-white solid, 82% yield, mp 148-151 °C. ^{1}H NMR (400 MHz, DMSO-d_6) 12.84 (s, 1H), 11.99 (s, 1H), 8.55 (d, J = 8.7 Hz, 1H), 8.32 (d, J = 7.9 Hz, 1H), 7.93 (d, J = 2.0 Hz, 1H), 7.71 – 7.68 (m, 1H), 7.67 – 7.63 (m, 1H), 7.49 (t, J = 7.1 Hz, 1H), 7.33 (t, J = 7.5 Hz, 1H); ^{13}C NMR (100 MHz, DMSO-d_6) δ 159.97, 139.74, 139.02, 133.40, 133.14, 129.07, 125.78, 125.29, 124.85, 122.90, 122.54, 121.29, 117.65, 116.06, 112.17, 110.19, 83.77.
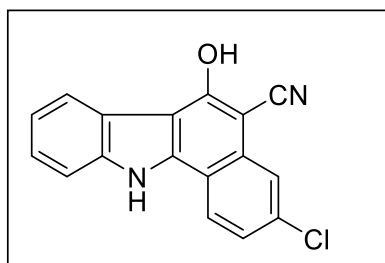
6-hydroxy-8-methoxy-11*H*-benzo[a]carbazole-5-carbonitrile (23e): Off-white solid, 75% yield, mp 145-148 °C. ^{1}H NMR (400 MHz, DMSO-d_6) 12.60 (s, 1H), 11.58 (s, 1H), 8.48 (d, J = 7.8 Hz, 1H), 7.99 (d, J = 8.1 Hz, 1H), 7.82 (d, J = 2.4 Hz, 1H), 7.72 – 7.67 (m, 1H), 7.58 (t, J = 8.0 Hz, 2H), 7.12 (dd, J = 8.8, 2.5 Hz, 1H), 3.88 (s, 3H); ^{13}C NMR (100 MHz, DMSO-d_6) δ 159.05, 154.72, 140.48, 133.78, 132.06, 128.31, 124.58, 124.22, 123.13, 122.94, 118.10, 117.72, 114.98, 112.80, 109.78, 104.81, 84.05, 56.06.
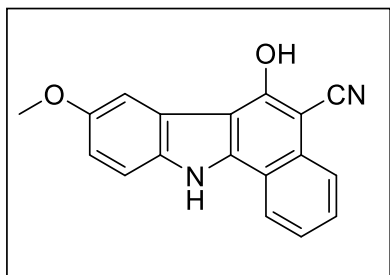
8-bromo-6-hydroxy-11*H*-benzo[a]carbazole-5-carbonitrile (23f): Off-white solid, 86% yield, mp 196−197 °C; ^{1}H NMR (400 MHz, DMSO-d_6) δ 12.92 (s, 1H), 11.84 (s, 1H), 8.51 (d, J = 8.1 Hz, 1H), 8.42 (d, J = 1.4 Hz, 1H), 8.01 (d, J = 8.3 Hz, 1H), 7.73 (t, J = 7.6 Hz, 1H), 7.68 – 7.58 (m, 3H); ^{13}C NMR (100 MHz, DMSO-d_6) δ 158.81, 140.71, 137.76, 132.38, 128.89, 127.98, 124.95, 124.46, 124.34, 123.16, 117.81, 117.44, 114.16, 113.19, 109.12, 84.91.
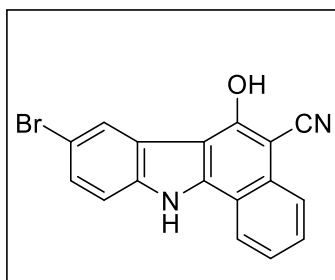
6-hydroxy-8,9-dimethoxy-11*H*-benzo[a]carbazole-5-carbonitrile (23g): Off-white solid, 75% yield, mp 220−221 °C; ^{1}H NMR (400 MHz, DMSO-d_6) δ 12.52 (s, 1H), 8.42 (dd, *J* = 8.3, 1.7 Hz, 1H), 7.95 (dd, *J* = 8.6, 1.0 Hz, 1H), 7.78 (s, 1H), 7.66 – 7.60 (m, 2H), 7.57 – 7.51 (m, 2H), 7.16 (s, 1H), 3.89 (s, 3H), 3.86 (s, 3H); ^{13}C NMR (100 MHz, DMSO-d$_6$) δ 149.26, 145.46, 139.10, 131.31, 130.45, 129.14, 127.61, 124.45, 124.15, 122.52, 118.26, 117.68, 114.84, 110.20, 104.69, 103.75, 95.38, 84.06, 56.50, 56.15.
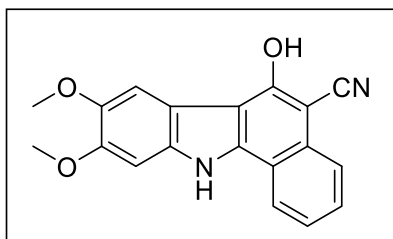
8-fluoro-5-hydroxy-10*H*-thieno[2,3-a]carbazole-4-carbonitrile (23h):
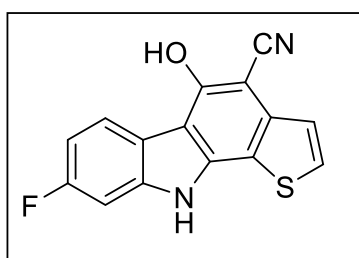
Off-white solid, 82% yield, mp 226−229, ^{1}H NMR (400 MHz, DMSO) δ 12.62 (s, 1H), 8.24 (dd, *J* = 8.7, 5.6 Hz, 1H), 7.96 (d, *J* = 5.3 Hz, 1H), 7.47 (d, *J* = 5.3 Hz, 1H), 7.35 (dd, *J* = 9.7, 2.4 Hz, 1H), 7.18 – 7.06 (m, 1H); ^{13}C NMR (100 MHz, DMSO-d_6) δ 184.03, 146.57, 135.93, 132.16, 130.44, 130.33, 129.13, 127.12, 123.83, 122.90

5-Fluoro-*N*-phenyl-1*H*-indole-3-carboxamide (22): Off-white solid, 70% yield, mp 211−213 °C; ^{1}H NMR (400 MHz, DMSO-d_6) δ 12.39 (s, 1H), 8.15 (dd, *J* = 5.3, 2.4 Hz, 1H), 7.69 – 7.64 (m, 2H), 7.61 – 7.54 (m, 3H), 7.46 (d, *J* = 7.5 Hz, 1H), 7.31 – 7.19 (m, 2H), 3.93 (s, 2H); ^{13}C NMR (100 MHz, DMSO-d_6) δ 184.03, 146.57, 135.93, 132.16, 130.44, 130.33, 129.13, 127.12, 123.83, 122.90, 121.75, 116.39, 112.37, 32.30.
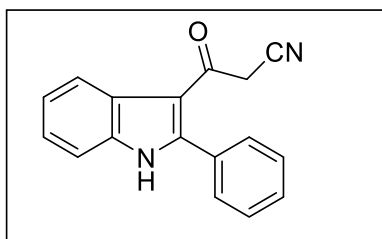
6.6 References

1. Ma, C.; Li, X.; Jin, K.; Cao, J.; Xu, W., Novel β-dicarbonyl derivatives as inhibitors of aminopeptidase N (APN). *Bioorganic and Medicinal Chemistry Letters* **2013,** *23* (17), 4948-4952.

2. Vaske, Y. S. M.; Mahoney, M. E.; Konopelski, J. P.; Rogow, D. L.; McDonald, W. J., Enantiomerically Pure trans-β-Lactams from α-Amino Acids via Compact Fluorescent Light (CFL) Continuous-Flow Photolysis. *Journal of American Chemical Society* **2010,** *132* (32), 11379-11385.

3. Rich, D. H.; Bernatowicz, M. S., Oxidation of statine-containing peptides to ketone analogs via novel peptide sulfonium ylides. *Journal of Organic Chemistry* **1983,** *48* (12), 1999-2001.

4. El-Meligie, S. E.; Khalil, N. A.; El-Nassan, H. B.; Ibraheem, A. A., A Review on the Synthetic Routes to β-Keto Amides. *Current Organic Chemistry* **2019,** *23* (19), 2005-2015.

5. Kato, T., Recent synthetic studies using diketene. *Accounts of Chemical Research* **1974,** *7* (8), 265-271.

6. Clemens, R. J., Diketene. *Chemical Reviews* **1986,** *86* (2), 241-318.

7. Han, M.; Nam, K.-D.; Hahn, H.-G.; Shin, D., Unexpected formation of new bicyclic γ-lactams by dimerization of α-chloroacetoacetanilides. *Tetrahedron Letters* **2008,** *49* (35), 5217-5219.

8. Zaleska, B.; Lis, S., Cerium (IV) Mediated Oxidative Dimerization of 3-Oxoacid Anilides and their Cyclizations. *Synthetic Communications* **2001,** *31* (2), 189-197.

9. Gao, B.; Sun, Y.; Wang, J.; Yuan, Z.; Zu, L.; Zhang, X.; Liu, W., Efficient and divergent synthesis of polyfunctionalized 2-pyridones from β-keto amides. *RSC advances* **2018,** *8* (59), 33625-33630.

10. Sai, K. K. S.; Gilbert, T. M.; Klumpp, D. A., Knorr cyclizations and distonic superelectrophiles. *Journal of Organic Chemistry* **2007,** *72* (25), 9761-9764.

11. Morris, J.; Wishka, D. G.; Fang, Y., A cyclodehydration route to 2-aminochromones. *Synthetic Communications* **1994,** *24* (6), 849-858.

12. Sosnovskikh, V. Y., Synthesis and reactions of halogen-containing chromones. *Russian Chemical Reviews* **2003,** *72* (6), 489-516.

13. O'Halloran, N.; James, J. P.; Downey, C. A., Inter-and intra-molecular cyclisation reactions of azoacetates derived from aryl hydrazones of ethyl acetoacetate and acetoacetanilides. *Heterocycles* **2008,** *75* (11), 2681-2701.

14. Suri, O.; Satti, N.; Suri, K., Microwave induced acetoacetylation of hetaryl and aryl amines. *Synthetic Communications* **2000,** *30* (20), 3709-3718.

15. Witzeman, J. S.; Nottingham, W. D., Transacetoacetylation with tert-butyl acetoacetate: synthetic applications. *Journal of Organic Chemistry* **1991,** *56* (5), 1713-1718.

16. Ancizu, S.; Moreno, E.; Solano, B.; Villar, R.; Burguete, A.; Torres, E.; Pérez-Silanes, S.; Aldana, I.; Monge, A., New 3-methylquinoxaline-2-carboxamide 1, 4-di-N-oxide derivatives as anti-Mycobacterium tuberculosis agents. *Bioorganic & Medicinal Chemistry* **2010,** *18* (7), 2713-2719.

17. Jaggavarapu, S. R.; Kamalakaran, A. S.; Jalli, V. P.; Gangisetty, S. K.; Ganesh, M. R.; Gaddamanugu, G., Facile eco-friendly synthesis of novel chromeno [4, 3-b] pyridine-2, 5-diones and evaluation of their antimicrobial and antioxidant properties. *Journal of Chemical Sciences* **2014,** *126* (1), 187-195.

18. Schieferdecker, S.; Exner, T. E.; Gross, H.; Roth, M.; Nett, M., New myxothiazols from the predatory bacterium Myxococcus fulvus. *The Journal of Antibiotics* **2014,** *67* (7), 519-525.

19. Nogawa, T.; Terai, A.; Amagai, K.; Hashimoto, J.; Futamura, Y.; Okano, A.; Fujie, M.; Satoh, N.; Ikeda, H.; Shin-Ya, K., Heterologous expression of the biosynthetic gene cluster for verticilactam and identification of analogues. *Journal of Natural Products* **2020,** *83* (12), 3598-3605.

20. Hoshino, S.; Okada, M.; Wakimoto, T.; Zhang, H.; Hayashi, F.; Onaka, H.; Abe, I., Niizalactams A–C, multicyclic macrolactams isolated from combined culture of Streptomyces with mycolic acid-containing bacterium. *Journal of Natural Products* **2015,** *78* (12), 3011-3017.

21. Smith, K. M.; Bu, Y.; Suga, H., Library screening for synthetic agonists and antagonists of a Pseudomonas aeruginosa autoinducer. *Chemistry & Biology* **2003,** *10* (6), 563-571.

22. Takahashi, L. H.; Radhakrishnan, R.; Rosenfield Jr, R. E.; Meyer Jr, E. F.; Trainor, D. A., Crystal structure of the covalent complex formed by a peptidyl. alpha.,. alpha.-difluoro-. beta.-keto amide with porcine pancreatic elastase at 1.78. ANG. resolution. *Journal of the American Chemical Society* **1989,** *111* (9), 3368-3374.

23. Kim, E. J.; Lee, J. H.; Choi, H.; Pereira, A. R.; Ban, Y. H.; Yoo, Y. J.; Kim, E.; Park, J. W.; Sherman, D. H.; Gerwick, W. H., Heterologous production of 4-O-demethylbarbamide, a marine cyanobacterial natural product. *Organic Letters* **2012,** *14* (23), 5824-5827.

24. Xin, X.; Wang, Y.; Kumar, S.; Liu, X.; Lin, Y.; Dong, D., Efficient one-pot synthesis of substituted pyridines through multicomponent reaction. *Organic & Biomolecular Chemistry* **2010,** *8* (13), 3078-3082.

25. Ramanjulu, J. M.; DeMartino, M. P.; Lan, Y.; Marquis, R., Titanium (IV) isopropoxide mediated synthesis of pyrimidin-4-ones. *Organic Letters* **2010,** *12* (10), 2270-2273.

26. Bonne, D.; Constantieux, T.; Coquerel, Y.; Rodriguez, J., Stereoselective multiple bond‐forming transformations (MBFTs): the power of 1, 2‐and 1, 3‐dicarbonyl compounds. *Chemistry‐A European Journal* **2013,** *19* (7), 2218-2231.

27. Chakraborty, A.; Majumdar, S.; Maiti, D. K., Selective exploitation of acetoacetate carbonyl groups using imidazolium based ionic liquids: synthesis of 3-oxo-amides and substituted benzimidazoles. *Tetrahedron Letters* **2016,** *57* (30), 3298-3302.

28. DeShong, P.; Cipollina, J. A.; Lowmaster, N. K., A general method for the synthesis of tetramic acid derivatives. *The Journal of Organic Chemistry* **1988,** *53* (7), 1356-1364.

29. Štefane, B.; Polanc, S., Aminolysis of 2, 2-difluoro-4-alkoxy-1, 3, 2-dioxaborinanes: Route to β-keto amides and β-enamino carboxamides. *Tetrahedron* **2007,** *63* (45), 10902-10913.

30. Zhang, Z.; Liu, Y.; Ling, L.; Li, Y.; Dong, Y.; Gong, M.; Zhao, X.; Zhang, Y.; Wang, J., Pd-catalyzed carbonylation of diazo compounds at atmospheric pressure: a catalytic approach to ketenes. *Journal of the American Chemical Society* **2011,** *133* (12), 4330-4341.

31. A. K. Kabi, R. Gujjarappa, N. Vodnala, D. Kaldhi, U. Tyagi, K. Mukherjee and C. C. Malakar, *Tetrahedron Letters*, **2020**, 61, 152535.

32. Huang, H.; Jiang, Z.-T.; Wu, Y.; Gan, C.-Y.; Li, J.-M.; Xiang, S.-K.; Feng, C.; Wang, B.-Q.; Yang, W.-T., Copper-Catalyzed Amidation of Arylboronic Acids with Nitriles. *Synlett* **2016,** *27* (06), 951-955.

33. Yoshimura, A.; Zhdankin, V. V., Advances in Synthetic Applications of Hypervalent Iodine Compounds. *Chemical Review* **2016,** *116* (5), 3328-3435.

34. Aradi, K.; Tóth, B. L.; Tolnai, G. L.; Novák, Z., Diaryliodonium Salts in Organic Syntheses: A Useful Compound Class for Novel Arylation Strategies. *Synlett* (EFirst).

35. Petersen, T. B.; Khan, R.; Olofsson, B., Metal-Free Synthesis of Aryl Esters from Carboxylic Acids and Diaryliodonium Salts. *Organic Letters* **2011,** *13* (13), 3462-3465.

36. Bielawski, M.; Zhu, M.; Olofsson, B., Efficient and General One-Pot Synthesis of Diaryliodonium Triflates: Optimization, Scope and Limitations. *Advanced Synthetic Catalyst* **2007,** *349* (17‐18), 2610-2618.

37. Malmgren, J.; Santoro, S.; Jalalian, N.; Himo, F.; Olofsson, B., Arylation with Unsymmetrical Diaryliodonium Salts: A Chemoselectivity Study. *Chemistry – A European Journal* **2013,** *19* (31), 10334-10342.

38. Olyaei, A.; Sadeghpour, M., Chemistry of 3-cyanoacetyl indoles: synthesis, reactions and applications: a recent update. *RSC Advances* **2023,** *13* (31), 21710-21745.

39. Li, M.; Wu, F.; Gu, Y., Brönsted acidic ionic liquid catalyzed synthesis of benzo[a]carbazole from renewable acetol and 2-phenylindoles in a biphasic system. *Chinese Journal of Catalysis* **2019,** *40* (8), 1135-1140.

40. Truax, N. J.; Banales Mejia, F.; Kwansare, D. O.; Lafferty, M. M.; Kean, M. H.; Pelkey, E. T., Synthesis of Benzo[a]carbazoles and an Indolo[2,3-a]carbazole from 3-Aryltetramic Acids. *Journal of Organic Chemistry* **2016,** *81* (15), 6808-6815.

41. Wu, L.; Huang, H.; Dang, P.; Liang, Y.; Pi, S., Construction of benzo[a]carbazole derivatives via Diels–Alder reaction of arynes with vinylindoles. *RSC Advances* **2015,** *5* (79), 64354-64357.

42. Tao, Y.; Zhang, F.; Tang, C.-Y.; Wu, X.-Y.; Sha, F., Direct Assembly of Benzo[a]carbazole-5-carboxylates via a Diels–Alder Reaction with Arynes and 3-Alkenylindoles. *Asian Journal of Organic Chemistry* **2014,** *3* (12), 1292-1301.

43. Li, B.; Zhang, B.; Zhang, X.; Fan, X., Regio-selective synthesis of diversely substituted benzo[a]carbazoles through Rh(iii)-catalyzed annulation of 2-arylindoles with α-diazo carbonyl compounds. *Chemical Communication* **2017,** *53* (7), 1297-1300.

44. Liu, A.; Han, Q.; Zhang, X.; Li, B.; Huang, Q., Transition-Metal-Controlled Synthesis of 11H-Benzo[a]carbazoles and 6-Alkylidene-6H-isoindo[2,1-a]indoles via Sequential Intermolecular/Intramolecular Cross-Dehydrogenative Coupling from 2-Phenylindoles. *Organic Letters* **2019,** *21* (17), 6839-6843.

45. Chen, G.; Zhang, X.; Jia, R.; Li, B.; Fan, X., Selective Synthesis of Benzo[a]Carbazoles and Indolo[2,1-a]-Isoquinolines via Rh(III)-Catalyzed C−H Functionalizations of 2-Arylindoles with Sulfoxonium Ylides. *Advanced Synthetic Catalyst* **2018,** *360* (19), 3781-3787.

46. Slaett, J.; Romero, I.; Bergman, J., Cyanoacetylation of indoles, pyrroles and aromatic amines with the combination cyanoacetic acid and acetic anhydride. *Synthesis* **2004,** *2004* (16), 2760-2765.

47. Bielawski, M.; Zhu, M.; Olofsson, B., Efficient and General One‐Pot Synthesis of Diaryliodonium Triflates: Optimization, Scope and Limitations. *Advanced Synthetic Catalyst* **2007,** *349* (17), 2610-2618.

48. Bielawski, M.; Aili, D.; Olofsson, B., Regiospecific one-pot synthesis of diaryliodonium tetrafluoroborates from arylboronic acids and aryl iodides. *Journal Organic Chemistry* **2008,** *73* (12), 4602-4607.

Chapter 7

Conclusions and Future Scope

7.1 General Conclusions

Among the azaheterocycles, indole has become leading pharmacophore which continues to receive increasing attention from medicinal chemists due to unique biological properties of indole derived compounds, especially and anticancer activity. Chemotherapy is very important and popular treatment among the available cancer therapies. In recent past, various chemotherapeutic agents such as paclitaxel, vincristine, and doxorubicin have lost their efficacy due to the development of drug resistance from prolonged exposure. Therefore, the development of novel and effective anticancer agents with an improved pharmacological profile remains a major challenge. The thesis deals with the design, synthesis and biological studies of indolylsulfoximines, indolyltriazoles and bisindoles. While synthesizing the indole-based compounds we developed mild, efficient and high yielding synthetic protocols for the construction of indolylsulfoximines, indolyl-1,3,4-triazoles, α-cyano bis(indolyl)chalcones, β-oxo amides and benzo[*a*]carbazoles. The thesis reports synthesis of N-arylindolyl sulfoximines as potent anticancer agents. The sulfoximine derivatives exhibited CDK5/p25 inhibition activity. Furthermore, colchicine derived sulfoximines and indolyl-1,2,4-triazoles were identified as potent tubulin inhibitors.

7.2 Specific conclusions

The **first chapter** deals the physical and chemical properties of indole and a brief overview of anticancer research and treatments of various types of cancers with special emphasizes on chemotherapy and classification of anticancer drugs present in market. This chapter described the utilities of natural and synthetic indole-based molecules in anticancer drug discovery. Further, this chapter provides the information for the rational design of novel indole containing chemical entities as potent anticancer agents. Also, it describes the current problems associated with the existing anticancer drugs and the scope for developing novel indole-based compounds by structural modifications of existing indole-based lead anticancer drug candidates with improved anticancer properties.
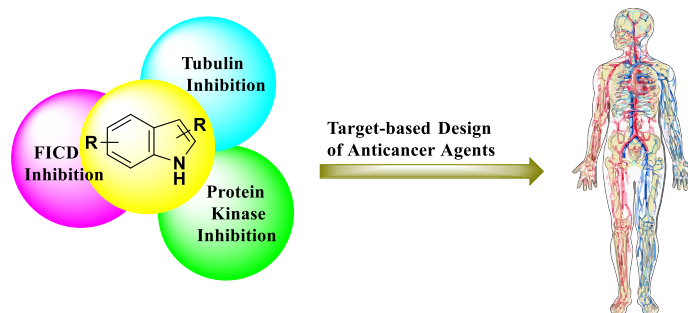
The **Second Chapter** highlights the design, synthesis and anticancer activities of two different novel sulfoximine series (indolylsulfoximines and colchicine sulfoximines). **Part 2A** of this chapter reports a copper-mediated cross-coupling reactions of *N*-Boc-3-indolylsulfoximines with aryl iodides to produce a diverse series of *N*-arylated indolylsulfoximines in excellent yields. From the prepared series of *N*-arylated indolylsulfoximines with 5-bromoindole (1.28 μM) and 5-methoxyindole (2.68 μM) moieties were found to be selectively cytotoxic against MCF7 and 22Rv1 cells. Particularly, the compound bearing fluorine at the C_6-position of indole, endowed broad cytotoxicity against C4-2, PC3, 22Rv1 and MCF7 with IC_{50} values of 8.1, 3.51, 1.91, and 1.7 μM, respectively. Mechanism of action studies suggested that compound displayed increased endogenous level of ROS, leading to the increased level of p-53 and c-jun, which ultimately induces apoptosis.
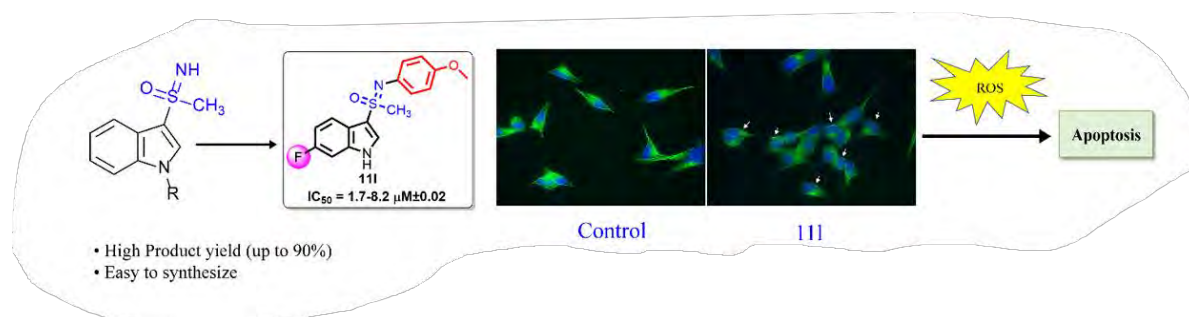
In **Part 2B** of the chapter, synthesis, characterization and anticancer activity of colchicine with sulfoximine moiety have been described. Preparation of colchicine sulfoximine involves the reaction of thiocolchicine with iodobenzene diacetate and ammonium carbamate in good yield. Cytotoxicity study showed that our sulfoximine analogue was more than eighty percent inhibition of cancerous cells. Tubulin polymerization assay also suggest that thiocolchicine and sulfoximine functionalized colchicine are comparable to the inhibitors of tubulin polymerization. Molecular docking studies also indicated that the potent compound exhibits strong binding affinity (-7.5 Kcal/mol) and potent H-bonding interaction with CYS241, surpassing that of colchicine.

The **Third Chapter** reports synthesis of a series of *N*-aryl indolylsulfoximines and *in vitro* kinase activities. Some of *N*-aryl indolylsulfoximines displayed potent and selective inhibition of CDK5/p25 (~ IC_{50} = 1.12 μM). Additionally, the docking results (binding affinity= -8.5 Kcal/mol) demonstrated a strong correlation with *in vitro* activity results.
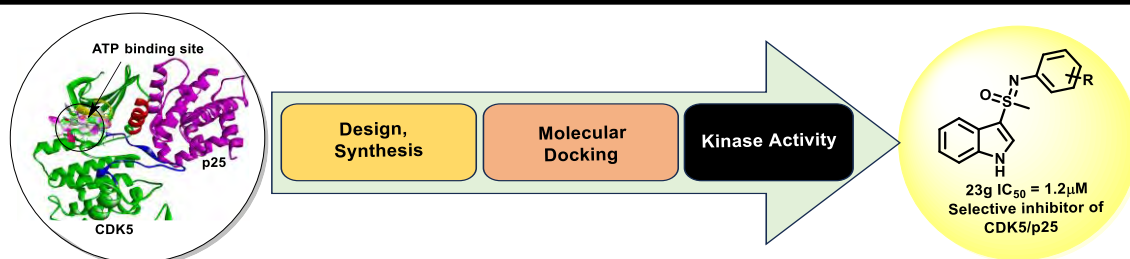
The **Chapter Four** of thesis elaborates design, synthesis and biological evaluation of indolyl-1,2,4-triazoles. These compounds were synthesized through the reaction of acylhydrazides and corresponding thioimidates, resulting in high product yields. The synthesized 5-bromoindolyl-1,2,4-triazoles exhibited remarkable cytotoxicity against a tested cancer cell line, HeLa cells, with $IC_{50} = 3.5$ µM. Molecular docking study of the potent indolyl-1,2,4-triazole showed good binding affinity at colchicine binding site.
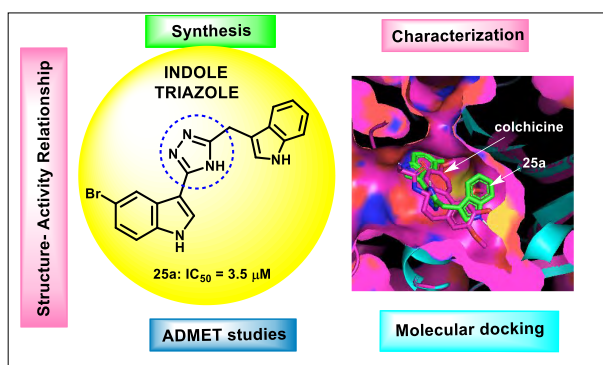
In Chapter Five, synthesis and anticancer activity studies of novel bisindoles are discussed and the chapter has been divided into two parts. **Part 5A** provides the high yielding synthesis of indolyl α-cyano bis(indolyl)chalcones was achieved from the L-proline catalysed reaction of appropriate aldehydes with 3-cyanoacetylindoles. Of the prepared eighteen α-cyano bis(indolyl)chalcones, compound **21j** demonstrated remarkable potency against the C4-2 prostate cancer cell line ($IC_{50} = 0.9$ µM). With broad spectrum of activity (0.98-5.6 µM), the compound 21j was found to increase the endogenous level of ROS, upregulate the level of p-53 and c-jun besides mitochondrial dysfunction, causes apoptosis.
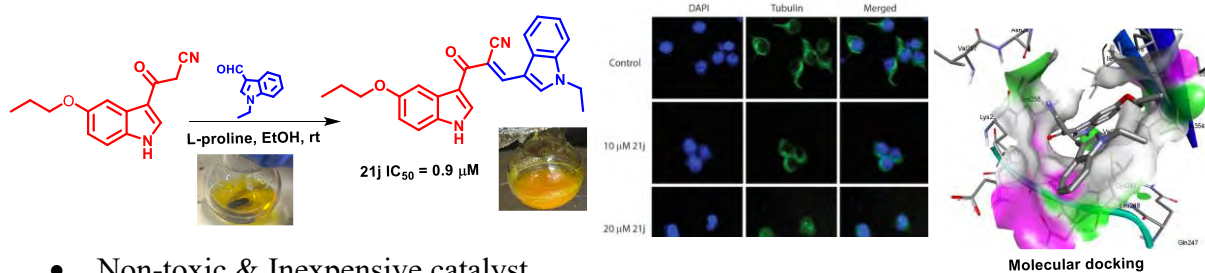
- Non-toxic & Inexpensive catalyst
- Easy experimentation & product isolation
- High product yields (upto 95%)

In **Part 5B**, synthesized α-cyano bis(indolyl)chalcones were screened for FICD inhibition activity and found to display significant potency ($IC_{50} = 7.9$ µM).
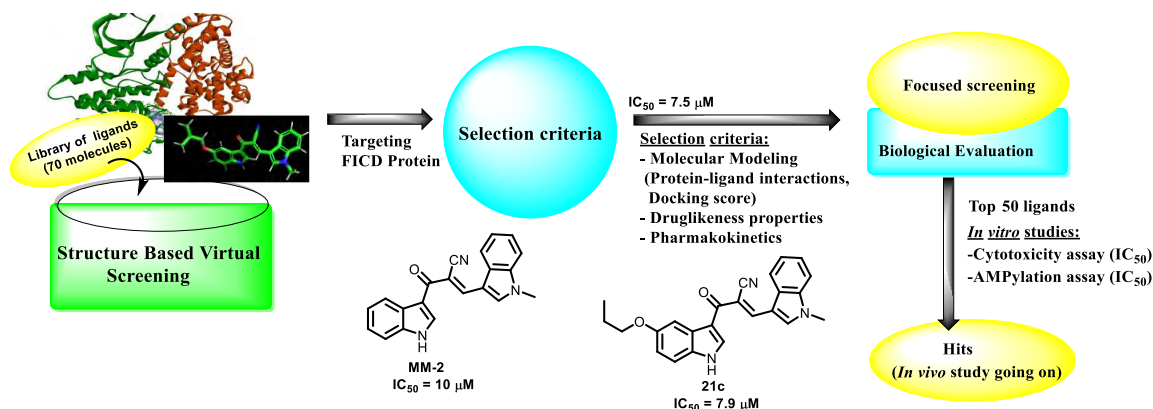
In **sixth chapter** preparation of diverse and biologically active β-oxo amides and benzo[*a*]carbazoles has been reported. Our copper-catalyzed strategy enables the synthesis of β-oxo amides using iodonium salts under mild reaction conditions. Additionally, approach offers a convenient route to diversely substituted benzo[*a*]carbazoles from 3-substituted acetylindoles and diaryliodonium salts under Pd-catalyzed conditions. The developed conditions were found to be advantegeous in term of high product yield, use of readily available starting materials and short synthesis of bioactive compounds.
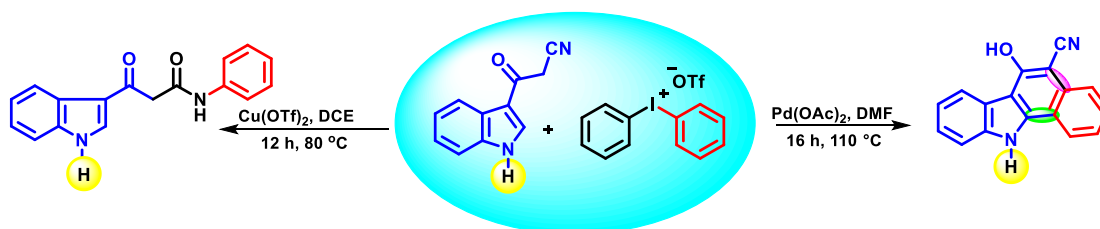
7.3 Future Scope of the Research Work

The synthesis and functionalization of biologically active heterocycles hold significant importance in organic chemistry. As heterocyclic motifs are prevalent in molecules entering clinical trials, the modification of these rings is crucial in drug development. Thus, there is a constant demand for the preparation and modification of heterocyclic ring systems under mild and feasible reaction conditions. Recent advancements in anticancer drug discovery have been noteworthy, with various efficient therapies like surgery, chemotherapy, radiation therapy, and immunotherapy being utilized. Moreover, the expanding knowledge of cancer biology aids in understanding the mechanistic pathways of cancer cell growth. Natural anticancer compounds like taxol, vinca alkaloids, and combretastatin A-4 have made significant contributions to the discovery of potent antitumor agents. However, despite the progress, challenges such as tumor

specificity, solubility, drug resistance, and toxicity-associated side effects persist, urging medicinal chemists to design novel drugs with improved safety profiles.

The scope of the thesis is to develop diverse structural classes of indoles as novel anticancer agents. The anticancer potential of indolylsulfoximine analogues, indolyl-1,2,4-triazoles and bisindolylchalcones, can be further enhanced through extensive structure-activity relationship studies. Based on observed *in vitro* cytotoxicity results, further structural modifications of the active compounds in different series are likely to yield drug-like candidates. Subsequent molecular target identification and *in vivo* screening of the potent compounds may also be explored. The relatively benign synthetic protocols developed for the preparation of indolylsulfoximines, colchicine analogues, indolyl-1,2,4-triazoles, bisindolylchalcones and carbazoles have the potential to generate a library of bioactive scaffolds.
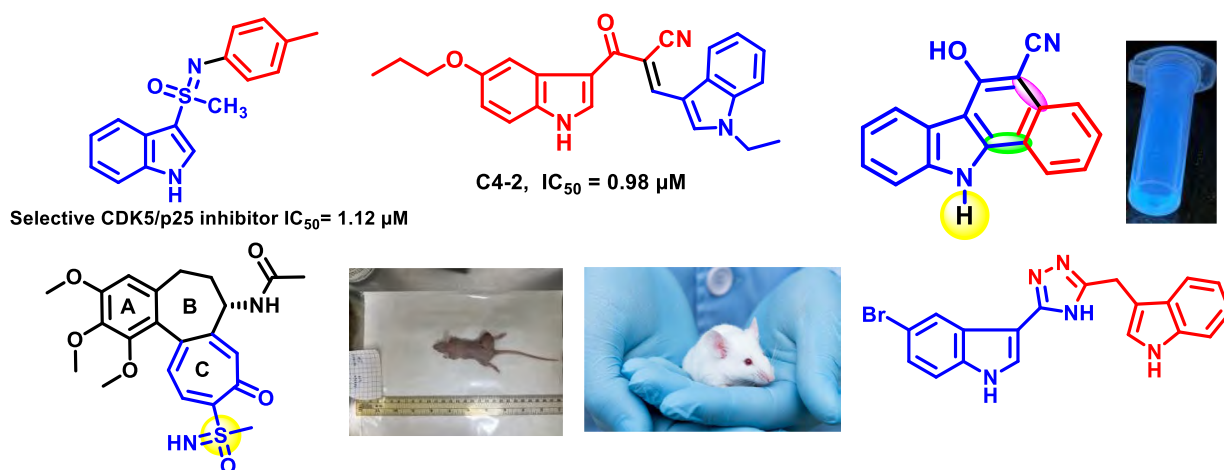

Figure 7.1 Future Scope of the Research Work

List of Publications

1. **<u>Monika Malik</u>**, Dinesh Kumar, Kavita Shah and Dalip Kumar " Design, synthesis and anticancer activity of N-aryl indolylsulfoximines: Identification of potent and selective anti-cancer agents" **Bioorg. Med. Chem., 2023, 93, 117459**.

2. Manish Kumar, **<u>Monika Malik</u>**, Bintu Kumar and Dalip Kumar. "Chemoselective Cu-catalyzed synthesis of diverse *N*-arylindole carboxamides, β-oxo amides and *N*-arylindole-3-carbonitriles using diaryliodonium salts" **Org. Biomol. Chem., 2021, 19, 1109**.

3. Mukund P. Tantak, **<u>Monika Malik,</u>** Linus Klingler, Zachary Olson, Anil Kumar, Rachna Sadana and Dalip Kumar. "Indolyl-α-keto-1,3,4-oxadiazoles: Synthesis, anti-cell proliferation activity, and inhibition of tubulin polymerization" **Bioorg. Med. Chem. Lett., 2021, 37, 127842**.

4. **<u>Monika Malik</u>**, Nandini Roy, Asha, Kavita Shah and Dalip Kumar "L-Proline catalysed synthesis and in-silico studies of novel α-cyano bis(indolyl)chalcones as potential anti-cancer agents" (**Manuscript submitted**)

5. **<u>Monika Malik</u>**, Manish Kumar and Dalip Kumar "Pd-catalyzed reactions of electron withdrawing group (EWG)-substituted acetyl indoles with diaryliodonium salts: A domino approach to potent benzo[*a*]carbazoles" (**Manuscript under preparation**)

6. **<u>Monika Malik</u>**, Kavita Shah and Dalip Kumar "Design, synthesis, molecular docking and biological study indolylsulfoximines of CDK5/p25, CDK2/CCNE and CDK1/CCNB with interesting selectivity against CDK5/p25 inhibitors in cancer" (**Manuscript under preparation**).

7. **<u>Monika Malik,</u>** Rachna Sadana, Dalip Kumar. "Design, synthesis, *in-silico* study and biological evaluation of novel sulfoximine modified colchicine derivative as potent tubulin-targeting anticancer agents" (**Manuscript under preparation**).

8. **<u>Monika Malik,</u>** Gopal Chakrabarti and Dalip Kumar. " Design and facile synthesis of Indolyl-1,2,4-triazoles as tubulin interacting anticancer agents" (**Manuscript under preparation**).

List of papers presented in conferences

Oral Presentations:

1. **Monika Malik,** Kavita Shah and Dalip Kumar "A facile and efficient synthesis of N-aryl indolylsulfoximines as potent and selective anti-cancer agents" held at **ISCB-24** International Conference, Marwadi University, Rajkot, Gujarat.

2. **Monika Malik** and Dalip Kumar, given oral presentation on "Design, synthesis and anti-tumor efficacy studies of indolyl-heterocycles as a prostate cancer inhibitor" Training Programme on Laboratory Animal Science-2023, BITS Pilani, Pilani Campus.

3. **Monika Malik**, Mukund P. Tantak, Rachna Sadana and Dalip Kumar, given oral presentation on "Indolyl- α- keto-1,3,4-oxadiazoles as tubulin interacting agents" at International Conference-2019 on "Modern Approaches of Chemical Science and Nanomaterials" Mody University, Lakshmangarh, Rajasthan.

Poster Presentations:

1. **Monika Malik** and Dalip Kumar, given poster presentation on "Diaryliodonium salt promoted regioselective and efficient synthesis of benzo-fused carbazoles" held at BITS Pilani, Pilani Campus, Rajasthan (**CRSI-2024**)

2. **Monika Malik,** Kavita Shah and Dalip Kumar, given poster presentation on "Diaryliodonium salts promoted chemoselective synthesis of diverse *N*-arylindole carboxamides and indole-based natural products" at International Conference on "Crossroads of Chemistry" at Indiana, USA (**ACS 2023, Spring**).

3. **Monika Malik** and Dalip Kumar, given poster presentation on "Chemoselective synthesis of *N*-arylindole carboxamides using diaryliodonium Salts" held at Indian Institute of Technology, IIT Delhi. (**ACC 2023**) (**Best Paper Presentation Award**)

4. **Monika Malik,** Rachna Sadana and Dalip Kumar, given poster presentation on "Indolyl-α-keto-1,3,4-oxadiazoles as tubulin interacting agents" at International Conference-2020 on "Integrating Chemical, Biological and Pharmaceutical Sciences for Innovations in Health Care" held at Institute of Pharmacy, Nirma University, Ahmedabad.

5. **Monika Malik**, "Synthesis and QSAR studies of some novel disubstituted 1,2,4-triazoles anti-microbial agents" National Seminar-2018 on "Recent Trends in Science & Technology A Computational Approach" CBLU University, Bhiwani, Haryana.

Brief biography of the candidate

Ms. Monika Malik was born on July10, 1995, in Bhiwani, Haryana, India. Ms. Monika began her academic journey by earning her Bachelor of Science degree from Adarsh College Bhiwani, affiliated with Maharshi Dayanand University, Rohtak, Haryana, in 2016. Subsequently, in 2018, she achieved her M.Sc degree with first class honors, specializing in Organic Chemistry, from Chaudhary Bansi Lal University, Bhiwani, Haryana. Driven by a passion for research, she applied for a fellow position in a CSIR sponsored Project. In March 2019, she commenced her professional career by joining the Department of Chemistry at BITS Pilani, Pilani Campus, as a project assistant for a CSIR project. In August 2019, she enrolled in the Ph.D. program. During her doctoral studies, she was selected as an Overseas Visiting Doctoral Fellow (OVDF) in 2022 at Purdue University, USA, where she expanded her expertise by studying biology and contributing to her doctoral research in the field of anti-cancer agents. Through out her Ph.D., Ms. Monika demonstrated outstanding research capabilities, resulting in five publications in peer-reviewed international journals. She actively participated in various national/international conferences and symposia, presenting her research findings through oral and poster presentations, and received accolades for her contributions, including the Best Paper Presentation awards. Her research endeavors are centered around the design, synthesis, and biological evaluation of novel indole-related heterocycles as anti-cancer agents.

.

Brief biography of the supervisor

Dr. Dalip Kumar is a Senior Professor of Chemistry at Department of Chemistry, Birla Institute of Technology and Science, Pilani. He completed his Ph.D degree from Kurukshetra University, Kurukshetra, Haryana in 1997 under the direction of Prof. Shiv P. Singh in the research area of heterocyclic chemistry. After his doctorate, he moved to Sam Houston State University, TX, USA for his post-doctoral research (1997-1999) with the guidance of Prof. Rajender S. Varma. He was also associated with Prof. Sean M. Kerwin as a post-doctoralfellow (1999-2000), College of Pharmacy, University of Texas at Austin, TX, USA. He joined BITS Pilani, Pilani campus, as a lecturer during 2000-2002. Later, in December 2002, he moved to University of Maryland, College Park, MD, USA as a Research Associate. In 2004, Prof. Kumar re-joined as an Assistant Professor at Department of Chemistry, BITS Pilani, Pilani campus, and since then he is continuing there. He was promoted to professor in year 2012. Now, he has been promoted to senior professor in year 2021. He has been involved in research for the last 22 years and in teaching for 13 years. As a result of his research accomplishment, he has greater than 140 international publications in peer reviewed journals.Prof. Kumar has guided fourteen Ph.D students and currently he is supervising eight Ph.D students. He has one US patent, one Indian patent and successfully completed several sponsored research projects from DST, DRDO, UGC, CSIR, DBT and DST-JSPS Indo-Japanproject. Currently, he has two Government of India sponsored projects from CSIR and DST and a collaborative industrial project from Sun Pharma Ltd.

Prof. Kumar is recipient of Honorary Diploma for Scientific Achievements and International Scientific Collaboration by Russian International Charitable Foundation "Scientific Partnership", Moscow, Russia (March 2013). He received the Prof. R. D. Desai 80th Birthday Commemoration Medal and Prize from Indian Chemical Society for year 2015. He is an Associate Editor of Chemistry & Biology Interface Journal published by Indian Society of Chemists and Biologists, Lucknow. Prof. Kumar is life member of Indian Chemical Society, Indian Society of Chemists and Biologists, and Indian Council of Chemists. His current research pursuit is focused on synthesis of novel heteroaryl substituted indole and indolyl analogues, porphyrin and BODIPYs for potential anticancer agents by employing transition metal catalyzed C−H functionalization, metal-free C-C, C-N, C-O bonds formation through greener synthetic approaches.

Brief biography of the Co-supervisor

Dr. Kavita Shah is a Walther Professor at the Department of Chemistry, Purdue University Center for Cancer Research, Purdue University, USA. In 1991, she completed her Ph.D degree from Indian Institute of Technology, Kanpur, India; under the direction of Prof. Y.D. Vankar in "Total Synthesis of Vitamin D3 Metabolites and Development of Novel Methodologies for Organic Synthesis". After this, she did her first post-doctoral reaseach, in Indian Institute of Technology, Kanpur, under the guidance of Prof. S. Ranganathan (1992-1993). She moved to US to do her second post-doctoral research under the supervision of Prof. T. M. Rana at UMDNJ-Robert Wood Johnson Medical School, Piscataway, NJ (1993-1994). She did her third post-doctoral research under the guidance of Prof. Kevan Shokat, at Princeton University, Princeton, NJ 08544 (1994-1999). She joined Genomics Institute of Novartis Research Foundation, San Diego, CA, as a Group Leader for the period of 1999 to 2004. Later, in July 2004, she moved to Purdue University Center for Cancer Research, USA and joinead as a Walther Associate Professor of Chemistry. In April, 2016 she was promoted to Walther Professor of Chemistry in Purdue University, USA and is continuing her research there. Prof. Shah has associated herself in the research field of chemistry and biology for the last 33 years. As a result of her research accomplishments, she has greater than 80 international publications in peer reviewed journals. Prof. Shah has guided more than eight Ph.D students and currently she is supervising three Ph.D and one post-doctoral student. She has completed various projects for academia and industries as a result of which Prof. Shah was awarded "Organizer and Chair of Scientific Meetings: Oncogenic Kinases Session" by American Chemical Society, Anaheim in March 30th, 2011. She is also the proud owner of the prestigious Lafayette Lions Club Award for Outstanding Achievements in Cancer Research (2015). She has also received the GIAN Award (2016) and JSPS Fellowship (2017). Lately, she received the prestigious IRAC-SRISTI Gandhian Technological Innovation (GYTI) Award in 2017 at Rashtrapati Bhavan India (2017). In her other achievements, Prof. Shah is lifetime member of ASBMB, ASCB, Society of Neuroscience. In 2008, she became the Editor of Current Protocols in Chemical Biology. From, 2008 to 2014 she was the Editorial Board member of Cell Biology Insights. From 2010 she is associated with Faculty of 1000. Prof. Shah is also a present member of Editorial Board member of Endocrinology and Metabolic Syndrome and Editorial Board member of Journal of Obesity & Weight loss Therapy, since 2011. From 2012 she is the on Editorial Board member of F1000 Research. Her current research pursuit is focused biological research of active pharmacological small molecules which can be targeted as anti-cancer agents. She also works on identification and elucidation of signalling pathways of various kinase proteins.